Journal of Engineering

ISSN 1726-4073

A Scientific Refereed Journal
Published by College of
Engineering University of
Baghdad

April

2015

Number 4

Volume 21

مجلة الهندسة

ISSN 1726-4073

مجلة علمية محكمة تصدرها
كلية الهندسة ـ جامعة بغداد

نيسان
2015

العدد 4
المجلد 21

English Section

القسم العربي

JOURNAL OF ENGINEERING ISSN 1726-4073

College of Engineering University of Baghdad Baghdad

Editorial Board

- **Chief Editor**

  Prof. Dr. Najdat Nashat Abdullah

- **Members**

  Prof. Dr. Safa N. Hamad
  Prof.Dr. Thamir K. Mahmood
  Prof.Dr. Ghada M.R.Razzouqi Al Sihiq
  Prof.Dr. Adanan Naji Jamael
  Asst. Prof. Dr. Sameera M. Hamad-Allah
  Asst. Prof. Dr. Zainab Ziad Ismail
  Asst. Prof. Hasan Farhood Makki
  Asst. Prof. Dr. Firas Mohammed Tuaimah
  Asst. Prof. Dr. Nadia Adnan Shiltagh

- **Scientific Consultant Committee**

  Prof. Dr.Saleem Mohammed Ridha Ali Taha
  Prof. Dr.Saba Jabbar Neamah Al khafaji
  Prof.Dr.Yasin Khdear Salman
  Prof.Dr.Ala Nasir ALjorany
  Prof. Dr. Hussein Yousif Mahmood
  Prof. Dr. Riyadh Zuhair Al Zubaidy
  Prof. Dr.Majid Ibrahim Abdulwahab
  Prof. Dr.Raad Sami Fyath
  Prof. Dr.Mohammed Othman Abdul -Razaq
  Prof. Dr.Abdul – Rassol Hamodi Shahab

- **Technical Supervision**

  Rafel M. Ali

The Journal of Engineering is a monthly refereed periodical
Correspondence should be addressed to:

THE EDITOR
JOURNAL OF ENGINEERING
COLLEGE OF ENGINEERING
UNIVERSITY OF BAGHDAD
P. O. BOX 47024 JADERIYAH
BAGHDAD – IRAQ

ISSN 1726-4073

مجلة الهندسة

كلية الهندسة جامعة بغداد

هيئة التحرير

- رئيس التحرير:

أ. د. نجدت نشأت عبد الله

- الاعضاء:
  - أ.د. صفاء نوري حمد
  - أ.د. ثامر خضير محمود
  - أ.د. غادة موسى رزوقي
  - أ.د. عدنان ناجي جميل
  - أ.م.د. سميرة محمد حمد الله
  - أ.م.د. زينب زياد اسماعيل
  - أ.م.د. حسن فرهود مكي
  - أ.م.د. فراس محمد طعيمة
  - أ.م.د. نادية عدنان شلتاغ

* الهيئة الاستشارية العلمية :

- أ.د. سليم محمد رضا علي طه
- أ.د. صبا جبار نعمة الخفاجي
- أ.د. ياسين خضير سلمان
- أ. علاء ناصر الجوراني
- أ.د. حسين يوسف محمود
- أ.د. رياض زهير الزبيدي
- أ.د. ماجد ابراهيم عبد الوهاب
- أ.د. رعد سامي فياض
- أ.د. محمد عثمان عبد الرزاق
- أ.د. عبد الرسول حمودي شهاب

- الاشراف الفني:

رفل محمد علي

مجلة الهندسة: مجلة شهريه محكمة

تعنون كافة المراسلات وطلبات الاشتراك الى:

رئيس التحرير
مجلة الهندسة
كلية الهندسة
صندوق بريد 47024 الجادرية
بغداد - العراق

Software Implementation of Binary BCH Decoder Using Microcontroller

Lect. Mohammed Kasim Al-Haddad
Electronics and Communication Department
College of Engineering - Baghdad University
mkmih12@gmail.com

ABSTRACT

In this paper a decoder of binary BCH code is implemented using a PIC microcontroller for code length n=127 bits with multiple error correction capability, the results are presented for correcting errors up to 13 errors. The Berkelam-Massey decoding algorithm was chosen for its efficiency. The microcontroller PIC18f45k22 was chosen for the implementation and programmed using assembly language to achieve highest performance. This makes the BCH decoder implementable as a low cost module that can be used as a part of larger systems. The performance evaluation is presented in terms of total number of instructions and the bit rate.

Key Words: bch code, berlekamp-massey algorithm, chien search, pic microcontroller.

التنفيذ البرمجي لفك ترميز شفرة BCH الثنائية باستعمال المسيطر الدقيق

م. محمد قاسم محمد الحداد
قسم الهندسة الالكترونية والاتصالات
كلية الهندسة – جامعة بغداد

الخلاصة

في هذا البحث تم تنفيذ منظومة لفك ترميز BCH الثنائية باستعمال المسيطر الدقيق نوع PIC لطول ترميز يساوي 127 مرتبة ثنائية مع قدرة على تصحيح اخطاء متعددة، وقد تم عرض النتائج لتصحيح الاخطاء يصل عددها حتى 13 خطأ. تم اختيار خوارزية بيركيلام-ميسي في عملية فك الترميز لكفاءتها. تم اختيار المسيطر الدقيق PIC18f45k22 للتنفيذ وقد تمت برمجته بواسطة لغة التجميع للحصول على اعلى اداء. وهذا يجعل فك ترميز BCH قابل للتنفيذ كوحدة بنائية واطئة الكلفة وممكن استعمالها كجزئ من انظمة اكبر. وكان تقيم الاداء عن طريق استعراض عدد التعليمات الكلي ومعدل الترميز.

الكلمات الرئيسية: ترميز BCH، خوارزية بيركيلام-ميسي، بحث تشين، المعالج الدقيق PIC.

1. INTRODUCTION

Bose-Chaudhuri-Hocquenghem (BCH) codes are an important subclass of the linear cyclic block codes that can be considered as a generalization of Hamming codes. Unlike Hamming codes, BCH codes has multiple error correction capability. There are efficient decoding algorithms for the BCH codes due to their special algebraic structure و ,**Jiang, 2010**. Two important subclasses of the BCH Codes are the Reed-Solomon Codes, which are nonbinary and the binary BCH codes. This paper is about the binary BCH code.

,Chu, and **Sung, 2009.** presented a technique for improving Chien search base on Constant Galois Field Multiplication (CGFM) where a multiplication by a constant is implemented by shift register. Multiplications can be performed in a single shift operation if proper lookup tables are used. Higher speed performance can be achieved by larger lookup tables. ,**Taki El-Din *et al*., 3013.** proposed an algorithm for detecting the undetectable received codewords i.e. when the number of errors is greater than the design error correction capability *t*. This is achieved by transforming the error locating polynomial to another polynomial whose coefficients must satisfy certain conditions. If the conditions are satisfied, the decoder can proceed to Chien search and correct the received codeword, otherwise, the Chien search is skipped and decoding failure is declared and repeat request is transmitted. ,**Schipani *et al*., 2011.** made a comparison study of the different decoding algorithms of the generalized nonbinary BCH codes with the binary BCH codes as a special case. Schipani proposed an algorithm for syndrome evaluation that is based on rearranging the received codeword polynomial as a linear combination of polynomials with special grouping of powers of *x*. This arrangement reduces the number of multiplications over the direct evaluation of the received codeword polynomial. ,**Lin *et at*., 2010.** proposed a hardware-based soft decision decoding algorithm of BCH codes where the syndrome calculations and error location stages are processed in parallel. Simulation was for the t=2 error correcting code (255,239,2), Lin suggested that the proposed algorithm can correct at most $2t$+1 errors. ,**Wu, 2008.** presented a modification to the Berkelamp-Massey algorithm that can produce a list of candidates of correct codewords (list decoding) for both Reed-Solomon and BCH codes where the number of correctable errors of these codes is extended beyond their design error correcting capability.

2. MATHEMATICAL BACKGROUND

Finite fields especially Galois Field (GF) play an important role in coding theory, here is a brief introduction. A finite field has a finite number of elements, their number is either a prime p or a power of a prime $q=p^m$. If p=2, the GF field is referred to by GF(2^m), a special but yet important case where m=1 which yields GF(2) has the only two elements 0 and 1. There are to operations defined over the field; addition (+) and multiplication (·). Other than number of elements being finite all properties if fields apply, like closure, commutative and associative operations, the identity and inverse elements of addition and multiplication. The elements of a GF(2^m) are defined as remainder obtained when dividing the powers of x by a generator polynomial $g(x)$ whose coefficients $\in$ GF(2), i.e. 0 or 1, the roots of $g(x) \in$ GF(2^m). A polynomial with coefficients $\in$ GF(2) is called a binary polynomial. A generator polynomial must be a binary polynomial and irreducible that is it cannot be factored into two or more binary polynomials. Such a polynomial is also called a primitive polynomial and its root α is called primitive element because all elements can be represented in terms of powers of α. The above can be stated mathematically as

$$x^i = s(x)g(x) + r(x) \qquad \deg(r(x))<\deg(g(x)) \tag{1}$$

Equation (1) tells us simply that x^i (considered as a polynomial) when divided by $g(x)$, the remainder $r(x)$ represents the element of the GF(2^m) field in polynomial form. **Table 1.** shows an example of GF(2^3) field generated using the primitive polynomial $g(x)=x^3+x+1$. **Table 1.** also shows the two forms representing the GF elements, one is the power of α, here the element 0 cannot be represented as an integer power of α, so, it is represented as $\alpha^{-\infty}$ by convention. The second representation is by the binary polynomial $r(x)$. The third representation will be explained later in system implantation section. The addition operation is performed by adding the polynomial form of the elements where the coefficients are added modulo-2 for example: $\alpha^3+\alpha^4=(x+1)+(x^2+x)=x^2+1=\alpha^6$. Note that modulo-2 addition implies that addition is the same as subtraction i.e., $x+x=x-x=0$. Multiplication is performed in the power for with $\alpha^{q-1}=1$ where $q=2^m$, for example: $\alpha^4\alpha^5=\alpha^9=\alpha^7\alpha^2=1\cdot\alpha^2=\alpha^2$. From the above it is clear that every element is the additive inverse of itself and the multiplicative inverse of α^i is $\alpha^{q-1-i}$for more details and proofs of claims stated above the reader may refer to references ,**Justesen, Høholdt, 2004.** and ,**Jiang, 2010**. The elements of a GF field can be generated by hardware using a linear feedback shift register (LFSR), **Jiang, 2010**. as shown in **Fig. 1**, where the branches represent the coefficients of $g(x)$, the contents of the LFSR can be initialized by any element other than 0. A single clock to the LFSR represents a multiplication by x when the LFSR overflows; $g(x)$ is subtracted from the content. Clocking j times is equivalent to multiplication by x^j. One more thing that needs to be addressed before leaving this section is the minimal polynomials. A minimal polynomial $\phi_l(x)$ of element α^j is a binary irreducible polynomial with α^j as its root. The polynomial $\phi_1(x)=(x+\alpha)(x+\alpha^2)(x+\alpha^4)=x^3+x^2+1$ is a minimal polynomial of α because it is binary, irreducible and has α as root, and there is no binary polynomial of degree less than 3 with α as a root, the polynomial $x+\alpha$ is not minimal although it is of degree 1 because it has the coefficient α which is not a binary value. The roots of $\phi_l(x)$: α, α^2, α^4 are called conjugates.

3. BINARY BCH CODES

Generalized BCH codes are of length $n=q^v-1$ where q is a power of prime and v is positive integer. Two important subclasses of the generalized BCH codes are the binary BCH codes when $q=2$ and the Reed-Solomon (RS) codes when $v=1$, **Moreira** and **Farrell, 2006**. In this paper we are interested in the binary BCH codes, which can be described as follows; for $m\geq 3$ and $t<2^m-1$ there exist a binary BCH code C(n,k,t) with the following properties:

1- Code length: $n=2^m-1$
2- Number of parity bits: $n-k\leq mt$
3- Minimum hamming distance: $d_{min}\geq 2t+1$
4- Error correcting capability: t errors in a codeword

The generator polynomial $g(x)$ of binary BCH code with above parameters is the minimum-degree binary polynomial that has α, α^2, α^3,...., α^{2t} as roots, i.e.

$$g(\alpha^i)=0 \qquad i=1,2,3,\cdots,2t \tag{2}$$

The binary polynomial that satisfies Eq. (2) can be described in terms of the minimal polynomials of the roots α^i as

$$g(x) = \mathrm{LCM}(\phi_1(x), \phi_2(x), \cdots, \phi_{2t}(x)) \tag{3}$$

Where LCM(a,b) is the least common multiple of a and b. It can be shown that GF elements α^i and α^{2i} are both conjugates, that is they are both roots of the same minimal polynomial. Therefore the even indexed minimal polynomials can be removed and Eq. (3) becomes

$$g(x) = \mathrm{LCM}(\phi_1(x), \phi_3(x), \cdots, \phi_{2t-1}(x)) \tag{4}$$

Hamming codes are special case of BCH codes with $g(x)$= ($\phi_1(x)$) and t=1. If the massage k-bits are represented in a polynomial form

$$m(x) = m_0 + m_1 x + m_2 x^2 + \cdots + m_{k-1} x^{k-1} \tag{5}$$

The BCH code can be generated by multiplying $m(x)$ by the generator polynomial

$$c(x) = m(x) g(x) \tag{6}$$

This is a nonsystematic encoding, for the systematic encoding the codeword $c(x)$ is given by Eq. (7), ,**Moreira** and ,**Farrell, 2006.**

$$c(x) = x^{n-k} m(x) + p(x) = q(x) g(x) \tag{7}$$

Where, $p(x)$ and $q(x)$ are the remainder and quotient when dividing $x^{n-k}m(x)$ by $g(x)$. In both equations (7) & (8) the codeword $c(x)$ is a multiple of the generator polynomial $g(x)$, this means that the roots of $g(x)$ (Eq. (2)) are also roots of $c(x)$, i.e.

$$c(\alpha^i) = c_0 + c_1\alpha^i + c_2\alpha^{2i} + \cdots + c_{n-1}\alpha^{i(n-1)} = 0 \qquad i = 1,2,\cdots,2t \tag{8}$$

These 2t equations can be written in matrix form

$$[c_0 \quad c_1 \quad c_2,...,c_{n-1}] \begin{bmatrix} 1 & \alpha & \alpha^2 & \cdots & \alpha^{n-1} \\ 1 & \alpha^2 & (\alpha^2)^2 & \cdots & (\alpha^2)^{n-1} \\ 1 & \alpha^3 & (\alpha^3)^2 & \cdots & (\alpha^3)^{n-1} \\ \vdots & \vdots & \vdots & \vdots & \vdots \\ 1 & \alpha^{2t} & (\alpha^{2t})^2 & \cdots & (\alpha^{2t})^{n-1} \end{bmatrix}^T = CH^T = \mathbf{0} \tag{9}$$

Equation (9) gives the parity check matrix H. It has been mentioned earlier that if α^j is a root of one of the minimal polynomials in Eq. (4) and hence $g(x)$, then its conjugates are also roots, these conjugates appear in the even rows of Eq. (9), so, these rows can be removed from H

$$H = \begin{bmatrix} 1 & \alpha & \alpha^2 & \cdots & \alpha^{n-1} \\ 1 & \alpha^3 & (\alpha^3)^2 & \cdots & (\alpha^3)^{n-1} \\ 1 & \alpha^5 & (\alpha^5)^2 & \cdots & (\alpha^5)^{n-1} \\ \vdots & \vdots & \vdots & \vdots & \vdots \\ 1 & \alpha^{2t-1} & (\alpha^{2t-1})^2 & \cdots & (\alpha^{2t-1})^{n-1} \end{bmatrix} \tag{10}$$

where, Each element of H is a GF(2^m) element which can be represented by a vector of m bits.

4. DECODING OF BINARY BCH CODES

The process of decoding BCH codes is described by the block diagram shown in **Fig. 2**. It consists of 3 main stages; the first is the syndrome calculations, the second is to use these syndrome values to find a polynomial whose roots represents the error locations, the third step is to solve the error locating polynomial to find the error positions. Since we are dealing with a binary code (unlike RS codes) there is no need for an error evaluation step as the error values in the binary case are always 1's. These 3 main blocks are describes next.

4.1 Syndrome Calculations

Like any other block code, the received word and the error pattern are related in polynomial form by

$$r(x) = c(x) + e(x) \tag{11}$$

Since CH^T=0, the syndrome can be calculated by

$$S_j = r(\alpha^j) = \sum_{i=0}^{n-1} r_j \alpha^{ij} \qquad j = 1,2,\cdots,2t \tag{12}$$

Equation (12) involves calculating the syndrome values either using polynomial evaluation over GF(2^m) field or using matrix multiplication as in

$$S = RH^T \tag{13}$$

where, R is the received word as a vector. There is another way of calculation which involves polynomial division. The received word as a polynomial is divided by the minimal polynomials and the remainder polynomials are evaluated for the values of the roots α^j as below

$$r(x) = a_j(x)\phi_j(x) + b_j(x) \tag{14}$$

Recall that α^j, j=1,2,…, 2t are roots of $\phi_j(x)$ therefore Eq. (12) becomes

$$S_j = r(\alpha^j) = b_j(\alpha^j) = \sum_{i=0}^{m-1} b_j \alpha^{ij} \tag{15}$$

The difference between Eq. (12) and Eq. (15) is that Eq. (12) is about evaluating the polynomial $r(x)$ which of degree n-1 while Eq. (15) is about evaluating the polynomials $b_j(x)$ which of degree m which is less than the order of $r(x)$. But in order to obtain the polynomials $b_j(x)$, 2t divisions must be performed in order to obtain the 2t polynomials $b_j(x)$. One last thing is that in binary case Eq. (12) and Eq. (15) can be used to calculate the syndromes of odd indices and the syndromes of even indices can be obtained using the equation below which applies for any binary polynomial, ,**Moreira** and **Farrell, 2006.**

$$S_{2i} = (S_i)^2 \tag{16}$$

4.2 Error Locating Polynomial

The error locating polynomial is of the form

$$(1-\beta_1 x)(1-\beta_2 x)\cdots(1-\beta_v x) = 1+\sigma_1 x+\cdots+\sigma_v x^v = 0 \tag{17}$$

Where β_j, j=1, 2,…, v are GF(2^m) elements that represent the error location through their power representation, i.e.

$$\beta_j = \alpha^{i_j} \tag{18}$$

The value of i_j in Eq. (18) is the error location in the codeword vector R. The roots of Eq. (17) are the multiplicative inverses of β_j. The value of v is the order of the equation and the number of errors and it is unknown. There are different algorithms for finding the error locating polynomial

1- Peterson's Algorithm
2- Euclidean Algorithm
3- Berlekamp-Massey (BM) Algorithm

There are other algorithms which are beyond the scope of this work. These 3 algorithms share the common ground that the syndrome values and the coefficient of the error locating polynomial are related through the so-called Newton's identity

$$\begin{aligned}
&S_1+\sigma_1 = 0\\
&S_2+\sigma_1 S_1+2\sigma_2 = 0\\
&S_3+\sigma_1 S_2+\sigma_2 S_1+2\sigma_2 = 0\\
&S_v+\sigma_1 S_{v-1}+\sigma_2 S_{v-2}+\cdots+\sigma_{v-1} S_1+v\sigma_v = 0\\
&S_{v+1}+\sigma_1 S_v+\sigma_2 S_{v-1}+\cdots+\sigma_{v-1} S_2+\sigma_v S_1 = 0
\end{aligned} \tag{19}$$

$$S_{v+2}+\sigma_1 S_{v+1}+\sigma_2 S_v+\cdots+\sigma_{v-1}S_3+\sigma_v S_2=0$$
$$S_{2t}+\sigma_1 S_{2t-1}+\sigma_2 S_{2t-2}+\cdots+\sigma_{v-1}S_{2t-v+1}+\sigma_v S_{2t-v}=0$$

In the binary case the term $v\sigma_v$ reduces to 0 when v is even or 1 when v is odd. In the above equations the syndrome values S_i are given and the coefficients σ_i are the unknowns. Peterson's algorithm solves these linear equations for σ_i. Although Peterson's algorithm seems straight forward but it becomes very complex in terms of amount of computations for large number of errors, especially the degree of the error locating polynomial v which is the number of actual errors is unknown, so the algorithms has to start with the maximum number of correctable errors allowed by the design i.e., $v=t$ and go backwards by reducing the order v until the actual number of errors is reached. For details the reader can refer to ,**Jiang, 2010**. The Euclidean algorithm is a general algorithm with many applications. Here the Euclidean algorithm can be applied to find the so-called key equation given by

$$\sigma(x)S(x)-\mu(x)x^{n-k}=-W(x) \tag{20}$$

The algorithm involves repeated polynomial divisions, it starts with x^{n-k} and $S(x)$ as inputs, First x^{n-k} is divided by $S(x)$ then $S(x)$ is divided by the remainder of the first step then the remainder of the first step is divided by the remainder of the second step and so on recursively. The algorithm stops when the remainder of the last step which becomes $W(x)$ has a degree such that

$$\deg(W(x))\le\lfloor(n-k)/2\rfloor+1 \tag{21}$$

Although the Euclidean algorithm is more efficient than the Peterson's algorithm in terms of amount of calculations but the Berlekamp-Massey algorithm is preferred over the Euclidean algorithm because the Euclidean algorithm starts with polynomials of degrees larger than the actual degree of the error locating polynomial $\sigma(x)$ and goes down till the actual degree of $\sigma(x)$ is reached, While BM Algorithm starts with polynomial of order 1 and goes up to the actual degree of $\sigma(x)$ and this makes it more efficient than the Euclidean algorithm. Since in this work, the BM algorithm is adopted in the implantation of the decoder, this algorithm is presented with more details.
The idea of BM algorithm depends on the Newton identity given by Eq. (19) where the $\sigma(x)$ is suppose to satisfy the Newton identity for syndrome values up to S_{2t}. in the beginning $\sigma(x)$ is initialized by

$$\sigma^{(1)}(x)=1+S_1x,\ B^{(1)}(x)=S_1^{-1},\ v^{(1)}=1,\ j=2$$

Where $B^{(j)}(x)$ is the correction polynomial and the superscript in parentheses is the iteration count. Newton identity in Eq. (19) is used to estimate the next syndrome value

$$\tilde{S}_j=\sum_{i=1}^{v_{j-1}}\sigma_i^{j-1}S_{j-i} \tag{22}$$

The discrepancy between the estimated value of syndrome and the actual one is calculated

$$\Delta^{(j)} = S_j - \tilde{S}_j \tag{23}$$

If the value of $\Delta^{(j)}=0$ then $\sigma^{(j)}(x)$ left unchanged, but $B^{(j)}(x)$ is updated as below

$$B^{(j)}(x) = xB^{(j-1)}(x) \tag{24}$$

If $\Delta^{(j)}\neq 0$, $\sigma^{(j)}(x)$ is updated as below

$$\sigma^{(j)}(x) = \sigma^{(j-1)}(x) - \Delta^{(j)} xB^{(j-1)}(x) \tag{25}$$

In addition to the condition $\Delta^{(j)} \neq 0$, if the condition $2v^{(j-1)}<j-1$ is satisfied both $B(x)$ and v are updated as in Eq. (26) and Eq. (27) below otherwise $B^{(j)}(x)$ is updates by Eq. (24) and v is kept the same

$$B^{(j)}(x) = (\Delta^{(j)})^{-1}\sigma^{(j-1)}(x) \tag{26}$$

$$v^{(j)} = j - v^{(j-1)} \tag{27}$$

The process is repeated $2t$ steps. The block diagram of BM algorithm is shown in **Fig. 3.** The reader may find that this block diagram and variable initialization are different than what is found in literature, this is because the block diagram has been modified in a way to be suitable for efficient programming. So, Basically **Fig. 3** shows the flowchart of the actual implemented program for decoding binary BCH codes in this work.

4.3 Error Position Locating and Chien Search

The final step of the decoding is to find the roots of the error locating polynomial and from the roots values, the error position will be found. The algorithm used to find the roots of a GF polynomial is Chien search, ,**Jiang, 2010**. Chien search is simply to evaluate the GF polynomial over all the elements of the GF(2^m) field. Recursive calculation is performed in order to make the search efficient. Suppose that the error locating polynomial $\sigma(x)$ is evaluated for the GF element α^i

$$\sigma(\alpha^i) = 1 + \sigma_1\alpha^i + \sigma_2\alpha^{2i} + \cdots + \sigma_t\alpha^{vi} \tag{28}$$

In the next iteration $\sigma(x)$ is evaluated for the next GF element α^i

$$\sigma(\alpha^{i+1}) = 1 + \sigma_1\alpha^{i+1} + \sigma_2\alpha^{2(i+1)} + \cdots + \sigma_t\alpha^{v(i+1)}$$

$$\sigma(\alpha^{i+1}) = 1 + \sigma_1\alpha^i\alpha^1 + \sigma_2\alpha^{2i}\alpha^2 + \cdots + \sigma_t\alpha^{vi}\alpha^v \tag{29}$$

So, by defining each term of the ith iteration of Eq. (28) by

$$\sigma_j^{(i)} = \sigma_j \alpha^{ji} \tag{30}$$

These terms will be updated in the next iteration by

$$\sigma_j^{(i+1)} = \sigma_j^{(i)} \alpha^{j} \tag{31}$$

With initial values equal the coefficients of $\sigma(x)$ i.e. $\sigma_j^{(0)} = \sigma_j$. Recalling Eq. (17), the error positions are obtained from the multiplicative inverses of the roots of σ(x), so, if the roots were found as α^{i_1}, α^{i_2},…, α^{i_v}, the error positions will be at 2^m-1-i_1, 2^m-1-i_2,…, 2^m-1-i_v. In other words if α^{i_k} is a root, then the error position ep_k will be given by

$$ep_k = 2^m - 1 - i_k \tag{32}$$

5. THE PIC18F45K22 MICROCONTROLLER

The PIC18F45K22 is one of the PIC18(L)F4X/5XK22 family that has many features suitable for many applications. In this section a brief overview is presented about its features that are relevant to application of this paper. One of the most attractive features of the PIC18F45K22 is that its price is around 3$ and the system of binary BCH decoder is entirely implemented by this microcontroller without any external hardware. The PIC18F45K22 will be referred to throughout this paper by (PIC) for simplicity. The PIC has a 16-bit wide instructions and 8-bit wide data. It can operate up to 64MHz clock frequency using internal multiply-by-4 PLL. Each instruction is executed by 4 clock cycles that makes the instruction cycle execution frequency 16MHz which is referred to as Million Instructions Per Second (MIPS). The Program memory is 32kB (16k instructions), the data memory is 1536 bytes SRAM, this RAM contains both special Function Registers (SFR) and General Purpose Registers (GPR). FSR's are used for control and status of the controller and peripheral functions, GPR used for general data storage for user applications. The RAM address range is from 0 to 4k addressable with 12-bit data address bus. This address range is divided to 16 banks of 256B. The FSR's are located at the end of the addressable range F38h-FFFh. The GPR are implemented in the first 6 banks 000h-5FFh, the remaining addressable range is not implemented. When a location in the RAM is to be addressed, the lower 8 bits are specified in the instruction addressing the byte location within a specific bank, the higher 4 pits should be loaded in the Bank Select Register (BSR), a special function register, to specify one bank out of the 16 banks. There is an alternative way to address part of the RAM called the Access RAM. The Access RAM contains the first 96 bytes of the RAM (00h-5Fh) in bank 0 and the last 160 bytes of the RAM (60h-FFh) in bank 15. The combined 256 bytes are treated as one bank (Access Bank) and the BSR is ignored. This addressing mode is specified by an operand 'a' in the instruction, if a=0, access bank is used and the content of BSR is ignored, if a=1 the bank is specified by the BSR contents.

Another mode of RAM addressing is the indirect mode. Indirect addressing allows the user to access a location in data memory without giving a fixed address in the instruction. This is done by using File Select Registers (FSR's) as pointers to the locations which are to be accessed. Indirect addressing is implemented through either of 3 registers FSR0, FSR1, FSR2, each is a pair of 8-bit registers, FSRnL and FSRnH. Each FSR holds the 12-bit address value, so, the upper 4 bits of the register is not used. In a given instruction, the memory location is accessed by indirect mode using

the operands INDF0 through INDF2. These are thought of as virtual registers, the actual register is defined by the FSRn contents. In the implemented program indirect addressing is widely used along with access bank mode. Direct addressing using the BSR is never needed within the program core.

6. SYSTEM IMPLEMENTATION

The implemented system was designed to correct binary BCH codes of length n=127 bits for any value of t, only the results shown at the end are for up to t=13 errors. The programming was made by assembly language using MPLAB IDE V8.70. The start is to find a GF generator polynomial, and since n=127 the generator polynomial should be of degree m=7. The value of m also represent the number of bits required to represent the GF(2^m) elements. There are tables for GF generator polynomials as in ,**Justesen,** and **Høholdt, 2004.** and ,**Lin,** and **Costello1, 1983**. the GF generator polynomial that is commonly used is

$$g(x) = 1 + x^3 + x^7 \tag{33}$$

One important issue that needs to be addressed is that which representation we should use for the GF elements? As has been discussed in **section 2**, there are two representations of the GF elements; one is the polynomial representation and the other is the powers of primitive element, see **Table 1**. Each has its advantages and disadvantages and these are discussed in the following

1- The polynomial representation: Advantages is that all 2^m elements can be represented in binary without special treatment and the addition is simply bitwise XOR. Disadvantage is that the multiplication is not straightforward; it can only be implemented if one of the multiplicands is in the power form and the other operand is in polynomial as described in **section 2**. Since the power of the elements has a maximum of 2^{m-2}, this means that there are cases where 2^m-2 (126 in our case) sub-operations may be needed for a single multiplication. This is not practical and therefore the polynomial representation is not used in the system.

2- The power representation: Advantages is that the multiplication is made by addition of powers mod 2^{m-1}, which can be implemented by few steps. Disadvantages are that the addition is not possible and requires lookup table and since there are two operands the lookup table will be of 2^mX2^m dimension and this is not practical. The other disadvantage is that the zero has no integer power representation, therefore special treatment is required.

3- The modified representation: It is decided to adopt a representation close to the power representation where the powers are represented by adding 1 to the actual power and the GF element 0 is represented by 0. In this way all elements are represented by 0 through 2^m-1. The addition will be implemented by converting the power representation of the operand to polynomials and converting the result to power (if needed). The conversion from power to polynomial and vice versa is implemented by lookup tables, so, there will be 2 size 2^m=128 lookup tables.

Table 2. shows the memory organization of the program data, the first four entries of the table are with the range of 0h-60h to make it possible to access them by access bank mode (without specifying the BSR content) this is useful for reducing program instructions especially these contents are accessed frequently within loops in the program. The lookup tables are located each in a separate bank for ease of access, where each table starts at address 0 within the respective bank. The received codeword although contains 127 bits but is stored in 127 bytes where each bit is stored in a separate memory location. This might seem like a waist of memory but it is actually not. If the

received codeword is stored compactly in 16 bytes, it would be very difficult and time consuming (in terms of number of instructions) to access an individual bit. While storing each bit in a separate memory location (byte) makes it much easier to access the individual bits, especially accessing the individual bits is needed in the syndrome calculations and Chien search, which are time consuming parts of the program.

6.1 Implementation of Syndrome Calculations

The syndrome calculation has been discussed in **Section 4.1** and it was mentioned that direct calculation involves evaluation of polynomials, Eq. (12), of higher degree than the remainder polynomials given by Eq. (15). Because the method of Eq. (15) requires *t* polynomial divisions in advance it cannot be considered better than the direct calculation method unless parallelism is adopted in the implementation which is possible by hardware implementation, where the *t* polynomial divisions can be implemented by *t* separate LFSR's. Since the implantation of the system in this work is a software implantation, the direct calculation is adopted with the following considerations:

1- All calculations are made by using the polynomial representation so there will be no need for conversion from one form to the other.

2- The values of α^{ij} are calculated in advance in polynomial form using MATLAB and stored in a lookup table in the program memory because of its large size.

3- Only the syndromes of odd indices are calculated using Eq. (12) and the syndromes of even indices are calculated using Eq. (16).

Fig.4 shows a flowchart used to implement the syndrome calculation. The values α^{ij} are the elements of the parity check matrix given by Eq. (10) which are stored as a table in the end of the program memory in polynomial form. These values are addressed by the table pointer register TBLPTR which is a 3-byte register. The content of the table is read by the instruction TBLRD*+ that reads the content of the table into a memory register TABLAT which is an SFR and at the same time increments the contents of TBLPTR making it ready for the next read instruction. Since the received codeword *C* is binary, the multiplication $c_i\alpha^{ij}$ of Eq. (9) is simple where the value of c_i is checked for zero value, if so, nothing is done; otherwise the value of α^{ij} is used to calculate S_j. When the inner loop is completed the value of S_j is obtained in polynomial form and since the calculations of the next stage of the BM algorithm requires that the values of syndromes to be in the power form the value of S_j is converted immediately to power form. This is made easily by lookup table that is stored in the RAM as in **Table 2**. The lookup table used to convert from polynomial form to power form is called GFINV. The polynomial form of S_j is stored in the FSR2L register with FSR2H loaded with a fixed value of 2 which is the bank address of GFINV table. The contents of the FSR2 is retrieved and stored in place of the old S_j, and the value of S_j becomes in power form. The counter of the outer loop is incremented by 2 to calculate the odd indexed syndromes. The even indexed syndromes are later calculated using Eq. (16) which is much faster than the direct calculations.

6.2 Implementation of BM Algorithm

Before going into the details of implementing the BM algorithm, the operation of GF elements multiplication is considered first because there are few details that need to be considered. It has been mentioned before that the multiplication in power form is easier than in polynomial form because it is basically addition of powers mod 2^m-1. An algorithm presented by ,**Deschamps *et al.*, 2009.** for

mod n addition that is suitable for hardware implementation. Since the addition used in this work is mod 2^m-1 and mod n is more general, the algorithm is slightly modified for mod 2^m-1 addition to make it easier than the mod n addition as shown in **Fig. 5**. In this algorithm the two integers a and b are added (which are both represented by m bits) and the result, c, is incremented by 1, then the result is tested for overflow, if $c<M=2^m$ (no overflow) then the addition without incrimination is the correct result so c is decremented, otherwise when there is an overflow and the mth bit is set then the mth bit of c is simply cleared and the algorithm terminates. It can be seen that the clearing of the mth bit is common for both sides of the condition this does not affect the other branch of the condition because the mth bit is already 0. The test of the mth bit is simply made using the instruction (BTFSS f,b,a) or (BTFSC f,b,a), where, the bit whose address (b (0-7)) within the file register (f) is tested if set (or clear) the next instruction is skipped. The operand a=0,1 is for the memory access mode. The clearing of a specific bit (b) of a file register (f) is cleared by the instruction BCF f,b,a. The mod addition algorithm is not implemented in the way described above because the powers of the GF elements are stored as i+1 rather than i. This requires the algorithm to be further modified as in **Fig. 6**. This algorithm is used throughout the main program whenever is needed and it is first used for evaluation of the even indexed syndromes using Eq. (16).

Now some details about BM algorithm implementation is presented by providing more insight for the main blocks of the algorithms block diagram shown in **Fig. 3**. The first quantity to calculate is the estimate of the jth syndrome as in Eq. (22), see **Fig. 7**. Here a temporary variable (T) is assigned the value of $\sigma_i S_{j-1}$ obtained as a multiplication of two GF elements which are represented by the alternative power form, so, the algorithm of mod addition shown in **Fig. 5** is used. Before carrying out the multiplication as mod addition of powers, the values of σ_i and S_{j-1} are checked if either one equals to 0. If so, the whole multiplication and addition is skipped and a new iteration is started. Since the value of T should be added to $\tilde{S}_j$, it should be converted to polynomial form in a way similar to what has been described earlier using lookup table. Here the lookup table used is GF lookup table where the value of T is used as an address stored in FSR1 and the value pointed by that address is retrieved as the value of T in polynomial form. Now the addition is performed as a simple XOR of the two quantities. Next the discrepancy $\Delta^{(j)}$ is calculated as in Eq. (23) which also requires the conversion of S_j to polynomial form.

The implementation of the block related to Eq. (25) is separated into two parts; the first is to calculate the discrepancy part (denoted as $D(x)$) in a temporary location

$$D(x) = \Delta^{(j)} x B^{(j-1)}(x) \tag{34}$$

The Flowchart of implementation of Eq. (34) is shown in **Fig. 8**, here the coefficient B_i of the term x^i is multiplied by $\Delta^{(j)}$ and assigned for $D(x)$ as the coefficient D_{i+1} of the term x^{i+1}. This is obvious because of the term x in the expression of Eq. (34). Of course the coefficient B_i should be checked for zero value as explained earlier. Later the two terms of $D(x)$ and $\sigma^{(j-1)}(x)$ are added to update $\sigma^{(j)}(x)$. No special treatment is required except for changing the coefficient of $D(x)$ and $\sigma^{(j-1)}(x)$ to polynomial form for addition and back to power form using GF and GFINV lookup tables. One last point is that the block of Eq. (25) appears twice in **Fig. 3**. A natural way to do it is to position it before the ($2v^{(j-1)}$-j<0) condition test and on the (No) branch of the ($\Delta^{(j)}$=0) condition test. This is not suitable for in-place calculation of $\sigma^{(j)}(x)$, since updating $\sigma^{(j-1)}(x)$ to $\sigma^{(j)}(x)$ would cause loosing the value of $\sigma^{(j-1)}(x)$ that is needed for the $B^{(j)}(x)$ calculation (as in Eq. (26)) which is implemented in a

later stage. The block of Eq. (26) is simply implemented by multiplying the multiplicative inverse of $\Delta^{(j)}$ by $\sigma^{(j-1)}(x)$. The multiplicative inverse $(\Delta^{(j)})^{-1}$ is obtained easily when $\Delta^{(j)}$ is in power form $(\Delta^{(j)}=\alpha^k)$ as $(\Delta^{(j)})^{-1}=(a^k)^{-1}=a^{q-1-k}$ where $q=2^m-1$. The quantity q-1-k is simply the 1's complement of k. Since the $\Delta^{(j)}$ is represented in the alternative power form, where the stored value is the power plus 1, a decrement is needed before the binary inversion. Implementation of Eq. (24) is only a shifting of coefficients and no calculations are involved. The remaining blocks of the BM algorithm flowchart are straight forward and there is no need to elaborate.

6.3 Implementation of Chien Search

The efficient implementation of Chien search described earlier can be implemented by updating the coefficients of the error locating polynomial σ_j recursively for each iteration as in Eq. (31). Where, i^{th} iteration represents the evaluation of $\sigma(x)$ for α^i. This is faster than the direct evaluation using Eq. (28) and it suitable for in-place calculations because the initial coefficients are no longer needed. The flowchart of Chien Search is shown in **Fig. 9**. The product part is implemented using the alternate power for of the GF elements and since this product is on one hand needed for the other iterations, and on the other hand is required to be converted polynomial form for summation part, a temporary variable T is used to convert to the polynomial form. For practical considerations the evaluation of $\sigma(x)$ for the element 1 (i=0) is made separately outside the loop where the coefficients σ_j are simply summed and the result is check if equal to zero. When all of the roots of $\sigma(x)$ are found before reaching the final value of the counter i, the process of the Chien search can be terminated to save the extra unnecessary computations time as suggested by ,**Wu, 2004**. For each root found, the error position is found as in Eq. (32) which is simply the 1's complement of the roots power representation.

7. PERFORMANCE EVALUATION

In general the implementation of decoding algorithms can be made either by hardware or software. Hardware implementation is advantageous in terms of speed so higher bit rates can be accomplished, but on the other hand its cost is high because of the amount of hardware components used. The software implementation is better in terms of cost because it needs only a processor and possibly some input-output peripherals. Fortunately the PIC microcontrollers became a very cost effective engineering solution because of their high performance and low cost with on chip input-output peripherals. The implantation of the decoder being entirely software running by a PIC microcontroller makes the decoder cost only the market price of the used microcontroller (PIC18F45K22) which is around 3$. The disadvantage is that the speed performance is lower than the direct hardware implementation because of the sequential execution of instructions and the limitation of clock frequency. Now the performance analysis of the implemented system will be given in terms of number of instructions cycles for the three main blocks of the system: syndrome calculations, BM algorithm and Chien Search, for different values of the decoding capability t. The code length is fixed as n=127, and the values of the number of correctable errors t is varied from 4 to 13. The choice of the code parameters: n (no. of code bits), k (no. of message bits) and t (no. of correctable errors) is not arbitrary and these values can be found in tables as in ,**Lin,** and **Costello**, **1983**. **Table 3.** shows the number of instructions for each component of the decoder. The first 8 rows of the table show the number of instructions for different values of t with the number of actual errors is maximum i.e. v=t. In the next 7 rows t is fixed to 13 and the number of actual errors is

varied from 12 to 0. It can be seen that the syndrome calculations depends only on t and not on the actual number of errors v, this is expected because syndrome calculations is made of two nested loops one of length n and one of length t which makes the number of instructions proportional to nt. The BM algorithm requires a number of instructions that depends on the number of actual errors occurred in the received codeword in spite of the fact that it has a fixed number of iterations ($2t$) but the different paths of the algorithm (see **Fig. 3**) have different amount of calculations. In general it has a number of calculations proportional to t^2 ,**Schipani *et al.*, 2011**. The number of instructions of Chien search depends not only on the number of actual errors v (which represents the degree of the error locating polynomial) but also on the errors locations. Since the loop of Chien search is terminated when all the error locations are found (see **Fig. 9**). The number of instructions of Chien search is given as minimum and maximum, the minimum number of the loop iterations is v, this is a special case when all errors are found in the first v iterations. The maximum number of iterations is when the Chien search loop has to go throw all the n-1 GF elements i.e. when the last error position is found by the last iteration. The next column of **Table 3.** shows the total number of instruction of the three decoder components with the Chien search number of instructions taken as maximum. Finally the achievable bit rate R_b in kilo bits per second (kbps) is given by the last column it is calculated as

$$R_b = nF / N_t \tag{35}$$

Where F is the instruction cycle execution frequency which is in our case 16 MHz and N_t is the total instructions of the decoder for decoding n bits. It is important to note that the system bit rate R_b is calculated based on the worst case when the number of actual errors is maximum i.e. $v=t$ and the Chien search iterations is maximum. Therefore, the values of R_b given in **Table 3**. where $v \neq t$ is not realistic but it is shown for the sake of comparison especially the last entry where a correct codeword is received v=0. In this case (which is usually the most probable caser) the execution time is very small (the rate is high) because only the first syndrome value is needed to decide if the codeword is correct which is when S_1=0, there will be no need to calculate the other syndrome values and this is more easily seen from Peterson's algorithm, ,**Jiang, 2010**.

As a final discussion, the increase of the bit rate is considered. To increase the bit rate, one possibility is to increase the system frequency and this can be done by using a higher level PIC microcontroller like PIC24 family where frequency can be increased up to 40 Mhz. This option is simple but still the outcome is limited. Another way is to use a sort of distributed system like the one described in **Fig. 10** where N decoders are used in parallel and fed by a buffer that is filled from the incoming data stream which can be of bit rate equals MR_b where M>1 is a factor, and R_b is the operating bit rate of the individual decoder as given in **Table 3**.The input buffer feeds the individual decoders asynchronously, that is whenever a decoder is free, an n-bit block is fed to it. The output buffer is to rearrange the decoded messages according to their original sequence. It is assumed that the occurrence of the cases where v is high and error positions requiring high number of iterations have a low probability. This arrangement should give the sufficient time for and individual decoder to decode up to the maximum time required by the worst case but also less overall time for the while N decoders to decode N codewords that are not necessarily require the maximum time of decoding. Of course, there can be situations where the cases of high decoding time can occur more than once in the buffer and the time imposed by the incoming bit rate (MR_b) is insufficient. This will create the

situation when the input buffer encounter an all busy decoders when trying to allocate a decoder to specific codeword, in this case a decoding failure is declared and a retransmission request is issued. This will make the decoder a suboptimal in the sense that there are situations where the number of errors $v \leq t$ but the time assigned to the decoder is insufficient. The performance evaluation of this system can be investigated as a future work to find the best choice of the parameters *M* and *N*.

CONCLUSION

A binary BCH decoder is implemented in PIC microcontroller platform using assembly language with n=127 bits and adjustable error correction capability t, the number of code bits n can be increased to 255 bits with slight modifications to the program. Results shows that the time consumption of the decoding algorithm depend on the actual number of errors and that suggests using the designed decoder in a distributed system fashion in order to enhance the performance.

REFERENCES

- Cho, J. and Sung, W., 2009, *Efficient Software-Based Encoding and Decoding of BCH Codes*, IEEE Transactions On Computers, Vol. 58, No. 7 pp 878-889.
- Deschamps, J. P., Imaña, J. J., Sutter, G. D., 2009, *Hardware Implementation of Finite-Field Arithmetic*, McGrow Hill.
- Jiang, Y., 2010, *A Practical Guide to Error-Control Coding Using MATLAB*, Artech House.
- Justesen, J., and Høholdt, T., 2004, *A Course In Error-Correcting Codes*, European Mathematical Society.
- Lin, S. and Costello, D. J., Jr., 1983, *Error Control Coding: Fundamentals and Applications*, Prentice Hall, Englewood Cliffs, New Jersey.
- Lin, Y., Chang, H., and Lee, C., 2010, *An Improved Soft BCH Decoder with One Extra Error Compensation*, Proceedings of 2010 IEEE International Symposium on Circuits and Systems, Paris, pp 3941-3944.
- Lee, Y., Yoo, H. , Yoo, I. and Park, I., 2014, *High-Throughput and Low-Complexity BCH Decoding Architecture for Solid-State Drives*, IEEE Transactions on Very Large Scale Integration (VLSI) Systems, Vol. 22 , No. 5. 1183-1187.
- Moreira, J. C, and Farrell, P. G., 2006, *Essentials of Error-Control Coding*, John Wiley.
- Namba, K., Pontarelli, S.,Ottavi, M. and Lombardi, F, 2014, *A Single-Bit and Double-Adjacent Error Correcting Parallel Decoder for Multiple-Bit Error Correcting BCH Codes*, IEEE Transactions on Device and Materials Reliability, Vol. 14 , No. 2, pp 664–671.
- Schipani, D., Elia, M., Rosenthal, J., 2011 *On the Decoding Complexity of Cyclic Codes Up to the BCH Bound* IEEE International Symposium on Information Theory Proceedings, St. Petersburg, pp 835-839.
- Taki El-Din, R. F., El-Hassani, R. M. and El-Ramly, S. H., 2013, *Optimizing Chien Search Usage in the BCH Decoder for High Error Rate Transmission*, IEEE Communications Letters, Vol. 17, No. 4, pp 741-744.
- Wu, Y., New, 2008, *List Decoding Algorithms for Reed-Solomon and BCH Codes*, IEEE Transactions on Information Theory, Vol. 54, No. 8, pp 3611-3630.
- Wu, Y., *Low Power Decoding of BCH Codes*, 2004, Proceedings of 2010 IEEE International Symposium on Circuits and Systems, Canada pp 369-372.
- www.microchip.com, 2012, PIC18(*L)F2X/4XK22 Data Sheet*, Microchip.

Table 1. GF elements and their representation.

i	GF elements power form		GF elements polynomial form		GF elements alternative form	
	α^i	i in Binary Representation	$r(x)$	Binary Representation	α^i	i+1 Binary Representation
-	$0=\alpha^{-\infty}$	-	0	000	$0=\alpha^{-\infty}$	000
0	$1=\alpha^0$	000	1	001	$1=\alpha^0$	001
1	α^1	001	x	010	α^1	010
2	α^2	010	x^2	100	α^2	011
3	α^3	011	$x+1$	011	α^3	100
4	α^4	100	x^2+x	110	α^4	101
5	α^5	101	x^2+x+1	111	α^5	110
6	α^6	110	x^2+1	101	α^6	111

Table 2. Program Memory Organization.

Bank	Address	Contents
0	0h-1Fh	General variables
0	20h-3Fh	Syndrome values
0	40h-4Fh	Error locating polynomial coefficients $\sigma(x)$
0	50h-5Fh	Correction polynomial coefficients $B(x)$
1	00-7Fh	GF elements lookup table
2	0h-7Fh	GFINV elements lookup table
3	0h-7Eh	Received/Corrected code in bits

Table 3. Performance analysis of the implemented binary BCH decoder.

n=127, Instruction Cycle Frequency=16 Mhz								
t	k	v	Syndrome Calculations	BM Algorithm	Chien Search		Total Instructions	Bit Rate (kbps)
					Min.	Max.		
4	99	4	4702	1455	453	11799	17956	113.17
5	92	5	5874	2087	658	14210	22171	91.66
6	85	6	7046	2833	901	16621	26500	76.68
7	78	7	8218	3693	1182	19032	30943	65.67
9	71	9	10562	5711	1858	23854	40127	50.64
10	64	10	11734	6957	2253	26265	44956	45.20
11	57	11	12906	8273	2686	28676	49855	40.76
13	50	13	15250	11184	3666	33498	59934	33.90
13	50	12	15250	10547	3157	31087	56884	35.72
13	50	10	15250	9195	2253	26265	50710	40.07
13	50	8	15250	7907	1501	21443	44600	45.56
13	50	6	15250	6683	901	16621	38554	52.71
13	50	4	15250	5523	453	11799	32572	62.38
13	50	2	15250	4427	157	6977	26654	76.24
13	50	0	15250	-	-	-	1178	1724.96

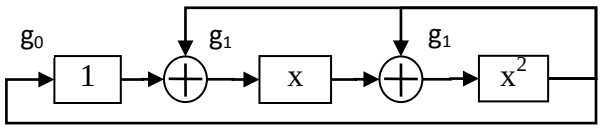

Figure 1. Implementation of LFSR for generating GF elements.

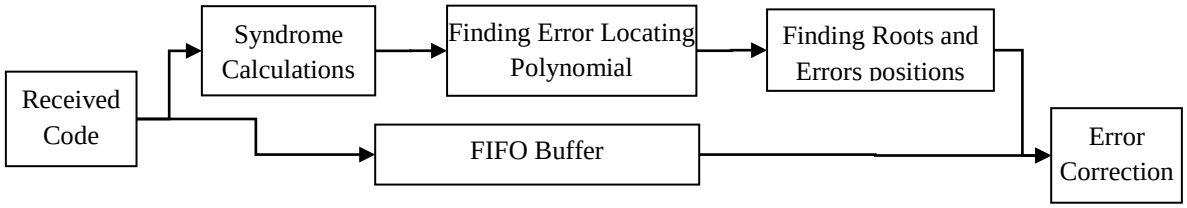

Figure 2. Block diagram for Binary BCH Decoding.

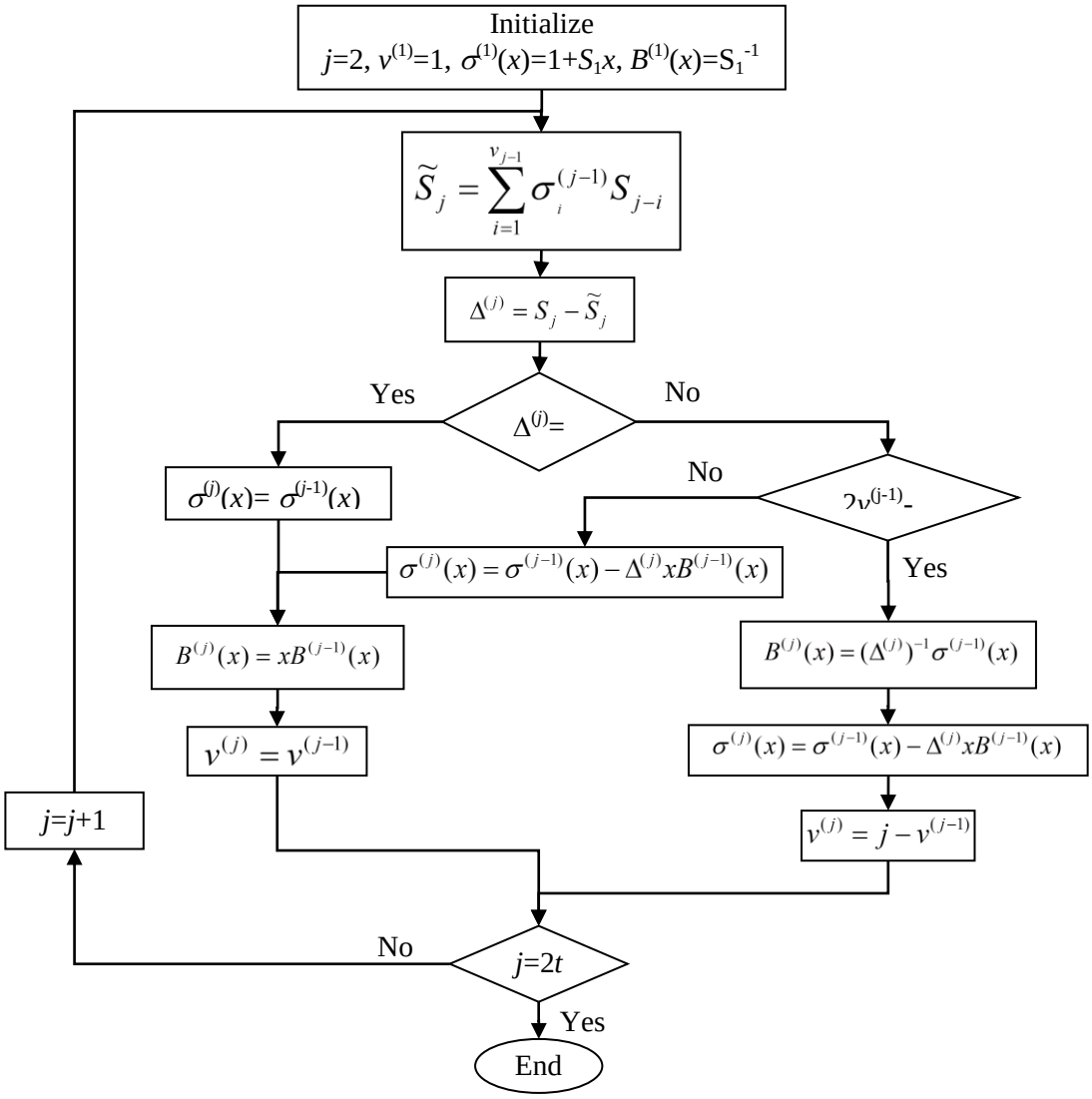

Figure 3. Block Diagram of BM algorithm.

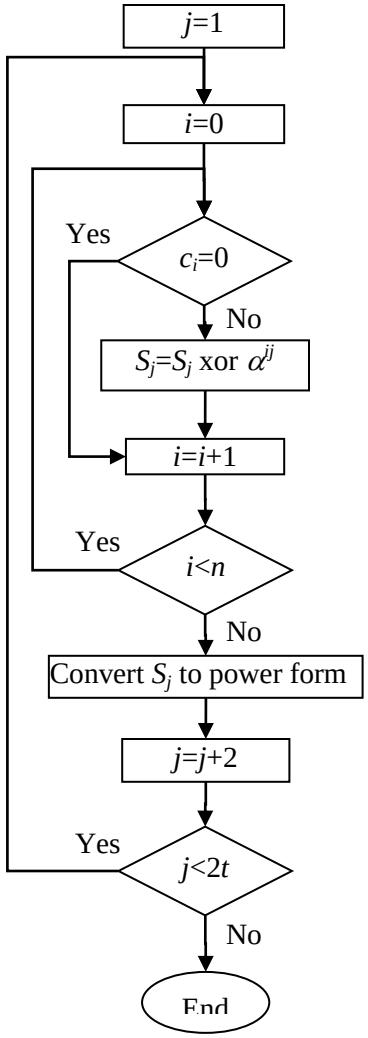

Figure 4. Flowchart for odd index syndrome calculations.

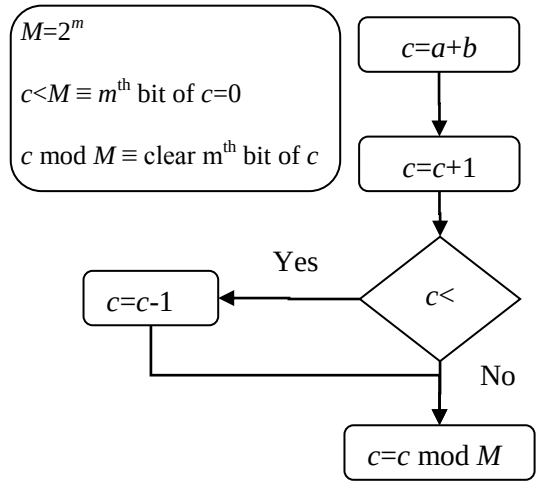

Figure 5. An algorithm for mod 2^m-1 addition.

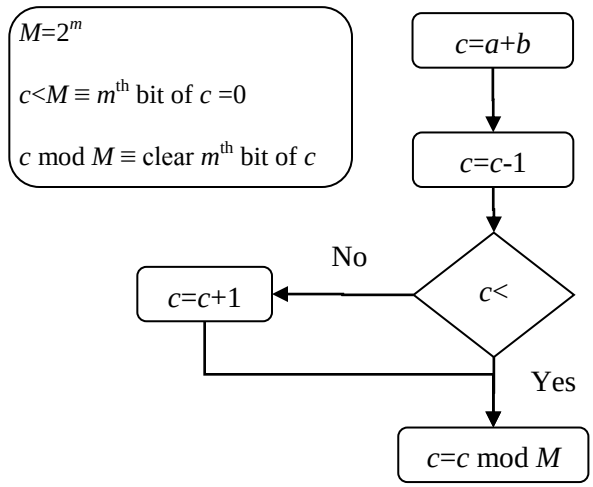

Figure 6. An algorithm for mod 2^m-1 addition suitable for the used GF elements alternative form.

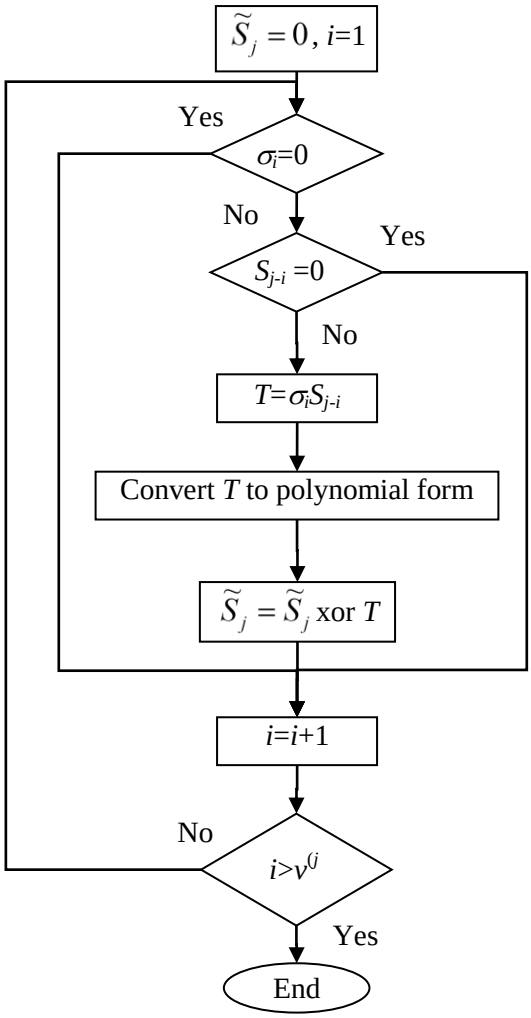

Figure 7. Flowchart for implementing Eq. (22) of BM algorithm.

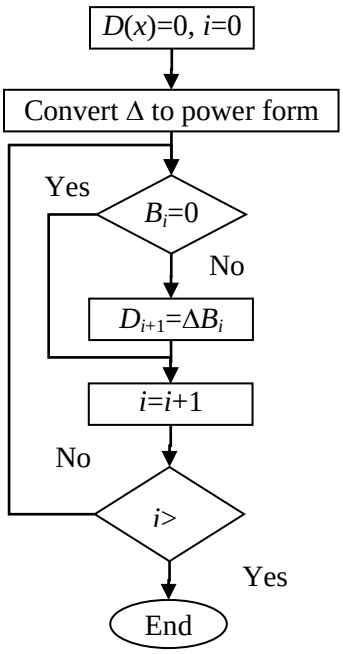

Figure 8. Flowchart for implementing Eq. (34) of BM algorithm.

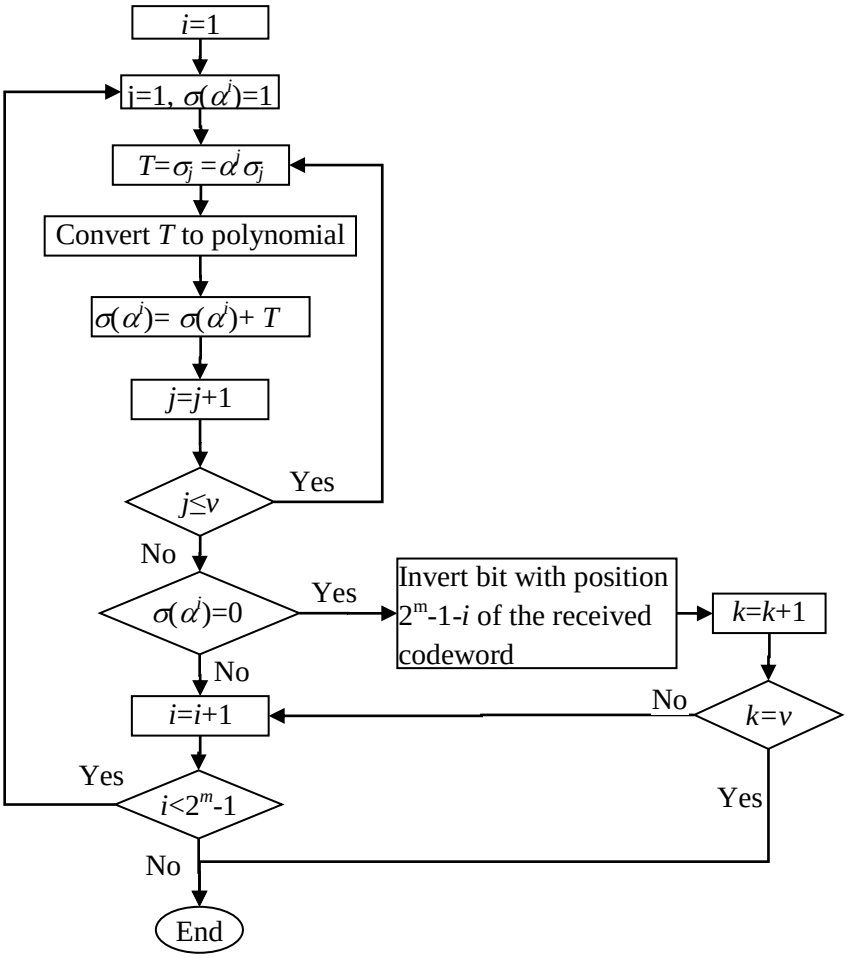

Figure 9. Flowchart for implementing Chien search**.**

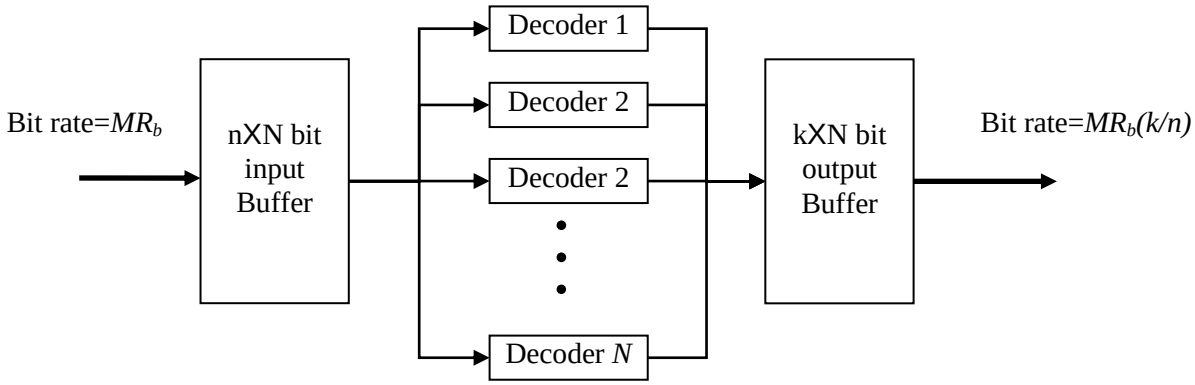

Figure 10. A proposed Distributive Decoder**.**

Digital Image Authentication Algorithm Based on Fragile Invisible Watermark and MD-5 Function in the DWT Domain

Asst. Lect. Nehad Hameed Hussein
Department of Software Engineering
Baghdad College of Economic Sciences
Email: it_engineer85@yahoo.com

ABSTRACT

Using watermarking techniques and digital signatures can better solve the problems of digital images transmitted on the Internet like forgery, tampering, altering, etc. In this paper we proposed invisible fragile watermark and MD-5 based algorithm for digital image authenticating and tampers detecting in the Discrete Wavelet Transform DWT domain. The digital image is decomposed using 2-level DWT and the middle and high frequency sub-bands are used for watermark and digital signature embedding. The authentication data are embedded in number of the coefficients of these sub-bands according to the adaptive threshold based on the watermark length and the coefficients of each DWT level. These sub-bands are used because they are less sensitive to the Human Visual System (HVS) and preserve high image fidelity. MD-5 and RSA algorithms are used for generating the digital signature from the watermark data that is also embedded in the medical image. We apply the algorithm on number of medical images. The Electronic Patient Record (EPR) is used as watermark data. Experiments demonstrate the effectiveness of our algorithm in terms of robustness, invisibility, and fragility. Watermark and digital signature can be extracted without the need to the original image.

Keywords: fragile watermark; image authentication; dwt; adaptive threshold; hvs; md-5; rsa.

خوارزمية أثبات اصالة الصور الرقمية بالاعتماد على العلامة المائية الهشة المخفية و دالة ملخص الرسالة الخامسة ضمن نطاق تحويل المويجات المنفصلة

م.م. نهاد حميد حسين
قسم هندسة البرامجيات
كلية بغداد للعلوم الاقتصادية

الخلاصة

في هذا البحث تم عمل خوارزمية للتحقق من اصالة الصور الرقمية من خلال الاعتماد على تقنيات العلامة المائية والتوقيع الرقمي. اولا يتم تحويل الصورة الى المجال الترددي باستخدام تقنية تحويل المويجات المنفصلة DWT وثم ادخال العلامة المائية في الصورة بعد تحويلها الى النظام الثنائي. قمنا باستخدام الترددات العالية والمتوسطة في الصورة لغرض اخفاء العلامة المائية لضمان عدم تأثر الصورة و عدم رؤية العلامة المائية المضافة بالعين البشرية. يتم اخفاء البيانات في عدد من الترددات العالية في الصورة التي يتم اختيارها من خلال معادلة متغيرة مع كل مستوى من التحويل المويجي. اضافة الى وجود العلامة المائية يتم اخفاء خلاصة العلامة المائية والتي يتم احتسابها باستخدام خوارزميات (MD5, RSA). تم تطبيق الطريقة على عدد من الصور الطبية مع

استخدام بيانات سجل المريض الالكتروني كعلامة مائية. التجارب العملية اثبتت قوة الخوارزمية وامكانية كشفها لاي هجوم او تعديل على الصورة.

الكلمات الرئيسية: العلامة المائية الهشة, اصالة الصور الرقمية, تحويل المويجات المنفصلة, نظام الرؤية البشري, خلاصة الرسالة.

1. INTRODUCTION:

The evolution of information systems, supported by advances in information and communication technologies, enables digital information likes digital images to be shared between organizations and personals more easily. At the same time, more attention should be paid to protect and authenticate these information. Image watermarking and digital signatures technologies are an effective solutions to meet such requirements. Medical images are good example of images that required to be authenticated before sharing it between the consultants or healthcare centers.

Digital watermarking is a technology that embeds watermark data (copyright information) such as identification numbers, personal information, or serial numbers, into digital data **Cox, et al. 2000**. In digital images watermarking should take care the image fidelity degradation so that the embedded watermark should be small as possible and not be visible. A high fidelity means that the watermarked image is very similar to its original image or more precisely, they are indistinguishable.

Image authentication is a technique for inserting information (digital signature) into an image for authentication and integrity. In the receiver side, the inserted information will be extracted and compared with the original information to decide image authenticity and integrity. MD-5 and SHA-1 are the well-known algorithms used for digital signature creation.

In this paper, a new method for digital image authentication based on the watermark and digital signature is proposed. The proposed algorithm aims to achieve image authentication through fragile invisible watermark and MD-5/RSA algorithms. Medical images are selected as test images and the watermark will be taken from Electronic Patient Record (EPR) including: Patient record number, Patient name, Age, Gender, Medical state, Dr. Name, Hospital name, and Region of residence.

In addition to the watermark, the digital signature will be computed and embedded in the image. MD5 and RSA (Rivest-Shamir-Adleman) algorithms are used to generate the digital signature from the watermark. MD5 used for computing 128-bit digest and RSA used for encrypting the computed digest.

After that, the image is decomposed by 2-level DWT and the watermark and digital signature are embedded in the selected coefficients in the middle and high frequency sub-bands according to the adaptive threshold that based on the watermark length and the middle and high frequencies coefficients of each DWT level. These sub-bands are used for authentication data embedding in order to ensure the watermark invisibility and high image fidelity.

The remaining of the paper is organized as follows: Literature survey is discussed in section 2, methods used in this paper are studied in section 3, and the algorithm details including authentication data generation, embedding, and extraction are discussed in section 4. The experimental results and performance analysis are evaluated in section 5. Finally, conclusions are detailed in section 6.

2. LITERATURE SURVEY

In the literatures mainly two types of watermarking techniques are discussed: (1) spatial domain based and (2) frequency domain based approaches. In spatial domain approaches, the watermark data are embedded in the least significant bit (LSB) of the cover image pixels. However, the LSB insertion method is easy to be attacked.

In frequency domain approaches, a mathematical transform is applied to the image to embed watermark into the transform coefficients, then apply inverse transform to get the embedded image. The most frequent used methods are Discrete Wavelet Transform (DWT)**,** Discrete Cosine Transform (DCT), and Discrete Fourier Transform (DFT). As the frequency domain methods always have good robustness to common image processing such as compression, noise, filtering, rotation, cutting, etc., they now come into more widespread used ,**Wang et al., 2009.** and **,C. Li and H Song, 2008**.

,Sinha and ,Singh, 2003. proposed a technique to encrypt an image for secure transmission using digital signature of the image. They embedded the authentication data in the spatial domain. ,**Chang, C., Tseng, H. 2004**. proposed spatial domain method by exploiting the correlation between adjoining pixels for determining the bit number to be embedded at certain specific pixel. If the pixel is located in edge areas, we can embed more data than the smooth areas. ,**Cong Jin et.al., 2006.** described watermarking scheme using wavelet transform and HVS. In this method watermark is embedded using adaptive embedding based on HVS. It considers sensitivity of human eye towards noise, luminous and textures. Watermark is inserted using adaptive gain factor which is calculated from noise sensitivity, luminosity, edge distance and texture area.

,Po. Chen and ,Y. Tseng, 2007. proposed a new frequency domain method for image watermarking. In this system, first transform the cover image into sub bands. The secret image is embedded into LL sub band of cover image. ,**Yang, Hengfu and ,Sun, Xingming, 2007.** proposed an image-adaptive semi-fragile watermarking technique for image authentication and tamper detection. The algorithm embeds the watermark in coefficients of the vertical and the horizontal detail sub-bands of image sub-block. It is utilizing HVS so it is highly adaptive to the original image characteristics.

,Chuanmu L. and Haiming S., 2008. proposed invisible watermarking scheme for image authentication in DWT. The binary watermark is generated by a chaotic map using adaptive threshold. Using a secret key, select some perceptually significant coefficients from detail sub-bands of 3-level DWT of the host image for watermark embedding.

In **2012. Baisa, L. et.al.,** explored method of watermark in medical images using Region of Interest ROI method. In this method watermark is embedded in ROI only. They use Arnold transform for watermark scrambling and wavelet transform for host image decomposition. ,**K. Raval and S. Zafar, 2013.** proposed adaptive watermark embedding procedure using DWT and DCT, first watermarked image is decomposed through DWT transform and choosing the high frequency bands for watermark embedding according to adaptive factor function. DCT transform is applied for watermark message for reformatting and reshaping before embedding it. ,**N. Grover and A. Mohapatra, 2013.** proposed technique for authenticating the shared images on the social networks through embedding the secret data related to person's login detail and current timestamp in the original image using adaptive steganography. The watermark bits are embedded in the DWT low frequency bands.

,M. Dhoka, J. Kadam, 2014. proposed a method of invisible watermark to medical image using Bi-orthogonal wavelet filter and transformed domain watermark embedding. In their method, they transformed both original image and watermark using DWT and Bi-orthogonal wavelet filter coefficients. Comparison is made on basis of PSNR and normalized correlation (NC).

Our contribution is based on new methods in the watermarking embedding techniques, where the image is watermarked in the frequency domain providing watermark robust, invisibility, and more security against many attacks types. However while the recent papers are influenced on the image authentication through watermarking embedding only, we will focus on embedding the digital signature of watermark also in the image in the invisible manner without affecting the image fidelity. This gives two ways for ensuring the image authentication through watermark and digital signature.

3. METHODS

3.1 Discrete Wavelet Transform

DWT is information processing method was presented in the late 1980's. It's used for multi-resolution analysis, it is particularly useful for the analysis of non-stationary signals, including image processing ,**Chang Gao, 2009**.

The basic idea is to decompose the image into sub-bands at different frequency and different space. In DWT, the image is first decomposed in four sub-bands, low frequency band (LL1), horizontal detail band (HL1), vertical detail band (LH1), and diagonal detail band (HH1). The LL1 band is further can be decomposed into four sub-bands obtaining LL2, HL2, LH2 and HH2. LLi sub-band can be further decomposed to generate other four sub-bands and so on **,Al-Haj and ,T. Manasrah, 2007.**

The LL band can be treated as an approximation of the image. Any modification done to this band is visually most perceptible. The other three bands are high frequency bands that characterize the marginal information of the corresponding direction and have little energy. These bands contain the detail information of an image like the edge information and texture. **Fig. 1** depicts a two level decomposition of MRI medical image using DWT.

Since human eyes are much more sensitive to the low-frequency part (LL sub-band), in the suggested algorithm, we will use regions that known to be less sensitive to human visual system (HVS) that are high frequency sub-bands for watermark and signature embedding. This makes the watermark is invisible and maintains better image fidelity and quality.

3.2 Human Visual System

Visual psychology researchers have found that masking characteristics of the human visual system when embedding authentication information improves digital watermarking robustness and imperceptibility **,Dumitru et al., 2008.**

The advantage of using the DWT is that it is known to more accurately model the aspects of the HVS as compared to the FFT or DCT **,Cong Jin, et al., 2006.** Some of the significant features the DWT provides are excellent spatial localization, frequency spread, and multi-resolution characteristics, which are similar to the theoretical models of the HVS **,Dumitru et al., 2008.**

We will benefit from the HVS characteristic that is known to be less sensitive to the middle and high resolution sub-bands (LH, HL, and HH) for generating invisible watermark through embedding the watermark and digital signature in the middle and high frequencies sub-bands only. This causes to increase in the robustness with a little or no impact on image quality and fidelity **,Dumitru et al., 2008.**

3.3 Performance Evaluation Metrics

3.3.1 peak signal-to-noise ratio (PSNR)

PSNR is the ratio between the maximum possible value (pixel) of image and the power of distorting noise that affects the quality of its representation. The proposal is that the higher the PSNR, the better degraded image has been reconstructed to match the original image and the better the reconstructive algorithm **,Rajendra et al., 2012.** PSNR is defined via the mean squared error (MSE). Given M x N image I and its reconstructed one K, MSE is:

$$MSE = \frac{1}{mn}\sum_{i=0}^{m-1}\sum_{j=0}^{n-1}[I(i,j) - K(i,j)]^2 \quad (1)$$

$$PSNR = 10.\log_{10}\left(\frac{MAX^2}{MSE}\right) \quad (2)$$

Here, *MAX* is the maximum possible pixel value of the image.

3.3.2 structural similarity (SSIM)

SSIM index measures the similarity between two images in a manner that is more consistent with human perception than MSE and PSNR. It attempts to measure the change in luminance, contrast, and structure in an image. SSIM result closer to 1 means the reconstructed image very similar to the original image **,Wang et al., 2004.** The SSIM metric is calculated between the original image x and reconstructed image y images with common size N x M is:

$$\mathrm{SSIM}(x,y) = \frac{(2\mu_x\mu_y + c_1)(2\sigma_{xy} + c_2)}{(\mu_x^2 + \mu_y^2 + c_1)(\sigma_x^2 + \sigma_y^2 + c_2)} \quad (3)$$

Where, μ_x is the average of x, μ_y is the average of y, σ^2_x is the variance of x, σ^2_y is the variance of y, and finally σ_{xy} is the covariance of x and y;

3.3.3 Normalized Hamming Distance (NHD)

NHD is used for measuring the similarity between the embedded and extracted watermarks **,Z. M. Lu and ,S. H. Sun, 2009.** The correct watermark extraction percentage (CWEP) and correct signature extraction percentage (CSEP) are defined as normalized hamming distance between embedded and extracted watermarks and digital signature signatures, respectively.

$$CWEP = 1 - \frac{1}{L}\sum_{i=1}^{L}(W_i \oplus W1_i) \quad (4)$$

$$CSEP = 1 - \frac{1}{N}\sum_{i=1}^{N}(S_i \oplus S1_i) \quad (5)$$

Where W, W1 denote the embedded and extracted watermarks with L bits length. S, S1 are the embedded and extracted digital signature with N bits length. $\oplus$ is X-OR logic operator. The higher the CWEP and CSEP value, the more similarity there is between W and W1, and S and S1 respectively. When CWEP and CSEP values equal to 1, means W1= W and S1=S.

4. PROPOSED DIGITAL IMAGE AUTHENTICATION ALGORITHM

The proposed algorithm is fragile invisible watermark and digital signature based for digital image authentication and tampers detecting. The watermark invisibility mains the embedded watermark cannot be perceived in HVS **,Mahavir D., and Jitendra K., 2014.** Fragile watermark is readily altered or destroyed when the host image is modified through a linear or nonlinear transformation **,Chang Gao, 2009.** That is, it may interest for parties to verify that an image has not been edited, damaged, or altered since it was marked.

The data that will be embedded in the digital image includes watermark and digital signature. Watermark data is patient-related data or EPR that includes: Patient record number, Patient Name, Age, Gender, Medical state, Dr. Name, Hospital name, Country, and Region of residence.

Digital signature is computed for the watermark data using MD-5 and RSA algorithms. MD-5 algorithm is used to generate 128-bit digest from the watermark. RSA algorithm is used for encrypting the digest that results the digital signature.

The suggested technique based on adaptive threshold to embedding the watermark and digital signature into the digital image in such a way that it is undetectable by the HVS. The adaptive thresholding method is employed to determine appropriate coefficients to hiding watermark and digital signature in the high frequencies regions in the image.

The threshold is variable according to the middle and high frequencies sub-bands coefficients of each DWT level making the hiding coefficients are different for each image.

First, the digital image is decomposed into seven regions using 2-level DWT and the middle and high frequency regions are selected for watermark and digital signature hiding. These frequencies give the details of the image and any changes in them are not easy notes by HVS, so that we will use them in order to ensure watermark invisibility and image fidelity. In this technique, low frequencies are excluded when inserting authentication data in order to preserve ROI and digital image fidelity.

Second, according to the computed adaptive threshold, the watermark data and digital signature are embedded in the appropriate coefficients. By using the adaptive threshold, the watermark and signature aren't hidden in all middle and high frequencies coefficients but in number of them only.

However, the suggested algorithm is composed of three sections: authentication data generation, authentication data embedding, and its extraction or verification. **Table 1.** shows the main symbols used in the paper and **Fig. 2** shows the block diagram of the algorithm (embedding and extracting).

4.1 Authentication Data Generation Process:

One of the most important features of the suggested algorithm is the type of the watermark data. The suggested watermark data is text type, like patient information. The watermark data used in the algorithm testing is collected from the EPR that is storing in the hospital database.

However, EPR data that used as watermark include: Patient record number, Patient Name, Age, Gender, Medical state, Dr. Name, Hospital name, and Country or Region of residence.

These data will be collected in one string and converted from ASCII to binary to forming the binary watermark $W= \{W_0\ W_1\ W_2 \ldots\ W_{L-1}\}$ where W_i $(1 \geq i \leq L)$ is the *ith* bit in the binary watermark.

The digital signature *S* is used for demonstrating the authenticity of image. Here we used MD-5 and RSA algorithms for generating the digital signature from the watermark data. The depending of the digital signature on the watermark itself making any attempt to change or remove the watermark is detectable. This means the algorithm provides dual methods for image authenticating.
The watermark and its digital signature forming the authentication data used in the embedding process. However, the authentication data generation steps are listed in the algorithm below *algorithm_1* and its flowchart is shown in **Fig. 3**.

ALGORITHM_1: Authentication Data Generation

Input*: Text Watermark and Encryption Private Key Kp.*
Output*: Authentication Data String (Watermark W, Digital Signature S)*
BEGIN:
Step1: Collect the data that forming the watermark data in one string.
Step2: Binarize the collected watermark data and store in W_L variable string.
Step3: Compute the digital signature *S* using the following steps.

i. Generating a 128-bits digest *D* from the binary watermark W_L using MD-5 algorithm.
ii. Encrypting the digest using RSA algorithm for providing the digital signature *S*. The digest will be encrypted using sender private key K_p.

Step4: Concatenate *S* and W_L and store in one string of binary numbers called authentication string *Auth_S*.

$$Auth_S = \{S_0\ S_1\ S_2 \ldots S_{127}\} \parallel \{W_0\ W_1\ W_2 \ldots W_{L-1}\}$$

END:

4.2 Authentication Data Embedding Process

The aim of this algorithm is to hiding the watermark data and digital signature (*Auth_S*) into the digital image. This algorithm should be implemented in the image sender side. However, this algorithm consists of five steps.

1. Applying 2-level DWT to the digital image.
2. Computing the adaptive threshold for each level.
3. Determining the hiding coefficients which are used for hiding the watermark and signature bits.
4. Embedding the authentication data (*Auth_S*) in the determined hiding coefficients.
5. Performing the inverse wavelet transform IDWT to construct the watermarked medical image.

4.2.1 Apply Discrete Wavelet Transformation

DWT is applied twice to decomposing the image to seven sub-bands in the frequency domain. The first level of DWT produces four sub-bands, termed LL1, LH1, HL1 and HH1. The LL1 band is iteratively decomposed to obtain four levels are LL2, LH2, HL2, and HH2. The six DWT sub-bands (LHi, HLi, and HHi) are used in the embedding process.

4.2.2 Compute of Adaptive Threshold

After transforming the image into frequency domain through DWT, the adaptive thresholds are computed for each level. Here, we describes the method for computing threshold value (*T*), which is adaptive to different level characteristics. The threshold value is calculated according to the decomposition level and watermark length *L*. In the 2-level decomposition, the average of

coefficients C for 1-level high frequency sub-bands (LH1, HL1, HH1) is computed and the threshold T_1 is calculated by Eq. (6), also the average of coefficients C for the 2-level high frequency sub-bands (LH2, HL2, HH2) is computed and the threshold T_2 is calculated by the same equation.

$$T_i = 2^{|(log_{10}\, AVR(C_i))|}\, mod\ (L+i) \qquad (6)$$

AVR (C_i) function finds the average of coefficient C in i-level. The authentication bits are embedded only in the selected coefficients in the high and middle frequency bands according to the adaptive threshold. **Fig. 4** shows how the adaptive threshold can be computed. The computed threshold is adaptive because it depends on the DWT level and the largest coefficient in the level.
The algorithm which computes threshold values in wavelet domain it very simple to implement and computationally is more efficient. It has following steps (algorithm_2):

ALGORITHM_2: Adaptive Thresholding Algorithm

Input: *DWT middle and high frequency sub-bands (LHi, HLi, HHi) and Watermark length L*
Output: *Adaptive threshold of each DWT level* (T_1, T_2).
Step1: For every DWT level, do the following.
BEGIN:
Step2: Load the coefficients C of LHi, HLi, and HHi sub-bands of i-level DWT.
Step3: Find the average of coefficients in i-level sub-bands (LHi, HLi, and HHi).
Step4: Compute the threshold value (T_i) using Eq. (6).
Step5: Save the threshold values results in T_i.
END:

4.2.3 Watermark and Digital Signature Hiding

This step is used to decide what the sub-bands and coefficients are to be used for the authentication data hiding. Some of the coefficients in the high levels (HH_1 and HH_2) and the middle levels (HL_1, LH_1, HL_2 and LH_2) will be used for authentication bits embedding. Embedding data in the middle and high sub-bands (LH, HL and HH) ensures a higher image fidelity and authentication data invisibility.
On the contrary, we exclude LL_2 sub-band to preserve image ROI. In spite of embedding data in the low frequency sub-band improve the watermark robustness but it is highly perceptible by human eye making the embedded authentication data is visible.
However, the coefficients are selected using adaptive threshold according to the following steps:

1. For each level, all coefficients of the LH_i, HL_i and HH_i sub-bands are firstly concatenated into a single sequence. Three coefficients with the same coordinate of the three sub-bands, which correspond to the same spatial location, are continuously adjacent in the new sequence. However the coefficients are rearranged in the following way:

$\{C_{LHi}(0,0),\ C_{HLi}(0,0),\ C_{HHi}(0,0),\ C_{LHi}(0,1),\ C_{HLi}(0,1),\ C_{HHi}(0,1),....,\ C_{LHi}(N-1,M-1),\ C_{HL2}(N-1,M-1),\ C_{HH2}(N-1,M-1)\}$.

Where N and M are the horizontal and vertical size of the sub-band respectively.

2. Then, the *Auth_S* bits are embedded in the LSB of the hiding coefficients which are satisfying the condition as follows:

$$|\ Coefficient\ Magnitude\ | > Threshold\ of\ Level\ (T) \qquad (7)$$

All the coefficients in i-level sub-bands (LHi, HLi, and HHi) are tested for satisfying the previous condition. However, the pseudocode of embedding process is listed below.

```
j=0;  // the start of the Auth_S string.
FOR  i= 1 TO i≤2   // i=1,2 (the number of DWT levels)
Begin:
Sort (C)
WHILE ({C_i-level} ≠ {Ø})
Begin:
IF (|C_k| > T_i-level)     //k is the kth coefficient in the i-Level.
Auth_S_j → LSB (|C_k|)
End IF
j= j+1;
k= k+1;
End WHILE
End FOR
```

4.2.4 Inverse of Wavelet Decomposition

Finally, the authenticated image is reconstructed by performing the inverse wavelet transformation IDWT.

However, the embedding algorithm of the suggested technique is listed below (algorithm_3) while its flowchart is shown in **Fig. 5**.

ALGORITHM_3: Authentication Data Embedding

Input: Digital Image $I_{M\ x\ N}$, and Authentication String (*Auth_S*)
Output: Authenticated Image $AI_{M\ x\ N}$.
BEGIN:
Step1: Perform 2-level DWT for the input image.
Step2: For each level do the following
BEGIN:

1. Compute adaptive threshold value T_i according to the Algorithm_2:
2. Determine hiding coefficients according to the following steps:
   i. Sorting the coefficients of the sub-bands LHi, HLi, and HHi where the three coefficients with the same coordinate of the three sub-bands, which correspond to the same spatial location, are continuously adjacent in the new sequence.

      $\{C_{LHi}(0,0),\ C_{HLi}(0,0),\ C_{HHi}(0,0),\ C_{LHi}(0,1),\ C_{HLi}(0,1),\ C_{HHi}(0,1)\ ,\ldots,\ C_{LHi}(n-1,m-1),\ C_{HLi}(n-1,m-1),\ C_{HHi}(n-1,m-1)\}$.

   ii. For coefficients in LHi, HLi, and HHi sub-bands, the hiding coefficients are determine by using computed adaptive thresholding.
3. Repeat the following steps until every bit in *Auth_S* string is embedded.
   i. Read the high and middle frequency coefficients of current DWT level sequentially and

select the coefficients which are satisfying the condition in Eq. (7):

| Coefficient Magnitude | > i-level Threshold.

ii. Embed the *jth* bit from *Auth_S* string in the LSB of the *jth* hiding Coefficient.

End:
Step3: Reconstruct the authenticated image $AI_{M \text{ x } N}$ by using IDWT.
Step4: Save and display the authenticated image.
End:

4.3 Extraction and Verification Algorithm

The first step of the extraction algorithm consists also of decomposition of the authenticated image with the same wavelet levels used in the embedding process. The authentication string bits are extracted from DWT coefficients which are selected according to the same method used in embedding process after computing the adaptive threshold for each level. Another necessary procedure is to acquire the digital signature and watermark from the extracted data.

In addition to its dependency on the watermark extraction, the verification process is also depended on the extracted digest, the extracted digest is compared with the computed digest of the extracted watermark data before making the decision about the image authenticity.

The below algorithm is used to extract an authentication data and acquire the watermark and digital signature from the authenticated medical image. **Fig. 6** shows the extraction process flowchart.

ALGORITHM_4: Extraction & Verification Algorithm

Input: *Authenticated Image* $AI_{M \text{ x } N}$ *and Decryption Key* K_u
Output: *Watermark W, Digital Signature S, and Decision about image authenticity.*
BEGIN:
Step1: Load the authenticated image.
Step2: Perform 2-level DWT for the input image.
Step3: For each level, do the following:

i. Compute the adaptive threshold T_i according to the Algorithm_2:
ii. Sort the coefficients of i-level sub-bands (LHi, HLi, and HHi) in sequential manner as in the embedding process.
iii. Find the coefficients which are its magnitude greater than the value of i-level threshold T_i.

| Coefficient Magnitude | > i-level Threshold.

iv. Extract the embedded bit from each coefficient which is satisfying the previous condition.
v. Create new string called *Auth_S1* string that will receive the extracted bits.
vi. Insert the extracted bit in the *Auth_S1* string. The extracted bits are inserted sequentially in the *Auth_S1* string.

Step5: Do the following after extract all authentication bits from that coefficients which are satisfying the stated condition.

i. Take the first 128-bits from *Auth_S1* string and store in new string called *S1* that is the

extracted digital signature.

ii. Store the remaining bits from *Auth_S1* string in new string called *W1* that includes the extracted watermark *W1*.

iii. Decrypt the extracted digital signature *S1* using RSA algorithm with K_u as decryption public key.

iv. Store the decrypted *S1* in new string called *D1* that is the extracted digest *D1*.

v. Compute the Digest value for the extracted watermark *W1* using MD-5 algorithm

vi. Store the result digest in new string called *D*.

Step6: Decision if the image is authentic or unauthentic.

i. **If *D=D1*** then the image is authentic and display the ***extracted watermark*** on the screen.

ii. **Else**: Display error message "the medical image is unauthentic"; this means the medical image is either replaced or modified.

End.

The experimental results and performance analysis of the technique will be presented in the next section, we will apply the algorithm on some medical images with different sizes of authentication data and test the technique robustness through applying some attacks on the authenticated images.

5. EXPERIMENTAL RESULTS

In order to test the proposed algorithm, we will apply the algorithm on medical images for different medical cases with various characteristics. The medical images are selected because of the importance of the authentication process in the medical applications over Internet like tele-radiology, tele-surgery, and telemedicine. The images are captured using MRI technique with size of 512×512 and 8-bits gray level. Also, these medical images are present different textural characteristics, various percentage of homogeneous regions, edges, and details.

The algorithm is applied on all ten images but the results of four images only exhibited. **Fig. 7** shows the original medical images which are used in this experiment.

For the purpose of proving the effectiveness of the proposed algorithm, the authentication data (watermark and digital signature) is hidden in the ten medical images with three different sizes are: 400, 600, and 800 Bytes. The digital signature size is constant in each case that is 128-bits. **Fig. 8, 9,** and **10** show the original medical images and their watermarked versions with 400, 600, and 800 Bytes authentication data capacity, respectively.

As can be seen in **Fig. 8**, the original images are in upper row and the authenticated images are appeared in the lower row. The amount of degradation caused by the embedding of watermark and signature is very difficult to distinguish by the HVS and thus the fidelity of the medical image was not affected.

The main reason for this is due to exclude areas of important details and textures during the embedding of watermark data into the medical image (LL2) sub-band. Also, the amount of authentication data play main role in as this situation.

By contrast, the results images shown in **Fig. 9** display a tiny amount of degradation that it is possible to distinguish by the expert person. While the watermarked images shown in **Fig. 10** have significant amount (also acceptable) of degradation that can be denoted by the general humans. The reason for this is the large amount of watermark data that affect the reconstruction image process (inverse of wavelet) after the data is embedded.

As a result, the degradation in the reconstructed medical image increases when the amount of embedded data is increased. This also confirms the conflicting relationship between two factors are quality and capacity. Thus, there must be a tradeoff between these two factors to achieve the ideal solution to resolve the conflict.

This problem was relatively solved through defining the maximum authentication data that can be embedded in the algorithm by 800 bytes or 100 ASCII characters. This number seems enough in the text watermark length for using personal information or secret message as watermark data. The maximum number of embedded data can be updated in the algorithm code.

However, in any case the image degradation remains acceptable because the main image details (LL2 sub-band) is not affected by the algorithm in any case.

5.1 Image Fidelity Evaluation

In additional to above, the proposed algorithm is evaluated in terms of fidelity of digital image in numerical form for more accuracy. For that, two image quality metrics are used that are PSNR and SSIM. PSNR and SSIM metrics are computed using Eq. 2 and 3, respectively.

A larger PSNR and SSIM indicate that the authenticated image more closely resembles the original image, meaning that the algorithm makes the embedded data more imperceptible.

Table 2. shows the calculated results for ten authenticated medical images which are used in this experiment with three authentication data (400, 600, and 800 byte).

As shown in **Table 2.** as long as the size of embedding data is small the PSNR and SSIM metrics are high, hence the fidelity of the reconstructed images is high. These metrics are decreased as long as the watermark size is increased causing to affect the image fidelity. But even with 800 byte authentication data, the image quality is acceptable where the metrics remains relatively high.

Generally speaking, image with PSNR greater than 35 dB and SSIM closer to 1 is acceptable as HVS cannot distinguish the difference **,Cox, et al., 2000. and ,T. Ahsan,** and **,T. Mohammad, 2012.** Therefore, the suggested algorithm produces authenticated image with very much acceptable fidelity because the PSNR in all the tests with different authentication data sizes remains more than 35 dB and SSIM is very closer to 1.

In numerical form, for the suggested technique application on the ten selected images with 400 byte of authentication data the average of PSNR is 43.817 and the average of SSIM is 0.9142. With 600 byte the average of PSNR is 40.969 and the average of SSIM is 0.8759. While with 800 byte, the average of PSNR is 38.281 and the average of SSIM is 0.8227.

Fig. 11 and **12** shows the comparison of the PSNR and SSIM metrics respectively of the ten images after embedding the authentication data with 400 byte, 600 byte, and finally 800 byte capacity.

5.2 Tests of Tampering Detection

There are many ways to tamper the digital images that may be intended or unintended like noise adding, image cropping, resizing, compressing, blurring, filtering, cutting, contrast adjustment, objects insertion, etc. Therefore, for testing algorithm robustness and watermark fragility we will apply some of the tampers and attacks that cause to modifying or changing the digital images and then check the authenticity of the images by the watermark and digital signature means.

Fig. 13 shows the eight examples of attacked medical images which are previously authenticated by using the suggested technique with 400 bytes. Here, all medical images are unauthentic, because the attacks cause to changing the values of images pixels hence the DWT coefficients.

The similarity between the embedded and extracted watermark and digital signature is measured by the CWEP and CSEP using Eq. 4 and 5, respectively. CWEP and CSEP values equal one in the previous tests because the authenticated images are not geometrically processed or attacked. This means the embedded and extracted watermarks and signatures are identical demonstrating the watermark fragility. On the other side, when the authenticated image is attacked, the CWEP and CSEP metrics results are not equal one (just nearing to one) as shown in **Table 3**.

Table 3. shows the computed PSNR, CWEP and CSEP after applying many attacks on the authenticated images with 400 bytes. The images are unauthentic because the original and extracted watermark and signature aren't identical where CWEP and CSEP aren't equal one.

6. CONLUSIONS

An efficient digital images authentication scheme based on adaptive fragile watermark and MD-5 has been presented. The algorithm used middle and high DWT frequencies for watermark and digital signature embedding. This makes the watermark is invisible and fragile where the HVS can't distinguish the changing in images when embedding the watermark in the high frequencies.

Moreover, the algorithm can't only achieve image authentication purpose, but also achieves copyright protection and tamper detection purpose. For authentication purpose, the digital signature is computed for the watermark using MD-5 and RSA algorithms and embedded in the digital image.

Experimental results demonstrate that the proposed scheme can be used for copyright protection and tamper detection by the invisible fragile watermark. The main characteristics of our scheme are as follows. (1) The fragile watermark for image copyright protection is robust to many mild and maliciously attacks. (2) By employing adaptation of watermarking method, enhancing watermark security, distributing, and fragility. (4) The authenticity of medical image is improved through providing double methods for copyright protection and authentication through watermark and digital signature.

REFERENCES:

- Cox J., Miller M.L., Linnartz J.M., and Kalker T., 2000, *A Review of Watermarking Principles and Practices, in Digital Signal Processing for Multimedia Systems*, K.K. Parhi, T. Nishitani, eds., New York, Marcel Dekker, Inc. P 332.
- Chuanmu L. and Haiming S., 2008, *A Novel Watermarking Scheme for Image Authentication in DWT Domain*", IEEE Transactions on Image Processing, Vol. 5, No. 3, pp 122-129.
- Ali Al-Haj and Tuqa Manasrah. 2007, *Non-Invertible Copyright Protection of Digital Images Using DWT and SVD*, Springer, 2nd International Conference on Digital Information Management, ICDIM '07. Vol. 27, No. 13, 114–118.
- Wang Z., Alan C. B., Hamid R. H., and Ereo P. S, 2004, *Image Quality Assessment: From Error Visibility to Structural Similarity,* IEEE, Transactions on Image Processing, VOL. 13, NO. 4, PP. 600-612
- Rajendra B. P., Vinayaka k., Mysura B. R, 2012, *Biorthogonal Wavelet Transform Digital Image Watermarking*, Springer, Proceedings in 2nd Conference of Advanced Computer Security Techniques, Vol. 2 NO.3 PP. 1223- 1229.

- Mahavir D. and Jitendra K., 2014, *Digital Watermarking for Medical Images using Biorthogonal Wavelet Filters and Transformed Watermark Embedding*, International Journal of Advanced Computer Research, ISSN: 2249-7277 ISSN Vol. 4 NO. 2, PP. 2277-2284.
- Chang Gao, 2009, *Image Authentication Method Based On DWT In Color JPEG Images*, IEEE, International Conference on Environmental Science and Information Application, Vol. 1, No. 1, pp 70-80.
- O.Dumitru, M. Mitrea, and F. Prêteux, 2008, *Theoretical limits in DWT image and video watermarking*, Mathematics of Data/Image Pattern Recognition, Compression, and Encryption with Applications, SPIE, USA, Vol. 8, No. 5, pp 823-829.
- Cong J., Feng T. and Yru F., 2006, *Image Watermarking Based HVS Characteristic of Wavelet Transform*, IEEE, International Conference on Intelligent Information Hiding and Multimedia Signal Processing, Vol. 11, No. 13, pp 660-668.
- Lu Z. M. and Sun S. H., 2009, *Digital Image Watermarking Technique Based on Vector Quantization*, Springer, 2nd International Conference on Information Security, Vol. 1, No. 2, pp 230-237.
- Tanveer A., and Tahseen M., 2012, *Digital Watermarking Based Image Authentication and Restoration by Quantization of Integer Wavelet Transform Coefficients*, IEEE/OSA/IAPR International Conference on Informatics, Electronics & Vision, Vol. 15, No. 27, pp 222-228.
- N. Grover and A. Mohapatra 2013, *Digital Image Authentication Model Based on Edge Adaptive Steganography*, Second International Conference on Advanced Computing, Networking and Security, PP 233 – 239.
- K. Raval and S. Zafar, 2013, *Digital Watermarking with Copyright Authentication for Image Communication*, International Conference on Intelligent Systems and Signal Processing (ISSP), Page(s):102-109.
- Yang, Hengfu and Sun, Xingming, 2007, *Semi-Fragile Watermarking for Image Authentication and Tamper Detection Using HVS Model*. Page(s):1112-1117.
- Chang, C.C, Tseng, H.W., 2004, *A Steganographic method for digital images using side match*, Pattern Recognition, vol. 25, pp.1431-1437.
- Po-Yueh Chen and Yue-chi Tseng, 2007, *A Study of DWT based steganography using Coefficient analysis*, pp.242-248.
- Sinha and K. Singh, 2003, *A technique for image encryption using digital signature," optics communications*, vol. 218, no.4, pp.229-234.
- Baisa L. Gunjal, Suresh N. 2012, *ROI Based Embedded Watermarking of Medical Images for Secured Communication in Telemedicine*, World Academy of Science, Engineering and Technology Vol: 6.

Table 1. Paper symbols and abbreviations.

Symbol	Description
$I_{M \times N}$	Digital image with M X N dimensions
$AI_{M \times N}$	Authenticated image with M X N dimensions
W_L	Watermark data with L-bits length
W1	Extracted Watermark Data
D	Digest
D1	New Digest
S	Embedded Digital Signature
S1	Extracted Digital Signature
Auth_S	Embedded Authentication Data (concatenation of S and W)
Auth_S1	Extracted Authentication Data
C_{DWT}	Selected Hiding DWT Coefficients
ThF	Threshold Computation Function
T_i	Computed Threshold for i-level DWT
EmA	Embedding Algorithm
ExA	Extraction Algorithm
EA	Encryption Algorithm (RSA)
DA	Decryption Algorithm
RSA	Rivest-Shamir-Adleman Cryptosystem
MD-5	Message-digest algorithm
K_p	Sender Private Key
K_u	Receiver Public Key

Table 2. PSNR and SSIM metrics of three watermark capacity.

Authenticated images	Auth. data Size=400 Bytes		Auth. data Size=600 Bytes		Auth. data Size=800 Bytes	
	PSNR	SSIM	PSNR	SSIM	PSNR	SSIM
Image01	44.85	0.928	42.65	0.892	40.12	0.819
Image02	43.45	0.898	41.63	0.834	38.59	0.782
Image03	46.13	0.934	43.05	0.902	40.86	0.860
Image04	43.06	0.918	40.98	0.887	38.30	0.847
Image05	42.33	0.909	40.12	0.882	37.56	0.824
Image06	43.92	0.902	39.97	0.875	36.88	0.837
Image07	43.25	0.927	41.15	0.841	39.11	0.787
Image08	45.23	0.921	41.97	0.886	38.66	0.815
Image09	43.52	0.912	40.35	0.884	37.44	0.821
Image10	42.43	0.893	37.82	0.876	35.29	0.835

Table 3. PSNR, CWEP, and CSEP of attacked watermarked image**.**

Attack Type	PSNR	CWEP	CSEP
Gaussian Noise (5%)	18.5573	0.782	0.817
Salt & Pepper Noise (5%)	15.8391	0.804	0.771
Object Insertion	22.7751	0.865	0.870
Contrast Adjustment	23.8749	0.906	0.842
Image Sharpening	19.7101	0.868	0.905
JPEG Compression (70%)	21.0298	0.842	0.858
Region Cutting	17.9011	0.818	0.763
Image Blurring	22.0881	0.917	0.711

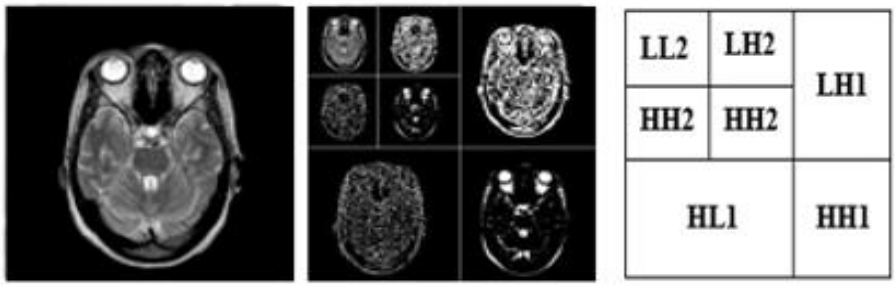

Figure 1. 2-level DWT decomposition.

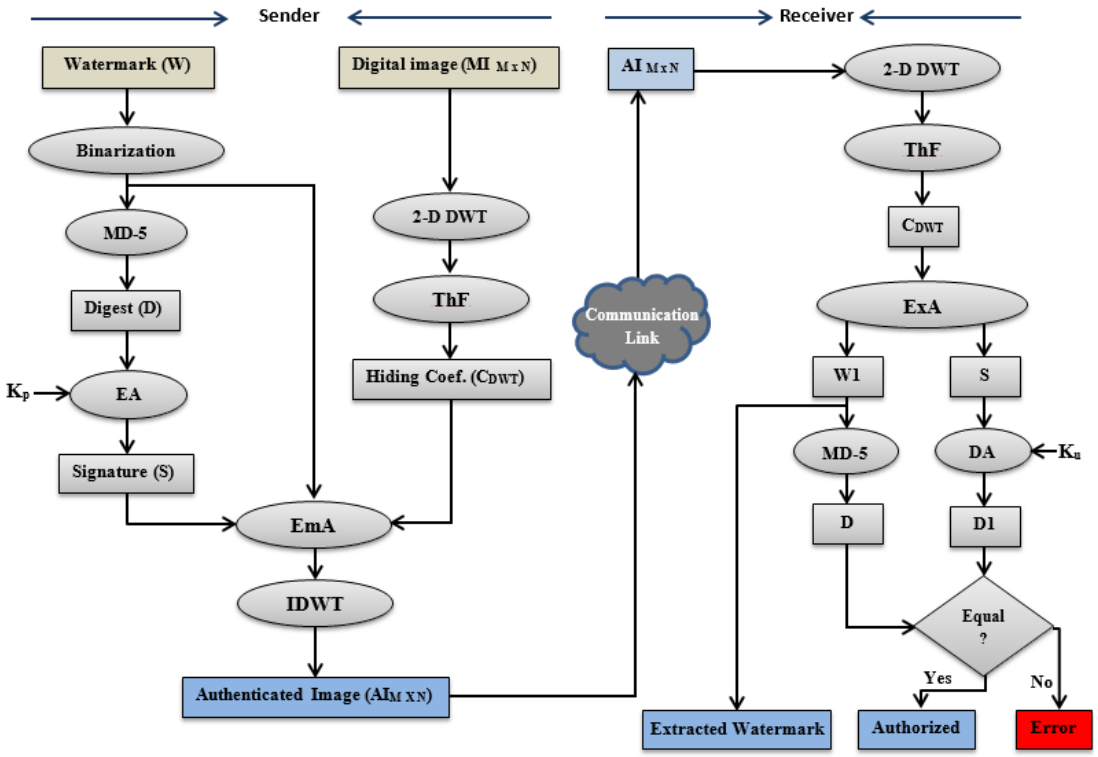

Figure 2. Proposed authentication model.

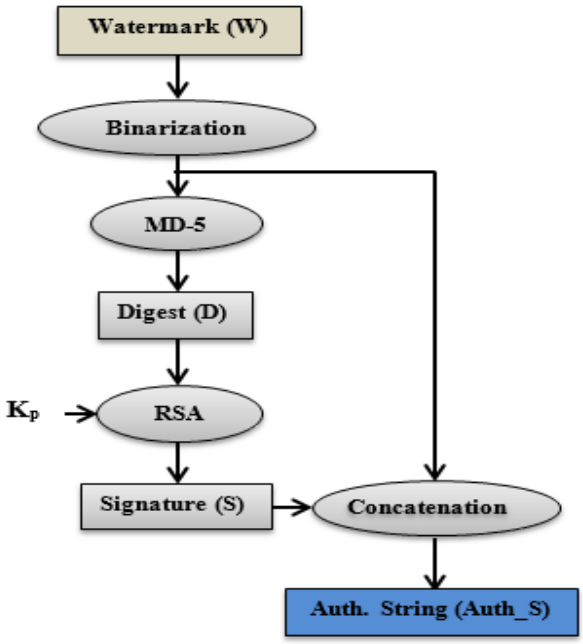

Figure 3. Authentication data generation algorithm.

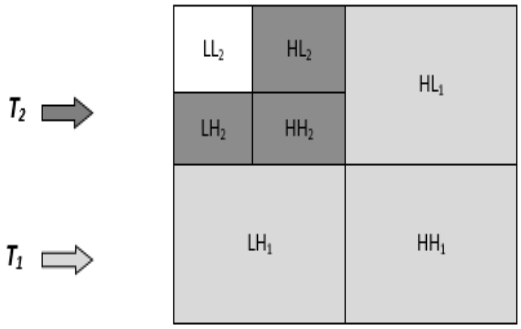

Figure 4. Adaptive thresholding.

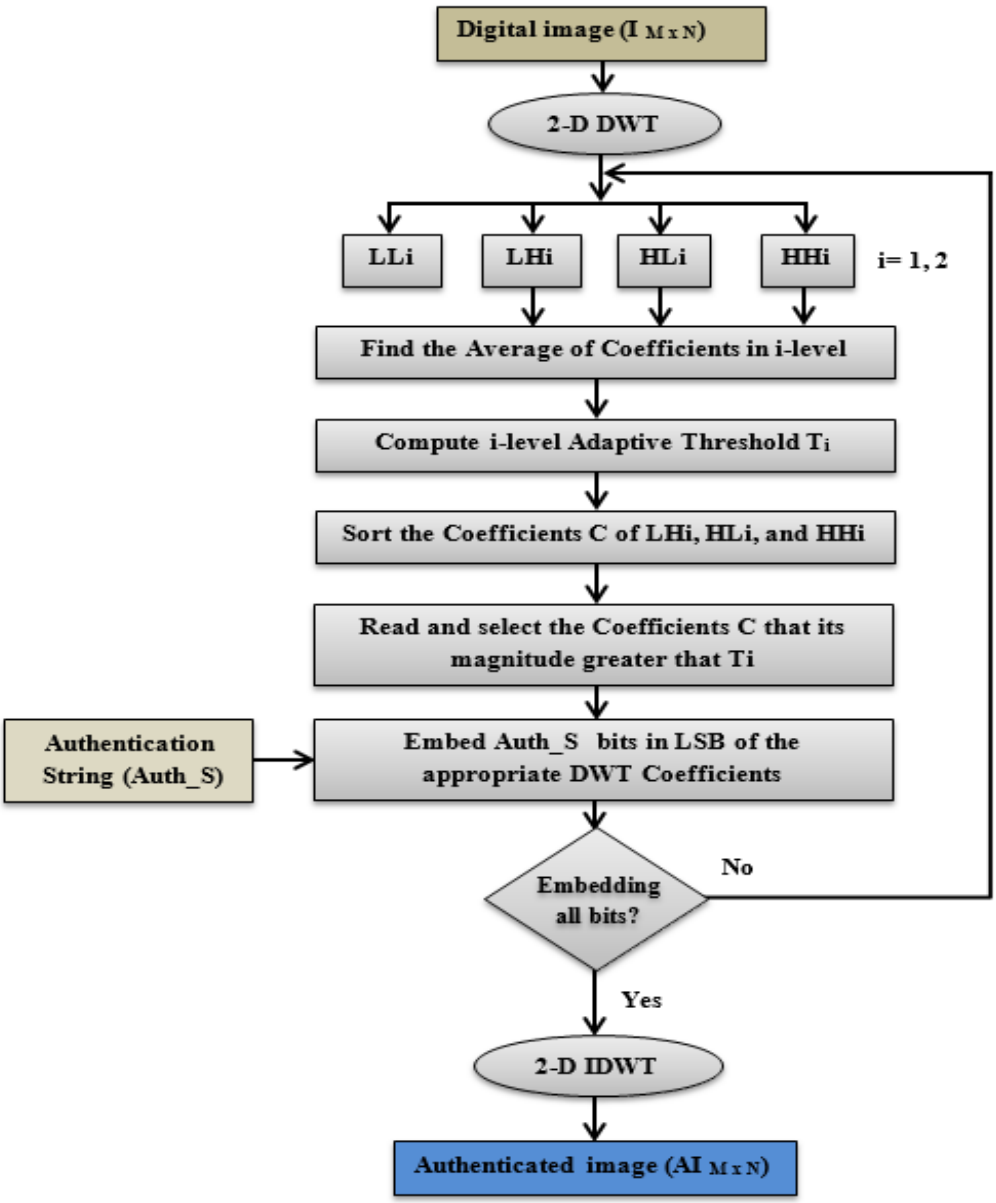

Figure 5. Watermark and digital signature embedding algorithm.

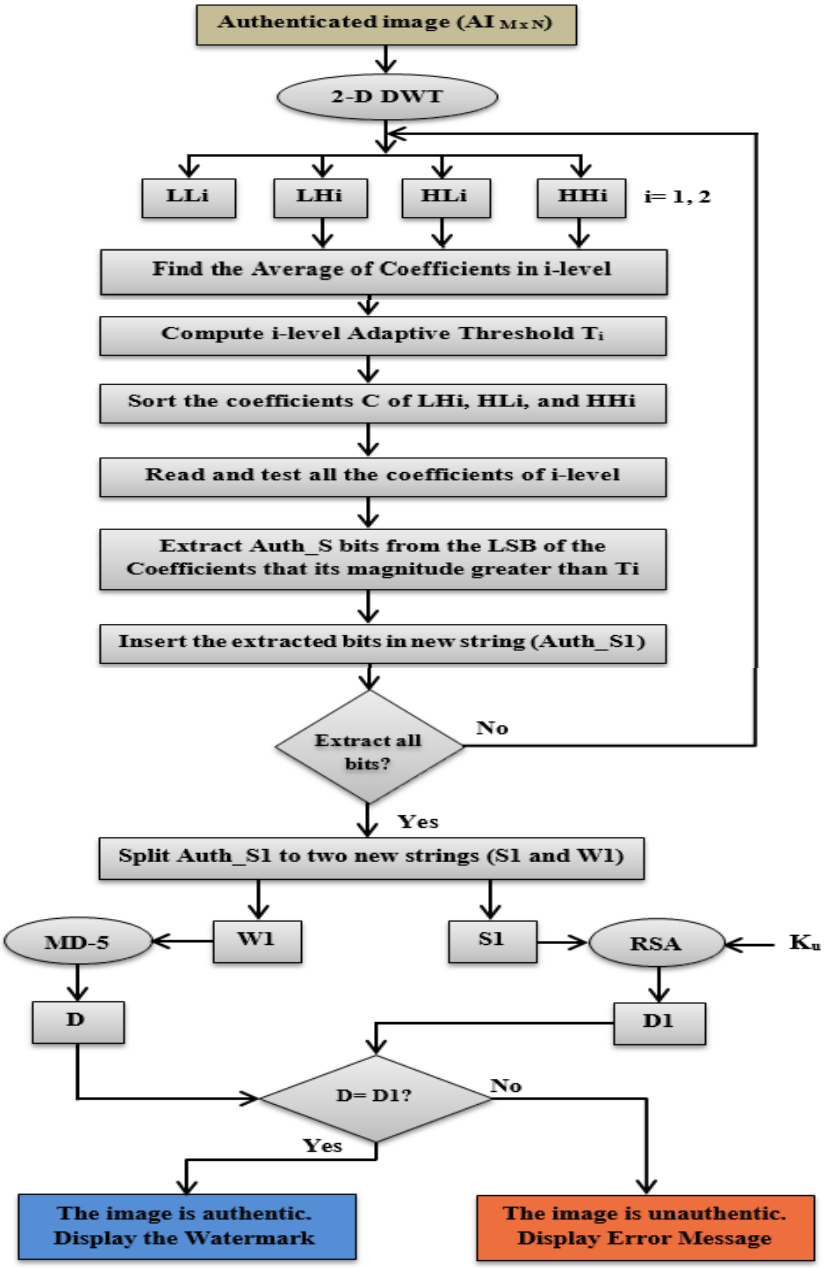

Figure 6. Extraction and verification algorithm.

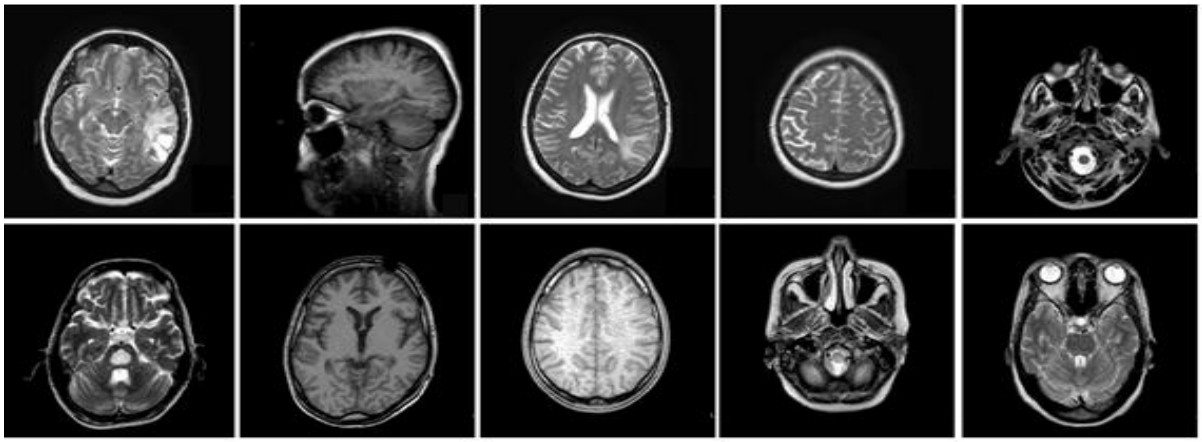

Figure 7: Test images used in the experience.

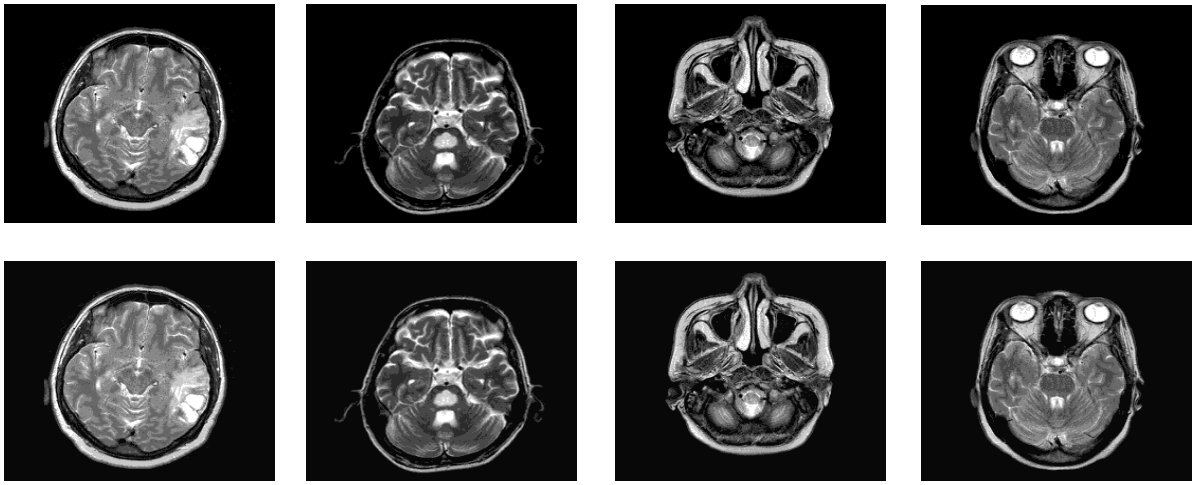

Figure 8 Test images with its authenticated versions (*Auth_S*= 400 Bytes).

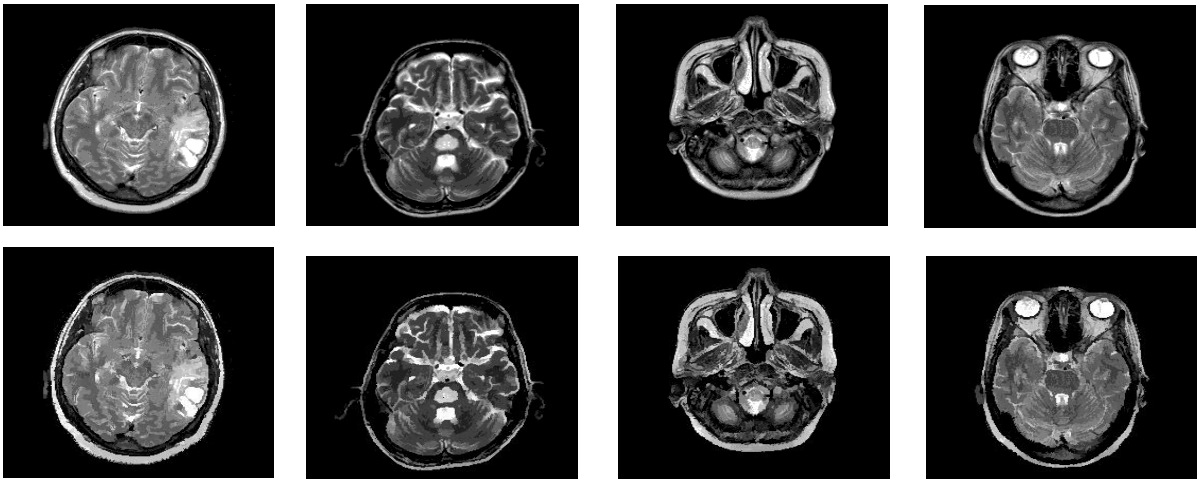

Figure 9 Test images with its authenticated versions (*Auth_S*= 600 Bytes).

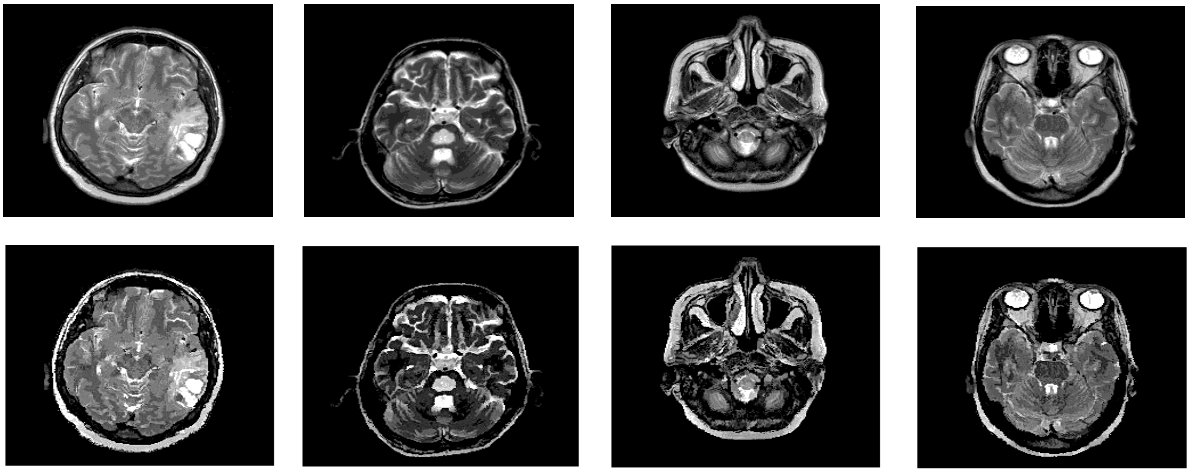

Figure 10 Test images with its authenticated versions (*Auth_S*= 800 Bytes).

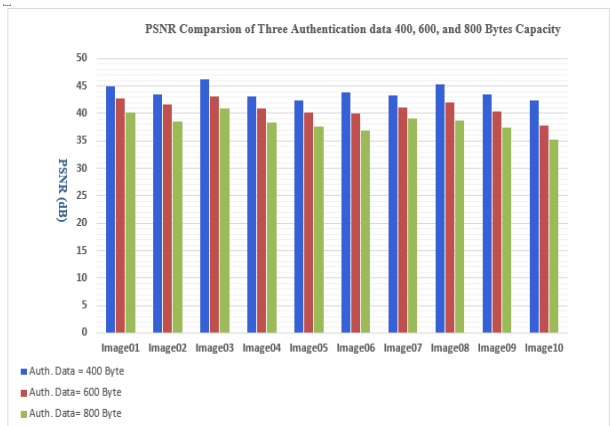

Figure 11. PSNR comparison of three Auth. data (400, 600, and 800 Byte)

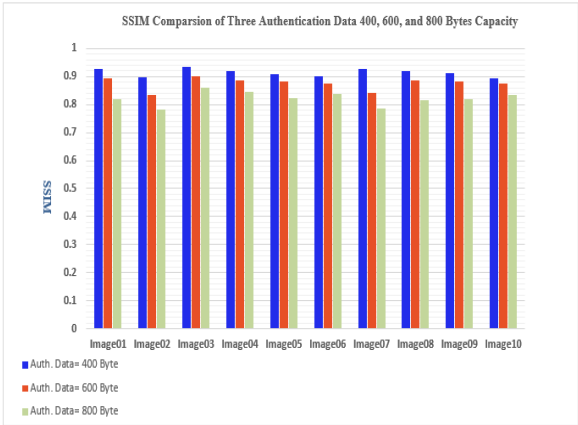

Figure 12. SSIM comparison of three Auth. data (400, 600, and 800 Byte)

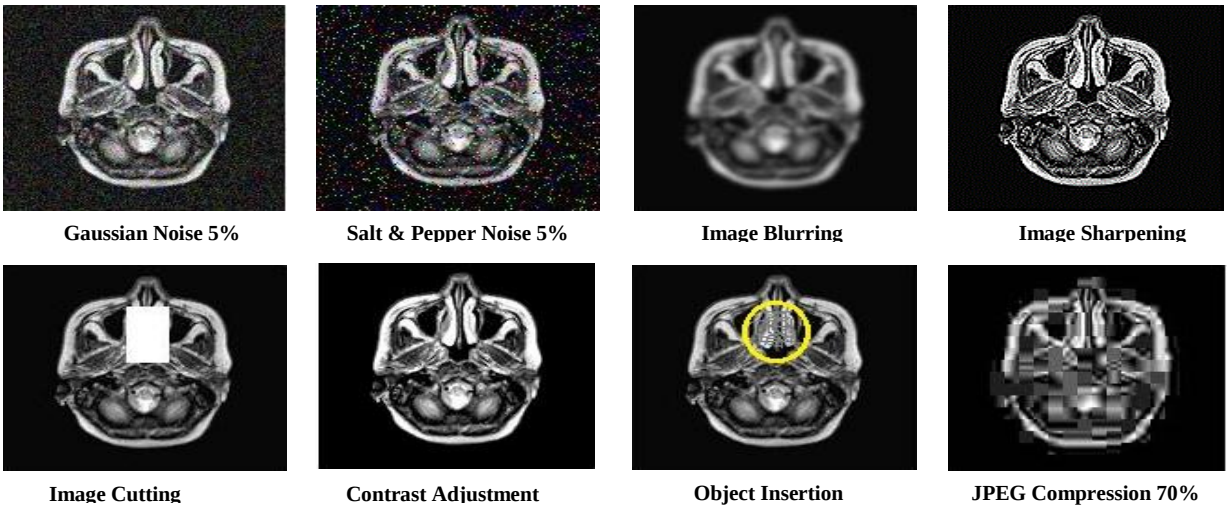

Figure 13. Authenticated images after Sample Attacks.

Data Aggregation in Wireless Sensor Networks Using Modified Voronoi Fuzzy Clustering Algorithm

Nadia Adnan Shiltagh
Assistant professor Dr.
Computer Engineering/ Baghdad University
E-mail:dr-nadiaat@hotmail.com.

Maab Alaa Hussein
Computer Engineering/Baghdad University
E-mail:maab_alaa@yahoo.com

ABSTRACT

Data centric techniques, like data aggregation via modified algorithm based on fuzzy clustering algorithm with voronoi diagram which is called modified Voronoi Fuzzy Clustering Algorithm (VFCA) is presented in this paper. In the modified algorithm, the sensed area divided into number of voronoi cells by applying voronoi diagram, these cells are clustered by a fuzzy C-means method (FCM) to reduce the transmission distance. Then an appropriate cluster head (CH) for each cluster is elected. Three parameters are used for this election process, the energy, distance between CH and its neighbor sensors and packet loss values. Furthermore, data aggregation is employed in each CH to reduce the amount of data transmission which lead to extend the network lifetime and reduce the traffic that may be accrue in the buffer of sink node. Each cluster head collected data from its members and forwards it to the sink node. A comparative study between modified VFCA and LEACH protocol is implemented in this paper and shows that the modified VFCA is more efficient than LEACH protocol in terms of network lifetime and average energy consumption. Another comparative study between modified VFCA and K-Means clustering algorithm is presented and shows that the modified VFCA is more efficient than K-Means clustering algorithm in terms of packets transmitted to sink node, buffer utilization, packet loss values and running time. A simulation process is developed and tested using Matlab R2010a program in a computer having the following properties: windows 7 (32-bit operating system), core i7, RAM 4GB, hard 1TB.

Keywords: voronoi fuzzy, fuzzy c-means ,clustering algorithm, data aggregation.

تجميع البيانات في شبكات المتحسسات اللاسلكية باستخدام خوارزميه التجميع المعدلة VFCA

أ.م.د. نادية عدنان شلتاغ
هندسة الحاسبات/جامعة بغداد

مآب علاء حسين
هندسة الحاسبات/جامعة بغداد

الخلاصة

تقنيات مركزية البيانات مثل تجميع البيانات عن طريق خوارزمية معدلة على أساس خوارزمية التجميع الـ FCM , مع مخطط الرسم البياني voronoi ستوضح في هذا العمل. من خلال الخوارزمية المعدلة (VFCA). في الخوارزمية المعدلة، المنطقة المراقبة تقسم إلى عدد من الخلايا تسمى voronoi cells من خلال تطبيق مخطط voronoi، على المنطقة المراد مراقبتها. كل خلية ممثلة بواحدة من أجهزة الاستشعار(العقد) التي وزعت بشكل عشوائي في المنطقة المستشعرة. يتم تقسيم هذه الخلايا الى مجاميع باستخدام طريقة التجميع (FCM) لتقليل المسافة التي تقطعها المعلومة للوصول إلى الهدف وتقليل إرسال البيانات

المكررة من العقد المتجاورة. ثم يتم اختيار العقدة المناسبة لتمثل كل مجموعة (رئيس المجموعة). واستخدمت ثلاثة معايير لعملية اختيار رؤساء المجاميع وهي: الطاقة، بعد المسافة بين رئيس المجموعة والعقد المجاورة له , و قيم الخسارة من مخزن العقدة. علاوة على ذلك، يعمل تجميع البيانات عند كل رئيس مجموعة على تقليل كمية البيانات المنقولة خلال الشبكة وهذا يؤدي إلى تمديد عمر الشبكة وتقليل حركة المرور التي قد تتراكم في المخزن الخاص بالـ Sink Node. رئيس كل مجموعة يجمع البيانات من أجهزة الاستشعار المنتمية اليه ويحولها إلى الـ (Sink Node).

أظهرت نتائج المحاكاة لدراسة مقارنة بين الخوارزمية المعدلة VFCA والبروتوكول LEACH أن VFCA المعدلة هي أكثر كفاءة من البروتوكول LEACH من حيث عمر الشبكة و من حيث متوسط تبديد الطاقة ومعدل استهلاك الطاقة. وتبين دراسة أُخرى للمقارنة بين الخوارزمية المعدلة VFCA و K–Means أن VFCA المعدلة هي أكثر كفاءة من K–Means من حيث الحزم المرسلة للعقدة المسؤولة عن الشبكة (Sink). و من حيث قيم الخسارة من مخزن كل عقدة ومن حيث والوقت المستغرق لإتمام العملية. ، تم تطوير عملية المحاكاة والاختبار باستخدام برنامج MATLAB R2010a في حاسوب يحمل المواصفات التالية: ويندوز 7 (32 بت نظام التشغيل)، كور i7، ذاكرة الوصول العشوائي 4GB، القرص الثابت 1TB.

1. INTRODUCTION

Nodes in a WSN sense the environment and send the collected data to the base station. Many nodes report similar readings as data in a WSN are correlated. Thus, a large amount of energy is spent during the transmission of thousands of redundant data. Furthermore, as nodes transmit sensed values to the base station by transiting through intermediate nodes, significant energy is spent in communication. One technique used to decrease the number of redundant messages transmitted and thus pro-long the network lifetime is data aggregation. During data aggregation, intermediate nodes merge the data received from other nodes into a single representative value. The energy of the network is conserved through a reduction in the number of messages being exchanged among nodes, **,Khedo, et al., 2010.** The general data aggregation algorithm works as shown in **Fig.1, Patil,2010.**

2. DATA AGGREGATIO IN CLUSTER BASED NETWORKS

Various protocols are being used for the clustering of the sensor networks like Direct Communication(DC), Minimal Transmission Energy(MTE), LEACH, K-Means, and Fuzzy C-Means. In DC, the sensor nodes far away from the base station get depleted with its energy at a faster rate, whereas in MTE, the nodes near to the base station get depleted. In LEACH, the selection of cluster heads is based on predetermined probability; other nodes choose the cluster by computing the nearest distance to the cluster heads elected. However, there is a randomized selection of cluster heads, where some of the clusters are devoid of cluster heads, resulting in poor clustering. In K-Means clustering, also known as hard clustering, the nodes near the boundary region are affected since the degree of belongingness is described in terms of either zero or one, the edge nodes may have the same degree of belongingness to more than one clusters, resulting in poor cluster formation. In the Fuzzy C-Means algorithm, which is an unsupervised, nondeterministic iterative method, there is an optimal cluster formation. The sensor nodes are assigned to a cluster, based on the degree of belongingness to different cluster in the deployed area, but the degree of belongingness needs to be computed in each and every round for every sensor node, **,Keerthi and Babu,2012.**

3- THE MODIFIED VORONOI FUZZY CLUSTERING ALGORITHM(VFCA)

The main purpose of the Voronoi Fuzzy Clustering Algorithm (VFCA) is to increase the network lifetime. Sensors are placed to detect an event occurring in the sensing area the sensed data need to be transmitted to the sink node for acquiring knowledge. The process of transmitting of sensed data from sensor nodes to the sink node may lead to consume the energy of nodes to transmit and receive data. Data aggregation helps the nodes in the network to save their energy by fusion of data from different sensors to eliminate redundant transmissions to the base station. This significantly reduces the amount of data traffic as well as the distances over which the data needs to be transmitted and increase the network life time, data aggregation and modified Voronoi Fuzzy Clustering Algorithm are proposed in this algorithm. Initially voronoi method is applied to construct voronoi diagram for the network by partitioning the sensed area into subareas each of which controlled by one sensor node these subarea called voronoi cell, then clustering process is starting by applying FCM then data transmission and aggregation is implemented. The modified VFCA is shown in **Fig.2**.

3.1 The Voronoi Method

In the modified algorithm, all nodes are assumed to be stationary and any sensor node position is projected by **x** and **y** coordinate. That is for any sensor node $\mathbf{p_i=s=(x_i,y_i)}$ the calculation of distance between nodes to construct voronoi diagram is done by using Euclidean distance function to given by Eq. (1), **Nithyakalyani and Kumar, 2013.**

$$dis(s,r)=\sqrt{(x_s-x_r)^2+(y_s-y_r)^2} \tag{1}$$

,Where **dis (s,r):** is the Euclidean distance between node (s) and set of all neighbor nodes (r).
P is a set of distinct points (sites) in the plane which is represents a set of points as $\{p_1,p_2, \ldots, p_n\}$. We subdivide the plane into **n** cells so that each cell contains exactly one site. An arbitrary point **(x,y)** is in a cell corresponding to a site $\mathbf{p_i}$with coordinates $\mathbf{(x_{pi}, y_{pi})}$ if and only if for all $\mathbf{p_j}$with $\mathbf{j\neq i,\ 1 \leq i,j\leq n}$. That is, the Euclidean distance from **(x,y)** to any other site is greater than the distance from **(x,y)**to $\mathbf{p_i}$ **, Mumm ,2009.**

$$\sqrt{(x-X_{pi})^2+(y-Y_{pi})^2} < \sqrt{(x-X_{pj})^2+(y-Y_{pj})^2} \tag{2}$$

3.2 Setup phase of VFCA

Formation of clusters and cluster head election are the main goal of setup phase. After the division of the sensed area into voronoi cells the network of sensors should be divided into clusters and this process is called “Clustering”. The clustering process for nodes is formed by using Fuzzy C-Means clustering algorithm, the first requirement of clustering is to the selection of cluster head node and then assign nodes to the best cluster head to become as members for cluster. Each cluster contains a set of nodes and the number of nodes is not necessary equal in the clusters, a cluster head is initially elected in each cluster. The node nearest to the center selected as cluster head . This is done only at the first round but for the next rounds the selection of cluster head based on the distance and energy for the nodes. **Fig.3** shows the five clusters. Which shows the location of final centers when choosing number of clusters for example (5-clusters).

3.3. The Steady-State phase of VFCA

Once the clusters are created and cluster heads are elected, data transmission can begin. The data transfer is begin starting from each node in the cell or cluster to communicate with the base station. This communication doesn't pass directly, the node communicates with CH, and all heads transfer data directly to the main base station. Every member in each cluster transmits the sensed data ($V(p_i)(d)$) to its corresponding cluster head, ($V(p_i)(d)$) comprises value of sensed data for cell $V(p_i)$. The cluster head nodes received the data until it's buffer full then the data aggregation computing using one of the following equations, **,Nithyakalyani and Kumar, 2013.**

$$\boldsymbol{Avg}=\frac{\sum_{i=1}^{n} di}{n} \quad (3)$$

$$\boldsymbol{Max} = \max(D) \quad (4)$$

$$\boldsymbol{Min} = \min(D) \quad (5)$$

Where : di : is the data sensed by node i.
D: is the total sensed data received in each cluster head.
Avg: average value of (d_i).
Max: maximum value of (d_i).
Min: minimum value of (d_i).
By taking the aggregation function for the received data in each cluster head the cluster heads send the aggregated data which is represent the maximum degree for each cluster to the sink node which is also take the same aggregation function for the received data. For each sensor node, the energy is consumed due to the receiving and transmitting for the data. Depending on the distance between transmitter and receiver. After sending data, the dissipated energy for each node and each cluster head to transmit and receive data should be calculated in order to use it as parameter behind the distance to select new cluster head. If the energy of cluster head reach to zero this means that the cluster head will be die and new node from that cluster should be chosen with highest remaining energy and nearest to the center. The energy dissipated for transmitting and receiving data for normal nodes is calculated as in the following Eqs. (6) and (7).

$$ETX_node = E * distance(i,j) \quad (6)$$

$$ERX_node = E * distance(i,j) \quad (7)$$

Where:
ETX_node: Transmitter Electronics Energy dissipated for each node.
ERX_node : Receiver Electronics Energy dissipated for each node.
distance(i,j) : Distance between node i and its cluster head j.
E : Initial Energy for each node.

Then the remaining energy for each node can be calculated by subtracting dissipated energy for transmitted and received from the energy of that node.

The energy dissipated for data transmitting and receiving data for cluster head nodes is calculated as in the following Eqs. (8) and (9).

$$ETX_CH = ETX_CH - (Sum(ETX_node(cluster))) \quad (8)$$

ERX_CH = ERX_CH - (sum(ERX_node(cluster)) (9)

Where:
ETX_CH: Transmitted energy dissipated for each cluster head.
ERX_CH : Received energy dissipated for each cluster head.

From the above equations one can conclude that the cluster head node has dissipated energy in transmitting data to sink and dissipated energy to receiving data from its members, while the normal nodes has only dissipated energy for sending data to its CH, and sink node has dissipated energy to received data from cluster heads.

- The selection of cluster head node usually depends on several parameters, this paper was used energy as parameters as explained above and then was used packet loss value from the buffer of cluster head node which can be calculated as explained in Eq.(10).Each cluster head after receiving data from its members should check if there is packets was lost from its buffer as in Eq.(10)

Pl= BUF – P **(**10)
Where:
Pl: packet loss.
BUF: size of the buffer.
P: Number of the received packets.
whereby each time cluster head receive sensed data from its members the cluster head subtract received data packets from its buffer size to see if there is space in its buffer for the receiving packets or not and if it is find that some of the received packets was loss it calculate the value of packet loss and then re-cluster the network again in the second round and chose the new cluster head nodes with low packet loss and nearest to the final centers of FCM clustering.

4- SIMULATION SETUP AND RESULTS

In this section the simulation of the modified VFCA in the network environment and comparison with LEACH protocol in WSN are presented. Simulation is implemented with GUI (Graphical User Interface) in Matlab and it is achieved with n-sensor nodes that are randomly distributed within a (100x100) m region. These nodes are assumed to be stationary, the proposed algorithm is simulated in a wireless sensor network and is compared with LEACH protocol. All simulation parameters in the modified algorithm are presented in Table(1).
To evaluate the performance of the modified VFCA, the number of sensor nodes should be inserted for example 100-stationary sensor nodes are randomly placed in a sensed area also number of clusters should be insert for example 5 - clusters. **Fig.4** illustrates the model of the 100-nodes simulation network after applying voronoi diagram and then FCM clustering for the first round.

The running time taken to construct voronoi diagram represented in **Fig.5**. From the figure one can see that voronoi diagram take less time for constructing and increasing in low rate with increased the number of nodes.

The running time taken by FCM for 100 sensor nodes divided to different number of clusters represented in **Fig.6**. From the figure one can see that FCM take minimum time to divide the voronoi cells to clusters and this time increasing in low rate with increased the number of clusters.

Then after divide the voronoi cells to clusters should press the next button illustrated in **Fig.4** and second button illustrated in **Fig.7** to see the information about each cluster these information include the distance between each node in the cluster and the cluster head ,the sensed data for each node in each cluster represented by temperature degrees and the energy for each node in the cluster all these information are shown in **Fig.8**.
The modified VFCA choosing the optimal cluster head node at each new round depending on the division of the voronoi cells that cover all the sensed area to clusters using FCM and the process of election of cluster head depending on the highest node energy, this may be lead to enhance the Performance of the applying modified VFCA to the WSN from hand of running time of the network and the energy dissipated and network lifetime to better than LEACH protocol as seen following.

4.1 Network Lifetime

The lifetime of the network for the modified VFCA and, LEACH protocol with respect to alive nodes in the number of rounds is shown in **Fig.9**. As compared with LEACH, the modified VFCA has an improvement over the stability period as compared with LEACH protocol. As it is clear from **Fig.9**, the first node dies in LEACH protocol at round 932 and last node dies at round 1312, whereas in modified VFCA, the first dead node is at round 977 and last node die at round 1520 as illustrated in Table(2). This shows an improvement due to the use of the voronoi diagram. This help the network to cover all area and reduce transmission distance. Also by using Fuzzy C-Means clustering (FCM) with voronoi diagram will be reduced the transmission distance. The modified VFCA is chose the best node as the cluster head node depending on the cluster node with highest energy and this will be lead to increase the network lifetime.

4.2 Average Energy Consumption

For any routing protocol, lesser energy consumption is an important issue so that the network stays alive for longer period or for more number of rounds. **Fig.10** shows the average energy dissipation for all nodes with respect to number of rounds. The rate of energy consumption of the modified VFCA is lower than the rate of LEACH. Nodes in the modified VFCA deplete their energy in very slow rate as compared to LEACH. Eq. (11) shows how to calculate the average energy conception for the network, **,Anitha andKamalakkannan, 2013.**

$$E_a = \frac{\sum_{K=1}^{N} (E_{iK} - E_{ck})}{N} \qquad (11)$$

Where, E_{ik} = The initial energy level of a node.
E_{ck} = The current energy level of a node.
N = Number of nodes in the simulation.

5- PERFORMANCE OF THE MODIFIED VFCA WITH K-MEANS ALGORITHM

The simulations run with the parameters mentioned in Table (1). To evaluate the performance of the modified VFCA, 20-stationary sensor nodes are randomly placed in a sensed area with one sink node. **Fig.11** illustrates the model of the 20-nodes simulation network. The numbers of elected cluster heads from all nodes in the network is chosen randomly. In the modified VFCA the role of CH node rotates between all sensor nodes in the network if the selected cluster head

has packet lost from its buffer because the congestion traffic in its buffer the cluster head sends the packets that are in its buffer and all other cluster heads also send the aggregated data in their buffers and then the process of clustering repeated and chose new cluster head nodes depending on the value of packet loss and the distance between sensor nodes and the centers that gets it from FCM clustering algorithm.

5.1 Total Number of Packets at Buffer of Sink Node

The total number of packets can be computed according to the packets reached to the buffer of the sink node. The network model that is used for implementing varying the number of cluster heads consists of 400 nodes. **Fig.12**. illustrates the compression between the modified VFCA and K-Means algorithm in terms of the total number of packets received at the sink node in the network, when varying the number of clusters in the network (5-10-15-20-25) clusters, this may lead to increased number of packets arrived at sink node as shown in Table (3).

From **Fig.12** one can conclude that the modified VFCA divides the area into cells and this will lead to optimization in distribution and aggregation of data from the network then the sink node may reach the data that needed from the sensed area without losses and congested. In K-Means algorithm ,although the sink node received more data than modified VFCA when increasing the number of clusters but this may be lead to congestion at sink node and losses some of the important data, where as in the modified VFCA the congestion and losses not accrue. Therefore, the VFCA is better than K-Means algorithm.

5.2 Buffer Utilization (BU)

The buffer utilization of sink node can be computed according to the buffer of sink node when increasing number of nodes and fixing number of clusters once and increasing number of clusters and fixing number of nodes in the other once. as described in Eq. (12).

$$BU = \frac{P_{total}}{BU_{\sin k}} \tag{12}$$

Where, BU: Buffer Utilization.
P_{total}: total packets received at sink buffer.
BU_{sink}: size of the sink buffer.

a. (BU)When Increasing the Number of Nodes and Fixing Number of Clusters:

Fig.13 denotes the Buffer Utilization of sink node after applying Eq.(12) , by increasing number of nodes in the network and fixing numbers of clusters to 5. One can see from **Fig.13** every time number of nodes increase the buffer utilization is increased because when increasing number of nodes and fixing the number of clusters this lead to increase the number of nodes in each cluster and then when cluster head aggregate the packets that is received from its members, the sink received values from only five nodes represent data of its members. The best value of buffer utilization should be less than or equal to one but not greater than one from the **Fig.13** one can see that the buffer utilization for K-Means algorithm begin smaller than one when number of nodes equal to 20-nodes and when the number of nodes increased the value of BU increased to value greater than one. But the value of BU when apply modified VFCA does not arise greater than one. This mean that the modified VFCA is better than K-Means algorithm because the modified VFCA managing the buffer accurately so that no losing in packets are happened. Table (4) shows the values of buffer utilization in the sink node.

b. (BU)When Increasing Number of Clusters And Fixing Number of Sensor Nodes:

Fig.14 denotes the Buffer Utilization of the sink node by increasing number clusters in the network and fixing number of sensor nodes to 400. One can see from **Fig.14** when the number of clusters increase the buffer utilization approaches to one because when increasing number of clusters the numbers of cluster heads sending their data packets to sink node will be increased and this leads to increase the number of data packets arrived at sink node and then approximately all space in the CH buffer will be filled by data packets.

The behavior of the modified VFCA is better than k-Means algorithm. This is because the modified VFCA managing the buffer of sink more efficient than the K-Means algorithm. Table (5) shows the values of buffer utilization of the sink with respect to the number of clusters in the network.

5.3 Packet loss value

Fig.15 illustrates packet loss value for each node in the network that consists of 20 sensor nodes divided to 20 voronoi cells and these cells are divided to five clusters for the first round. One can see from the figure that only cluster head nodes has packet lost from its buffer because the CH received data from its members and these data may be huge lead to packet loss from CH buffer. From **Fig.16** one can see that the modified VFCA is better than K-mean because the cluster head approximately received all data from its member. Table (6) shows the cluster head nodes, number of received data at each CH and packet loss values for both VFCA and K-Means algorithm for the first round.

5.4 Running Time

Fig.16 shows the Comparison between modified VFCA and K-means algorithm in terms of running time for the network in **Fig.12**. The number of nodes is changed at each time of execution and evaluate the time in both algorithms, the number of clusters constant for both algorithms to find the running time. The number of cluster heads equal to 5. **Fig.16** shows that the running time of VFCA less than running time of K-Means algorithm. This is because the method of computing the membership function in the modified VFCA which is repeated in a single voronoi cell, so that the execution of this function is just in the cell and not in all nodes in the cell, and hence the running time will be reduced.

6- CONCLUSION

In this paper, a modified VFCA for data aggregation is presented. In order to reduce the average energy dissipated in the sensor network and increased the network lifetime. At first the voronoi diagram is applied for the sensed area based on energy of each node once and packet loss value for other once. Consequently, the cluster head node is selected by applying FCM clustering algorithm. Then every node send its sensed data to its cluster head. Cluster head aggregate the received data by taking maximum value and send the aggregated data to sink node. Finally, the results shows that the behavior of modified VFCA is better than both LEACH protocol and K-Means clustering algorithm.

REFRENCES

- Anitha R. U. and Kamalakkannan D. P.,2013, *Enhanced Cluster Based Routing Protocol for Mobile Nodes in Wireless Sensor Network*, Proceedings of the International Conference on Pattern Recognition, Informatics and Mobile Engineering (PRIME), IEEE, India, 20-22 February, PP.187-193.
- Keerthi, M, and Babu, B.S., 2012, *An Improved FCM's Clustering Protocol for Wireless Sensor Networks*, International Journal of Electronics and Communications (IJEC), Vol.1, Issue 1, PP. 69-73.
- Khedo, K., Doomun, R., and Aucharuz, S.,2010, *READA: Redundancy Elimination for Accurate Data Aggregation in Wireless Sensor Networks*, Wireless Sensor Network, Vol. 2 No. 4, 2010, pp. 300-308.
- Mumm M.,2009, *Voronoi Diagrams*, The Montana Mathmatic Enthusiast (TMME), Vol 1, no.2, pp.44.
- Nithyakalyani, S., and Kumar S. S. ,2013, *An approach to Data Aggregation in Wireless Sensor Network Using Voronoi Fuzzy Clustering Algorithm*, Journal of Scientific & Industrial Research,Vol. 72, PP. 287-293.
- Patil, N. S., and Patil, P. R. ,2010, *Data Aggregation in Wireless Sensor Network*, ICCIC International Conference on Computational Intelligence and Computing Research, B.V. Tamilnadu college of Engineering coimbatore, India, 28-29 Dec.2010, PP. 162-168.

List of symbols

(x_i,y_i)=X-coordinate and Y-coordinate of sensor node.

BU: Buffer Utilization.

BUF: size of the buffer.
BU_{sink}: Size of the sink buffer.
D: is the total sensed data received in each cluster head.
di = The data sensed by node i, m^2.
distance(i,j) : Distance between node i and its cluster head j, m^2.
E : Initial Energy for each node, Joule.
Ec = The current energy level of a node, Joule.
Ei = The initial energy level of a node, Joule.
ERX_CH : Received energy dissipated for each cluster head, Joule.
ERX_node : Receiver Electronics Energy dissipated for each node, Joule.
ETX_CH: Transmitted energy dissipated for each cluster head, Joule.
ETX_node: Transmitter Electronics Energy dissipated for each node, Joule.
N = Number of nodes in the simulation.
P: received packets.
p_i= The location of sensor node.
Pl: packet loss.
P_{total}: Total packets received at sink buffer.
s= senson node.
V(pi) = The voronoi cell of node (p_i).

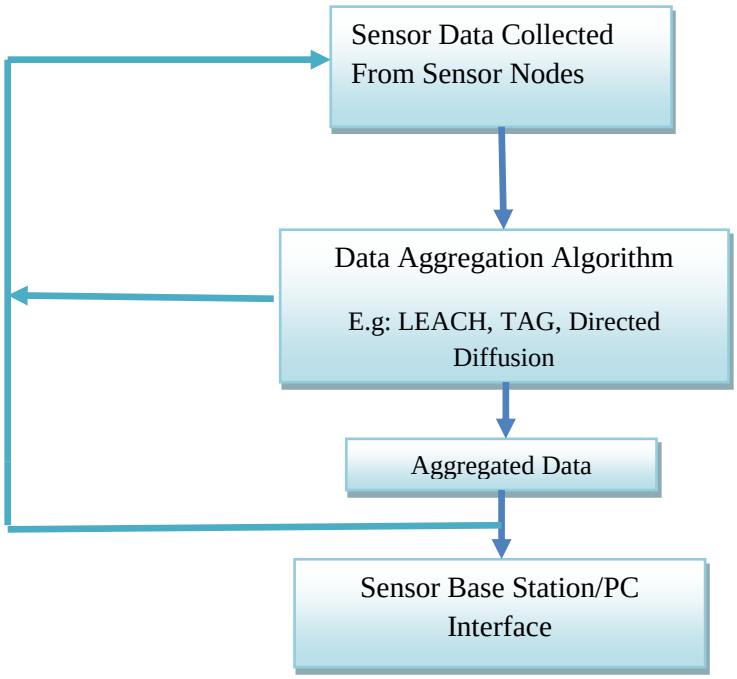

Figure 1. General architecture of the data aggregation algorithm.

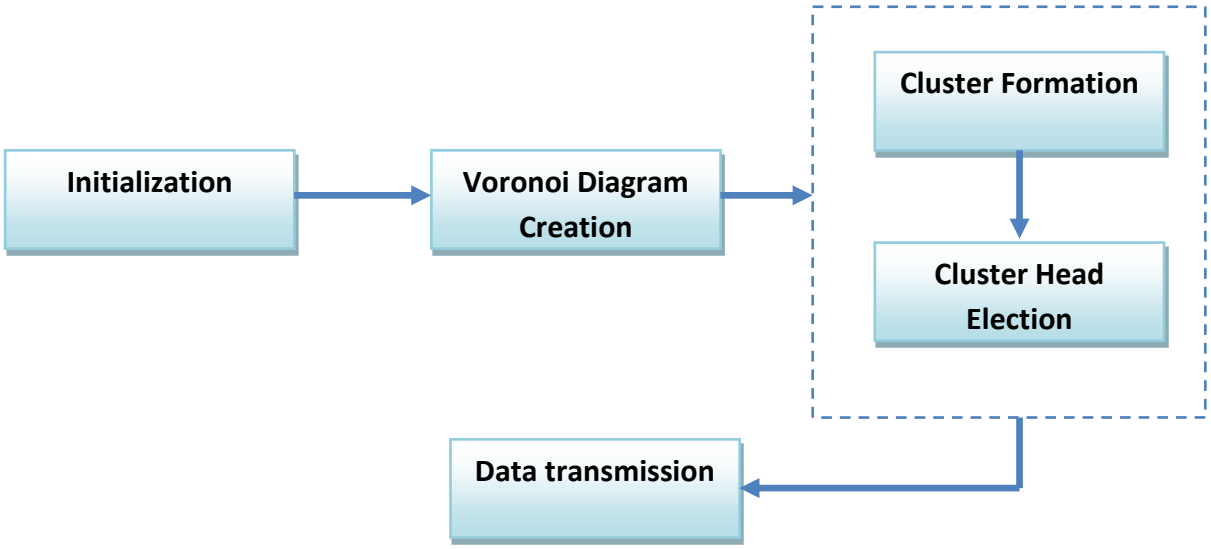

Figure 2. Modified voronoi fuzzy clustering algorithm.

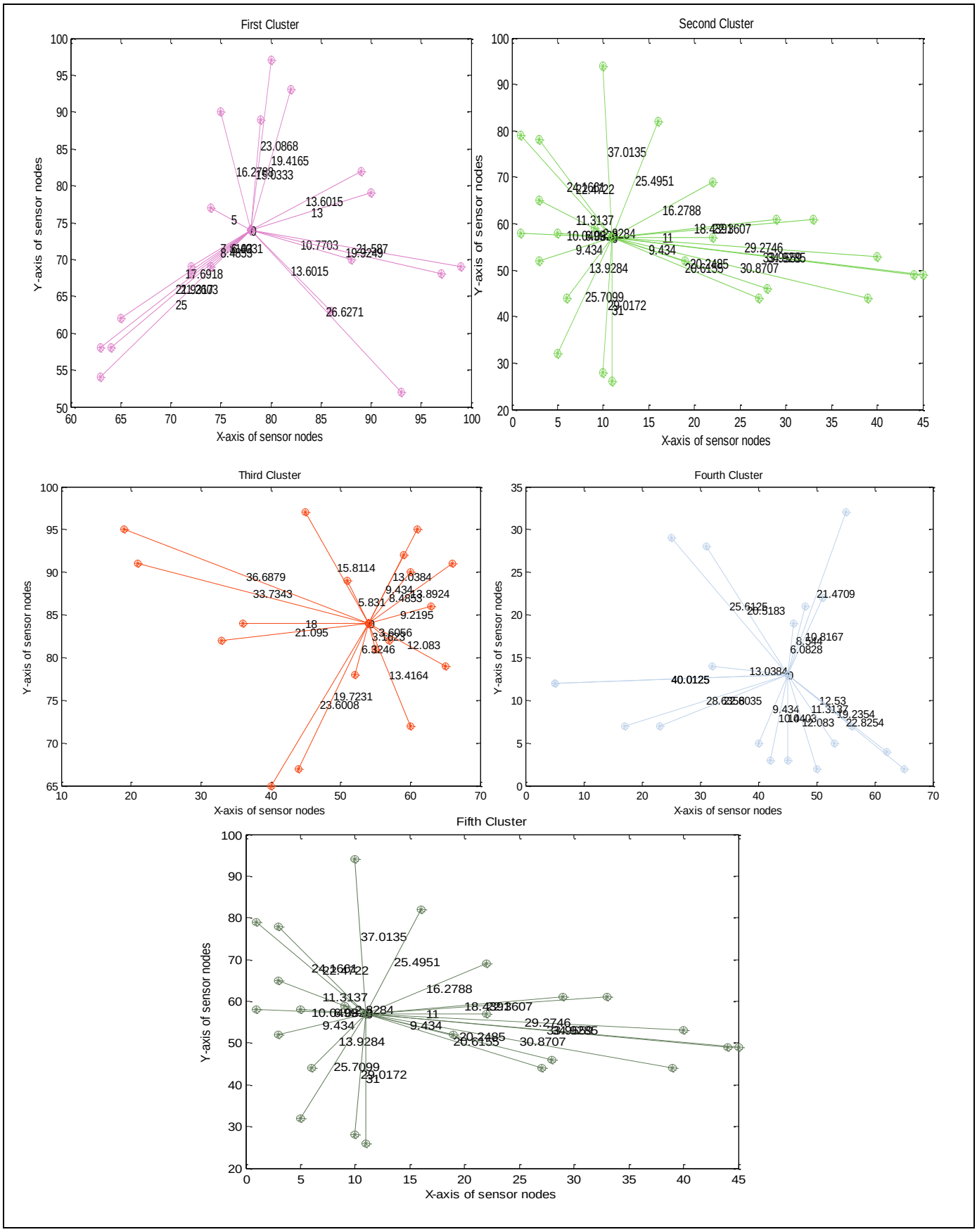

Figure 3. Sensors after applying fuzzy c-means clustering.

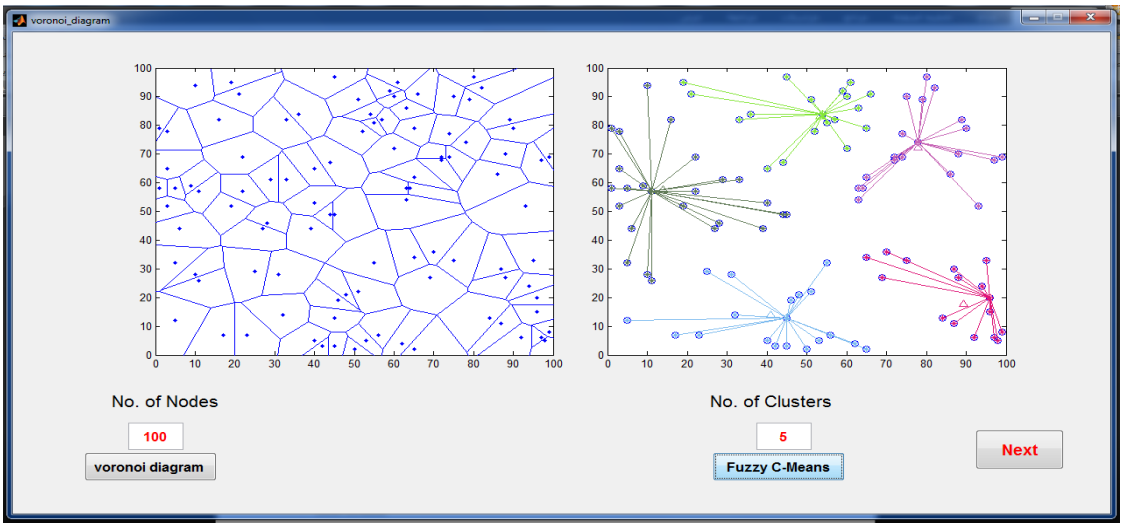

Figure 4. Sensor nodes after applying voronoi diagram and FCM.

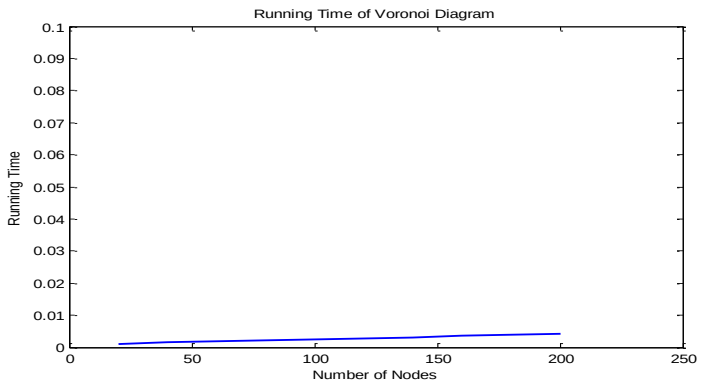

Figure 5. Running time of voronoi diagram vs number of nodes.

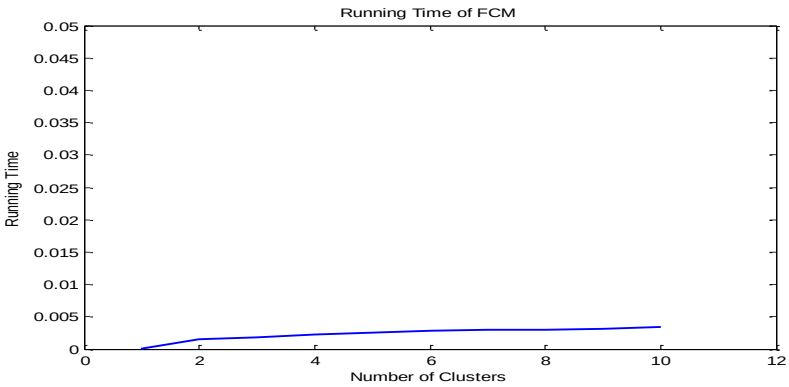

Figure 6. Running time of FCM vs number of clusters.

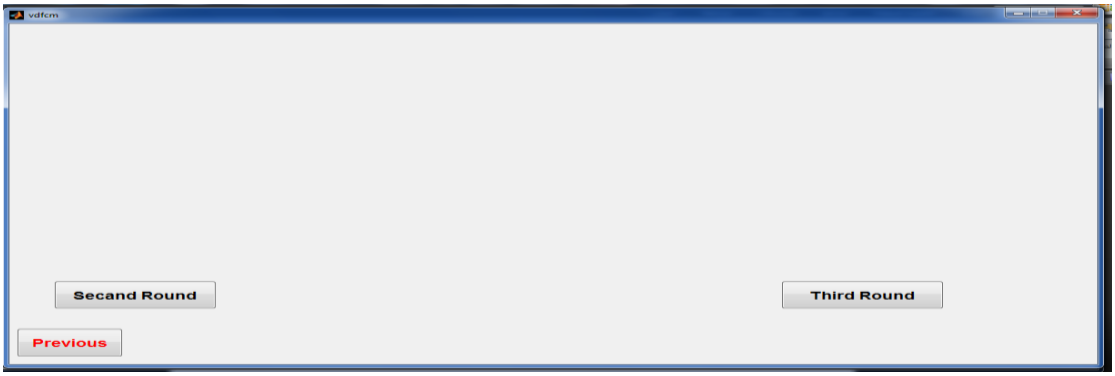

Figure 7. Represent the button to run the second and third round.

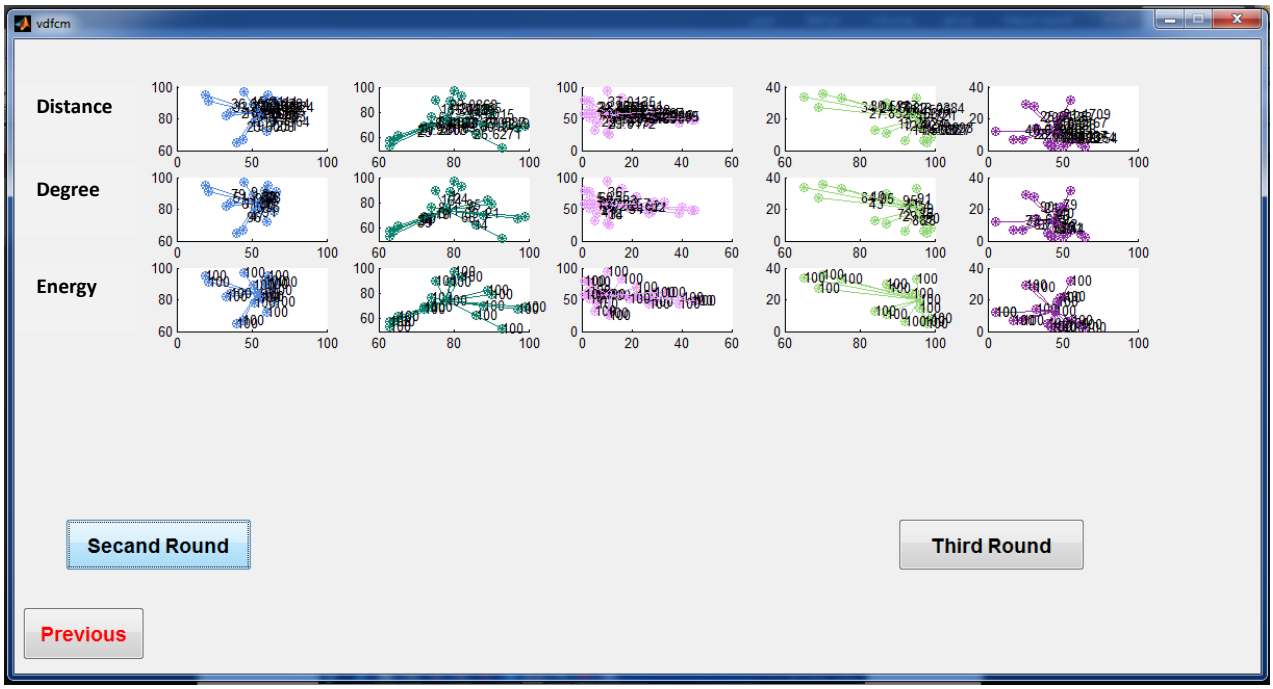

Figure 8. Information for each node in each cluster for first round.

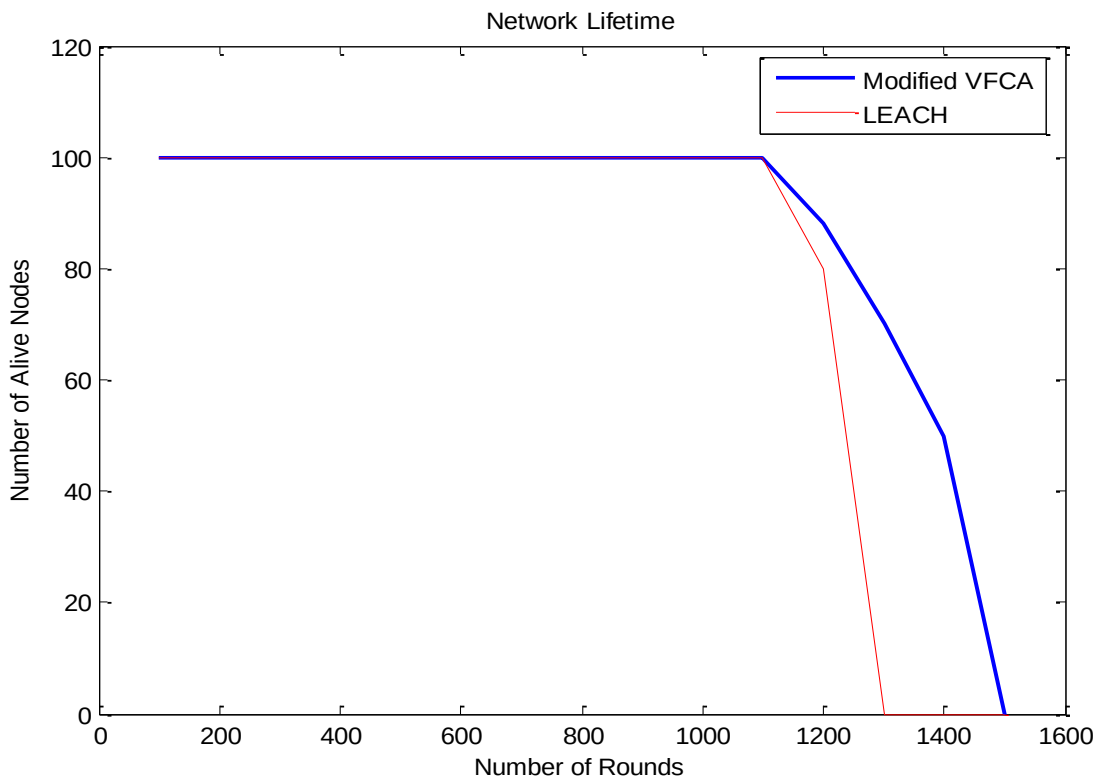

Figure 9. Network lifetime.

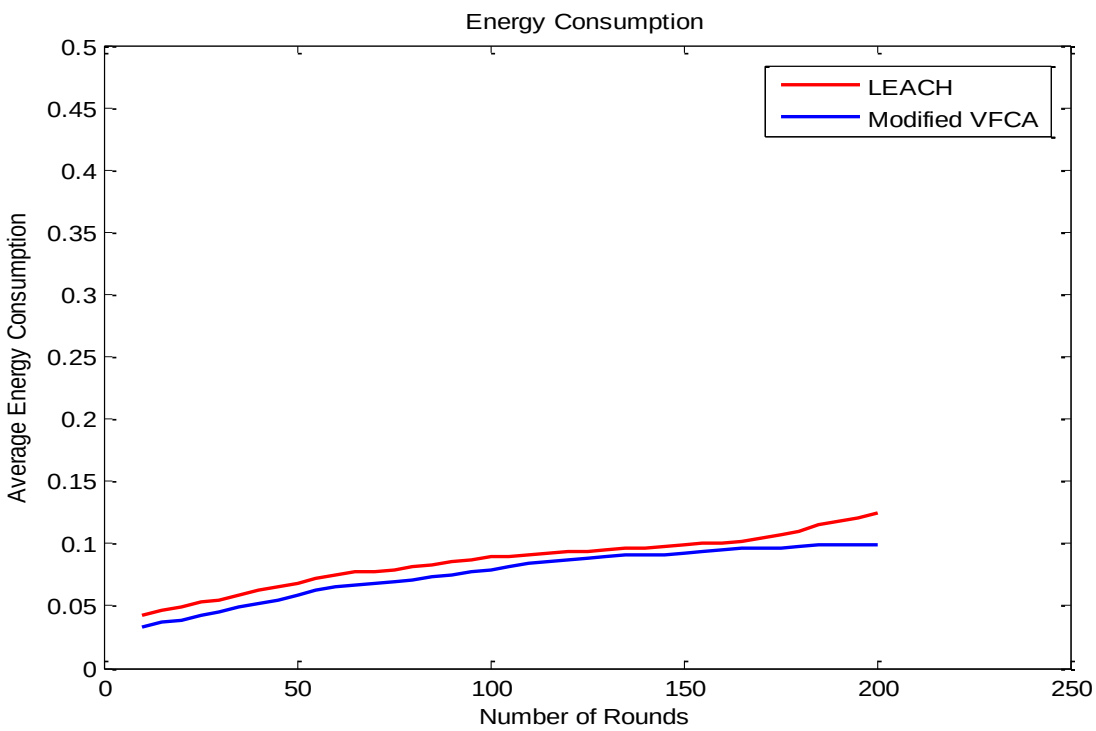

Figure 10. Average energy consumption for the network.

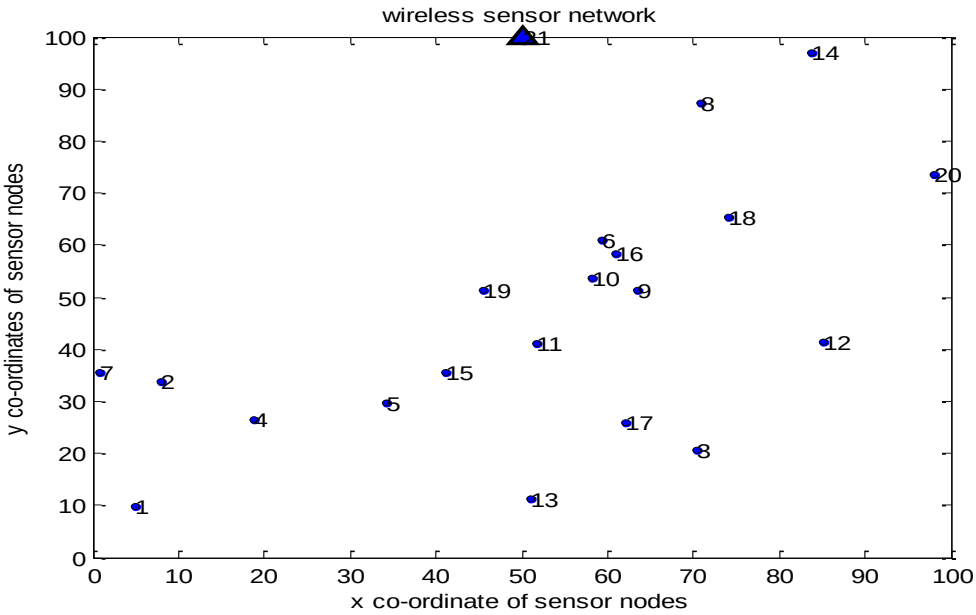

Figure 11. The nodes distribution over the sensed area.

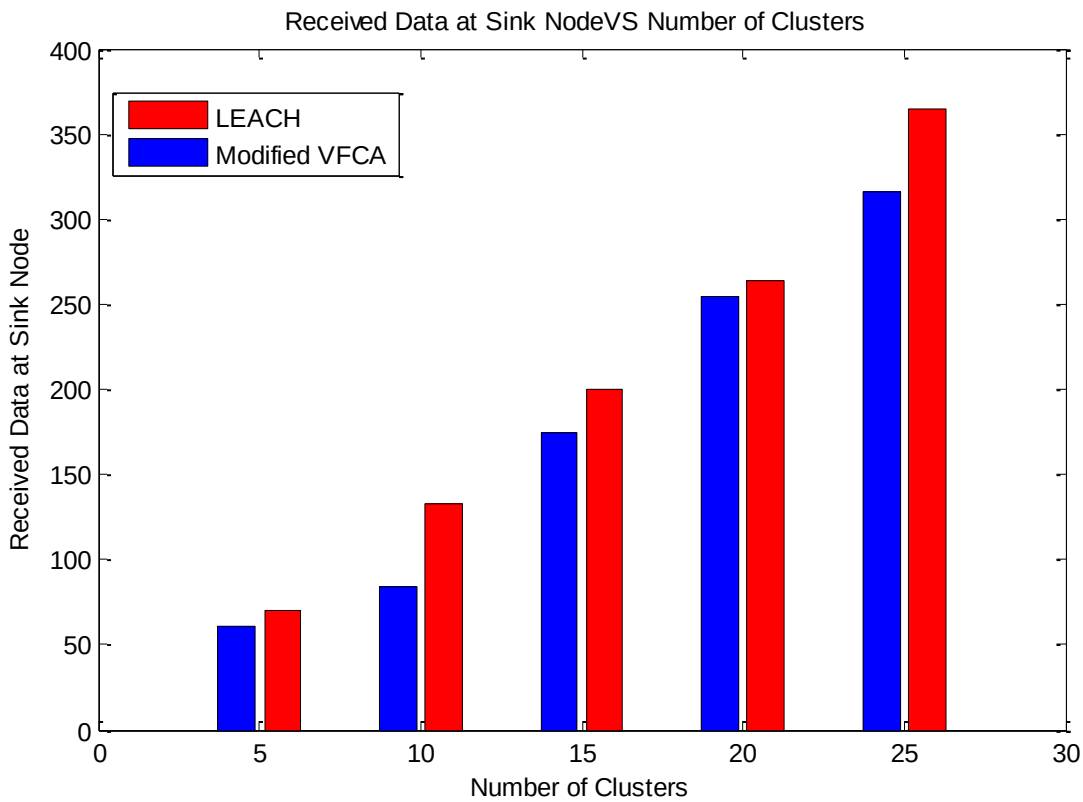

Figure 12. Received data at sink node vs number of clusters.

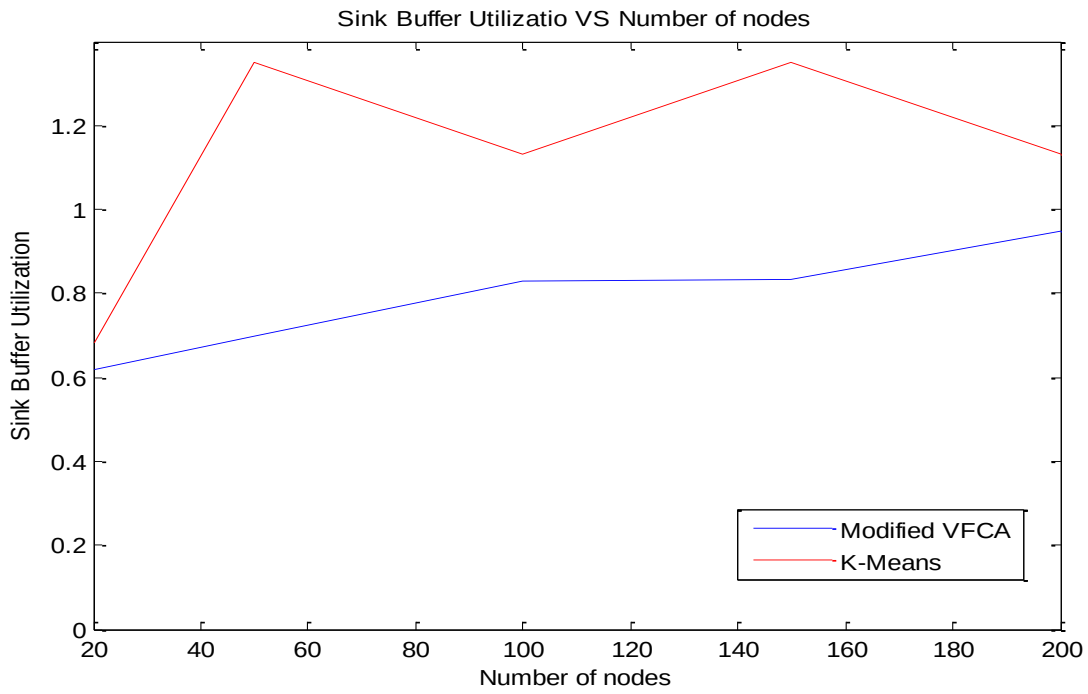

Figure 13. Buffer utilization of sink node vs number of nodes.

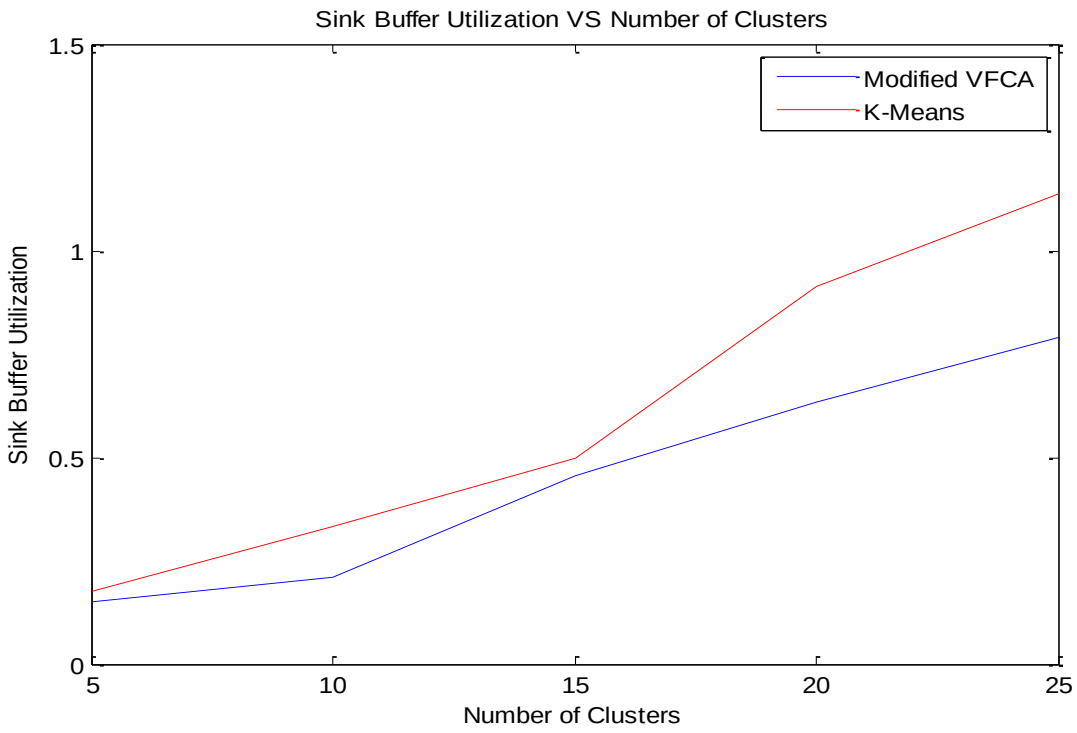

Figure 14. Buffer utilization of sink vs Number of clusters.

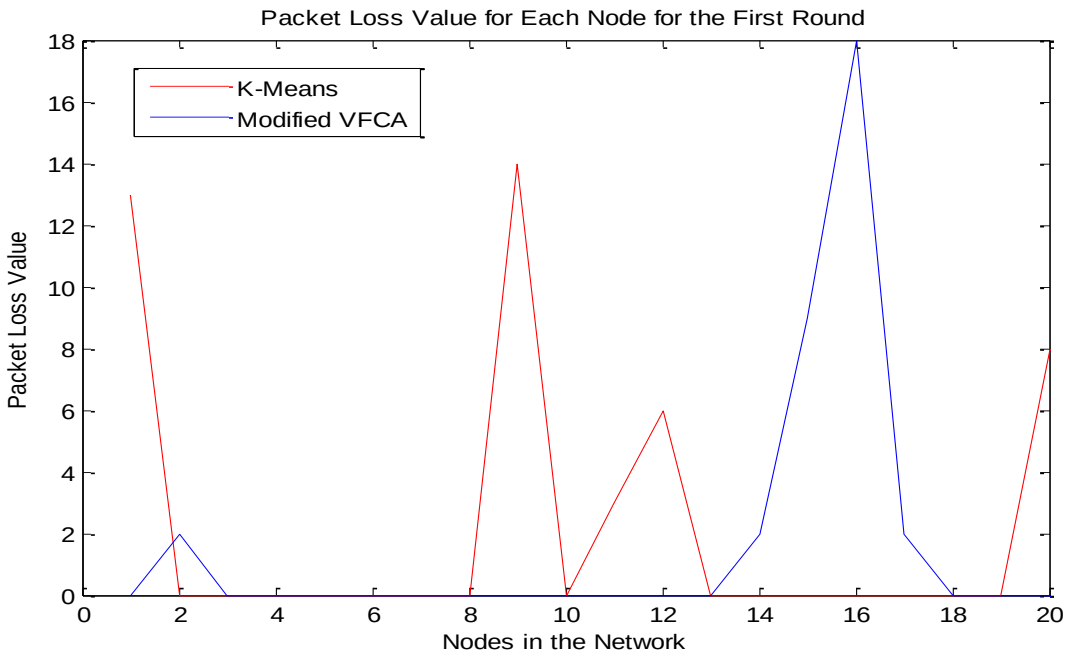

Figure 15. Packet loss value for each node in the network.

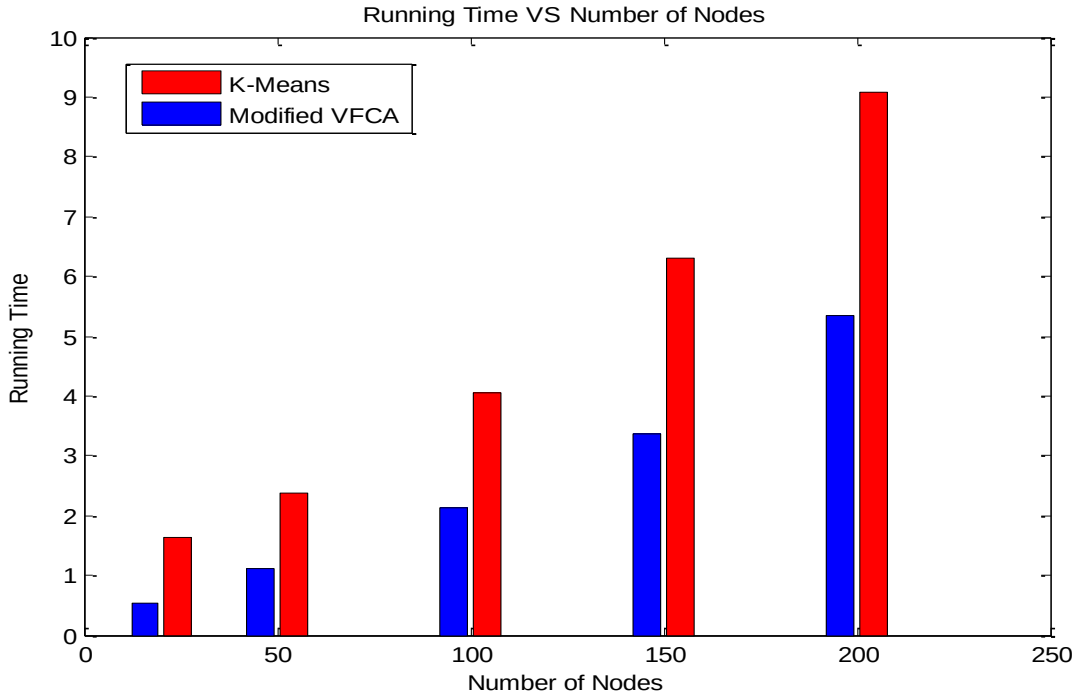

Figure 16. Running time vs number of nodes.

Table 1. The simulation parameters.

Parameter	Value
Network size	100mx100m
Number of nodes	n=100
Number of sinks	1
Behavior of nodes	Static
Base Station position	[50,100]
Number of clusters	k=5
Iteration steps	1000
Termination condition	0.00001
Buffer size of nodes	35 packet
Buffer size of sink	100 packet
Initial energy	100 nJ/bit
ETX=ERX	50nJ/bit

Table 2. Alive nodes in both LEACH and VFCA when every time increasing rounds (Network lifetime).

No. on Rounds	Alive nodes in LEACH	Alive Nodes in VFCA
100	100	100
200	100	100
300	100	100
400	100	100
500	100	100
600	100	100
700	100	100
800	100	100
900	100	100
1000	100	100
1100	100	100
1200	80	88
1300	23	70
1400	0	50
1500	0	0

Table 3. Received packets at sink node vs number of clusters.

Number of Clusters	Number of Received Packets at Sink Node (VFCA)	Number of Received Packets at Sink Node (K-Means)
5	61	70
10	84	133
15	175	200
20	254	264
25	316	365

Table 4. Buffer utilization in sink node vs number of nodes.

Number of nodes	Sink Buffer Utilization (VFCA)	Sink Buffer Utilization (K-Means)
20	0.6167	0.6833
50	0.7	1.35
100	0.83	1.133
150	0.8334	1.35
200	0.95	1.133

Table 5. Buffer utilization of the sink vs number of clusters.

Number of clusters	**Sink Buffer Utilization (VFCA)**	**Sink Buffer Utilization (K-Means)**
5	0.1525	*0.176*
10	0.21	*0.3325*
15	0.4575	*0.5*
20	0.635	*0.9125*
25	0.79	*1.1375*

Table 6. Packet loss value for each cluster head node.

Cluster head nodes		**Packet loss Value**
K-Means	Node 2 - cluster head of first cluster	13
	Node 9 - cluster head of second cluster	14
	Node 11 - cluster head of third cluster	3
	Node 12 - cluster head of fourth cluster	6
	Node 9 - cluster head of fifth cluster	8
Modified VFCA	Node 2 - cluster head of first cluster	2
	Node 2 - cluster head of first cluster	2
	Node 2 - cluster head of first cluster	9
	Node 2 - cluster head of first cluster	18
	Node 2 - cluster head of first cluster	2

Improved Automatic Registration Adjustment of Multi-source Remote Sensing Datasets

Rawaa Abdul Jabbar Mohammed
Engineer
College of Engineering - Diyala University
rrr_rys_1979@yahoo.com

Dr. Fanar Mansour Abed
Lecturer
College of Engineering- Baghdad University
fanar.mansou@coeng.uobaghdad.edu.iq

Dr. Loay Edwar George
Assistant professor
College of Science - Baghdad University
loayedwar57@yahoo.com

ABSTRACT

Registration techniques are still considered challenging tasks to remote sensing users, especially after enormous increase in the volume of remotely sensed data being acquired by an ever-growing number of earth observation sensors. This surge in use mandates the development of accurate and robust registration procedures that can handle these data with varying geometric and radiometric properties. This paper aims to develop the traditional registration scenarios to reduce discrepancies between registered datasets in two dimensions (2D) space for remote sensing images. This is achieved by designing a computer program written in Visual Basic language following two main stages: The first stage is a traditional registration process by defining a set of control point pairs using manual selection, then comput the parameters of global affine transformation model to match them and resample the images. The second stage included matching process refinement by determining the shift value in control points (CPs) location depending on radiometric similarity measure. Then shift map technique was adjusted to adjust the process using 2nd order polynomial transformation function. This function has chosen after conducting statistical analyses, comparing between the common transformation functions (similarity, affine, projection and 2nd order polynomial). The results showed that the developed approach reduced the root mean square error (RMSE) of registration process and decreasing the discrepancies between registered datasets with 60%, 57% and 48% respectively for each one of the three tested datasets.

key words: Remote Sensing, Registration, Matching, Similarity Measure, Adjustment.

تحسين عمليات تسجيل بيانات التحسس النائي آلياً

د. فنار منصور عبد
مدرس
كلية الهندسة- جامعة بغداد

د. لؤي ادورد جورج
استاذ مساعد
كلية العلوم- جامعة بغداد

رواء عبد الجبار محمد
مهندس
قسم الشؤون الهندسة- جامعة ديالى

الخلاصة

تقنية التسجيل لازالت تعتبر من المهام الصعبة لمستخدمي بيانات التحسس النائي خصوصا بعد الزيادة الهائلة بحجم البيانات المكتسبة من الاعداد المتزايدة والمطورة للمتحسسات وهذه الطفرة بحاجة لتطويروتحسين دقة وقوة خطوات التسجيل التي بامكانها التعامل مع هذه البيانات المختلفة الخصائص الراديومترية والهندسية . يهدف هذا البحث الى تطوير وتحسين عملية

التسجيل التقليدية لتقليل الفرق بين البيانات المسجلة في المجال الثنائي الابعاد لصور التحسس النائي. هذا يتحقق من خلال تصميم برنامج بلغة visual basic باتباع مرحلتين اساسيتين: الاولى هي القيام بعملية التسجيل بالطريقة التقليدية من خلال تحديد مجموعة من أزواج نقطة الضبط باستخدام الاختيار اليدوي، ثم حساب ثوابت موديل التحويل العالمي affine لمطابقة واعادة تشكيل الصور. المرحلة الثانية تتضمن عملية تحسين المطابقة بقياس مقدارالازاحة لمواقع نقاط الضبط بالاعتماد على قياس التشابه الراديومتري ومن ثم تم تحسين تقنية shift map لتحسين عملية التسجيل باستخدام دالة التحويل 2nd order polynomial والتي تم اختيارها بعد اجراء تحليل احصائي والمقارنة بين اكثر الدوال شيوعا . أظهرت النتائج أن النهج المطور خفض RMSE من عملية التسجيل وقلل الاختلاف بين مجموعة البيانات المسجلة بنسبة 60٪، 57٪ و 48٪ على التوالي لكل واحدة من مجموعة البيانات الثلاثة التي تم اختبارها.

الكلمات الرئيسية: التحسس النائي، تسجيل الصور، موائمة الصور، معامل التشابه، تصحيح الصور.

1. INTRODUCTION

Image registration is a process to determine the geometric transform that aligns points of a certain object in one view with the corresponding points of that object in another view to minimize position shifting errors. This process is often necessary for integrating information taken from different sensors, transponders, finding changes in images taken at different times, elevation or under different conditions. This is applied for model based object recognition and inferring three-dimensional information from images in which either the camera on satellite or the objects in the scene has moved **,Singhai, R., and Singhai, J., 2012.** Images registration remains challenging for several reasons. First, images are usually acquired using different sensor types, each having its inherent noise. Furthermore, radiometric as well as geometric properties of the same objects in the involved imageries might differ as a result of changes in the sensor view point, imaging methodology, imaging conditions (e.g., atmospheric changes, cloud coverage, and shadows), and spectral sensitivity of the implemented imaging systems (e.g., panchromatic, multi- and hyper-spectral imaging systems) **,Jensen, 1986. Jia, 2003.** Finally, the registration process can be complicated because of changes in object space caused by movements, deformations, and urban development between the epochs of capture associated with the involved images **,Martinez and Abad, 2000.**

In general, any image registration methodology must deal with four issues. First, the choice of primitives for the registration procedure. Then, establishing the registration transformation function that mathematically related the images under consideration. The third issue concerns the similarity measure which should be devised to ensure the correspondence of the conjugate primitives. Finally, after establishing the registration primitives, transformation function, and similarity measure, one should focus on how to establish the correspondence between conjugate primitives. Corresponding primitives in the reference and input images can be identified manually. The need for fast registration methods mandates the automation of the process of identifying conjugate primitives **,Alruzouq, R.I., 2004.** Therefore, a matching strategy has to be developed to manipulate the registration primitives, the transformation function, and the similarity measure to automatically establish the correspondence between conjugate primitives.

In this paper, a developed matching strategy is adopted to attain high accuracy for image registration process. There are several attempts to improve image registration. **,Wong, A., 2007.** presented an automatic registration method for remote-sensing images obtained at different times and/or from different sensors. The introduced method uses a set of features that are invariant to intensity mappings during the control-point matching process. He addressed global and local contrast issues associated with remotely sensed images and intensity-difference issues associated with multimodal registration of remotely sensed images. **,Wong, A., 2008.** referred that the error residue can be minimized by applying a combination of efficient globally exhaustive optimization techniques and subpixel-level locally optimization techniques. This combination can further improve robustness in situations with small initial overlap. **,Sang, L.,**

2010. introduced automatic coarse-to-fine image registration algorithm for satellite images, based on Haar Wavelet Transform (HWT) and the Speeded Up Robust Features (SURF) algorithm in the coarse registration. He used the normalized cross-correlation and Random Sample Consensus (RANSAC) algorithm to achieve fine registration. However, **,Gang, H. and Yun, 2008.** introduced image registration technique, which is based on wavelet-based feature extraction technique, a normalized cross-correlation matching and relaxation-based image matching techniques. On the other hand, **,Fatiha, M. et al., 2010.** presented an efficient image registration algorithm that is based on using genetic algorithms and the cross-correlation similarity measure for matching within a multi-resolution framework based on the Non-Subsampled Contourlet Transform (NSCT).

In this paper, a developed image registration of remote sensing images was presented, based on two main steps; first steps is traditional registration using manually selection of control points and global affine transformation model to match them and second stage; matching process refinement by determining a shift map using 2nd order polynomial transformation function. Whereas the shift values were calculated for CPs by applying radiometric similarity measure. The remainder of this paper was organized as follows; data sets and study sits used was described in section two. The methodology was discussed in detail in section three; the obtained results were presented in details in section four and conclusions discussed in section five.

2. STUDY SITES AND DATA SETS

Three sets of remote sensing data have been derived from Digital Globe and used in this research. The utilized datasets can be divided into two categories; data from different passive panchromatic sensors and data from active LiDAR systems. Then data from passive sensors include Spot satellite image and Quick Bird panchromatic image, as shown in **Fig. 1.a** and **Fig. 1.b** respectively. Both acquired over Ramadi city and they are having 2.5 m and 0.6 m spatial resolution respectively. In this test set, a rural area was used to test adjusted process capability of making more accurate registration process. The size of images (a) is 2501 x 2698 pixels, and the size of image (b) is 1259 x 1545 pixels. The second set data was Panchromatic image from Ikonos satellite as shown in **Fig.2.a** and the corresponding panchromatic image from Quick Bird satellite as shown in **Fig. 2.b**. Both acquired over Baghdad city; they have 1.0 m and 0.6 m spatial resolution respectively. In this test set, an urban area was used to test the method capability of registering data of dense area, the size of image (a) is 1492 x 1508 pixels and the size of image (b) is 1288 x 1501 pixels. Third test data was LiDAR data sets over Niagara city in USA acquired with 1km flying height and delivered as LAS data format from the Finnish terrasolid company (www.Terrasolid.com) for training purposes. Laser point clouds data sets of two overlapping flight lines are shown in **Fig. 3.a** and **3.b** respectively.

3.METHODOLOGY

A developed registration technique for different remote sensing data source are critically needed, because an enormous increase in the volume of remote sensing data being acquired by an ever-growing number of earth observation sensors. In this section, the developed methodology of the adjusted registration process is presented including the traditional registration process, the statistical analyses, and the refinement of images matching process by shift map using 2nd order polynomial for satellite images and LIDAR data are presented as shown in **Fig .4**

3.1 Transform the 3D LiDAR Data into 2D Images

LiDAR data is 3D digital representation of the scanned features. It has transformed into two dimension images using QTM software for next registration process steps. This is achieved

by generating digital surface model, interpolate the surface and export the surface as 2-D images as shown in **Fig .5**
The LAS files containing the LiDAR data points which require further manipulation to generate a DSM.

3.1.1 Grid size for digital surface models

Before generating any LiDAR derived Digital Surface Model (DSM), selection of grid size for DSM raster layer is crucial for minimizing the data loss during conversion **,Kumar V., 2012.** The optimized DSM resolution must match the density of LiDAR data and should able to reflect the variability of the terrain surface to represent the majority of terrain features. **,Liu, 2008. and ,McCullagh, 1988.** suggested that the number of grids should be roughly equivalent to the number of LiDAR points in the covered area. The grid resolution (S) of a DSM can be estimated using Eq. (1) ,**Hu et al., 2003.**

$$S = \sqrt{\frac{A}{n}} \quad (1)$$

where n is the number of terrain points and A is the covered area. This means that the DSM resolution should match the sampling density of the original terrain points.

3.1.2 Model selection

The points used to generate surfaces by different model selections have been developed to represent surfaces: regular grid (usually square grid); triangular irregular network (TIN); and contour line model. However, it introduces discontinuity in representation of the terrain surfaces due to same elevation value. This effect is minimized by the high density characteristic of LiDAR data **,Liu, 2008.**
The simplest way to generate a closed surface from the point cloud is by triangulation process, and it is a method used in QT Modeler software v.5.1.5, where every three adjacent 3D points combine to form a triangular surface element. Delaunay triangulation offers an appropriate method of creating such a triangular mesh. This identifies groups of three neighboring points whose maximum inscribed which circle does not include any other surface point. Each triangle can be defined as a plane in space using Eq. (2) and the result is a polyhedron representation or wire model of the surface. There is normally has no topological relation between the 3D points. Differential area elements must be established between adjacent points in order to generate a topologically closed surface which enables further processing as a surface description. All 3D points on the plane are defined by the following equation:

$$a(x - x_0) + b(y - y_0) + c(z - z_0) = 0 \quad (2)$$

where:
x,y, z are the coordinates of each point.
x_0,y_0, z_0 are the coordinate of the origin point.

3.1.3 DSM interpolation

Interpolation is the process of predicting the values of certain variable using their neighboring values. It is assumed that a terrain surface is continuous and that a high correlation exists between the neighboring data points. Interpolation methods are classified into deterministic such as Inverse Distance Weighted (IDW) and spline-based and geostatistic such as Kriging. **,Liu, 2008.** found there is no single interpolation method that is the most accurate one in all cases.

After DSM is created, the surface is exported as two dimensions (image) as 24-bit intensity color – TIF format. This process delivers two images for Niagara city ready for insertion to the developed registration program.

3.2 Comparison between Common Transformation Methods

In order to assess the accuracy of the selected transformation methods, polynomial, affine, conformal and projection methods, a set of selected distinct feature points extracted from datasets have been tested and validated statistically. The analysis aimed to investigate the deviation of the mean values between CPs in the overlapping region delivered from each method individually. This allows for inspection of discrepancies between individual feature points in the overlapping regions in both reference and sensed images after transformation. In order to compare between the four transformation methods, (30) feature points from sensed and reference images were selected and the parameters of the transformation function for each method were calculated using least square criterion as shown in **Table .1** The coordinates of the control points belong to the sensed image are mapped to the coordinate system of the reference image. After the determination of transformation function coefficients, optimization method was applied that is based on statistical bases to adjust the geometric errors. T-test statistical method is used to compare the matched pairs of the coordinates.

Before this analysis, we must check the comparative dataset variances using F-test. Testing means and variances of the discrepancies between the selected feature points from both matched pairs are translated by P-values indicators to show the accuracy and the degree of confidence of matching process. All these statistical analysis should be applied after testing the degree of confidence of how well these data are normally distributed and fitted with the normal distribution curve. This is an essential step to make sure that the statistical hypothesis and the delivered results are valid for the current datasets. These tests determine the appropriateness of accepting or rejecting the null hypothesis which assumes the data are similar and perfectly matched based on P-value reports. If the p-value of a statistical test is less than 0.05, we reject the null hypothesis. From the T-test results shown in **Table .2** it can be realized that the 2nd order polynomial transformation method is the best transformation function to use with our current datasets. Following these results, this function was used in the developed images registration process to correct the geometric shift.

3.3 Images Registration Process

In this stage, the traditional registration process is conducted and it is consists of four steps; manual selection of CPs, transformation function, similarity measurement, and matching with resample image registration.

3.3.1 Manual feature extraction and selection

Choosing points of interest within the image pixel space is not an easy task, because we need to easily identify significant and distinct high-level features such as line intersections, road crossings, centroids of water regions, oil and gas pads, high variance points, local curvature discontinuities, curve inflection points, most distinctive points of similarity measure, etc. ., which are possibly uniformly spread over the images and easily detectable, as shown in **Fig. 6, 7, and 8.**

3.3.2 Two-dimensional transformation method

Two-dimensional (2D) transformation is transforming the coordinates of points in one rectangular system (x, y) into coordinates in another rectangular system (X, Y) **,Deakin, 2004.**

After the feature correspondence has been established, the mapping function is constructed. It should transform the sensed image to overlay it over the reference one. The CP from the sensed image that the corresponding CP from reference images should be as close as possible after the sensed image transformation is employed in the mapping function design. The task in this stage consists of choosing the type of the mapping function and its parameter estimation. The most fundamental characteristic of any image registration technique is the type of spatial transformation or mapping needed to properly overlay two images. Although many types of distortion may be present in each image, the registration technique must select the class of transformation which will remove only the spatial distortions between images due to differences in acquisition and not due to differences in scene characteristics to be detected. The primary general transformations are affine, projective, conformal, and high order polynomial. These are all well-defined mappings of one image into another **,Brown, 1992. and ,Zitova and Flusser, 2003.** In this research affine transformation has used in the first stage (traditional registration) as shown its parameters in **Table. 3,4 and 5.** sequentially for each one of the three tested datasets and 2nd order polynomial transformation has used in the second stage (adjusted registration) as shown its parameters in **Table 6.** for the three tested datasets.

A. Affine Transformation

Affine transformation is also used for the mapping of two coordinate systems in 2D plane. This 6-parameter transformation defines two displacements, one rotation, and two separate scaling factors as shown in **Fig. 9.**

For a point P in the source system, the XY coordinates in the target system are given by Eq. 3 and 4. **,Ghosh, 1979. and ,Luhmann et al., 2011.**

$$X = a_0 + a_1 x + a_2 y \quad (3)$$
$$Y = b_0 + b_1 x + b_2 y \quad (4)$$

or in non-linear form with $a_0 = X_0$ and $b_0 = Y_0$ as

$$X = X_0 + m_X x \cos\alpha - m_y y \sin(\alpha + \beta) \quad (5)$$
$$Y = b_0 + m_X x \sin\alpha + m_y y \cos(\alpha + \beta) \quad (6)$$

The parameters a_0 and b_0 (X_0 and Y_0) define the displacement of the origin, α and β are the rotation angle, and m_X, m_y are the scaling factors for x and y.

In order to determine the six coefficients a minimum of three identical points is required in both systems. With more than three identical points, the transformation parameters can be calculated by over-determined least-squares adjustment.

In matrix notation, the affine transformation can be written as:

$$X = Ax + a \quad (7)$$

$$\begin{bmatrix} X \\ Y \end{bmatrix} = \begin{bmatrix} a_1 & -b_1 \\ b_1 & a_1 \end{bmatrix} \begin{bmatrix} x \\ y \end{bmatrix} + \begin{bmatrix} a_0 \\ b_0 \end{bmatrix} \quad (8)$$

or

$$\begin{bmatrix} X \\ Y \end{bmatrix} = \begin{bmatrix} m_X x\, cos\alpha & -m_y y \sin(\alpha+\beta) \\ m_X x\, sin\alpha & m_y y\, cos(\alpha+\beta) \end{bmatrix} \begin{bmatrix} x \\ y \end{bmatrix} + \begin{bmatrix} X_0 \\ Y_0 \end{bmatrix} \quad (9)$$

A is the affine transformation matrix. For lightly rotated and sheared systems the parameter $a_1$corresponds to the scaling factor m_X and the parameter b_1 to the scaling factor m_y.

B. Polynomial Transformation

Non-linear deformations can be described by polynomials of degree (n), **Fig. 10** shown the Plane polynomial transformations process. In general, the transformation model can be written as **,Ghosh, 1979. ,Luhmann et al., 2011.**

$$X = \sum_{j=0}^{n} \sum_{i=0}^{j} a_{ji}\, x^{j-i} y^{i} \quad (10)$$

$$Y = \sum_{j=0}^{n} \sum_{i=0}^{j} b_{ji}\, x^{j-i} y^{i} \quad (11)$$

where n is degree of polynomial. A polynomial of n=2 are given by:

$$X = a_{00} + a_{10}x + a_{11}y + a_{20}x^2 + a_{21}xy + a_{22}y^2 \quad (12)$$

$$Y = b_{00} + b_{10}x + b_{11}y + b_{20}x^2 + b_{21}xy + b_{22}y^2 \quad (13)$$

The polynomial of n=1 is identical to the affine transformation Eq. (3) and (4). In general, the number of coefficients required to define a polynomial transformation of degree n is:
u = (n+1) (n+2) and in order to determine the u coefficients, a minimum of u/2 identical points is required in both systems.

3.3.3 Least squares adjustment

The least squares Gauss-Markov adjustment model is based on the idea that the unknown parameters are estimated with maximum probability. Assuming a data set with an infinite number of measured values and normally distributed errors, the following condition for the residuals results should be used **,Luhmann et al., 2011.** The sum of the squares of the residuals must be minimized. Eq. (14) expresses the fundamental principle of least squares **,Charles and Paulr, 2006.**

$$\sum v^2 = v_1^2 + v_2^2 + \cdots + v_n^2 = minimum \quad (14)$$

The following subsections present the matrix methods used in performing a least squares adjustment for the matrix expressions, an analogy will be made with the systematic procedures let a system of observation equations be represented by the matrix notation **,Charles and Paulr, 2006.**

$$AX = L + V \quad (15)$$

Where

$$A = \begin{bmatrix} a_{11} & a_{12} & \dots & a_{1n} \\ a_{21} & a_{22} & \dots & a_{2a} \\ \vdots & \vdots & \vdots & \vdots \\ a_{m1} & a_{m2} & \dots & a_{mn} \end{bmatrix}$$

$$X = \begin{bmatrix} x_1 \\ x_2 \\ \vdots \\ x_n \end{bmatrix} \qquad L = \begin{bmatrix} l_1 \\ l_2 \\ \vdots \\ l_m \end{bmatrix} \qquad V = \begin{bmatrix} v_1 \\ v_2 \\ \vdots \\ v_m \end{bmatrix}$$

$x_1, x_2, \ldots\ldots\ldots x_n$ are the unknowns
$a_{11}, a_{12,} \ldots\ldots a_{1n}$ are the coefficients of the unknowns

$$A^{\mathrm{T}}AX = A^{\mathrm{T}}L \quad \ldots\ldots\ldots\ldots\ldots\ldots\ldots\ldots\ldots\ldots\ldots \text{(16a)}$$

Eq. (16a) can also be expressed as

$$NX = A^{\mathrm{T}}L \quad \ldots\ldots\ldots\ldots\ldots\ldots\ldots\ldots\ldots\ldots\ldots\ldots \text{(16b)}$$

Eq. (16a) and (16b) produce the normal equations of a least squares adjustment. By inspection, it can also be seen that the N matrix is always symmetric $(i.e\ldots, n_{ij} = n_{ji})$. By employing matrix algebra, the solution of normal equations such as Eq. (16a) is:

$$X = (A^{\mathrm{T}}A)^{-1}A^{\mathrm{T}}L = N^{-1}A^{\mathrm{T}}L \qquad (17)$$

3.3.4 Measuring similarity for image registration

Similarity measures are used to register images by finding an accurate match between an input image and transformed versions of the reference image. The two types of the similarity measuring techniques are geometric and radiometric similarity measuring discussed in **,Brown, 1992.** The similarity measuring used in this research is geometric to measure the degree of matching images in the first stage (traditional registration) and radiometric similarity measuring to determine the discrepancies in Corresponding CPs in the second stage (refine the registration process).

A geometric similarity measure is mathematically describes the fact that conjugate primitives should coincide with each other after application of the proper registration transformation function. Geometric similarity measure depends on the selected registration primitive (e.g., points, linear features, areal regions) as well as the registration transformation function (e.g., 2-D similarity or affine transformation) is expressed as follows **,Habib et al., 2001.**

$$x_r - f_{g_x}(x_i, y_i) = 0 \qquad (18)$$

$$y_r - f_{g_y}(x_i, y_i) = 0 \qquad (19)$$

where f_{g_x} & f_{g_y} represent the registration transformation function. For affine function, the geometric similarity measure is described as follows **,Habib et al., 2001.**

$$x_r - a_0 - a_1 x_i - a_2 y_i = 0 \qquad (20)$$

$$y_r - b_0 - b_1 x_i - b_2 y_i = 0 \qquad (21)$$

Excluding mismatches is one of the tasks connected to image matching. One possibility of how to avoid some of outliers in matching is by setting thresholds for similarity measures. After measuring the amount of similarity measure between the points in the reference and sensed image, the points that have large values have been rejected (at least of similarity) by threshold. An outlier is an observation point that is distant from other observations, as shown in **Fig. 11**
At least, similarities values are not always outliers because they may not be unusually far from other observations. Therefore, the threshold determines the acceptance or rejection of the points and the values larger than these are points of unaccepted similarity and which must be rejected which considered as outliers later on. Using the threshold similarity measures is so needed to excluding the false matches.

3.3.5 Matching strategy

In photogrammetric and remote sensing, matching can be defined as the establishment of the correspondence between various data sets. The matching problem is also referred to as the correspondence problem. The datasets involved in matching might include images, maps and GIS data. Image matching process is an important and prerequisite step for many applications, such as image registration, image orientation, DEM generation, orthorectification, data fusion and relative orientation. Matching strategy refers to the concept or overall scheme of the solution of the matching problem **,Schenk, 1999.** It encompasses the selected primitives, transformation functions and similarity measures for solving the registration problems automatically.

3.3.6 Images re-sampling techniques

Image re-sampling is a process by which new pixel values are interpolated from existing pixel values whenever the raster's structure is modified such as during projection, datum transformation, or cell resizing operations **,Wade and Sommer, 2006.**
Bilinear filtering is a method used to smooth out when the images are displayed larger or smaller than they actually are. Bilinear filtering uses points to perform bilinear interpolation. This is done by interpolating between the pixels nearest to the point that best represents that pixel. Bilinear re-sampling interpolation takes a weighted average of pixels in the original image nearest to the new pixel location. The averaging process alters the original pixel values and creates entirely new digital values in the output image **,Santhosh et al., 2010**.

3.4 The Registration Adjustment Following Images Matching Process

After establishing the registration primitives, transformation function, similarity measure, and matching scenario, the second stage is due in order to adjusted matching strategy that has been developed to manipulate the registration primitives, the transformation function, and the similarity measure.
In this stage, the matching strategy has been developed by determining the shift value of CPs through dependence on concept of radiometric similarity measure and using shift map for adjusting matching process using 2nd order polynomial transformation.
Radiometric similarity measure describes the degree of similarity between the gray level distribution functions at the vicinity of the selected point. Small windows composed of gray values serve as primitive points where the center pixel of the window can be used for the definition of the location of a point **,Habib et al., 2001.**
An image patch cut from one image, so called template, is searched in the second image. The template consists of m x n pixels, mostly m=n. The position of the template is referred to as the central pixel that is why m and n are odd numbers. The template is compared with patches of

the same size in the second image. An approximate position of the corresponding point in the second image can be derived (e.g. when approximations of orientation parameters of two overlapping images are known). The comparison is then restricted to an area called a search area or window. Geometric distortions caused by relief and different orientation of images will influence the matching of large templates, and in order to get acceptable results, a size of the template has to be small, therefore a template of 3x3 pixel size has been selected. However, the size of the search window depends on how precise it is located. Whereas a search window of 7x7 pixel size was used. A value of a similarity measure is calculated at each position of the template within the search window.

Depending on the similarity measure, a corresponding point to the center of the template is assumed to be in the position where maximal value of the similarity measure is obtained.

The sum of absolute differences (SAD) is used which is a known criteria for similarity measure. These criteria represent a quantitative measure of how well conjugate points correspond to each other.

In digital image processing, the sum of absolute differences, defined in Eq. (22) as shown in **,Ulysses and Conci, 2010. ,Richardson and Iain, 2003.** works by taking the absolute value of the difference between each pixel in the template of original image (I_1) and the corresponding pixel in the matching window of transformed image for comparison (I_2) as shown in **Fig. 12** These differences are summed to get the similarity value of center point in matching window, with each move of the matching window inside the search window, the sum absolute difference between template and match window has been determined. The position where the sum absolute difference reaches its lowest value represents more similar point and its position achieves the best match /fit.

$$SAD = \sum_{(i,j \in U)} | I_1(x+i, y+j) - I_2(x+dx+i, y+dy+j) | \quad (22)$$

A new representation of the shift map operation is described by using second order polynomial to improve matching strategy. After determining the more similar point to CPs, we calculate the shift value for them in both X-axis and Y-axis, then calculate the parameter of polynomial transformation function use Eq. (23) and (24), thereafter determine the shift value of each pixel in transformed image by 2nd order polynomial transformation function. Finally, the shift map (is the relative shift of every pixel in the output image from its source in an input image) was used to apply the geometric rearrangement of the transformed image. The relationship between an input image I (x, y) and an output image B(u, v) in image rearrangement and retargeting is defined by a shift-map M(u, v) = (t_x, t_y) as shown in **Fig.13**. The output pixel B (u, v) will be derived from the input pixel I (x + t_x , y + t_y).and the 2nd order polynomial can be expressed as shown below:

$$\Delta X = a_{00} + a_{10}x + a_{11}y + a_{20}x^2 + a_{21}xy + a_{22}y^2 \quad (23)$$

$$\Delta Y = b_{00} + b_{10}x + b_{11}y + b_{20}x^2 + b_{21}xy + b_{22}y^2 \quad (24)$$

where

xy : are the coordinates in the transformed image system

ΔX ΔY : are the shifts magnitudes

a_{00} ... b_{00}.. : are the transformation coefficients

4. RESULTS

To evaluate the accuracy of the proposed registration approach, the Root Mean Square Error RMSE was calculated to determine the quality of the developed registration process **,Congalton, 2009.**

$$RMSE = \sqrt{\frac{1}{N}\sum_{i=1}^{n}((X_i - X_i')^2 + (Y_i - Y_i')^2)} \quad (25)$$

where N is the total number of matched control points, the (X_i , Y_i) are coordinates of control points in the reference image, and the (X_i', Y_i') are the estimated coordinates of the corresponding point in the sensed image based on the transformation model.

The RMSE results of the developed approach (second stage), compared with the traditional registration (first stage), are shown in **Table 7.** It can be observed that image registration using the adjusted registration process results has a lower RMSE values than traditional registration by around 60%, 57% and 48% sequentially for each one of the three tested datasets. Furthermore, the visual results of the three data sets of multi-source (Ikonos, Spot, Quick bird satellite image and LiDAR images) are shown in **Fig 14, 15, 16 and 17**. Based on the visual inspection, it can be seen that results of adjusted registration are more accurate and valid for all datasets.

5. CONCLUSIONS

- The adjusted registration method refined the traditional registration and gives less RMSE of matching from many pixels in the traditional registration to fewer pixels in the adjusted registration, percentage 60%, 57% and 48% sequentially for each one of the three dataset use in this paper.
- The developed registration method is more accuracy and efficiency than selection of the CPs manually, because this method reduces the Local error (displacement of the CPs coordinates) therefore we found more refinement when comparing with feature selection manually.
- From the applied statistical tests on the common transformation methods (affine, polynomial, projective and conformal), the results showed that the 2nd order polynomial function is more accurate and more appropriate to use in matching and registration process to correct geometric distortion.
- The registration for LiDAR images is more accuracy than the registration for satellite images and this was clear in the first stages of registration process, and this is due to the high accuracy for LiDAR system and the LiDAR images are comes from the same sensor while the satellite images comes from different sensor (this images was used in dataset in this research).

REFERENCES

- Alruzouq, R.I., 2004, *Semi-Automatic Registration of Multi-Source Satellite Imagery with Varying Geometric Resolutions*. Department of Geomatics Engineering, University of Calgary, Canada.

- Bartoli, G., 2007, *Image Registration Techniques*, Universit_a degli Studi di Siena, Visual Information Processing and Protection Group.

- Brown, L., 1992, *A survey of image registration techniques*, ACM Computing Surveys 24(4): 325-376.

- Charles D. Ghilani and Paulr R.Wolf, 2006, *Adjustment Computation Spatial Data Analysis*, fourth edition, published by John Wiley and Soons, Inc., Hoboken, New Jersey and Canada.

- Congalton R.G and K. Green, 2009, *Assessing The Accuracy of Remotely Sensed Data*, principles and practices.

- Deakin, R.E. 2004, *The standard and Abridged Molodensky Coordinate Transformation Formulae*, Department of Mathematical and Geospatial Sciences, RMIT University pp.121.

- Fatiha, M., Miloud, El.M. and Nasreddine, T., 2010, *A rigid image registration based on the Nonsubsampled Contourlet transform and genetic algorithms*, Sensors 2010, 10, 8553-8571, doi: 10.3390/s100908553.

- Gang, H. and Yun, Z., 2008, *Wavelet-based image registration technique for high resolution remote sensing images*, Computers & Geosciences 34.1708–1720.

- Ghosh, S. K., 1979, *Analytical Photogrammetry*, Pergamon Press, New York, 203 pp.

- Habib, A., Lee, Y. and Morgan, M., 2001, *Surface matching and change detection using modified iterative Hough transform for robust parameter estimation*, Photogrammetric Record, 17 (98): 303-315.

- Hu, J., et al. 2003, *Approaches to large-scale urban modeling*, Computer Graphics and Applications, IEEE, 23(6), 62-69.

- Jensen, R. J (1986), *Introductory Digital Image Processing*, pp (234-258), Prentice-Hall, New Jersey.

- Jia, X. (2003) *On error correction and accuracy assessment of satellite imagery registration* journal of the Australian map circle inc

- *Kumar V., 2012, Forest Inventory Parameters and Carbon Mapping From Airborne LiDAR*, Geo-Information Science and Earth Observation of the University of Twente.

- Liu, X. 2008, *Airborne LiDAR for DEM Generation: Some Critical Issues*, [Electronic version]. Progress in Physical Geography, 32(1), 31-49.

- Luhmann, T.,Robson,S., Kyle,S. and Harley, I., 2011, *Close Range Photogrammetry, Principles, techniques and applications*. Whittles Publishing, Dunbeath, Caithness KW66EG, Scotland, UK. www.whittlespublishing.com.

- Martinez, A., Abad, F.J. (2000), *Remote Sensing Image Rectification in an Automatic Way*, Remote Sensing in the 21st.century.

- McCullagh, M., 1988, *Terrain and surface modelling systems: theory and practice*, The photogrammetric record, 12(72), 747-779.

- Richardson, E. G., Iain, 2003, *H.264 and MPEG-4 Video Compression: Video Coding for Next-generation Multimedia*. Chichester: John Wiley & Sons Ltd.

- Sang, L., 2010, *A coarse-to-fine approach for remote-sensing image registration based on a Local method*, International Journal on Smart Sensing and Intelligent Systems Vol. 3, No. 4.

- Santhosh Baboo1, S., Renuka Devi2, M., Keith T. Weber, 2010, *An Analysis of Different Resampling Methods in Coimbatore, District*. Global Journal of Computer and Technology vol. 10 Issue15 (ver.1.0).

- Schenk, T., 1999, *Digital photogrammetry*, TerraScience.

- Singhai, R. and Singhai, J., 2012, *Registration of Satellite Imagery Using Genetic Algorithm* ,Proceedings of the World Congress on Engineering 2012 Vol II WCE 2012, July 4 - 6, 2012, London, U.K.

- Ulysses, J. N. and Conci, A., 2010, *Measuring Similarity in Medical Registration*, IWSSIP 2010-17th International Conference on Systems, Signals and Image Processing.

- Wade, T., and Sommer, S., 2006. *A to Z GIS. Redlands*: ESRI Press.

- Wong, A., 2008, *Efficient FFT-Accelerated Approach to Invariant Optical-LIDAR Registration*. IEEE Transactions on Geoscience and Remote Sensing.

- Wong, A., 2007, *ARRSI: Automatic Registration of Remote-Sensing Images*, IEEE Transactions on Geoscience and Remote Sensing, vol.45, no.5.

- Zitova, B. and Flusser, J., 2003, *Image registration methods: a survey*, Image and Vision Computing 977–1000.

Table 1. The parameters of common transformation methods**.**

Parameter of transformation	Transformation function			
	Polynomial	Affine	Projective	Conformal
a1	290.4499	285.7838	0.5335	0.5469
a2	0.5328	0.5413	-0.0033	-0.0003
a3	-0.0103	-0.0014	287.6293	
a4	0.0000		-0.0037	
a5	0.0000			
a6	0.0000			
b1	40.1580	38.2148	0.5441	280.7047
b2	-0.0059	-0.0015	40.1622	38.7970

b3	0.5474	0.5492	-0.0000	
b4	0.0000		-0.0000	
b5	0.0000			
b6	-0.0000			

Table 2. Statistical test (P-value) for transformation Functions.

Statistic test of Transformation Function (P-value)					
data set	function	Normality test		Test for two Variances F-test	Test for two samples (T)
		P-value for CPs of the input image after registration	P-value for CPs of the reference image		
From Satellite images	Affine	0.080	0.080	0.996	0.998
	Projective	0.081		0.998	0.997
	Similarity	0.069		0.971	0.995
	Polynomial	0.077		0.998	0.999

Table 3. List of determined parameters of the affine transformation function for the first test set after rejection of the outlier CPs.

	After 1st try
a0	712.710143485467
a1	0.938865715880
a2	0.054032096416
b0	139.791791952421
b1	-0.055409236370
b2	0.938147043380

Table 4. List of determined parameters of the affine transformation function for the second test data.

	1st try	2nd try	3rd try
a0	274.754234133331	277.989788041552	279.8225439838
a1	0.553534903583065	0.550614983484924	0.54683422990834
a2	3.79930994934679E-03	5.37154906337874E-04	7.89680002129255E-04
b0	36.5435927227175	35.8653071871626	36.2180616016215
b1	1.12075860510604E-04	7.24193483558933E-04	-3.49615769592351E-06
b2	0.549094685011655	0.549094685011655	0.549827151117229

Table 5. List of determined parameters of the affine transformation function for the third test data LiDAR.

	1st try
a0	19.2314384309789
a1	0.998351120839234
a2	2.31913326432581E-02
b0	360.118951765439
b1	-6.74618282949926E-03

b2	1.0064727707664

Table 6. List of determined parameters of the 2nd order polynomial transformation for second stage of adjusted registration.

	first test	second test	third test
a0	2.18282	-0.95978	87.33501
a1	-0.00148	0.00379	-0.28481
a2	-0.00651	-0.00085	-0.01376
a3	0.00000	-0.00001	0.00001
a4	0.00000	0.00000	0.00025
a5	0.00000	0.00000	0.00000
b0	-3.50464	-0.31758	-151.91735
b1	0.0072	-0.001	0.58212
b2	0.0021	-0.00044	0.00378
b3	0.00000	-0.00001	0.00001
b4	0.00000	0.00000	-0.00057
b5	0.00000	0.00001	0.00000

Table 7. RMSE values of the manual/classical and the developed methods.

Classical Registration				The proposed approach
Data set	Source data	No. of points of manual selection	RMSE(pixel) For first stage	RMSE(pixel) For second stage
First test	Satellite images	43	2.323	0.932
Second test	Satellite images	35	3.653	1.564
Third test	LiDAR images	14	1.871	0.987

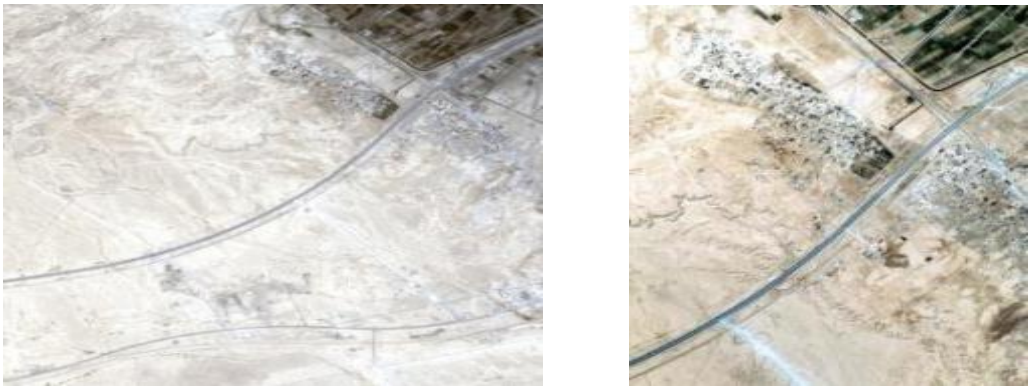

(a) **(b)**

Figure 1. Spot and Quick Bird satellite images.

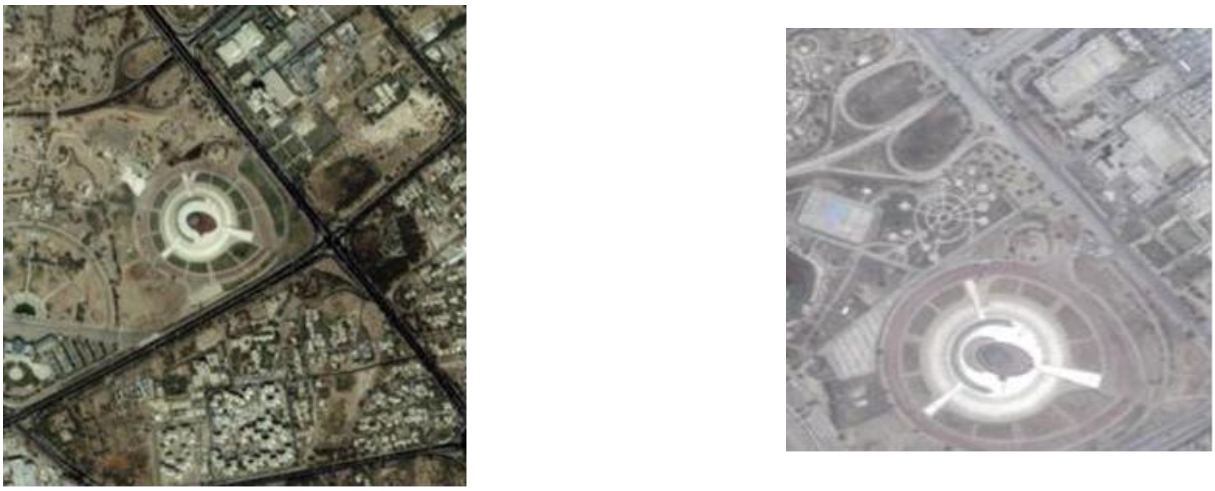

(a) (b)

Figure 2. Ikonos and Quick Bird satellite images.

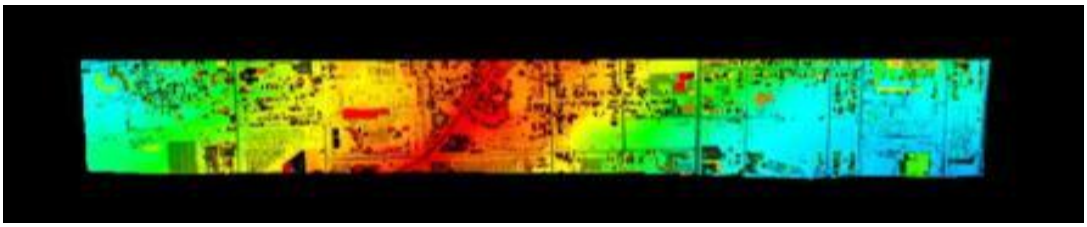

a.Strip_1

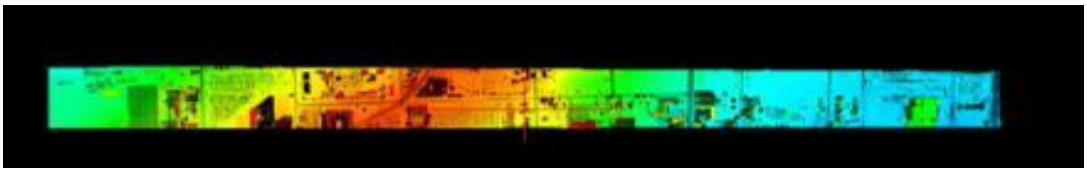

b.Strip_2

Figure 3. Laser point clouds dataset, a.Strip_1, and b.Strip_2.

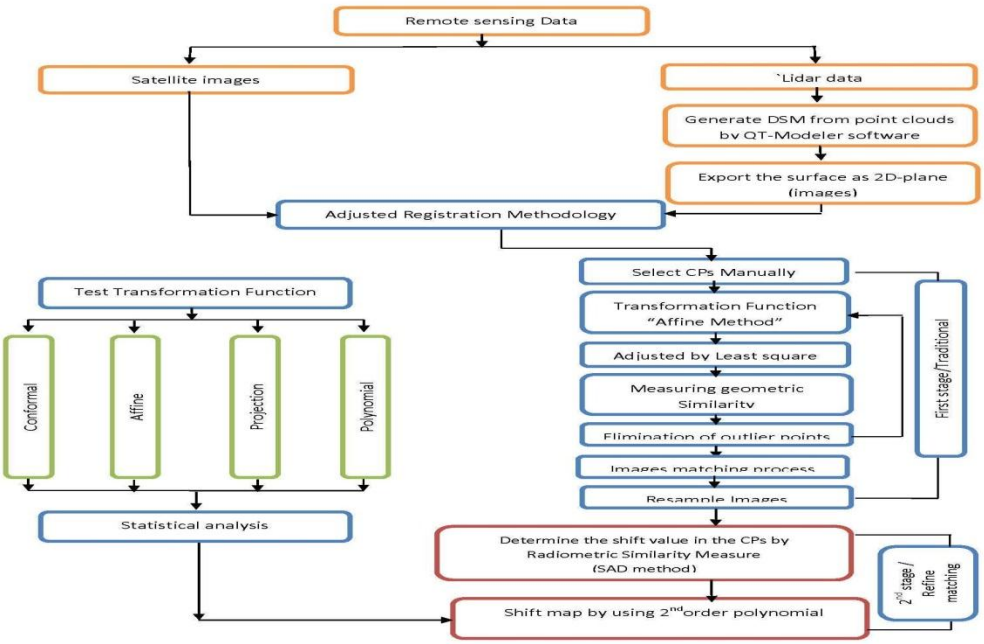

Figure 4. The

workflow of the adjusted registration.

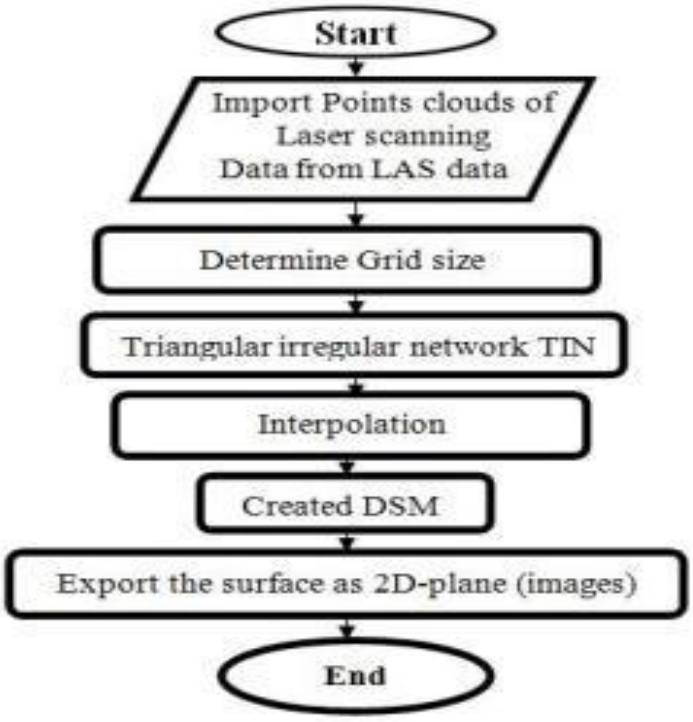

Figure 5. Transform 3D LiDAR data to 2D image.

a. Reference image

b. sensed image

Figure 6. Manual extraction of control points in reference and sensed image.

(a) (b)

Figure 7. Manual extraction of control points in reference and sensed image.

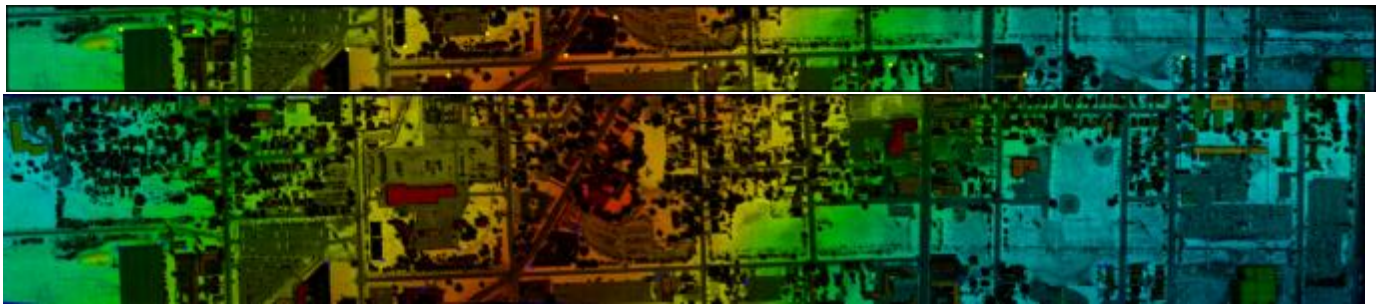

Figure 8. Manual extraction of control points in reference and sensed image.

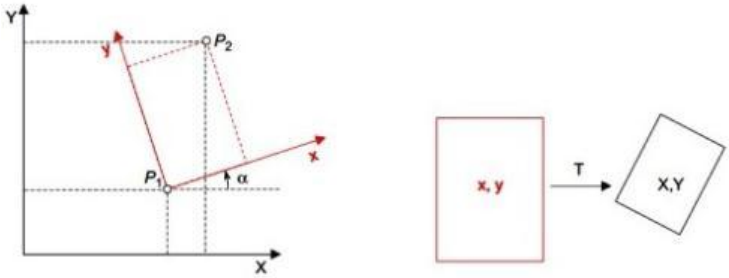

Figure 9. Plane similarity transformations (Luhmann et al., 2011).

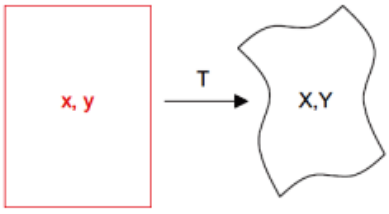

Figure 10. Plane polynomial transformations (Luhmann et al., 2011).

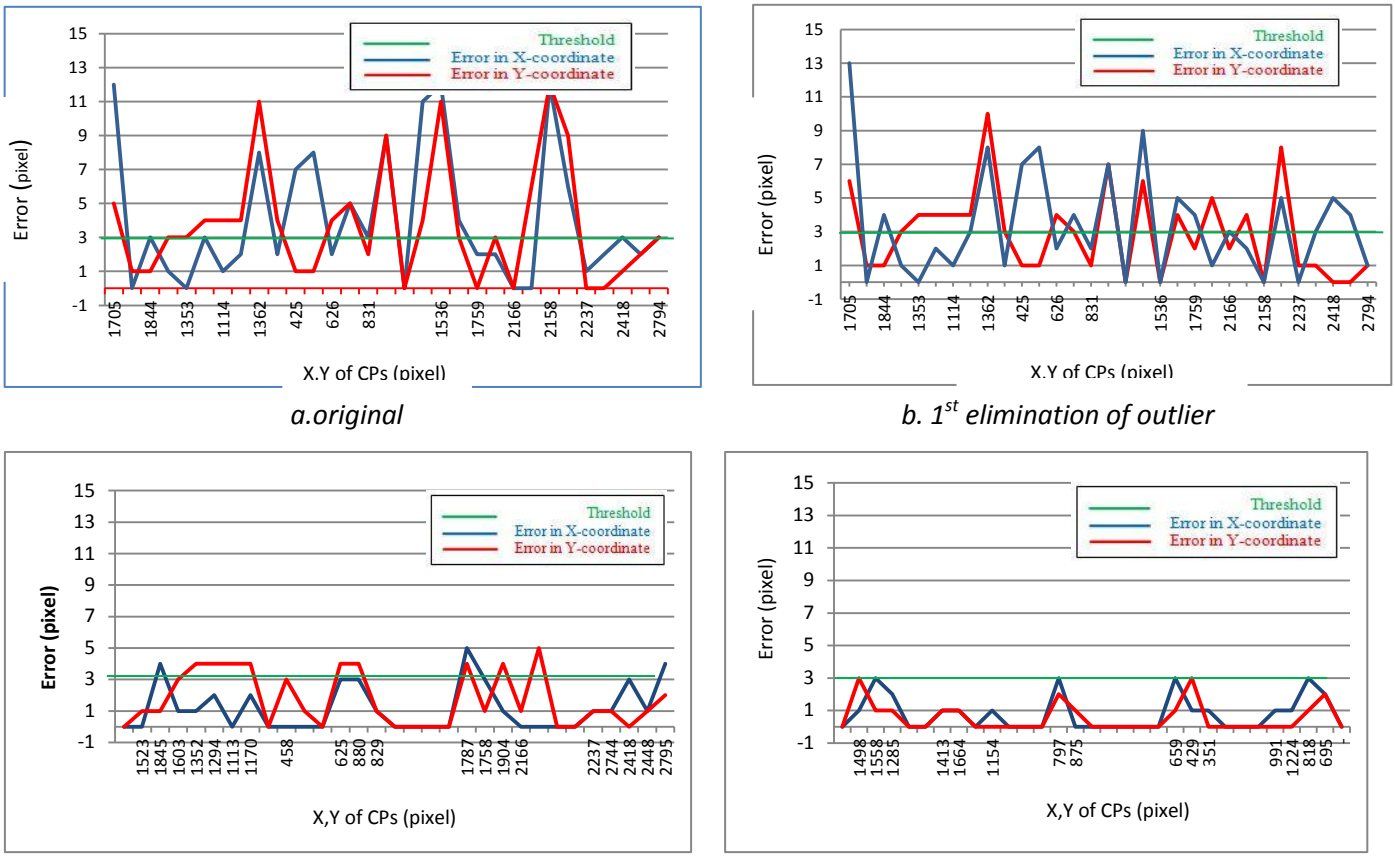

a.original

b. 1st elimination of outlier

c. 2nd elimination of outlier

d. 3rd elimination of outlier

Figure 11. The elimination process of outlier points over threshold

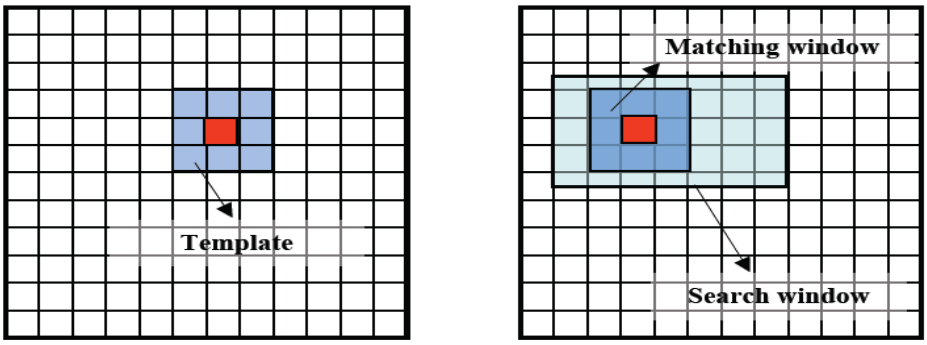

Reference Image (I1) **Input Image (I2)**

Figure 12. Concept of radiometric similarity measure ,Alruzouq, 2004.

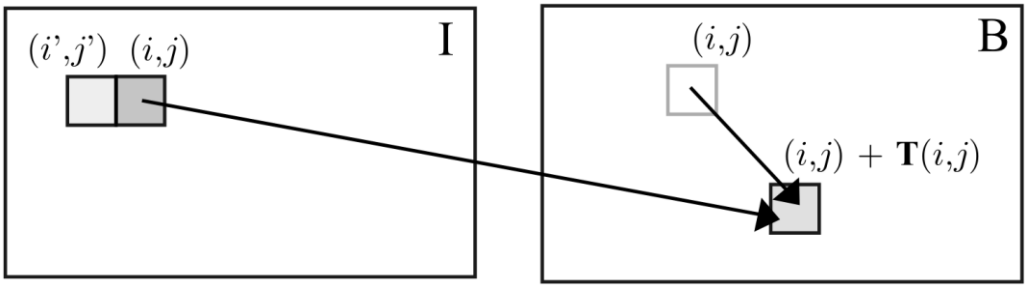

Figure 13. Shift-map between two images.

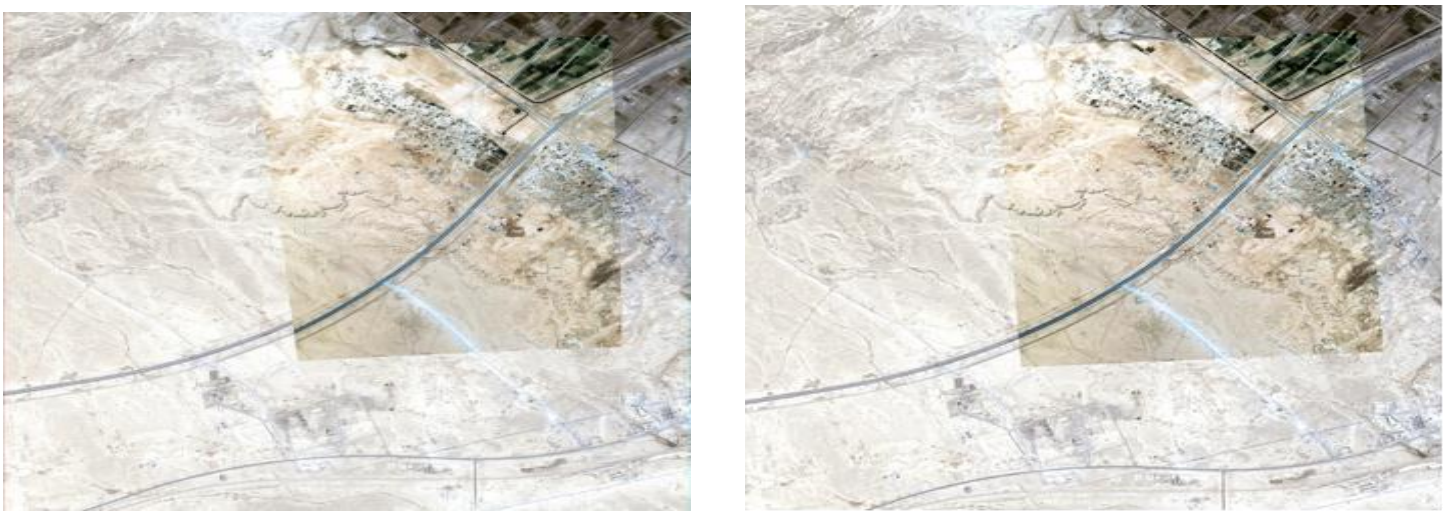

a. first stage /traditional registration b. second stage /adjusted registration

Figure 14. Image matching results between the image from spot satellite as reference image and quick bird satellite as sensed image a. the first stage /traditional registration b. second stage of image registration adjustment.

a. first stage /traditional registration b. second stage /adjusted registration

Figure 15. Image matching results between the image from spot satellite as reference image and quick bird satellite as sensed image a. the first stage /traditional registration b. second stage of image registration adjustment.

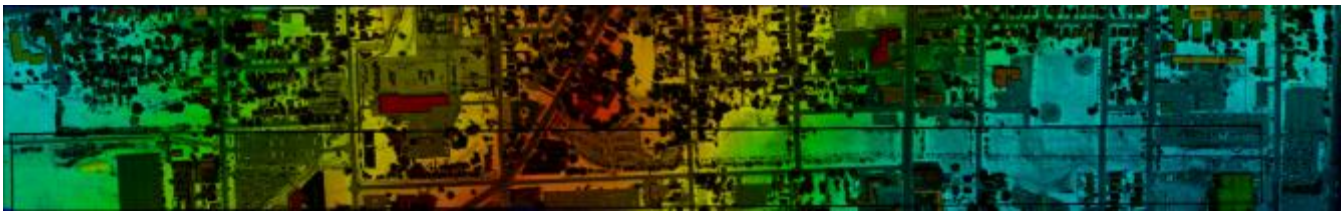

Figure 16. The image matching results between the strip 1 as reference image and strip 2 as sensed image (the first stage /traditional image registration).

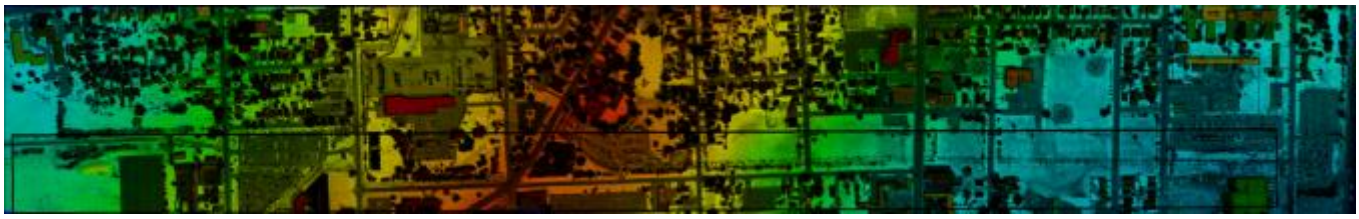

Figure 17. The image matching results between the strip 1 and strip 2 images

(second stage / adjusted registration process).

Equilibrium and Thermodynamic Studies of Reactive Orange Dye Biosorption by Garden Grass

Ahmed A. Mohammed
Assistant Professor
College of Engineering
University of Baghdad
ahmed.abedm@yahoo.com

Farrah Emad Al-Damluji
Assistant Lecturer
College of Engineering
University of Baghdad
farrah.damluji@yahoo.com

Tariq J. Al-Musawi
Lecturer
College of Engineering
University of Baghdad
tariqjwad@yahoo.com

ABSTRACT

The present study aims to evaluate the biosorption of reactive orange dye by using garden grass. Experiments were carried out in a batch reactor to obtain equilibrium and thermodynamic data. Experimental parameters affecting the biosorption process such as pH, shaking time, initial dye concentrations, and temperature were thoroughly examined. The optimum pH for removal was found to be 4. Fourier transform infrared spectroscopy analysis indicated that the electronegative groups on the surface of garden grass were the major groups responsible for the biosorption process. Four sorption isotherm models were employed to analyze the experimental data of which Temkin and Pyzhey model was found to be most suitable one. The maximum biosorption capacity was 12.2 mg/g at 30 °C. The maximum removal percent reached 90% at optimum conditions. Therefore, the pretreatment or modification of this biosorbent may enhance the biosorption capacity. Thermodynamic parameters (i.e., change in the free energy, the enthalpy, and the entropy) were also evaluated and their values revealed that the biosorption process was exothermic in nature and less favorable at high temperature.

Keywords: grass, orange dye, biosorption, isotherm model, thermodynamic.

دراسة توازن وثرموداينمكية الامتزاز الحيوي للصبغة البرتقالية باستخدام ثيل الحدائق

احمد عبد محمد
استاذ مساعد
جامعة بغداد/كلية الهندسة

فرح عماد الدملوجي
مدرس مساعد
جامعة بغداد/كلية الهندسة

طارق جواد الموسوي
مدرس
جامعة بغداد/كلية الهندسة

الخلاصة

تهدف الدراسة الحالية الى تقييم الامتزاز الحيوي للصبغة البرتقالية الفعالة باستخدام ثيل الحدائق. اجريت العديد من التجارب بطريقة الدفعات لغرض الحصول على بيانات الامتزاز الحيوي و الثرموديناميكية. تم دراسة تأثير بعض الظروف في عملية الامتزاز مثل الدالة الحامضية، سرعة الخلط، التركيز الابتدائي، والحرارة. وجد ان افضل ازالة حصلت عند قيمة دالة الحامضية 4. بينت نتائج تحليل الثيل باستخدام الاشعة تحت الحمراء (FTIR) ان المجاميع الفعالة سالبة الشحنة الموجودة على سطح الثيل كان لها الدور الكبير في عملية الامتزاز. تم مطابقة النتائج العملية مع اربعة موديلات رياضية حيث بينت النتائج تطابق كبير مع الموديل المقدم من قبل Temkin وPyzhey. وصلت اعلى قيمة لعملية الامتزاز الى 12.2 ملغم/غم عند درجة

حرارة 30 مئوية. و ان اعلى نسبة ازالة وصلت الى 90% بالظروف المثلى. لذا فان عملية المعالجة او التعديل للمادة الممتزة ربما تحسن عملية الازالة. اثبتت نتائج دراسة الثرموداينمك ان طبيعة الامتزاز هو باعث للحرارة و غير مفضل بدرجات الحرارة العالية.

كلمات رئيسية: ثيل، صبغة برتقالية، امتزاز الحيوي، موديل، ثرموداينمك.

1. INTRODUCTION

Reactive dyes are extensively used in textile, paper, leather, plastic, cosmetics, pharmaceuticals, and food industries to color various substances, **,Han,** and **Yun, 2007**. These dyes are widely used to dye cotton, wool, and polyamide fibers, due to their properties such as simple application procedure, good stability during washing, and bright colours. Dyes are bright in color due to presence of one or several azo bonds (-N=N-) associated with substituted aromatic structures, **,Moreira, et al., 1998. ,Bhatnagar,** and **Jain, 2005**. Wastewaters from textile industry contain large amounts of dyes, representing a major threat to the environment due to their toxicity and potential carcinogenic nature, ,**Bizani, et al., 2006**. Dyes are the most easily recognized contaminant because they are visible to the human eye. Dyestuff effluent is resistant to light and when discharged into the water bodies, it prevents the sunlight from penetrating through and reduces the aesthetic quality of water and photosynthesis **,Owoyokun, 2009.** and **,Jiang, et al., 2008.** Therefore, it is necessary for the dye effluents to be treated properly before they are discharged into the water bodies. A number of conventional treatment methods like coagulation, chemical precipitation, membrane filtration, solvent extraction, chemical oxidation, photolysis, reverse osmosis, and flocculation have been used for the treatment of dyes containing wastewaters, ,**Mittal, et al., 2009**. However, these methods are generally ineffective in color removal and expensive for the treatment of dyes containing wastewaters due to their complex poly-aromatic structure and hence cause health problems, **Mahmoud, et al., 2007.** and ,**Mall, et al., 2007**.

Adsorption techniques are generally considered as the preferred means for removing dyes due to their efficacy to separate chemical compounds from wastewater, simple operation, easy recovery and reuse of adsorbent. The most widely used adsorbent for this purpose is activated carbon**, ,El-Sayed, et al., 2011**. however, due to economic constraint, it's applications on industrial scale are limited, **Hammed, et al., 2008**. Biosorption is a process which utilizes inexpensive dead biomass to remove pollutants from waters, especially those that not easily degradable such as metals and dyes, **Kratochvil,** and **Volesky, 1998**. Biosorption is proven to be quite effective at removing pollutants from contaminated solutions in a low cost and environment-friendly manner, **Sulaymon, et al., 2013**. Biosorption of dyes from wastewater has attracted a significant attention in recent years. A number of studies have been focused on biomaterials that are capable of removing dyes from wastewater such as deolied soya, **Mittal, et al., 2009.** barely husk, **Haq, et al., 2011**. sunflower, **Thinakaran, et al., 2007**. rice milling waste, and ,**Bhatti,** and **Safa, 2012**. etc. However, these biosorbents have generally low biosorption capacities, high cost, not available in high quantity. Therefore, there is a need to find new, economically, easily available and effective biosorbent. Grass is an agricultural waste, environmentally friendly, and high yield material after mowing gardens, lawns, and parks. Grass is available in large quantities in gardens in University of Baghdad. Approximately, ten tons of grass is mower monthly from these gardens. Often, these quantities were dumped in a municipal solid waste landfill. In addition, GG is a low cost biosorbent, the unit cost of collecting 1 kg of virgin grass from Baghdad University

gardens is about US$ 0.5, **Sulaymon, et al., 2014**. Several studies have been carried out to examine the use of grass as biosorbent to remove heavy metals from aqueous solution. ,**Hossain, et al., 2012**. ,**Sulaymon, et al., 2014**. and ,**Chojnacka, 2006.** studied the heavy metal removal efficiency of grass. The results revealed that the garden grass was an effective biosorbent for the removal of heavy metals.

In this study, we focused on the removal of reactive orange (RO) dye from aqueous solution onto garden grass (GG). The preparation, characterization and sorption properties of GG were reported. RO dye sorption was investigated in batch system considering the effect of pH, temperature, contact time, and initial dye concentration.

2. MATERIALS AND METHODS

2.1. Biosorbent and Sorbate Preparation

The GG was collected from the gardens of University of Baghdad after mowing. The foreign matters were removed manually. To remove dirt and impurities, the GG washed several times with tap water then with distilled water. Cleaned GG was cut into small pieces, sundried, and then dried in oven at 60±3 °C until all the moistures are removed. The dried material was shredded, grounded into powder. The average particle size of powdered grass was measured by sieving method in a sieve shaker. The average size of GG particles that passed the 200 µm size screen (yield 50 %) were chosen as biosorbent then stored in an opaque air-tight polyethylene container at room temperature for using in the biosorption experiments with required amounts. No other physical or chemical treatment was used before biosorption experiments.

The commercial grade of RO dye with molecular formula $C_{20}H_{17}N_3Na_2O_{11}S_3$, molecular weight 617.42 g/mol, and wave length (λ_{max}) 490 nm, solubility 90 mg/l, pH 6.5, was obtained from SIGMA-ALDRICH Company. **Fig. 1** shows the chemical structure of RO dye used in this study. Simulated stock solution of RO dye had been prepared by dissolving 1 g of dry powdered dye in 1000 ml distilled water and stored in glass container at the room temperature. Experimental solutions of desired concentrations ranging from 10 to 100 mg/l were obtained by successive dilution of the stock solution. The initial pH of the working solutions was adjusted by addition drop-by-drop buffer solution under magnetic stirring. Standard curve were developed at λ_{max}490 nm for RO dye through the measurement of the dye solution absorbance by UV-VIS spectrophotometer (Model: APEL PD-303 UV, JAPAN). All the glassware used for dilution, storage and experimentation were cleaned with detergent, thoroughly rinsed with tap water, soaked overnight in a 20% HNO_3 solution and finally rinsed with distilled water before use.

2.2. Fourier Transfer Infrared Spectroscopy (FTIR) Analysis

The identification of functional groups on the surface of the GG was performed using Fourier transform infrared spectroscopy (FTIR) analysis. The FTIR offers excellent information on the nature of the bands present on the surface of the biosorbent and also presents three main advantages as an analytical technique: it is fast, nondestructive and requires only small sample quantities, ,**Pereira, et al., 2003.** Two samples of well powdered and dried GG were subjected to the FTIR analysis. The first sample contains 1 g of GG. The second sample was prepared by mixing 1 g of GG with 100 ml of 10 mg/l RO dye solution. The suspension was shaken at 200 rpm for 2 h using a shaker (Edmund Buhler, 7400 Tubingen Shaker-SM 25, Germany). The aqueous solution was withdrawn and then the residue was filtered and dried in oven at 50 °C for 24 h. The two samples were pressed into small discs by using a spectropically pure KBr matrix. Then, Spectra were registered from 4000 to 500 cm^{-1} using Fourier transform infrared spectroscopy (Model: SHIMADZU 8500S, Japan).

2.3. Batch Experiments

2.3.1. Effects studies

Optimization of various parameters such as pH, temperature, initial dye concentration, and shaking time on the removal efficiency were carried out in a batch reactor using classical approach. To study the effect of pH, several conical flasks were shaken at 200 rpm for 4 h. Each flask containing 1 g GG with 100 ml of 10 mg/l dye concentration at room temperature, and the pH range was from 2-8. The temperature effect experiment was conducted using seven flasks each one containing 100 ml of 10 mg/l dye concentration, and the solution temperatures were 20, 25, 30, 35, 40, 45, and 50°C (200 rpm for 2 h, at an optimum pH determined in the pH study). The temperature was maintained using shaker incubator. Effect of initial dye concentrations were conducted using 10, 20, 50 and 100 mg/l dye solutions at room temperature and optimum pH value. The effect of contact time on the sorption process was investigated at different GG dosages (1, 2, 5, and 10 g) with 100 ml of 10 mg/l dye solution. The system was subjected to an agitation speed of 200 rpm, and the samples were collected from 1 to 240 min to determine the remaining concentration of RO dye.

2.3.2. Equilibrium experiments

Equilibrium sorption isotherms are useful to understand the sorption interaction as well as to find the sorption capacity of the sorbent. Equilibrium experiments were carried out by agitation fixed amount of GG (0.2, 0.4, 0.6, 0.8, 1, 2, 3, 4, and 5 g) with 100 ml of 10 mg/l synthetic solution of RO dye at different temperature (10, 20, and 30 °C). The pH of solution was adjusted to the best value based on the pH study (i.e., 4). The flasks were placed in a shaker (Edmund Buhler, 7400 Tubingen Shaker-SM 25) with constant shaking speed at 200 rpm for 2 h. After the equilibrium time of biosorption process, the sorbent was separated from the aqueous solution by using a filter paper (WHATMAN, No.42; diameter, 7 cm) and determination of RO dye concentration was conducted by using UV-VIS spectrophotometer. Each sample was measured thrice in UV-VIS spectrophotometer and the results were given as the average value. The dye uptake and the percentage removal were calculated using the following equations:

$$q_e = \frac{(C_o - C_e)V}{m}$$, **Hossain, et al., 2012.** (1)

where, q_e is the equilibrium biosorption capacity (mg/g); C_o and C_e are the initial and equilibrium dye concentrations in the water (mg/l), respectively; V is the volume of used solution (l); and m is the mass of the used GG.

The percentage of RO dye removal (%) was calculated using the following equation:

$$\%\ Removal = \frac{C_o - C_e}{C_o} \times 100 \quad (2)$$

2.4. Methods

The sorption isotherm data can be modeled using a huge number of theoretical equations. In this study, the experimental isotherm data were fitted with the four isotherm models, namely, Langmuir, Freundlich, Redlich-Peterson, and Temkin and Pyzhey sorption isotherm models to describe the equilibrium characteristics of sorption. These models are presented in **Table 1**. Langmuir model assumes monolayer coverage of adsorbate over a homogeneous adsorbent surface, ,**Langmuir, 1918**. A basic assumption is that sorption takes place at specific homogeneous sites within the adsorbent. The Freundlich isotherm can be applied to non-ideal

adsorption on heterogeneous surfaces as well as multilayer sorption, ,**Freundlich, 1906**. Temkin and Pyzhey isotherm contains a factor that explicitly taking into the account of sorbent–sorbate interactions. By ignoring the extremely low and large value of concentrations, the model assumes that heat of sorption of all molecules in the layer would decrease linearly rather than logarithmic with coverage, as implied in the Freundlich equation, **,Temkin** and **Pyzhey, 1940**. The Redlich-Peterson isotherm model can be applied to expresses the sorption process when dealing with a certain pollutants at high concentration, **,Quintelas, et al., 2008**. In addition, the thermodynamics parameters of the sorption process such as enthalpy changes (ΔH°), entropy changes (ΔS°), and Gibbs free energy changes (ΔG°) were used to determine the spontaneity of biosorption process. These parameters have been determined using Van't Hoff and Gibbs free energy equations.

3. RESULTS AND DISCUSSION

3.1. Biosorbent Characterization

The Physicochemical properties of GG are presented in **Table 2**. The FTIR spectrum of GG **Fig.2** shows RO dye interaction with different chemical groups during the biosorption process. This figure shows that the hydroxyl (-OH), carboxyl (-COO), alcohol (C-O), sulfur groups such as C-S-O and S=O stretching and amide groups are involved in the biosorption process.After contact with RO dye solutions, the position of the band related to the -OH groups from cellulose materials and -NH groups from proteins, ,**Prasad and ,Santhi, 2012.** and **,Bertagnolli, et al., 2014**. shifts from 3338 cm^{-1} in the GG to 3303 cm^{-1} for RO dye loaded GG. The band observed at 2911cm^{-1} is assigned for the alkyl chains (-C-H), ,**Ahmad,** and **Kumar, 2010**. This band was slightly shifted to a new value of 2920 cm^{-1}. The band at 1641cm^{-1} could be owing to the presence of carboxylates (-COO) groups, ,**Arief, et al., 2008**. this group shifted to 1655cm^{-1} after RO sorption. The –C-O, C-C, and –C-OH stretching vibrations can be attributed to peaks in the region of 1440–1024 cm^{-1}.Some bands in the fingerprint regions (900–750 cm^{-1}) could be attributed to the aromatic (–C-H) groups, ,**Al-Rub, et al., 2006**. No change was obvious in these peaks values. The shift of the bands can probably be attributed to proton exchange occurring during the biosorption of the RO dye onto the GG.

3.2 Effect of pH

Fig.3 shows the results of pH effect study. It can be seen that the pH of solution played a significant role in the sorption process especially in the acidic values. It is noteworthy that varied removal efficiency values were observed in the pH range from 2 to 6. The removal efficiency increased with increasing pH from 2 to 4 and reached to the maximum value (58%) at pH 4. While it reached 90% at the same pH value with using 10g GG. This pattern of dye removal is characteristic of anion sorption. In the pH range 6-7 a small decrease in the removal efficiency is observed while the variation in removal efficiency remain negligible in the pH above 7. ,**Lodeiro, et al., 2004.** showed at high acidic solution, the active surface sites of the sorbent may dissociated, reducing the number of binding sites for the sorption of sorbate. Hence low sorption capacity was observed at pH below 3. At pH range from 3 to 5, the surface of GG becomes positively charged and this facilities sorption of RO dye leading to maximum removal efficiency at pH 4. The results obtained in this study are in a good agreement with those reported in previous studies, ,**Elwakeel, et al., 2014.** who noted that in acidic solutions more protons will be available to protonate amine groups to form $-NH_3^+$groups, leading to increase of available sorption sites on the adsorbent. A decline in the sorption capacity was observed at pH above 6, which may be attributed to the competition of OH^- and dye anions. Also, certain chemical compounds in RO dye such as phenols and acids that are proton donors become anions when the

solution pH reaches to the equilibrium condition, in this case the sorption capacity decreased with increase in pH, ,**Kookana,** and **Rogers, 1995**. Therefore, the optimum pH 4 was used for the subsequent experiments.

3.2 Effect of Temperature

The effect of temperature on the removal efficiency has been investigated within a temperature range of 20 to 50 °C and the results are depicted in **Fig. 4**. It can be seen that the maximum percentage removal for RO dyes observed between 20-30 °C. Several authors showed that further increases in temperature (above 30 °C) lead to a decrease the percentage removal. This may be attributed to an increase in the relative desorption of the dye from the solid phase to the liquid phase, deactivation of the biosorbent surface, destruction of active sites on the biosorbent surface due to bond disruption, ,**Saleem, et al., 2007.** and **,Meena, et al., 2005**. or due to the weakness of the sorbent active site binding forces and the sorbate species and also between the adjacent molecules of the sorbed phase, **,Sari,** and **Tuzen, 2008**. It can be seen from **Fig. 4** that the variation of temperature from 25 to 30 °C has minimal effect on the biosorption process, so that further experiments were carried out at room temperature without temperature adjustment.

3.3 Effect of Initial Dye Concentration

Fig. 5 shows the variation of the removal efficiency and uptake with the variation of initial RO dye concentration from 10 to 100 mg/l at 1 g of GG. The results indicated that the percentage removal was not altered greatly from concentrations between 10 to 20 mg/l, this may be due to the amount of GG used in this experiment contains enough sorption surfaces and sites for this concentration range, ,**Anwar, 2010**. thereafter the percentage removal rapidly decreased with the further increase in concentration to 20 mg/l. The decrease in the percentage removal of dye can be explained with the fact that all the sorbents had a limited number of active sites, which have become saturated above a certain concentration, ,**Li, et al., 2012**.

3.4 Effect of Contact Time and Dose

It was very important to know the required time to reach equilibrium sorption condition. **Fig. 6** shows the results of sorption efficiency versus contact time. The results revealed a rapid sorption of RO dye at the initial time (30 min). The equilibrium condition was attained within first hour contact time and a relatively slow phase was observed beyond this time period. Initial biosorption was rapid due to the sorption of dye onto exterior surface, after that dye molecules enter into pores (interior surface), relatively slow process. The figure also showed that the removal efficiency increased from (58%-90%) with increasing the GG dosage from (1g to 10g). A similar observation was previously reported from removal of hazardous cationic dyes from aqueous solution onto Acacia nilotica leaves, ,**Prasad,** and **Santhi, 2012**.

3.5 Equilibrium Isotherm Study

The biosorption isotherm is a plot that shows the equilibrium uptake (q_e, mg/g) against the weight of the biosorbent (g) or equilibrium concentration of the solute in the solution C_e (mg/g), ,**Radnia, et al., 2012**. In this study, this was obtained by the measurement of equilibrium uptake of RO dye using GG doses range from 0 to 5 g at different temperature (10, 20, and 30 °C) and the results are depicted in **Fig.7**. The sorption isotherm showed a steep initial slope followed by a progressive saturation of the sorbent. From **Fig.7** it can be seen that the values of biosorption capacity increased with the increase of the GG dose in the range from 0 to 3 g, and then the biosorption capacity reached a plateau. The static biosorption capacity (12.2 mg/g) of the GG sorbent for RO dye was obtained at 30 °C. The experimental isotherm data were fitted with

several equilibrium isotherm models. **Table 3.** summarized the parameters of each model; these parameters are obtained from the nonlinear regression using STATISTICA program. The Temkin and Pyzhey model gave the best fit for the experimental data for sorption system of RO dye onto GG compared with other models recognized by the highest coefficient of regression values (R^2). The best fit of experimental data by Temkin and Pyzhey isotherm assumes that the fall in the heat of sorption is linear rather than logarithmic**, ,Temkin,** and **Pyzhey, 1940**. In addition, the positive values of B of Temkin and Pyzhey model indicated that the biosorption process is a physical process, ,**Dada, et al., 2012**.

Several efforts have been made to characterize the organic materials binding properties of various forms of biomass. The uptake value by different biomass is summarized in **Table 4**. It can be seen that the GG has a low biosorption capacity, when compared with other biomass, which may be owing to the fact that these biosorbents were treated or modified before using it in the biosorption process.

3.6 Thermodynamics Study

Van't Hoff equation is used to obtain the thermodynamics parameters. The values of ΔH° (-43.521 kJ/mol) and ΔS° (-0.152 J/mol.K) are reported together with the Gibbs free energy values in **Table 5.** The negative value of ΔH° indicates the exothermic nature of biosorption process. The values of enthalpy are coherent with chemical nature of the interaction, which confirms the formation of a complex between GG active sites and RO dye. These results are in agreement with the ,**Elwakeel, et al., 2004.** The negative value of ΔS° means a decrease of the randomness of the system during biosorption of RO dye. Gibbs free energy of biosorption was calculated from the eq. (8) mentioned in **Table 1.** and the results were listed in **Table 5.** The positive values of ΔG° indicate that the biosorption reaction becomes less favorable at high temperature. The increase in the values of ΔG° with increasing temperature (from 1.28 to 6.1 kJ/mol) may be attributed to the exothermic nature of the reaction between GG sites and RO dye molecules.

4. CONCLUSIONS

This study entailed the equilibrium and thermodynamic studies of the biosorption of RO dye on GG. The results showed that garden grass is a good biosorbent towards reactive orange dye at slightly acidic solution (i.e., optimum pH 4) in which the removal efficiency reached to 90%. The maximum equilibrium uptake was 12.7 mg/g at the optimum condition. The biosorption process was examined by changing various parameters such as pH, temperature, and initial dye concentration, the results showed that the removal efficiency was affected due to the change in these parameters. FTIR analysis showed that the hydroxyl, carboxyl, alcohol, and amide groups are the major groups that responsible for the biosorption process. The sorption isotherm is successfully modeled by the Temkin and Pyzhey model. Thermodynamic study revealed that there is an exothermic nature of the reaction between GG sites and RO dye molecules.

Acknowledgments

We would like to express our sincere thanks to the Environmental Engineering Department, University of Baghdad, Iraq, for supporting this work.

References

- Ahmad, R. and Kumar, R., 2010, *Adsorption Studies of Hazardous Malachite Green onto Treated Ginger Waste*. J. Environ. Manage., Vol. (91), No. (4), PP. 1032-1038.
- Al-Rub, A.A., El-Naas, M.H., Ashour, I., and Al-Marzouqi, M., 2006, *Biosorption of copper on Chlorella vulgaris from single, binary and ternary metal aqueous solutions, process*, Biochem., Vol. (41), PP. 457-464.
- Anwar, J., Shafique, U., Waheeduz, Z., Salman, M., Dar, A. and Anwar, S., 2010, *Removal of Pb(II) and Cd(II) From Water by Adsorption on Peels of Banana*, J. Bioresource Technology, Vol.(101),PP. 1752–1755.
- Arief, V.O., Trilestari, K., Sunarso, J., Indraswati, N., and Ismadji, S., 2008, *Recent Progress on Biosorption of Heavy Metals From Liquids using Low Cost Biosorbents: Characterization, Biosorption Parameters and Mechanism Studies*, a review, Clean., Vol. (36), PP. 937-962.
- Bertagnolli, C., Da Silva, M., and Guibal, E., 2014, *Chromium Biosorption Using the Residue of Alginate Extraction from Sargassum Filipendula*, Chemical Engineering Journal, Vol. (237), PP. 362–371.
- Bhatnagar A., and Jain, A.K., 2005, *A Comparative Adsorption Study with Different Industrial Wastes as Adsorbents for the Removal of Cationic Dyes from Water*, J. Colloid Interface Sci., Vol.(281), PP. 49-55.
- Bhatti, H.N., and Safa, Y., 2012, *Removal of Anionic Dyes by Rice Milling Waste from Synthetic Effluents: Equilibrium and Thermodynamic Studies*, Desalination and Water Treatment, Vol. (48), PP. 267-277.
- Bizani, E., Fytianos, K., Poulios, I., and Tsiridis, V.,2006, *Photocatalytic Decolorization and Degradation of Dye Solutions and Wastewaters in the Presence of Titanium Dioxide*. J. hazard. Mater., Vol. (136), PP. 85-94.
- Chojnacka, K.,2006, *Biosorption of Cr(III) Ions by Wheat Straw and Grass: a Systematic Characterization of New Biosorbents*, Polish J. Environ Stud., Vol. (15), PP. 845–52.
- Chung, K.T., Fulk, G.E., and Andrews, A.W., 1981, *Mutagenicity Testing of Some Commonly Used Dyes*, Appl. Environ. Microbiol., Vol. (42), PP. 641-648.
- Dada, A.O., Olalekan, A.P., Olatunya, A.M., and Dada O., 2012, *Langmuir, Freundlich, Temkin and Dubinin–Radushkevich Isotherms Studies of Equilibrium Sorption of Zn^{2+} onto Phosphoric Acid Modified Rice Husk*, IOSR Journal of Applied Chemistry, Vol. (3), No. (1), PP. 38-45.
- El-Sayed, G.O., Aly, H.M., and Hussien, S.H.M., 2011, *Removal of Acrylic Dye Blue-5G from Aqueous Solution by Adsorption on Activated Carbon Prepared from Maize Cops*, International Journal of Research in Chemistry and Environment, Vol. (1), No. (2), PP. 132-140.
- Elwakeel, K.Z., Atia A.A., and Guibal E., 2014, *Fast Removal of Uranium from Aqueous Solutions using Tetraethylenepentamine Modified Magnetic Chitosan Resin*, Bioresour. Technol., http://dx.doi.org/10.1016/j.biortech.2014.01.037
- Freundlich, H.M.F., 1906, *Over the Adsorption in Solution*, Journal of Physical Chemistry, Vol. (57), PP. 385-407.
- Hameed, B.H., Mahmoud D.K., and Ahmed, A.L., 2008, *Sorption Equilibrium and Kinetics of Basic Dye from Aqueous Solution Using Banana Stalk Waste*, J. Hazar. Mater., Vol. (158), PP. 499-506.

- Han, M.H., and Yun, Y.S., 2007, *Mechanistic Understanding and Performance Enhancement of Biosorption of Reactive Dyestuffs by the Waste Biomass Generated from Amino Acid Fermentation Process*, Biochem. Eng. J., Vol. (36), PP. 2-7.
- Haq. J., Bhatti, H.N., and Asgher, M., 2011, *Removal of Solar Red BA Textile Dye from Aqueous Solution by Low Cost Barely Husk: Equilibrium, kinetic and thermodynamic study*, The Canadian J. Chem. Eng. Vol. (89), No (3), PP. 593-600.
- Hossain M.A., Ngo H.H., Guo W.S., and Setiadi T., 2012, *Adsorption and Desorption of Copper(II) Ions Onto Garden Grass*, J. Bioresource Tech., Vol.(121), PP. 386-395.
- Jiang. Y., Sun. Y., Lui. H., Zhu. F., and Yin H., 2008, *Solar Photocatalytic Decolorization of C.I. Basic Blue 41 in an Aqueous Suspension of TiO_2-ZnO*. Dyes Pigm.,Vol. (78), PP. 77-83.
- Kookana, R.S., and Rogers, S.L., 1995, *Effects of Pulp Mill Effluent Disposal on Soil*, Rev. Environ. Contam. Toxicol., Vol.(142), PP. 13-64.
- Kratochvil, D., and Volesky, B., 1998, *Advances in Biosorption of Heavy Metals*, J. Trend Biotechnol., Vol. (16), PP. 291–300.
- Langmuir, I., 1918, *The Adsorption of Gases on Plane Surfaces of Glass*, Mica and Platinum. J. Am. Chem. Soc., Vol. (40), No. (9), PP. 1361-1403.
- Li C., Li W., and Wei L., 2012, *Research on Absorption of Ammonia by Nitric Acid-Modified Bamboo Charcoal at Low Temperature*, Vol. (47), PP. 3-10.
- Liu Y., 2009, *Is the Free Energy Change of Adsorption Correctly Calculated?*, J. Chem. Eng. Data, Vol. (54), PP. 1981-1985.
- Lodeiro, P., Cordero, B., Grille, Z., Herrero, R., and Vicente, M.E., 2004, *Physicochemical Studies of Cadmium (II) Biosorptionby the Invasive Alga in Europe: SargassumMuticum*, Biotechnol. andBioeng., Vol. (88), No. (2), PP. 237-247.
- Mahmoud, A.S., Brooks, M.S., and Ghaly, A.E., 2007,*Decolonization of Remazol Brilliant Blue Dye Effluent by Advanced Photo Oxidation Process (H_2O_2/UV System)*. Amer. J. App. Sci., Vol. (4), No. (12), PP. 1054-1063.
- Mall, I.D., Srivastava, V.C., Agarwall, N.K., and Mishra I.M., 2007, *Removal of Congo Red on Coal Based Mesoporous Activated Carbon*, Dye Pigments, Vol. (74), PP. 34-40.
- Meena, A.K, Mishra, G.K., Rai, P.K., Rajagopal. C., and Nagar, P.N., 2005, *Removal of Heavy Metal Ions from Aqueous Solutions using Carbon Aerogel as an Adsorbe*nt, J. Hazard. Mat., Vol. (122), PP. 161–170.
- Mittal, A., 2006, *Adsorption Kinetics of Removal of a Toxic Dye, Malachite Green, from Wastewater by using Hen Feathers*, J. Hazard. Mater.,Vol. (133), No. (1-3), PP. 196-202.
- Mittal, A., Kaur, D., and Mittal, J., 2009, *Batch and Bulk Removal of Triarylmethane Dye, Fast Green FCF, from Wastewater by Adsorption over Waste Materials*. J.Hazard. Mater., Vol. (163), PP. 568-577.
- Moreira, R.F., Kuhen, N.C., and Peruch, M.G., 1998, *Adsorption of Reactive Dyes onto Granular Activated Carbon*, Latin Am. Appl. Res. Vol. (28), PP. 37–41.
- Owoyokun, T.O., 2009, *Biosorption of Methylene Blue Dye Aqueous Solution on Delonix Regia (Flamboyant Tree) Pod Biosorbent*, The Pacific Journal of Science and Technology,Vol. (10), No. (2), PP. 872-883.
- Pereira, L., Sousa, A., Coelho, H., Amado, A.M., and Ribeiro-Claro. P.J.A., 2003,*Use of FTIR, FT-Raman and 13C-NMR spectroscopy for identification of some seaweed phycocolloids*, J.Biomol. Eng., Vol. (20), PP. 223–228.

- Prasad, A.L., and Santhi, T., 2012, *Adsorption of Hazardous Cationic Dyes from Aqueous Solution onto Acacia Nilotica Leaves as an Ecofriendly Adsorbent*, Sustain. Environ. Res., Vol. (22), PP. 113-122.
- Quintelas, C., Fernandes, B., Castro, J., Figueiredo, H., and Tavares, T. 2008, *Biosorption of Cr(VI) by three different bacterial species supported on granular activated carbon—a comparative study*, J. Hazard. Mater., Vol. (153), PP. 799–809.
- Saleem, M., Pirzada, T., and Qadeer, R., 2007, *Sorption of Acid Violet 17 and Direct Red 80 Dyes on Cotton Fiber from Aqueous Solutions*, J. Colloids Surf., Vol. (292), PP. 246–250.
- Sari, A., and Tuzen, M., *2008, Biosorptionof Cadmium (II) from Aqueous Solution by Red Algae (Ceramium Virgatum): Equilibrium, Kinetic and Thermodynamic Studies*. J. Hazard. Mat., Vol. (157), PP. 448–454.
- Sharma, N., and Nandi, B.K., 2013, *Utilization of Sugarcane Baggase, an Agricultural Waste to Remove Malachite Green Dye from Aqueous Solutions*, J. Mater. Environ. Sci., Vol. (4), No. (6), PP. 1052-1065.
- Sulaymon, A.H, Mohammed, A.A, and Al-Musawi, T.J., 2014,*Comparative Study of Removal of Cadmium (II) and Chromium (III) Ions from Aqueous Solution Using Low-Cost Biosorbent*, Int. J. Chem. Reac. Eng., Vol (12), No. (1), PP. 1-10.
- Sulaymon, A.H., Mohammed, A.A., and Al-Musawi, T.J., 2013, *Removal of Lead, Cadmium, Copper, and Arsenic Ions using Biosorption: Equilibrium and Kinetic Studies*, Desalination and Water Treatment, Vol. (51), PP. 4424-4434.
- Temkin, M.J., and Pyzhey, V., 1940, *Recent Modification to Langmuir Isotherm*, Acta. Physiochim., Vol. (12), PP. 217-222.
- Thinakaran, N., Baskaralingam, P., Pulikesi, M., Panneerselvam, P., and Sivanesan, S., 2007, *Removal of Acid Violet 17 from Aqueous Solutions by Adsorption onto Activated Carbon Prepared from Sunflower Seed Hull*, J. Hazard. Mater., Vol.(151), PP. 316-312.

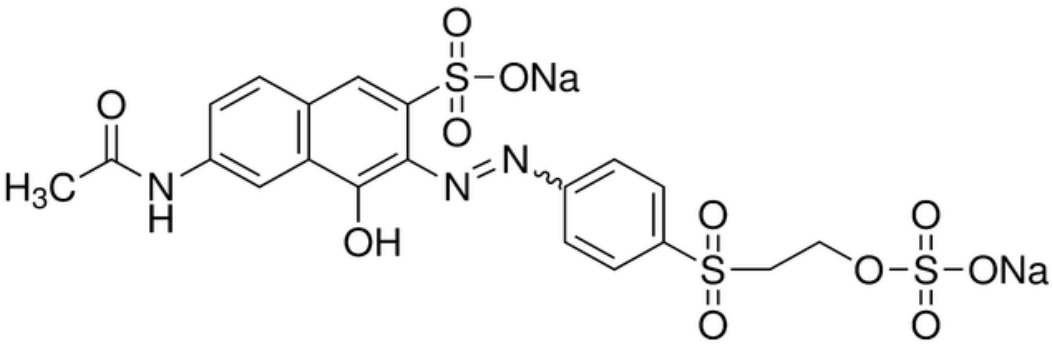

Figure 1. Chemical structure of RO dye, ,**Moreira, et al., 1998**.

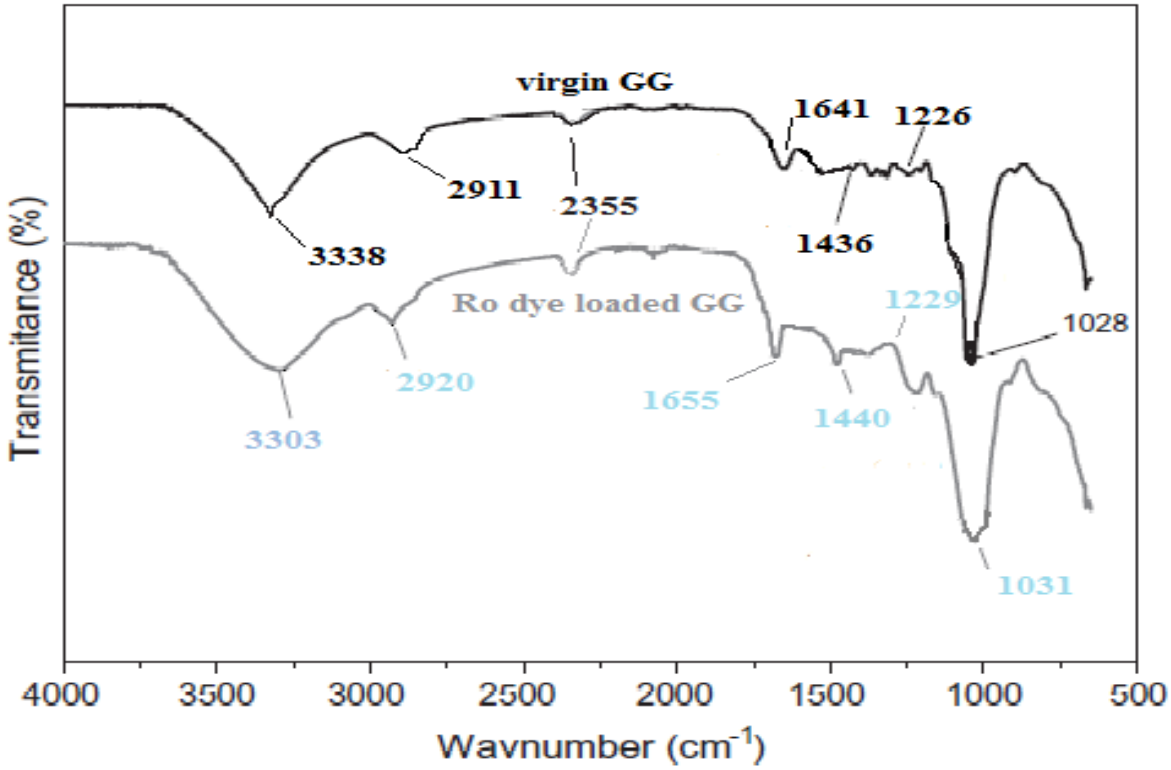

Figure 2. FTIR spectrum of virgin and RO loaded GG samples**.**

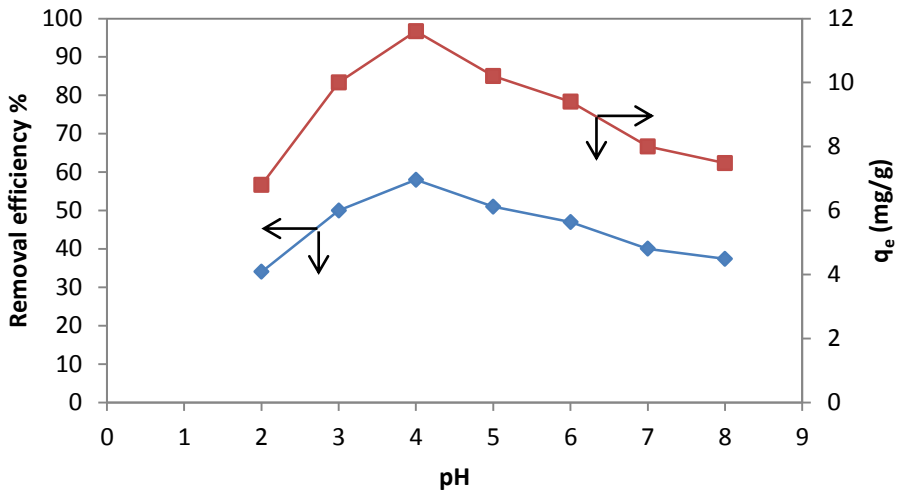

Figure 3. PH effect on RO dye sorption using GG (C_o=10 mg/l, GG dose=1 g, room temperature, 2 h contact time at 200 rpm).

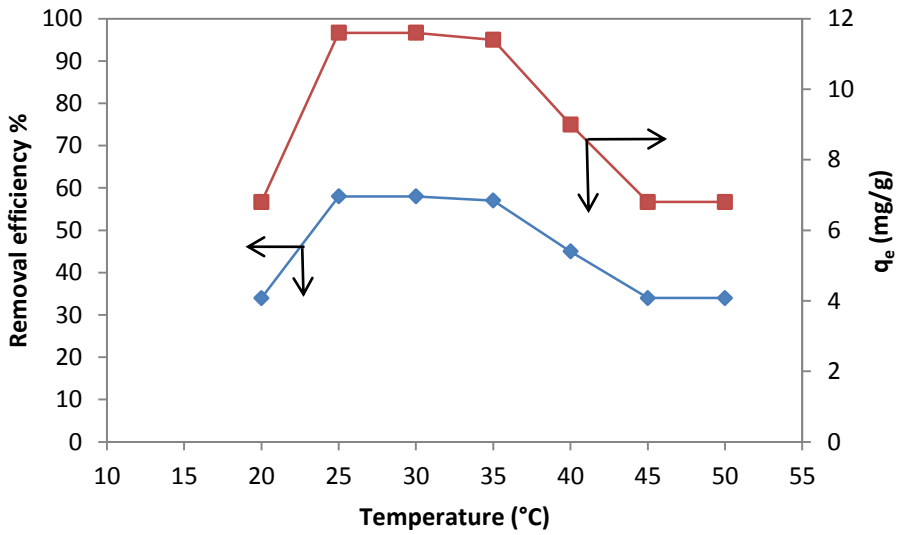

Figure 4. Temperature effect on RO dye sorption using GG (C_o=10 ppm, GG dose=1 g, pH=4, 2 h contact time at 200 rpm).

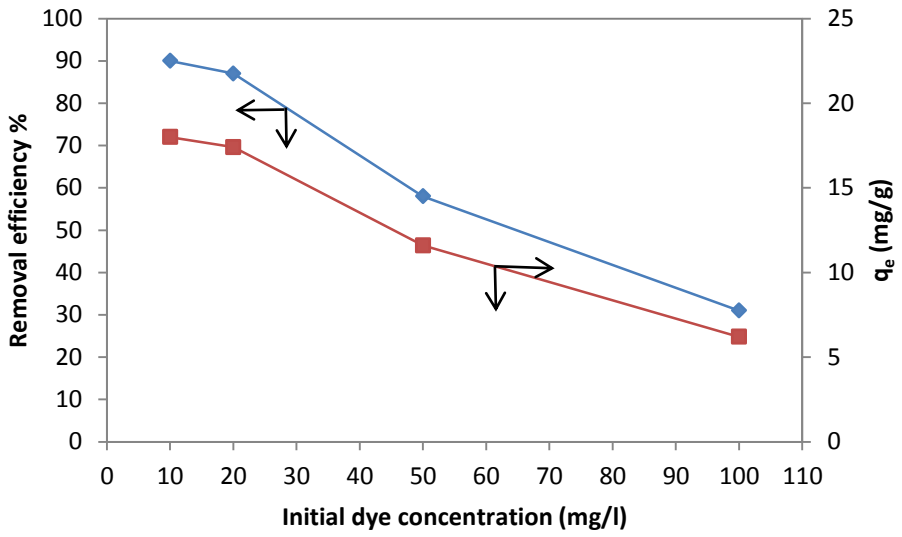

Figure 5. Initial RO dye concentration effect on the removal efficiency using GG: (GG dose=1 g, pH=4, room temperature, 2 h contact time at 200 rpm)**.**

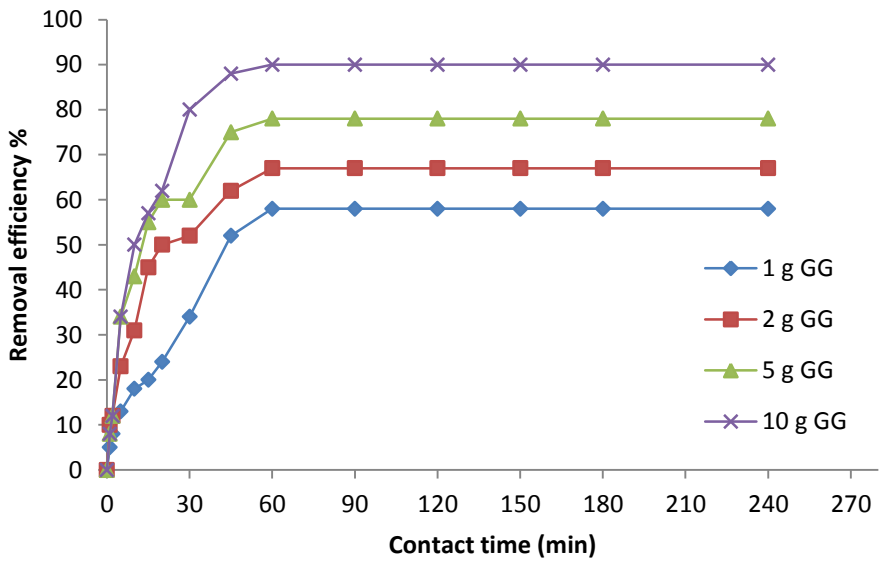

Figure 6. Effect of contact time on the removal efficiency of RO dye using different GG dosages: (pH=4, room temperature, at 200 rpm)**.**

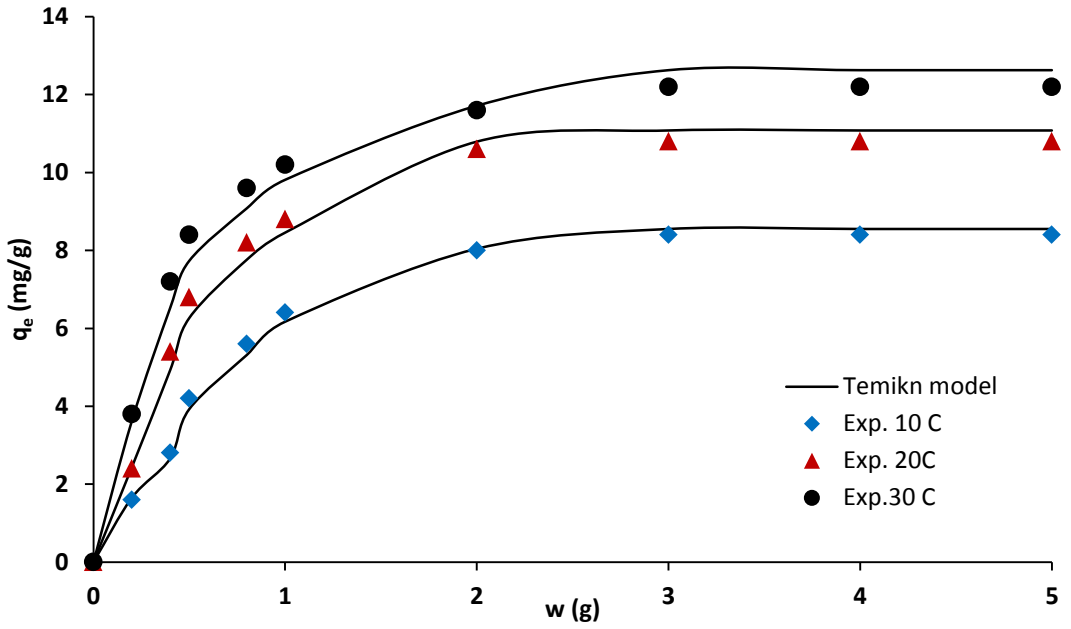

Figure 7. RO biosorption capacity using GG at different temperature: C_o=10 mg/l, GG weight (w) =0-5 g, pH=4, contact time= 2h, at 200 rpm.

Table1. The equations for the sorption isotherm.

Model	Equation Reference	No.
Langmuir	$q_e = \frac{q_m K_L C_e}{1+K_L C_e}$ **,Langmuir, 1918.** q_e is the sorption uptake (mg/g);C_e is the equilibrium concentration of the adsorbate (mg/l); q_m is the maximum amount of the adsorbate per unit weight of the adsorbent (mg/g); K_L is the Langmuir constant related to the free energy of sorption (l/mg).	(3)
Freundlich	$q_e = K_F C_e^{1/n}$ **,Freundlich, 1906.** q_e is the sorption uptake (mg/g); C_e is the equilibrium concentration of the adsorbate (mg/l); n is the Freundlich constant related to sorption intensity (g/l); K_F is the Freundlich constant related to the relative sorption capacity (mg/g).	(4)
Temkin and Pyzhey	$q_e = \frac{RT}{b_{Te}} ln(a_{Te} C_e)$ **,Temkin, and Pyzhey, 1940.** T is the absolute temperature (K), R is the universal gas constant (8.314 J/mol. K), a_{Te} is the equilibrium binding constant, b_{Te} is corresponding to the heat of sorption, and C_e is the equilibrium concentration of the adsorbate (mg/l).	(5)
Redlich-Peterson	$q_e = \frac{k_{RP} C_e}{1+\alpha_{RP} C_e^{\beta_{RP}}}$ **,Quintelas, et al., 2008.** q_e is the sorption uptake (mg/g);C_e is the equilibrium concentration of the adsorbate (mg/l); k_{RP}, α_{RP} and βRP are constants.	(6)
Van't Hoff	$ln\, K_c = -\frac{\Delta H^\circ}{RT} + \frac{\Delta S^\circ}{R}$ **,Liu, 2009.** K_c is the equilibrium constant (q_e/C_e), R is the universal gas constant (8.314 J/mol. K), ΔH° is the enthalpy of the sorption (kJ/mol), ΔS° is the entropy of the sorption (J/K.mol), and T is the solution temperature (K).	(7)
Gibbs free energy	$\Delta G^\circ = -RT\, ln\, K_c$ **,Liu, 2009.** $\Delta G^\circ$is the Gibbs free energy of biosorption (kJ/mol), K_c is the equilibrium constant (q_e/C_e), R is the universal gas constant (8.314 J/mol. K), and T is the solution temperature (K).	(8)

Table 2. Characterization of the powdered grass.

Parameter	Value
Particle size (mm)	<0.2
Surface area (m^2/g)	5.6
Apparent density (g/l)	0.48
Zero point charge (pH_{zpc})	5.1
Porosity (%)	60.5
Moisture content (%)	1.57
Ash content (%)	0.99

Table 3. Parameters of isotherm models for the biosorption of RO dye onto GG**.**

Model	Equation	Parameters	At 10 °C	At 20 °C	At 30 °C
Langmuir	$q_e = \frac{q_m K_L C_e}{1 + K_L C_e}$	q_m, mg/g K_L, l/mg R^2	0.857 -0.018 0.813	1.554 -0.023 0.826	2.616 -0.029 0.884
Freundlich	$q_e = K_F C_e^{1/n}$	K_f, mg/g n, g/l R^2	14.849 -0.321 0.925	10.079 -0.503 0.903	7.732 -0.709 0.917
Temkin and Pyzhey	$q_e = \frac{RT}{b_{Te}} ln(a_{Te} C_e)$	$B = {}^{RT}/_{b_{Te}}$, l/mg a_{Te}, mg/g R^2	14.962 102.713 0.995	13.332 105.603 0.988	12.330 108.630 0.980
Ridlich-Peterson	$q_e = \frac{k_{RP} C_e}{1 + \alpha_{RP} C_e^{\beta_{RP}}}$	k_{RP}, mg/g α_{RP},l/mg β_{RP}, R^2	22.040 0.991 0.567 0.891	12.553 1.133 1.041 0.789	30.339 1.008 0.889 0.782

Table 4. Uptake of organic materials by different biomasses**.**

Material	Biomass	q_e (mg/g)	Reference
Crystal Violet dye	Acacia nilotica leaves	33	**,Prasad and Santhi, 2012.**
Rhodamine B dye	Acacia nilotica leaves	37	**,Prasad and Santhi, 2012.**
Malachite green dye	Hen feather	26	**,Mittal, 2006.**
Malachite Green Dye	Sugarcane baggase	22	**,Sharma and Nandil, 2013.**
Reactive orange dye	Garden grass	12.7	This study

Table 5. Thermodynamic constants of biosorption of RO dye onto GG.

Temperature (K)	ΔG° (kJ/mol)	ΔH°(kJ/mol)	ΔS° (J/mol.K)	R^2
293	1.282	-43.521	-0.152	0.912
298	3.188			
303	3.241			
308	3.400			
313	4.710			
318	6.090			
323	6.103			

Competitive Removal of Cu^{2+}, $Cd^{2+}$and $Ni^{2+}$by Iron Oxide Nanoparticle (Fe_3O_4)

Shahlaa E. Ebrahim
Assistant Professor
College of engineering
University of Baghdad
Shahlaa.ebrahim@fulbrightmail.org

Hasanain Saad Alhares
Instructor
University of Baghdad
hassanian73@ yahoo.com

ABSTRACT

A competitive adsorption of Cu^{2+}, Ni^{2+}, and Cd^{2+} ions from a synthetic wastewater onto nanomaterial was studied.(Fe_3O_4) nanoparticles obtained from US Research Nanomaterials, Inc., Houston, TX 77084, (USA), was used as nanosorbent. Experimental parameters included pH, initial metal concentrations, and temperature were studied for nanosorbent. The uptake capacity 11.5, 6.07 and 11.1 mg/g for Cu^{2+}, $Ni^{2+}$and Cd^{2+}, respectively, onto nanosorbent . The optimum pH values was 6 and the contact time was 50 min. for Cu^{2+}, $Ni^{2+}$and Cd^{2+}, respectively. The equilibrium isotherm for nanosorbent single system component is of a favorable type and Freundlich isotherm model gives the best fit model for representing the experimental data for this system. Binary and ternary component systems were conducted in order to find the adsorption isotherm constants for each component system using nanosorbent. A set of adsorption models were tested to choose the best fit model for the experimental data, Combination of Langmuir- Freundlich model seems to give the best fitting. In single, binary and ternary component systems, Cu^{2+} always adsorbed more favorable onto nanosorbent than $Cd^{2+}$and Ni^{2+}. The adsorption capacity parameters were: Cu^{2+}> Cd^{2+}> Ni^{2+}. Thermodynamic study was carried out for these three pollutants onto nanosorbent. The results of adsorption show that the adsorption nature for heavy metals is an endothermic and physical nature process.

Key Words: adsorption, heavy metals, ions, competitive, nanosorbent.

الازالة التنافسية لايونات النحاس والكادميوم والنيكل بواسطة مادة النانو المازة(اوكسيد الحديد)

د. شهلاء اسماعيل ابراهيم
أستاذ مساعد
كلية الهندسة/قسم البيئة
جامعة بغداد

د.حسنين سعد عبد الزهرة الحارس
المدرس
جامعة بغداد

الخلاصة

الدراسة الحالية تهدف الى تقييم عملية الامتزاز للمعادن الثقيلة(النحاس،النيكل و الكادميوم) من المياه الصناعية بواسطة مادة النانو. وتم شراء مادة النانوالمازة وهي اوكسيد الحديد (Fe_3O_4) من الولايات المتحدة الامريكية. كذلك تم دراسة تغيير بعض العوامل المختبرية على عملية الامتزاز مثل الدالة الحامضية، التركيز الاولي، والحرارة لمادة النانو. ان سعة الازالة هي 11.1,6.07,11.5 mg/g لايونات النحاس والنيكل والكادميوم على التوالي باستخدام مادة النانو. وجد ان افضل نسب الازالة لمادة النانو تحصل عند قيمة الحامضية 6 لجميع الايونات وان وقت الازالة الامثل هو 50 دقيقة . تم القيام بسلسلة من تجارب الدفعات (batch experiment) للملوثات بصورة منفردة وثنائية وثلاثية لغرض الحصول على مخططات الامتزاز الحيوي لكل ملوث. وقد تم استخدام عدد من الموديلات الرياضية التي تصف عملية الامتزاز. وجد أن موديل (Freundlich) ، أفضل موديل رياضي يمثل النتائج العملية بالنسبه للمنفرده.اما بالنسبة الى التجارب الثنائية والثلاثية ، وجد ان موديل (Combination of Langmuir- Freundlich) افضل موديل رياضي يمثل النتائج العملية. وجد أن ايونات النحاس اعلى قدرة وملائمة على الامتزاز بواسطة مادة النانو بينما ايونات النيكل اقل قدرة من بقية الايونات . كما وجد ان طبيعية الامتزاز للمعادن الثقيلة هو ماص للحرارة من خلال التجارب الحرارية (thermodynamic study) وذو طبيعة فيزياوية.

الكلمات الرئيسية: امتزاز,المعادن الثقيلة,ايونات,التنافس,مادة النانو.

1. INTRODUCTION

Presence of heavy metals in wastewaters causes significant environmental problems. High concentrations of heavy metals are known to be toxic and carcinogenic to living organisms. When heavy metals are present even in a very low concentration, their concentration may be elevated through bio-magnification to a level that they start to exhibit toxic characteristics. Therefore, heavy metals are major pollutants in many industrial wastewaters and are toxic to human and aquatic life **,Taghi *et al.*, 2005**. Due to their elemental non-degradable nature, heavy metals always and regardless of their chemical form, pose serious ecological risk, when released into the environment. The metals which are of greatest environmental concern are cadmium, mercury, lead, chromium, cobalt, copper, nickel and zinc **,Sahmoune *et al.*, 2009**.The presence of heavy metal ions in the environment has been a matter of major concern due to their toxicity to human life. Unlike organic pollutants, the majority of which are susceptible to biological degradation, heavy metal ions will not degrade into harmless end products. Heavy metal ions such as cobalt (Co), copper (Cu), nickel (Ni),chromium (Cr), mercury (Hg), lead (Pb), cadmium (Cd), zinc (Zn) ions are detected in the waste streams from different industrial activities such as mining operations, tanneries, electronics , electroplating, petroleum refineries, and petrochemical industries **,Cheueh, 2005**.

The toxicity of heavy metals can be listed in order of decreasing toxicity as Hg > Cd > Cu > Zn > Ni > Pb > Cr >Al >Co, although this is only approximate as the vulnerability of species to individual metals varies. Toxicity also varies according to environmental conditions that control the chemical speciation of the metals**, Gray, 2005. ,Saleem *et al.*, 2011.**

Heavy metals can pose health hazards if their concentration exceeds the allowable limits. Even when the concentration of metals does not exceed these limits, there is still a potential for long-term contamination. As they are non-biodegradable, and persistence their threat is multiplied by their accumulation in the environment elements such as food chain and thus poses a significant danger to human health and life**, Manhan, 2005.**

The removal of heavy metals ions from wastewater involves high cost techniques such as ion-exchange, evaporation, precipitation, membrane separation etc. However, these common techniques are too expensive to treat low levels of heavy metals in wastewater. Adsorption techniques are widely used in the field of removing small quantities of pollutant present in large volume of fluid, which can be carried out in batch wise or continuous manner of operation **,Rao, 1994**. Many factors that affect the decision of choosing an adsorbent for removal of pollutants from water such as:

economical factor (cost of the adsorbent), abundance, availability and effectiveness of the adsorbent**, Sulaymon and ,Ahmed, 2008**.

The last decade has seen a continuous improvement in the development of effective\noble adsorbents in the form of activated carbon **,Huang et al., 2007.** zeolites **, Panuccio et al.,2009.** clay minerals **,Hizal and ,Apak, 2006.** chitosan **,Bamgbose et al., 2010.** lignocelluloses **,Shin,2007.** natural inorganic minerals **,Sevgi, 2009.** functionalized polymers **,Panda *et al.*,2008.** etc. However, most of these adsorbents are either not effective (due to diffusion limitation or the lack of enough active surface sites) or have shown problems like high cost,difficulties of separation from wastewater, or generation of secondary wastes. Nowadays there is a continuously increasing worldwide concern for the development of wastewater treatment technologies. Considering such drawbacks, recently nano-adsorbents viz. nano-alumina **,Srivastava *et* al.,2011.** functionalized carbon nanotubes **, Gupta et al., 2011.** and hydroxyapatite nanoparticles **, Feng *et* al.,2010.** have demonstrated high adsorption efficiency for metal ions removal. The utilization of iron oxide nanomaterials has received much attention due to their unique properties, such as extremely small size, high surface-area-to-volume ratio, surface modifiability, excellent magnetic properties, **,Xu *et al.*, 2012**. One such advanced class of adsorbent – magnetic nano-adsorbent with the help of an external magnetic field has been further successful in circumventing the solid–liquid separation problem usually encountered with nanoparticle. Such adsorbent combining nanotechnology and magnetic separation technique has not only demonstrated high adsorption efficiency due to its large surface to volume ratio, but have also shown additional benefits like ease of synthesis, easy recovery and manipulation via subsequent coating and functionalization, absence of secondary pollutants, cost-effectiveness and environmental friendliness **,Gupta and Nayak , 2012.** Till date, several magnetic nanomaterials, including maghaemite nanoparticles **,Hu et al., 2005.** Fe_3O_4 magnetic nanoparticles **,Shen et al.,2009.** Fe_3O_4 nanoparticles functionalized and stabilized with compounds like humic acid **,Liu *et al.*,2008.** have been explored for the removal of metal ions. In nanotechnology focuses on the fabrication of nano-sized adsorbents with enhanced adsorption capacity and rapid sorption rate for the removal of target contaminants. This is due to the large surface area and highly active surface sites of the nanoadsorbents **,Bhaumik et al.,2012.**Iron oxide nanoadsorbents are cost-effective adsorbents that provide high adsorption capacity, rapid adsorption rate and simple separation and regeneration **,Nassar, 2010.**In the present study, were used for the competitive removal of heavy metals (Cu^{2+}, Ni^{2+} and Cd^{2+}) in batch reactors at different operating conditions.

2. EQUILIBRIUM ISOTHERM BATCH MODELS FOR SORBENT

2.1 Single Component System

Empirical models are simple mathematical relationships, characterized by a limited number of adjustable parameters, which give a good description of the experimental behavior over a large range of operating conditions. The model used to describe the results should be capable of predicting sorbate binding at both low and high concentrations **,Vijayaraghavan and Yun, 2008.**

Although these conventional empirical models do not reflect the mechanisms of sorbate uptake, they are capable of reflecting the experimental curves of adsorption isotherm **,Vijayaraghavan *et al.*, 2008.**

2.1.1 Langmuir model (1916)
The Langmuir model can be represented as:

$$q_e = \frac{q_{max} b C_e}{(1+bC_e)} \quad (1)$$

Where q_e is the amount of adsorbate adsorbed per mass of adsorbent (mg/g).C_e is the equilibrium concentration (mg/l).

This classical model incorporates two easily interpretable constants: q_{max} , which corresponds to the maximum achievable uptake by a system; and b, which is related to the affinity between the sorbate and sorbent,(l/mg). The Langmuir constant "q_{max}" is often used to compare the performance of biosorbents; while the other constant "b" characterizes the initial slope of the isotherm. Thus, for a good biosorbent, a high q_{max} and a steep initial isotherm slope (i.e., high b) are generally desirable **,Aksu *et al.*, 2002. ,Kratochvil and Volesky, 1998.**

The Langmuir model assumes the following: (i) the surface consists of adsorption sites, (ii) all adsorbed species interact only with a site and not with each other, (iii) adsorption is limited to a monolayer, and (iv) adsorption energy of all the sites is identical and independent of the presence of adsorbed species on neighboring sites **, Ridha, 2011.**

Each component is adsorbed onto the surface according to ideal solute behavior; there is no interaction or competition between molecules involved under homogenous conditions, **,Mashitah *et al.*, 2008.**

The important characteristic of the Langmuir isotherm can be expressed in terms of dimensionless constant separation factor for equilibrium parameter R_L. This is defined by **,Sahmoune *et al.*, 2009.**

$$R_L = \frac{1}{b+C_o} \quad (2)$$

,Basha and Murthy, 2007. show, using mathematical calculation, that the parameter R_L indicates the shape of isotherm as follows in **Table 1.**

2.1.2 Freundlich model (1918)
The Freundlich isotherm can be represented as:

$$q = KC_e^{1/n} \quad n > 1 \quad (3)$$

The Freundlich isotherm was originally empirical in nature, but was later interpreted as the sorption to heterogeneous surfaces or surfaces supporting sites with various affinities. It is assumed that (i) the stronger binding sites are initially occupied, (ii) the binding strength decreasing with increasing degree of site occupation. It incorporates two constants: K, which corresponds to the maximum binding capacity; and n, which characterize the affinity between the sorbent and sorbate (adsorption intensity)**, Vijayaraghavan and ,Yun, 2008.**

2.1.3 Redlich–peterson model (1959)

$$q_e = \frac{K_{RP} C_e}{1 + a_{RP} C_e^{\beta_{RP}}} \quad (4)$$

Redlich–Peterson isotherm shows that an "area of stability" is reached after a frequent rise in the curve, i.e., several layers of adsorption occurs first. This isotherm assume (i) equilibrium for heterogeneous surfaces as it contains the heterogeneity factor β. (ii) It also converges to Henry's law at low surface coverage and is, therefore, (iii) thermodynamically consistent. However, it does not have as wide a practical application as the Langmuir and the Freundlich isotherms due to the inconvenience of evaluating three isotherm constants ,**Lawrence *et al.*, 2010.**

β_{RP} has values between 0 and 1. For β_{RP} = 1 the Redlich–Peterson model converts to the Langmuir model. β_{RP}=0 the Henry's Law form results

2.1.4 Sips model (1948)

$$q_e = \frac{K_s C_e^{\beta_s}}{1 + a_s C_e^{\beta_s}} \quad (5)$$

K_S is the Sips model isotherm constant; a_S the Sips model constant; β_S the Sips model exponent. This equation is also called Langmuir–Freundlich isotherm and the name derives from the limiting behavior of the equation. At low sorbate concentrations it effectively reduces to a Freundlich isotherm and thus does not obey Henry's law. At high sorbate concentrations, it predicts the monolayer sorption capacity characteristics of the Langmuir isotherm **,Padmesh *et al.*, 2006.**

2.1.5 Khan model (1997)

$$q_e = \frac{q_{max} b_k C_e}{(1 + b_k C_e)^{a_k}} \quad (6)$$

b_K is the Khan model constant; a_K Khan model exponent , q_{max} maximum uptake **,Vijayaraghavan and Yun, 2008.**

2.1.6 Toth Model (1971)

$$q_e = \frac{q_{max} b_T C_e}{\left[1 + (b_T C_e)^{\frac{1}{n_T}}\right]^{n_T}} \quad (7)$$

b_T the Toth model constant and n_T the Toth model exponent **,Vijayaraghavan and Yun, 2008.**

It derives from potential theory and is used in heterogeneous systems. Toth model assumes a quasi-Gaussian energy distribution; most sites have adsorption energy lower than the peak of maximum adsorption energy**, Jianlong and Can, 2009.**

2.2 Multi Component Systems

The adsorption of the solute of interest not only depends on the adsorbent surface properties and physical–chemical parameters of a solution such as pH and temperature, but also on the number of solutes and their concentrations. In such cases, the adsorption will become competitive, with one solute competing with another to occupy the binding sites**, ,Wang and Chen, 2009.**

Multicomponent biosorption has been the subject of limited studies .The uptake of a given metal ion is decreased to a greater extent in ternary combinations and furthermore in quaternary systems compared to the binary combinations. In the presence of co-ions in solution, chemical interactions between the ions themselves as well as with the adsorbent take place resulting in site competition. Therefore metal uptake from multicomponent systems is lower.

For binary solute cases, different isotherm models have been used to correlate single-solute isotherm data and to describe multi-solute sorption isotherms based on the time-consuming iterative algorithm **,César *et al.*, 2010.**

2.2.1 Extended langmuir model (ELM)

$$q_i = \frac{b_i q_{m,i} C_{e,i}}{\left(1+\sum_{j=1}^{n} b_j C_{e,j}\right)} \tag{8}$$

Where $C_{e,i}$ is the equilibrium concentration of the component i in the multicomponent solution, q_i is the equilibrium uptake of the component i, b_i and $q_{m,i}$ are the Langmuir isotherm model parameters obtained suitably from Eq. (1) in the single solute system.This model assumes (i) homogeneous surface with respect to the energy of sorption, (ii) no interaction between adsorbed species and (iii) that all sorption sites are equally available to all adsorbed species **,Aksu *et al.*, 2002.**

2.2.2 Redlich-peterson model

The three parameter isotherm of Redlich-Peterson that has been empirically developed for multi-component mixtures is given as**, Fahmi and Munther, 2003. , Sulaymon *et al.*, 2009.**

$$q_i = \frac{K_{R,i} q_{m,i} C_{e,i}}{\left(1+\sum_{j=1}^{n} a_{R,j} C_{e,j}^{Bj}\right)} \tag{9}$$

Where $K_{R,i}$ and $q_{m,i}$ are the Redlich-Peterson isotherm-model parameter suitably obtained from Eq. (4) in single solute system.

2.2.3 Combination of Langmuir-Freundlich Model

The competitive model related to individual isotherms parameters are expressed in the following equation**, Sips, 1984.**

$$q_i = \frac{q_{m,i} b_i C_{ei}^{(\frac{1}{n_i})}}{\left(1+\sum_{j=1}^{n} b_j C_{ej}^{(\frac{1}{n_j})}\right)} \quad (10)$$

3. EXPERIMENTAL WORK

The present study is to evaluate the competitive adsorption of heavy metals as inorganic pollutants from wastewater by nanosorbent (Fe_3O_4). In this research nanomaterial will be used for the competitive removal of heavy metals in batch reactors at different operating condition in single, binary and ternary systems.

3.1 Adsorbate (Stock Solutions)

A stock solution of copper, nickel and cadmium ions with a concentration of (1000 mg/l) were prepared by using $Cu(NO_3)_2$, $Ni(NO_3)_2$ and $Cd(NO_3)_2$ (minimum purity 99.5%). A 3.805, 4.945and 2.744g of copper nitrate, nickel nitrate and cadmium nitrate, respectively were dissolved in approximately 200 ml of distilled water.

A 10 ml concentrated HNO_3 was added then it was diluted to 1000 ml with distilled water **,APHA, 1995**. Concentrations of 50 ppm from these salts were used as adsorbate for different weights of nanosorbent.All the glassware used for dilution, storage and experiments were cleaned with extra detergent, thoroughly rinsed with tap water, soaked overnight in a 20% HNO_3 solution and finally rinsed with distilled water before use. Dissolved metal concentrations in solution were determined by a flame atomic absorption spectrophotometer (Buck, Accusys 211, USA).
Table 2. shows the main physicochemical properties of the metals tested.

3.2 Nanosorbent

(Fe_3O_4) nanoparticles obtained from US Research Nanomaterials, Inc., Houston, TX 77084, (USA) were used as nanosorbents. The main physical properties of the Nanopowder / Nanoparticales, Iron Oxide (Fe_3O_4) are listed in **Table 3. Table 4.** shows Certificate of Analysis -- % of Iron oxide Nanoparticales (Fe_3O_4).

The characteristics of the selected nanosorbents were evaluated ; namely: specific surface area, and external surface area. Results are presented in **Table 5**. External and specific surface areas of the nanosorbent were measured in Ministry of Oil / Petroleum Development and Research Centre. The results show that there is no significant difference between them. This indicates that the nanosorbents have no significant porosity and maintain a high external surface area. **Fig. 1** shows scanning electron micrographs for nanosorbent which carried out in Nano Research Center, University of Technology/Baghdad –Iraq.

3.2.1 Adsorption experiments for nanosorbents

A series of experiments were carried out in a batch system to obtain equilibrium data for adsorption of single, binary, ternary and quaternary metals solutions. **Table 6.** shows the major varied parameters used in these experiments.

3.2.2 Batch experiments for nanosorbent

3.2.2.1 Determination of the optimum pH

The effect of pH on Cu^{2+}, $Ni^{2+}$and Cd^{2+} ions adsorption onto nanosorbent was studied; 0.5 g nanosorbent of Fe_3O_4 was mixed with 100 ml of single metal ion solutions with concentration of 50 mg/l of Cu^{2+}, Ni^{2+} and Cd^{2+} ions respectively. These were maintained at different pH values ranging from 3 to 7 by using 0.1 M NaOH or HNO_3 solution at agitation speed of 200 rpm for a period of 30 min and at room temperature. Separation of nanosorbents from aqueous solution was evaluated by separating them via a small horseshoe magnet and wearing specific suits, thick gloves, special eye glasses, and special mask to prevent the direct contact with nanomaterial. Samples (10 ml) were taken from each volumetric flask and measured by using atomic absorption spectrophotometer AAS.

3.2.2.2 Equilibrium isotherm experiments

Different weights nanosorbent of Fe_3O_4 were used, (0.05, 0.1, 0.2, 0.4, 0.6, 0.8, 1, 1.2, and 1.4 g) , nanosorbents were placed in 9 volumetric flasks of 250 ml. A sample of 100 ml of measured concentration solution of 50 mg/l was added to each flask for single systems of Cu^{2+}, Ni^{2+} and Cd^{2+} respectively. The pH of the metal solutions was adjusted to the optimum pH value for each metal using 0.1M NaOH or 0.1M HNO_3. The flasks were then placed on a shaker (HV-2 ORBTAL, Germany) and agitated continuously for 50 min at 200 rpm and. A few drops of 0.1M HNO_3 were added to samples after separation of nanosorbent from aqueous solution to decrease the pH value below 2 in order to fix the concentration of the heavy metals during storage before analysis **,APHA, 1995.** The final equilibrium concentrations were measured by means of atomic absorption device. The residual concentration of cadmium, copper, and nickel in samples was determined using AAS in laboratory of Environmental Engineering Department/Baghdad University. The adsorbed amount is then calculated by the following equation:

$$q_e = \frac{V_l(C_o - C_e)}{W_{(nanosorbent)}} \quad (11)$$

The adsorption isotherms were obtained by plotting the weight of solute adsorbed per unit weight of biomass (q_e) against the equilibrium concentration of the solute in the solution (C_e) **,Vijayaraghavan and Yun, 2008**.

3.2.2.3 Thermodynamic parameters of adsorption

The effect of temperature on Cu^{2+}, Cd^{2+} and Ni^{2+} ions adsorption uptake onto nanosorbent was studied, 0.6 g of nanosorbent was mixed with 100 ml of single metal ion solutions with concentration of 50 mg/l of Cu^{2+}, Cd^{2+} and Ni^{2+} respectively. These were maintained at different temperature values ranging from 20 to 50°C for a period of 50 min, agitation speed was 200 rpm. Samples (10 ml) were taken from each volumetric flask and measured by AAS.

4. RESULTS AND DISCUSSION

4.1 Batch Systems for Nanosorbent

4.1.1 Effect of pH

The pH of the metal solution usually plays an important role in the adsorption of metals. As mentioned previously in sec.(3.2.2.1) **Fig. 2** shows the effect of over 6 pH values on the adsorption uptake of Cu^{2+}, Ni^{2+} and Cd^{2+} ions.

Beyond the value of pH 6.0 precipitation will occur to heavy metals, this due to the insoluble metal hydroxides start precipitating from the solutions at higher pH values and make the true sorption studies impossible. This should be avoided during sorption experiments which distinguish between sorption and precipitation metal removal becomes hard **,Quintelas et al., 2008.**At low pH, proton would compete for active binding sites with metal ions. The protonation of active sites thus tends to decrease the metal sorption. At low pH around 2 all the binding sites may be protonated, thereby desorbing all originally bound metals from the sorbent**, Aldre *et al.*, 2007.** Therefore optimum copper, nickel and cadmium ions adsorption process will be at pH 6 as shown in **Fig. 2**. These results agreed with the results obtained by **,Nassar, 2010.** And **,Grossl and Sparks,1994.**

4.1.2Effect of Contact time

Before the beginning the batch experiments, it was very important to know the required time to reach equilibrium adsorption. In other words, for all batch experiments, the contact time should be fixed at value to ensure reaching equilibrium concentrations. 0.6 g of nanosorbent of Fe_3O_4 was mixed with 100 ml of single metal ion solutions concentration of 50 mg/l of Cu^{2+}, Ni^{2+} and Cd^{2+} ions at pH 6. These were maintained at different time values ranging from 10 to 70 min. **Fig. 3** shows the results of removal efficiency (%) with the contact time of three metal solutions. It can be concluded that 50 min contact time is sufficient to reach equilibrium condition for all heavy metals.

4.1.3 Effect of initial heavy metal concentration

Different concentrations of 10, 50, 100 and 150 mg/l were selected to study the variation of removal efficiency with different initial concentrations at the same weight of nanosorbent (1 g) and at room temperature. The pH of heavy metal solutions was fixed at the optimum value for each heavy metal obtained from the isotherms experiments, and the agitation speed of the shaker was 200 rpm for contact time of 50min. as shown in **Fig.4.** It can be seen that the percentage removal efficiency was not altered greatly if the concentration increase from 10-50 mg/l, this behavior due to that 1 g of nanosorbent may contain enough sites for this concentration range, but when the concentrations increase to 100 and 150 mg/l the sites in 1 g will not be enough to accumulate these concentrations so that the depletion in percentage removal efficiency was obvious.

4.1.4 Effect of temperature and thermodynamic parameters

The effect of temperature on the equilibrium sorption capacity for Cu^{+2}, Ni^{+2} and Cd^{+2} ions has been investigated at temperature range between 20-50 °C. **Fig. 5** shows the variation of percentage removal efficiency with temperature.

From **Fig. 5**, it can be concluded that the increase in temperature leads to increase the percentage removal efficiency and the variation of temperature from 20-30 °C has no or little significant effect on the adsorption process, so that the adsorption experiments can be carried out at room temperature without any adjustment.

Thermodynamic parameters were obtained by varying temperature conditions over the range 20-50°C by keeping other variables constant. The values of the thermodynamic parameters such as $\Delta G°$, $\Delta H°$ and $\Delta S°$, describing copper, nickel and cadmium ions uptake by nanosorbent, were calculated using the thermodynamic equations: The apparent equilibrium constant for the process has been shown to be:

$$\Delta G = -RT\ ln(K_c) \quad (12)$$

Where

$$K_c = \frac{C_{ad}}{C_e} \quad (13)$$

Where K_c is the equilibrium constant, C_{ad} is the amount of metal adsorbed on the adsorbent per liter of the solution at equilibrium (mg/l), C_e is the equilibrium concentration of the metal in the solution (mg/l), T is absolute temperature (K) and R is the universal gas constant (8.314 J/mol K). Also, Gibbs free energy change ΔG^o , enthalpy changes (ΔH) and entropy changes (ΔS) can be estimated by the following equation **,Colak et al., 2009.**

$$\Delta G = \Delta H - \Delta S T \quad (14)$$

The positive values of $\Delta H°$ reveal the adsorption is endothermic and physical in nature. Generally, the change in adsorption enthalpy for physisorption is in the range of −20 to 40 kJ mol^{-1}, but chemisorptions is between −400 and −80 kJ mol^{-1}**,Zubeyde *et al.*, 2009. Fig. 6** and **Table 7.** show the thermodynamic constants of adsorption obtained for Cu^{2+}, Ni^{2+} and Cd^{2+} ions onto nanosorbents. **Table 7.** shows the values of enthalpy ΔH° were 12.8, 7.119 and 10.59 kJ.mo1^{-1} for Cu^{2+},Ni^{2+} and Cd^{2+} ions respectively, reveal the adsorption is endothermic and physical in nature. This is also supported by the increase in the values of uptake capacity of nanosorbents with the rise in temperature.

4.1.5 Estimation of adsorption isotherms constants

The adsorption for a single, binary,and ternary component systems of Cu^{2+}, Ni^{2+} and Cd^{2+} ions onto nanosorbent in batch experiments were conducted with initial concentration of (50 mg/l) and particle size of (20-30 nm) at room temperature in order to determine the isotherm constants for each system using different isotherm models.

4.1.6 Single component system

The adsorption isotherm for single component systems of of Cu^{2+}, Ni^{2+} and Cd^{2+} ions respectively, onto nanosorbent are shown in Fig. 7 to 9, whereas Fig. 10 shows a comparison between them. The data, for single component systems were correlated with six models illustrated in section (2.1). The parameters for each model obtained from non-linear statistical fit of the equation to the experimental data (STATISTICA software, version 6). **Table 8** shows parameters of single solute isotherm for Cu^{2+}, Ni^{2+} and Cd^{2+} ions uptake onto nanosorbent. **Fig. 11. to 13.** show comparison of some selective models applied in single system for copper, nickel and cadmium ions respectively.

Fig. 7 to 13 and **Table 8.** show the following:

- The equilibrium isotherm for each single component is of favorable type. n >1.
- The adsorption capacity q_e and heavy metals removal rate were related to the amount of adsorbent added; the greater adsorption capacity was obtained at lower adsorbent dose. The higher removal rate was achieved at higher adsorbent dose.
- The Freundlich model gives the best fit for the experimental data for single component adsorption system for copper, nickel and cadmium ions recognized by the highest values of (R^2),

this model has been used successfully to describe equilibrium adsorption. Results can be compared for the three adsorbates in term of maximum bending capacity and (n) parameters: $Cu^{2+} > Cd^{2+} > Ni^{2+}$.

- The copper which has the highest affinity order for being adsorbed by the nanosrbent, has the lowest hydration Van der Waals radius while nickel ions the least favorable by the nanosrbent, has the highest hydration Van der Waals radius, **Table 2.** This coincides with the fact that less hydrated ions radius is preferably accumulated at interface **,Hawari, 2006.**

4. 1.7 Binary component system

Binary systems are usually present in effluent from different industries. The data, for binary component systems were correlated with three models as mentioned in section (2.2). The parameters for each model obtained from non-linear statistical fit of the equation to the experimental data. The adsorption isotherms for binary component systems of Cu^{2+}, Ni^{2+} and Cd^{2+} ions onto nonabsorbent are shown in **Fig. 14. to 16**. **Table 9.** represents all parameters with correlation coefficient for binary systems.

Fig.17. to 22. show a three-dimensional adsorption surface for the simulation uptake for Cu^{2+}, Ni^{2+} and Cd^{2+} ions onto nanosorbents in binary mixtures.

4.1.8 Ternary component system

The adsorption isotherms for ternary component systems were correlated to which the best model was fitted in binary component system. The parameters for each model obtained from non-linear statistical fit of the equation to the experimental data.

The adsorption isotherms for ternary component systems of Cu^{2+}, Ni^{2+} and Cd^{2+} ions onto nanosorbent are shown in **Fig.23**.

Fig. 14 to 23. and **Tables 9. and 10.** show the following:

- For each the binary, ternary and quaternary systems the Combination of Langmuir- Freundlich model seems to give the best fitting for the experimental data at highest value of R^2. It can be seen from the figures, Cu^{2+} always adsorbed more favorable onto nanosrbent than Ni^{2+} and Cd^{2+} in binary and ternary systems.
- The decrease of adsorption capacity in binary and ternary systems compared to the single metal systems observed for all metals with exception of copper, reflects the existence of a competition between the metals studied for the binding sites present in nanoparticle wall. It seems that the total metal adsorption capacity onto the nanoparticle decreases when increasing the number of metals present. This fact supports the assumed competition between metals for the nano particle binding sites and tends to decrease the relative amount of each adsorbed element. These results agreed with the results obtained by **,Nassar, 2010**.

  Fig. 24 to 26 show that the metal removal efficiency of nanosorbent in single and mixed system was inhibited by the presence of the other heavy metals in the system. The removal efficiency of Cu^{2+} in single system is 100% reduced to 96.4% and 97.6% respectively in binary system with Cd^{2+} and Ni^{2+} ions respectively, while the removal efficiency of Cu^{2+} in ternary system reduced to 95% with [Cd^{2+} + Ni^{2+}]. The removal efficiency of Cd^{2+} in single system is 98.1% reduced to 64% and 88.6% respectively in binary system with Cu^{2+} and Ni^{2+} ions respectively, while the removal efficiency of Cd^{2+} in ternary system reduced to 47% with [Cu^{2+} + Ni^{2+}]. The removal efficiency of Ni^{2+} in single system is 82% reduced to 58.8% and 58%

respectively in binary system with Cd^{2+} and Cu^{2+} ions respectively, while the removal efficiency of Ni^{2+} in ternary system reduced to 20.4% with [Cd^{2+} + Cu^{2+}].

5. CONCLUSIONS

This study revealed the following conclusions, concerning the batch for nanosorbent Cu^{2+}, Cd^{2+}, and Ni^{2+} ions:

5.1 Batch Process for Nanosorbent

5.1.1 Single component system

1. Optimum pH was 6 for Cu^{2+}, Cd^{2+} and Ni^{2+}ions in adsorption process onto Fe_3O_4 nanoparticle (20-30 nm).
2. It can be concluded that 50 min contact time is sufficient to reach equilibrium condition for all heavy metals.
3. The equilibrium isotherm for each single component is of a favorable type and Freundlich isotherm gives the best fit model for representing the experimental data for this system.
4. In this system Cu^{2+} ions was the most favorable component rather than Cd^{2+} and Ni^{2+} ions, that due to its physiochemical characteristics that make the most favorable adsorbed component, due to the lowest hydration Van der Waals radius for copper. Results for the three adsorbates in term of adsorption capacity parameters were: Cu^{2+}>Cd^{2+}>Ni^{2+}.There were a good matching between experimental and predicted data.
5. It can be seen that the percentage removal efficiency was not altered greatly if the concentration increase from 10-50 mg/l, this behavior due to that the nanosorbent may contain enough sites for this concentration range, but when the concentrations increase to 100 and 150 mg/l the sites will not be enough to accumulate these concentrations so that the depletion in percentage removal was obvious.
6. Adsorption of Cu^{2+}, Cd^{2+} and Ni^{2+}ions was endothermic and physical in nature.

5.1.2 Binary and ternary component system

1. For each binary and ternary component systems, combination of Langmuir-Freundlich Isotherm gives the best fit for the experimental data.
2. The behavior of the equilibrium isotherm is of favorable type.
3. For each system Cu^{2+} ions is still most adsorbed component rather than Cd^{2+} and Ni^{2+}ions.
4. Due to the competitive effect of Cu^{2+}, Cd^{2+} and Ni^{2+}ions with each other to occupy the available site(s) of the nanosorbent, Cu^{2+}ions offers the strongest component that able to displace Cd^{2+} and Ni^{2+}ions from their sites, while Ni^{2+}ions was the weakest adsorbed component.
5. Compared with their adsorption in single component system the adsorption capacity of all three metals shows obvious decreases both in the binary and ternary system.

The percentage removal efficiency of each single component was decreased as each component presented with the other(s) in the binary and ternary system. This due to the presence of more than one component will enhance the competitive struggling race for occupying a certain site.

6. REFERENCE

- Aksu, Z., Gönen, F., Demircan, Z., 2002, *Biosorption of Chromium (VI) Ions by Mowital (R) B30H Resin immobilized Activated Sludge in a Packed Bed: Comparison with Granular Activated Carbon*, Process Biochem, 38,175–186.
- Aldre, J., Morais, B., Shiva, P., Valderi D. L., Antonio, G. S., 2007, *Biosorption of heavy metals in upflow sludge columns*, Bioresource Technology, 98 , 1418–1425.
- APHA, 1995, *Standard methods for the examination of water & wastewater*, 19th Edition, American Public Health Association,Washington, DC.
- Bamgbose, J.T., Adewuyi, S., Bamgbose, O., Adetoye, A.A., 2010, *Adsorption kinetics of cadmium and lead by chitosan*, Afr. J. Biotechnol. 9 2560–2565.
- Basha, S., and Murthy, Z., 2007, *Kinetic and equilibrium models for biosorption of Cr(VI) on chemically modified seaweed cystoseir indica*, Adv. Environ. Res, 42(11), 1521-1529.
- Bhaumik.M., Maity A., Srinivasu V.V., Onyango M.S. ,2012 , *Removal of hexavalent chromium from aqueous solution using polypyrrole-polyaniline nanofibers***,** Chemical Engineering Journal 181– 182 ,323– 333
- César, V., Joan, I., Adriana, F., José L., 2010, *Evaluating Binary Sorption of Phenol/Aniline from Aqueous Solutions onto Granular Activated Carbon and Hypercrosslinked Polymeric Resin (MN200)*, Water Air Soil Pollut, 210, 421–434.
- Cheueh, I. Z., 2005, *Ion Exchange Modeling of Silicotitanate Column for Chromium Removal from Arngentine Waste*, Wisting house Savannah River Company, USA.
- Colak, F., Atar, N., Olgun, A., 2009, *Biosorption of acidic dyes from aqueous solutionby Paenibacillus macerans: kinetic, thermodynamic and equilibrium studies*, Chem. Eng. J., 150 (1) 122–130.
- Fahmi, A. and Munther, K., 2003, *Competitive Adsorption of Nickel and Cadmium on Sheep Monure Waste, Experimental and Prediction Studies*, Separation Science and Technology, 38 (2), pp 483-497.
- Feng, Y., Gong, J.-L., Zeng, G.-M., Niu, Q.-Y., Zhang, H.-Y., Niu, C.-G., Deng J.-H., Yan ,M., 2010 , *Adsorption of Cd (II) and Zn (II) from aqueous solutions using magnetic hydroxyapatite nanoparticles as adsorbents*, Chem. Eng. J. 162 487–494.
- Gray, N.F., 2005, *Water technology; an introduction for environmental scientist's engineers*, Second edition, Elsevier Butterworth-Heinemann.
- Grossl,P.R., Sparks, D.L. , Ainsworth, C.C.,1994 , *Rapid kinetics of Cu(II) adsorption–desorption on goethite*, Environ. Sci. Technol. 28 1422–1429.
- Gupta ,V.K. ,Nayak, A. ,2012 , *Cadmium removal and recovery from aqueous solutions by novel adsorbentsprepared from orange peel and Fe_2O_3 nanoparticles*, Department of Chemistry, Indian Institute of Technology Roorkee, Roorkee 247667, India Chemical Engineering Journal 180 81– 90.
- Gupta V.K., Agarwal, S., Saleh, T.A.,2011, *Synthesis and characterization of alumina coated carbon nanotubes and their application for lead removal*, J. Hazard. Mater. 185 17–23.
- Hawari, H A., Mulligan N. C, 2006, *Biosorption of lead(II), cadium(II), copper(II) and nickel(II) by anaerobic granular biomass*, Bioresource technology, 97, 692-700.
- Hizal J., Apak, R.,2006, *Modeling of cadmium (II) adsorption on kaolinite-based clays in the absence and presence of humic acid*, Appl. Clay Sci. 32 232–244.

- Hu J, Chen, G.H., Lo I.M.C., 2005, *Removal and recovery of Cr (VI) from wastewater by maghemite nanoparticles*, Water Res;39(18):4528–36.
- Huang, X., Gao, N.Y., Zhang, Q.L., 2007, *Thermodynamics and kinetics of cadmium adsorption onto oxidized granular activated carbon*, J. Environ. Sci. 19 1287–1292.
- Jianlong, W., Can, C.,2009, "*Biosorbents for heavy metals removal and their future*, Biotechnology Advances, 27, 195–226.
- Khan, M. H., Keshtkar, A. R., Meysami B., Zarea, M. F., Jalali, R.,2006, *Biosorption of uranium from aqueous solutions bynonliving biomass of marinealgae Cystoseirandica*, Electronic Journal of Biotechnology, 9 (2), 100-106.
- Kratochvil, D., Volesky, B., 1998, *Advances in Biosorption of Heavy Metals*, Trend in Biotechnology, 16, 291-300.
- Lawrence, K. Wang, J. T., Stephen, T.T., Yung-Tse H., 2010 , *Handbook of environmental engineering, environmental bioengineering*, Springer New York Dordrecht Heidelberg London.
- Lin, C-C, Lai, Y-T., 2006, *Adsorption and recovery of lead(II) from aqueous solutions by immobilized Pseudomonas aeruginosa R08 beads*, J Hazard Mater, 137(105), 99–105.
- Liu ,J.F., Zhao, Z.S., Jiang, G.B., 2008, *Coating Fe_3O_4 magnetic nanoparticles with humic acid for high efficient removal of heavy metals in water*, Environ. Sci. Technol. 42 6949–6954.
- Manhan, S. T., 2005, *Controlling Heavy Metal in Water by Adsorption*, Bio. Che. J., 60(7), pp 801-803.
- Mashitah, M.D., Yus Azila, Y., Bhatia, S., 2008, *Biosorption of cadmium (II) ions by immobilized cells of Pycnoporus sanguineus from aqueous solution*, Bioresour. Technol, 99, 4742–4748.
- Maurya, N.S., Mitta, A.K., Cornel, P., Rother, E., 2006, *Biosorption of dyes suing dead macro fungi: effect of dye structure, ionic strength and pH*, Biores Technol, 97(21), 512–521.
- Nassar, N.N. ,2010 , "*Rapid removal and recovery of Pb(II) from wastewater by magnetic nanoadsorbents*"**,** Department of Chemical and Petroleum Engineering, University of Calgary, Calgary, Alberta, Canada ,Journal of Hazardous Materials 184 538–546
- Öztürk, A., Artan, T., Ayar, A., 2004, *Biosorption of nickel(II) and copper(II) ions from aqueous solution by Streptomyces coelicolor*, A3(2), Colloids and Surfaces B: Biointerfaces, 34(2), 105-111.
- Padmesh, T., Vijayaraghavan, K., Sekaran, G., Velan, M., 2006, *Application of Azolla rongpong on biosorption of acid red 88, acid green 3, acid orange 7 and acid blue 15 from synthetic solutions*, Chemical Engineering Journal, 122, 55–63.
- Panda ,G.C., Das, S.K., Guha ,A.K., 2008 , *Biosorption of cadmium and nickel by functionalized husk of Lathyrus sativus*, Colloids Surf. B: Biointerfaces 62 173–179.
- Panuccio ,M.R., Sorgonà, A., Rizzo, M., Cacco, G., 2009 , *Cadmium adsorption on vermiculite zeolite and pumice: batch experimental studies* ,J.Environ .Manage. 90 364–374.
- Quintelas, C., Fernandes, B., Castro, J., Figueiredo, H., Tavares, T., 2008, *Biosorption of Cr(VI) by three different bacterial species supported on granular activated carbon—A comparative study*, J, Hazardous Materials, 153, 799–809.
- Rao, C. S., 1994, *Environmental Pollution Control Engineering*, Wiley Estern, India.

- Ridha, M.J., 2011, *Competitive Biosorption of Heavy Metals Using Expanded Granular Sludge Bed Reactor*, Ph.D. Thesis, University of Baghdad, College of Engineering.
- Sahmoune, M., Louhab, K., Boukhiar, A., 2009, *Biosorption of Cr(iii) from aqueous solutions using bacterium biomass streptomyces rimosus*, Int. J. Environ. Res., 3(2), 229-238.
- Saleem, M., Chakrabarti, M.H., Irfan, M.F., Hajimolana, S.A., Hussain, M.A., 2011, *Electro-kinetic remediation of nickel from low permeability soil*, Int. J. Electrochem. Sci., 96, 4264-4275.
- Sevgi ,K., 2009 , *Adsorption of Cd (II), Cr (III) and Mn (II) on natural sepiolite*, Desalination 244 24–30.
- Shen, Y.F., Tang, J., Nie, Z.H., Wang, Y.D., Ren Y., Zuo, L., 2009, *Preparation and application of magnetic Fe_3O_4 nanoparticles for wastewater purification*, Sep. Sci. Technol.68 312–319.
- Shin, E.W., Karthikeyan, K.G., Tshabalala, M.A., 2007, *Adsorption mechanism of cadmium on juniper bark and wood*, Bioresour. Technol. 98 588–594.
- Sips, R., 1984 , *On the structure of a catalyst surface*, J. Chem. Phys. , 16, 490-495.
- Srivastava V., Weng, C.H., Singh, V.K., Sharma, Y.C., 2011, *Adsorption of nickel ions from aqueous solutions by nano alumina: kinetic, mass transfer, and equilibrium studies*, J. Chem. Eng. Data 56 1414–1422**.**
- Sulaymon, A. H., and Ahmed, K. W., 2008, *Competitive adsorption of furfural and phenolic compounds onto activated carbon in fixed bed column*, Environ. Sci. Technol. 42 (2), 392–397.
- Sulaymon, H. A., Abidb, A. B., and Al-Najar, A. J., 2009, *Removal of lead copper chromium and cobalt ions onto granular activated carbon in batch and fixed-bed adsorbers*, Chemical Engineering Journal.155(3), 647-653
- Taghi, g., Khosravi, M., and Rakhshaee, R., 2005 , *Biosorption of Pb, Cd, Cu and Zn from the wastewater by treated Azolla filiculoides with $H_2O_2/MgCl_2$*, International Journal of Environmental Science & Technology, 1(4), 265-271.
- Vijayaraghavan, K., Sung, W. W., Yeoung-S, Y., 2008, *Single- and dual-component biosorption of reactive black 5 and reactive orange 16 onto polysulfone-immobilized esterified corynebacterium glutamicum*, Ind. Eng. Chem. Res. 47, 3179-3185.
- Vijayaraghavan, K., Yun, Y.S., 2008, *Bacterial biosorbents and biosorption*, Biotechnology Advances, 26, 266–291.
- Wang, J., and Chen, C., 2009 , *Biosorbents for heavy metals removal and their future*, Biotechnology Advances, 27, 195–226.
- Wikipedia, *The Free Encyclopedia*, Internet Resource, 2 January 2014 <http://en.wikipedia .org/wiki/periodic_table#>.
- Xu , P., Zeng,M.,G. , Huang ,L.,D., Feng ,L.,C., Shuang Hu. ,S., Zhao H.,M.,Lai, C., Wei, Z., Huang ,C., Xie, X.,G., Liu, F.,Z., 2012 , *Use of iron oxide nanomaterials in wastewater treatment: A review* Science of the Total Environment 424 1–10
- Zubeyde, B., Ercan, C.¸ Mehmet, D., 2009, *Equilibrium and thermodynamic studies on biosorption of Pb(II) onto Candida albicans biomass*, Hazardous Materials 161, 62–67.

Table 1. Constant parameter R_L.

R_L	Type of isotherm
$R_L > 1$	unfavorable
$R_L = 1$	linear
$R_L = 0$	irreversible
$0 < R_L < 1$	favorable

Table 2. Main physicochemical properties of the metals tested **,Wikipedia,2014.**

Properties	Copper	Nickel	Cadmium
Formula	Cu^{2+} from $Cu(NO_3)_2$	Ni^{2+} from $Ni(NO_3)_2$	Cd^{2+} from $Cd(NO_3)_2$
Appearance	blue crystals	Emerald green solid	white crystals
Molar mass ($g \cdot mol^{-1}$)	241.6	290.79	236.42
Standard atomic weight	63.546	58.6934	112.414
Solubility in water g/100 ml	137.8 (0°C) 1270(100°C)	94.2 (20°C) 158 (60°C)	325 (15°C) 156 (25°C)
Melting point	114.5 °C	56.7 °C	59.5 °C
Boiling point	170 °C	136.7 °C	132 °C
Atomic Radius(pm)	128	124	151
Van der Waals radius(pm) *	140	163	158
Electronegativity (Pauling scale) **	1.9	1.91	1.69
Electrical resistivity nΩ·m(20 °C)	16.78	69.3	72.7(22 °C)
Magnetic ordering	diamagnetic	Ferromagnetic	diamagnetic
Density (g/cm^3)	2.32	2.05	2.455
Charge	2	2	2
Company	BDH (England)	Fluka (Switzerland)	RIEDEL-DE HAEN AG (Germany)

* pico meter $=10^{-12}$ m.
**Pauling Scale: A dimensionless quantity, on a relative scale running from around 0.7 to 3.98 (Hydrogen was chosen as the reference, its electronegativity was fixed first at 2.1, later revised to 2.20).

Table 3. The main physical properties of the Nanosorbent(manufactural reported).

Physical Properties of the Nanosorbent, Iron Oxide (Fe_3O_4)	
Purity	98+%
Average Particle Size	20-30 nm
Surface Area	40-60 m^2/g
Color Dark	Dark Brown

Morphology	spherical
Bulk Density	0.84 g/cm3
True Density	4.8-5.1 g/cm3

Table 4. Certificate of Analysis --% Iron oxide Nanoparticales (manufactural reported).

Certificate of Analysis --% Iron oxide Nanoparticales (Fe_3O_4)				
Ca	**Cr**	**K**	**Mn**	**SiO2**
0.02290<	0.0016<	0.0012<	0.086<	0.142<

Table 5. Characterizations of Fe_3O_4 nanosorbents considered in this study**.**

Manufacturer reported surface area (m^2/g)	**Specific surface area (m^2/g)**	**External surface areas(m^2/g)**
40-60	63	61

Table 6. Major experimental parameters that varied in batch experiments.

	Parameter	**Range**	**Purpose**
Batch	pH	3, 4, 5 ,6 and 7	To find the optimum pH of removal efficiency.
	Nanosorbent weight	0.05, 0.1, 0.2, 0.4, 0.6,0.8, 1,1.2, and 1.4 g	To plot the equilibrium isotherm curves.
	Temperature	20, 35, and 50 °C	To study the thermodynamic parameters of adsorption.
	Initial conc.	10, 50, 100, and 150 ppm	To study the effect of initial conc. on the adsorption.

Table 7. Thermodynamic constants of adsorption obtained for Cu^{+2}, $Cd^{+2}$and Ni^{+2} ions sorption onto nanoadsorbent.

Metal	Temperature (K)	ΔG^0 ($kj.mol^{-1}$)	ΔH^0 ($kj.mol^{-1}$)	ΔS^0 ($j.mol^{-1}K^{-1}$)	R^2
Cu^{+2}	293 308 323	-2.23055 -3.26050 -3.77921	12.8	0.051	0.964
Cd^{+2}	293 308 323	-0.9404 -1.69034 -2.12666	10.59	0.039	0.977
Ni^{+2}	293 308 323	-0.0359 -0.41427 -0.7686	7.119	0.024	0.999

Table (8). Parameters of single solute isotherm for Cu^{2+}, Ni^{2+} and Cd^{2+} ions for nanosorbent

MODEL	PERAMETER	SINGLE		
		Cu^{+2}	**Cd^{+2}**	**Ni^{+2}**
Langmuir $q = \frac{bq_m C_e}{1 + bC_e}$ **,Lin and lai, 2006.**	q_m(mg/g)	9.4223	11.698	5.7933
	b(l/mg)	0.4247	0.0613	0.0639
	R^2	0.8143	0.865	0.86
Freundlich $q = KC_e^{1/n}$ **,Öztürk *et al.*,2004.**	K, $(mg/g)(mg/l)^{(1/n)}$	3.544	1.8751	0.9446
	n,-	3.6695	2.4836	2.4801
	R^2	0.899	0.9217	0.8816
Redlich–Peterson $q_e = \frac{K_{RP} C_e}{1 + a_{RP} C_e^{\beta_{RP}}}$ **,Maurya *et al.*, 2006.**	k_{RP}(mg/g)	0.2138	0.1569	1.562e13
	a_{RB}(l/mg)	-0.2283	-0.3198	1.913e13
	ß,-	0.00002	0.000006	0.556
	R^2	0.5604	0.768	0.8807
Sips $q_e = \frac{K_s C_e^{\beta_s}}{1 + a_s C_e^{\beta_s}}$ **,Sips, 1984.**	k_s, (l/g)	0.46034	0.5227	0.05114
	ß	0.02268	0.0498	0.00684
	a_s,(l/mg)	-0.8729	-0.772	-0.963
	R^2	0.877	0.902	0.865
Khan $q_e = \frac{q_{max} b_k C_e}{(1 + b_k C_e)^{a_k}}$ **,Khan *et al.*, 2006.**	q_m (mg/g)	0.6502	0.25353	0.34003
	b_k,(l/mg	513.204	139.262	12.7709
	a_k	0.728	0.596	0.59743
	R^2	0.8887	0.9015	0.8714
Toth $q_e = \frac{q_{max} b_T C_e}{\left[1 + (b_T C_e)^{\frac{1}{n_T}}\right]^{n_T}}$	q_m (mg/g)	102.994	227.12	44.5025
	b_T	736.78	1.8023	0.4606
	n_T	8.789	7.443	5.2311
	R^2	0.8908	0.913	0.877

,Vijayaraghavan and Yun, 2008.				

Table 9. Parameters of binary systems solutes isotherms for copper,nickel and cadmium ions onto nanosorbent.

Binary system																							
	Cd^{+2},Ni^{+2} system				Cu^{+2},Ni^{+2} system				Cu^{+2},Cd^{+2} system				Parameter				Model						
	Ni^{+2}		Cd^{+2}		Ni^{+2}		Cu^{+2}		Cd^{+2}		Cu^{+2}		q_m (mg/g)		b (l/mg)		R^2	a,-		ß,-		R^2	Extended Langmuir Eq.(8)
1.856		5.822		2.537		8.939		3.311		7.7233		0.1		0.1		0.699	0.0034		2.064		0.866	Redlich-Peterson Eq.(9)
0.1		0.1		0.1		0.1		0.1		0.1		0.804		0.881		——		0.724	17.98		0.908		144.54		0.008	12.99		0.269	0.941	0.9228		6.71		0.1		3.218		0.299		4.9336		1.603	0.9336		0.1		0.1		0.1		2.3173		0.6575		161.69		1.823	0.269		0.1		1.895	3.0821		1.5657		1.5246		1.6444		2.962	1.894		0.956		0.897		0.983		0.912	0.938		0.936	Combination of Langmuir-Freundlich Eq.(10)

Table10. Parameters of ternary system solutes isotherms for copper,nickel and cadmium ions onto nanosorbent.

Ternary system				
Model	Parameters	Cu^{+2},Cd^{+2}, Ni^{+2} system		
		Cu^{+2}	Cd^{+2}	Ni^{+2}
Combination of Langmuir-Freundlich Eq.(10)	q_m (mg/g)	0.746	1.78	0.622
	b (l/mg)	2.482	0.098	0.103
	n	1.999	1.065	1.124
	R^2	0.95	0.874	0.833

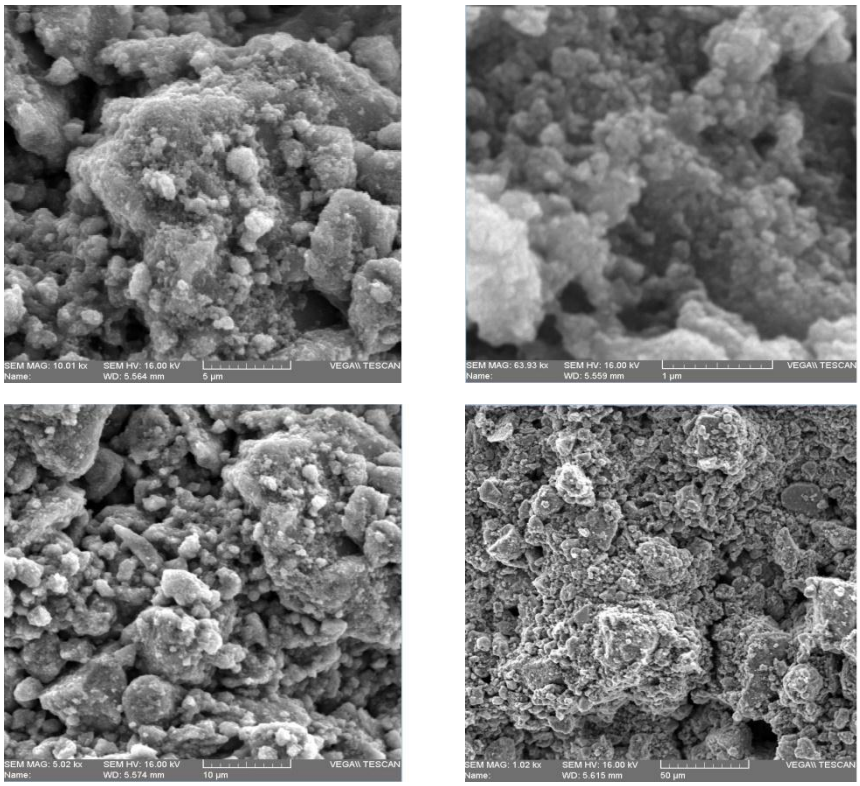

Figure 1. Scanning electron micrographs for nanosorbent.

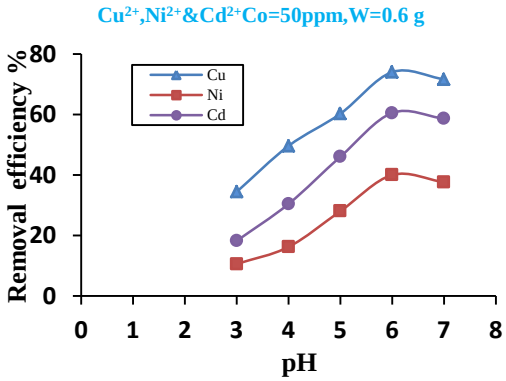

Figure 2. Effect of different pH values on copper, nickel and cadmium ions uptake by nanosorbents, $C_{nanosorbents}$= 6g/l, $C_{o(Cu, Ni and Cd)}$=50 mg/l.

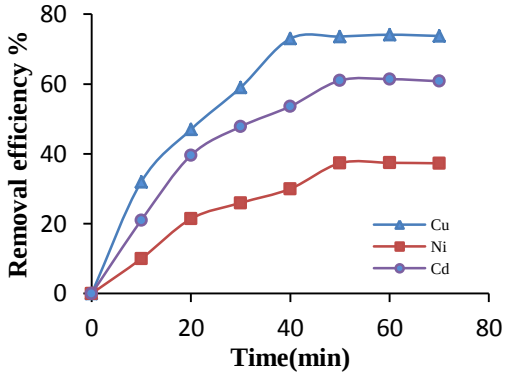

Figure 3. Adsorption efficiency for nanosorbent with different contact time, C_o=50 ppm, pH=6, $W_{nanosorbent}$=0.6 g, 200 rpm.

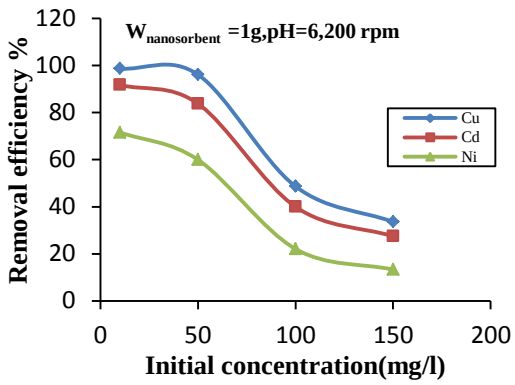

Figure 4. Percentage of removal adsorption efficiency with variation of initial concentration, contact time 50 min and 200rpm

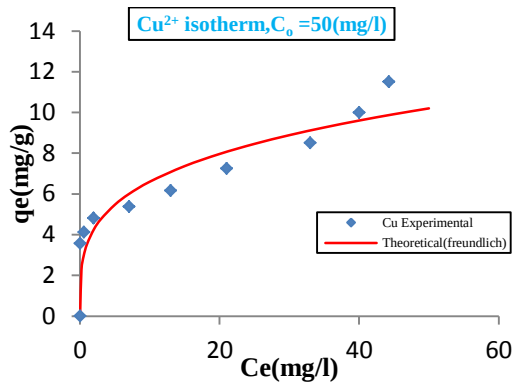

Figure 7. Adsorption isotherm for copper ions onto nanosorbent.

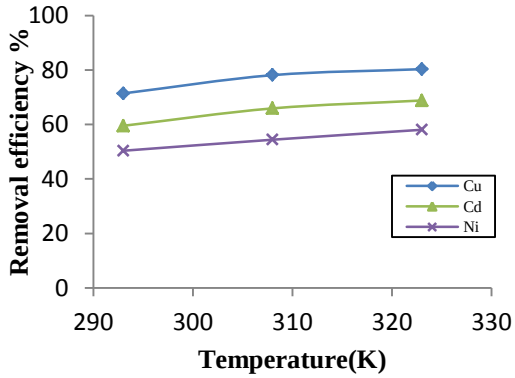

Figure 5. Variation of percentage removal with solution temperature, C_o=50 ppm, contact time 50min.,$W_{nanosorbent}$=0.6g, and 200rpm.

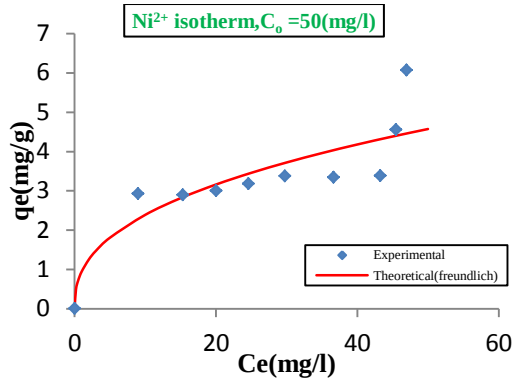

Figure 8. Adsorption isotherm for nickel ions onto nanosorbent.

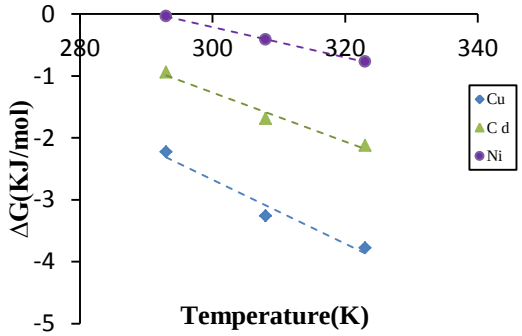

Figure 6. Change in free energy with temperature for the adsorption of Cu^{2+}, Ni^{2+} and Cd^{2+} ions by nanosorbent at initial concentration of 50 mg/l, and pH 6.

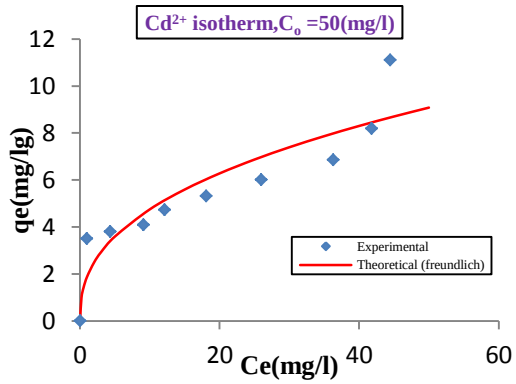

Figure 9. Adsorption isotherm for cadmium ions onto nanosorbent.

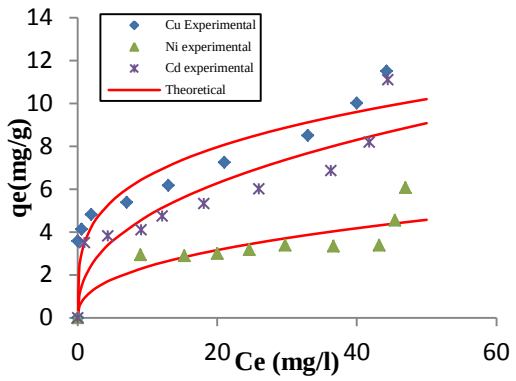

Figure 10. Adsorption isotherms of Cu, Ni and Cd ions as single solutes onto nanosorbent.

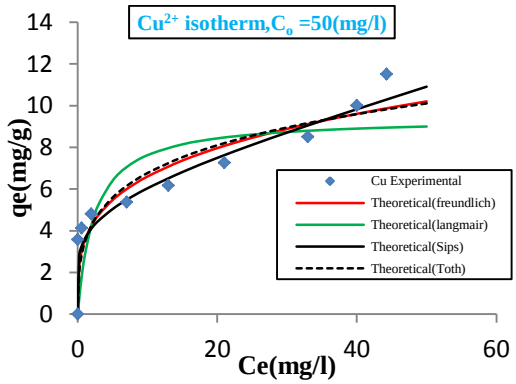

Figure 11. Comparison of some selective models applied in single system for copper ions onto nanosorbent.

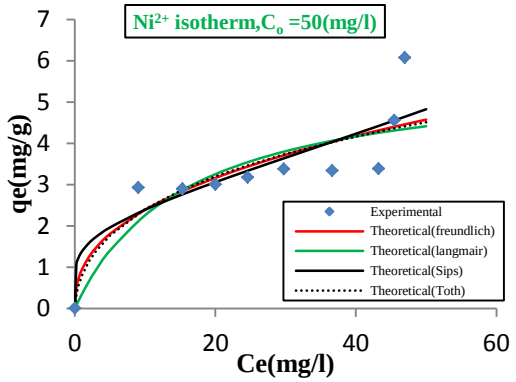

Figure 12. Comparison of some selective models applied in single system for nickel ions onto nanosorbent.

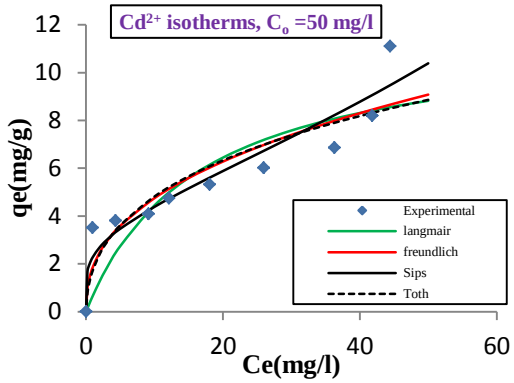

Figure 13. Comparison of some selective models applied in single system for cadmium ions onto nanosorbent.

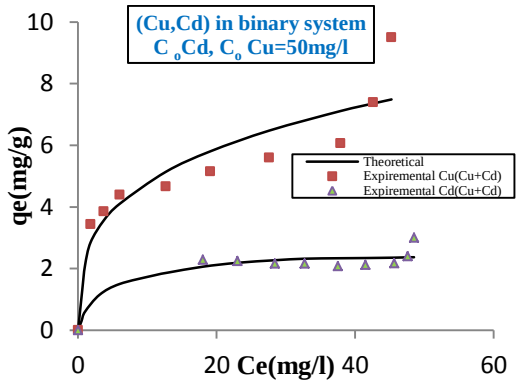

Figure 14. Adsorption isotherms of copper and cadmium ions onto nanosorbent.

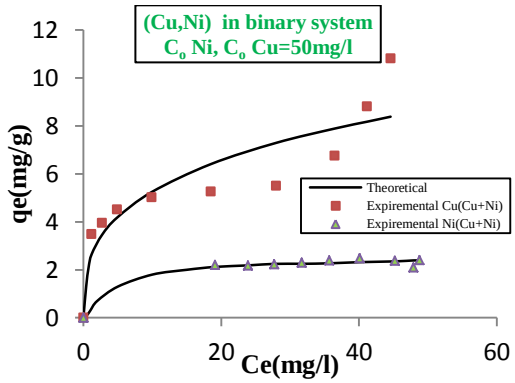

Figure 15. Adsorption isotherms of copper and nickel ions onto nanosorbent.

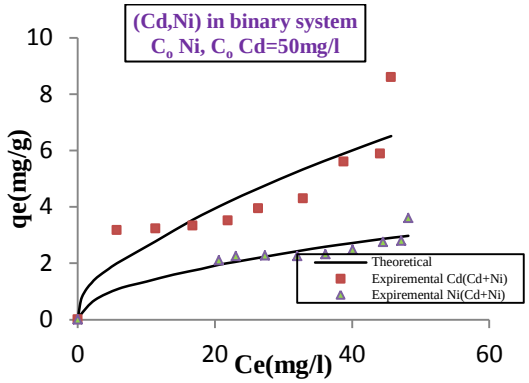

Figure 16. Adsorption isotherms of cadmium and nickel ions onto nanosorbent.

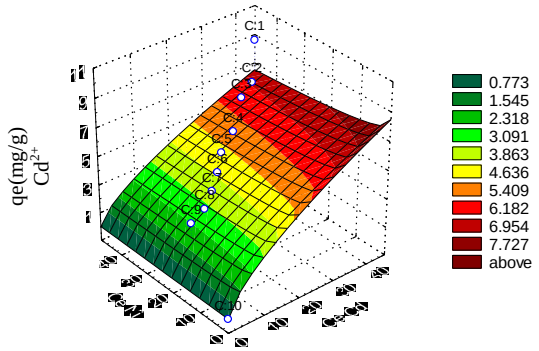

Figure 19. A three-dimensional adsorption surface for the simultaneous uptake of Cd ions onto nanosorbent from Cd ions and Ni ions binary mixtures.

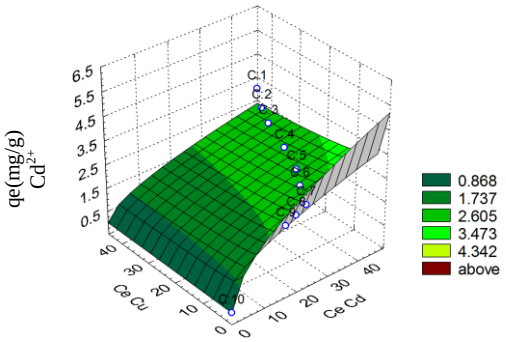

Figure 17. A three-dimensional adsorption surface for the simultaneous uptake of Cd ions onto nanosorbent from Cd ions and Cu ions binary mixtures.

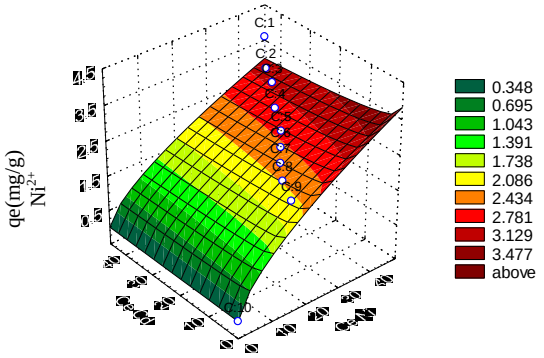

Figure 20. A three-dimensional adsorption surface for the simultaneous uptake of Ni ions onto nanosorbent from Ni ions and Cd ions binary mixtures.

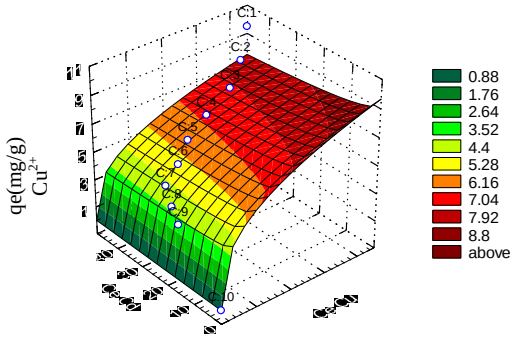

Figure 18. A three-dimensional adsorption surface for the simultaneous uptake of Cu ions onto nanosorbent from Cu ions and Cd ions binary mixtures.

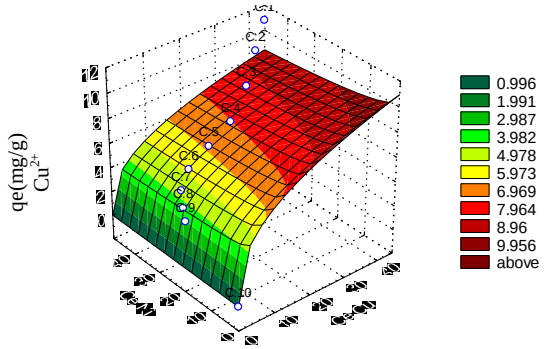

Figure 21. A three-dimensional adsorption surface for the simultaneous uptake of Cu ions onto nanosorbent from Cu ions and Ni ions binary mixtures.

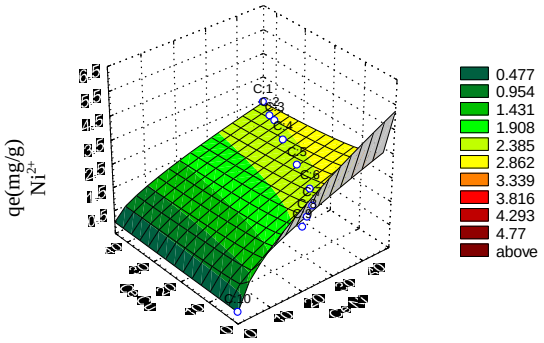

Figure 22. A three-dimensional adsorption surface for the simultaneous uptake of Ni ions onto nanosorbent from Ni ions and Cu ions binary mixture.

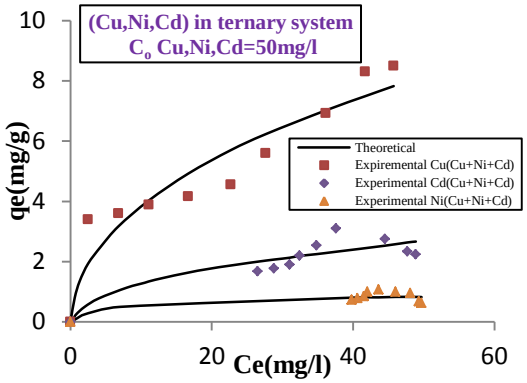

Figure 23. Adsorption isotherms of copper, cadmium and nickel ions onto nanosorbent.

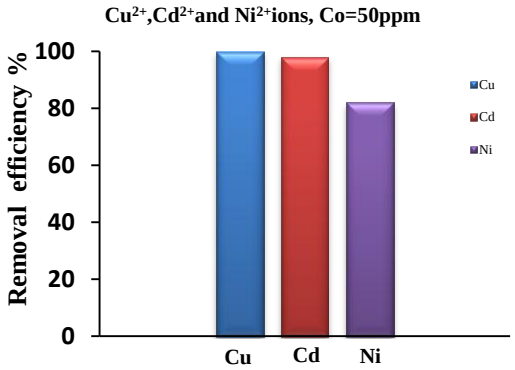

Figure 24. Adsorption of copper, nickel and cadmium ions, when used in single system.

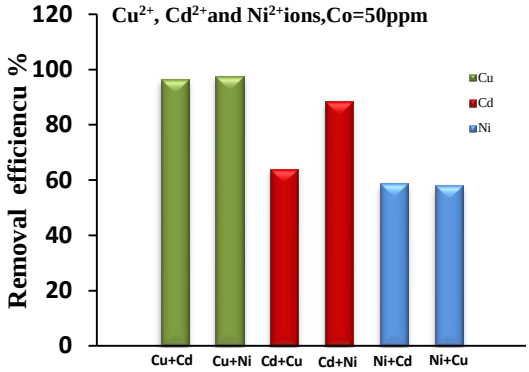

Figure 25. Adsorption of copper, nickel and cadmium ions, when used in binary system.

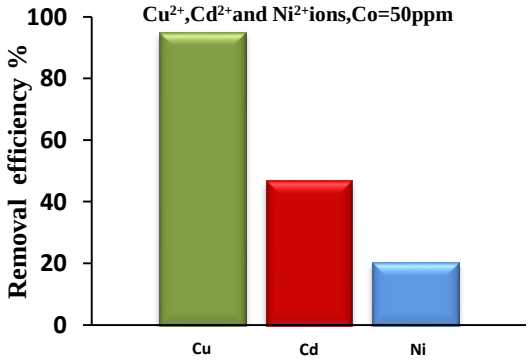

Figure 26. Adsorption of copper, nickel and cadmium ions, when used in ternary system.

Deterministic Analysis of Wind Loads Effects on High-Rise Buildings

Dr. Salah R. Al Zaidee
Instructor
College of Engineering
University of Baghdad
Email: salahalzaidee2004@gmail.com

Ashraf Hameed Alsalmani
Civil Engineer
College of Agriculture
University of Baghdad
Email: ashraf.hameed@gmail.com

ABSTRACT

This paper studies the effect of mean wind velocity on tall building. Wind velocity, wind profile and wind pressure have been considered as a deterministic phenomenon. Wind velocity has been modelled as a half-sinusoidal wave. Three exposures have been studied B, C, and D. Wind pressure has been evaluated by equation that joined wind pressure with mean wind velocity, air density, and drag coefficient.

Variations of dynamic load factor for building tip displacement and building base shear have been studied for different building heights, different mode shapes, different terrain exposures, and different aspect ratios of building plan. SAP software, has been used in modelling and dynamic analysis for all case studies.

Results For different building heights considered maximum dynamic load factor (DLF) occurs in height range from 100-150m because fundamental building frequency is so close as to dominate wind frequency. Effect of higher modes become insignificant for height greater than 175m. Effect of three different terrain exposures B, C, and D on DLF for tips displacement and building base shear have been insignificant effect on response of tip displacement and building base shear. . Finally, effect of aspect ratio λ for different building heights with dynamic load factor (DLF) for tips displacement and for building base shear have λ approaching 2, fundamental building frequency is so closed to dominate wind frequency.

KEY WORDS: dynamic load factor, frequency, terrain.

التحليلات المحددة لتأثير أحمال الرياح على البنايات العالية متعددة الطوابق

صلاح رحيمة عبيد
مدرس – دكتور
كلية الهندسة
جامعة بغداد

أشرف حميد السلماني
مدرس مساعد
كلية الزراعة
جامعة بغداد

الخلاصة

تمت دراسة تأثير الرياح في معدلاتها ، سرعة الرياح ، مقطع الرياح و ضغط الرياح والذي تم اعتباره كظاهرة محددة ، سرعة الرياح تمت معاملتها كدالة نصف جيبية. تم تصنيف الأرض الى ثلاث مناطق تعرض هي B و C و D. تم تقييم ضغط الرياح من خلال معادلة تربط ضغط الرياح بمعدل سرعة الرياح و كثافة الهواء و معامل الأعاقة.

تمت دراسة تأثير الرياح في معدلاتها ، على اختلاف معامل الحمولة الديناميكية لأقصى ازاحة واكبرقوة قص في القاعدة اخذين بنظر الأعتبار المعاملات التالية: ارتفاع البناية ، خشونة تضاريس المنطقة، طور الأهتزاز، نسبة الطول الى العرض بالنسبة للبناية.

كانت النتائج لعدة ارتفاعات للبناية لأقصى ازاحة واكبر قوة قص في القاعدة مع اختلاف معامل الحمولة الديناميكية تحدث في مدى ارتفاع البناية بين (100-150)م وذلك بسبب معامل الحمولة الديناميكية يزداد عند اقتراب تردد الرياح من أحد ترددات البناية.

بالنسبة لنتائج تأثير طور الأهتزاز مع اختلاف معامل الحمولة الديناميكية لأقصى ازاحة واكبرقوة قص في القاعدة كان التأثير غير مهم عندما يكون ارتفاع البناية اكبرمن 175م.
كانت نتائج تأثير مناطق التعرض الثلاث B و C و D مع اختلاف معامل الحمولة الديناميكية لأقصى ازاحة واكبرقوة قص في القاعدة تأثيرها غير مهم.
اخيرا كان تأثير اختلاف نسبة الطول الى العرض بالنسبة للبناية مع اختلاف معامل الحمولة الديناميكية لأقصى ازاحة واكبرقوة قص في القاعدة عندما تكون λ مساوية الى 2 وذلك بسبب معامل الحمولة الديناميكية يزداد عند اقتراب تردد الرياح من أحد ترددات البناية.

الكلمات الرئيسة: معامل الحمولة الديناميكية ، التردد ، التضاريس.

1. INTRODUCTION

To study the effect of mean wind velocity for high-rise buildings, different parameters have been studied in this study:

Time Function of Gust Front Winds

A half-sine wave could be used to describe time-varying feature of windstorms. Even though it may not represent the exact time variation of winds in a typical gust-front, it captures the underlying feature potentially responsible for enhanced loads. At a future time, this description may be revised once a sufficient number of measurements become available and an acceptable description of this function is arrived at based on an ensemble average of such observations. The function is defined as, **,Kwon, and Kareem, 2013**.

$$\bar{x}_{G-F}(t) = \bar{x}_o \sin(\frac{\pi}{t_d} t) \qquad (1)$$

where $\mathbf{t_d}$, is pulse duration of the excitation. The simplicity of above expression is an attractive feature, as it requires only a single parameter $\mathbf{t_d}$ in addition to $\bar{x}_o$ **,Kwon, and Kareem, 2013.**

Wind Profile

Every building site has its own unique characteristics in terms of surface roughness and length of upwind terrain associated with the roughness. Simplified code methods cannot account for the uniqueness of the site. Therefore, the code approach is to assign broad exposure categories for design purposes**, ,Taranath, 2005.**

Similar to the ASCE method, the UBC distinguishes between three exposure categories; B, C, and D. Exposure B is the least severe, representing urban, suburban, wooded, and other terrain with numerous closely spaced surface irregularities; Exposure C is for flat and generally open terrain with scattered obstructions; and the most severe, Exposure D, is for unobstructed coastal areas directly exposed to large bodies of water**, Taranath, 2005.**

Each exposure differs from another exposure in the thickness of boundary layer and power law. Exposure B is depicted with power law $\alpha = 0.14$ with thickness of boundary layer 366m. On the other hand, exposure C is depicted with power law $\alpha = 0.11$ with thickness of boundary layer 274.5m. Finally, exposure D is depicted with a power law $\alpha = 0.09$ with thickness of boundary layer 213.5m**, ,Taranath,2005**. Equations below depicted mean wind velocity within the atmospheric boundary layer:

$$\bar{x}(z) = \bar{x}(z_{ref})\left(\frac{z}{z_{ref}}\right)^{\alpha} \quad (2)$$

$\bar{x}(z)$ is the mean wind speed at height **z** above the ground, z_{ref} is the reference height, and α is the power law exponent, depending on the type of the exposure**,Balendra,1993.**

Wind Pressure:

For calculating the wind pressure, Eq. (3) that is prepared for wind force, should be adjusted by dividing by **B**:

$$F_D = \frac{1}{2}\rho C_D B\left[\bar{x}(z)\right]^2 \quad (3)$$

$$p_D = \frac{1}{2}\rho C_D\left[\bar{x}(z)\right]^2 \quad (4)$$

where p_D is the drag pressure in **Pa**, ρ is the density of air (1.2 kg/m^3), $\mathbf{C_D}$ is the drag coefficient, and $[\bar{x}(z)]^2$ is the square of mean wind velocity in m/sec, which, is within the atmospheric boundary layer is described by power law in Eq.(2).

By substitute Eq. (2) into Eq. (4), the drag pressure will be:

$$p_D = \frac{1}{2}\rho C_D\left[\bar{x}(z_{ref})\right]^2\left[\left(\frac{z}{z_{ref}}\right)^{\alpha}\right]^2 \quad (5)$$

Drag Coefficient:

For rectangular buildings, the drag coefficients depend strongly upon aspect ratio λ, which equal to **D/B**,

$$\lambda = \frac{\textit{plan dimension along wind direction "D"}}{\textit{plan dimension across wind direction "B"}} \quad (6)$$

See **Table1. ,Simiu, and Robert, 1996.**

Response Spectrum for Wind Load

Based on above discussions, it is clear that wind drag force and wind drag pressure will be in a quadratic proportional relation with wind velocity, which in turn is a sinusoidal function. Then wind pressure and wind force will be a sinusoidal function with second power order.

Dynamic load factor (DLF) for single degree of freedom systems when subjected to above second power sinusoidal function has been determined numerically based on Matlab routine. Results have been depicted graphically in **Fig.1**.

2. SAP MODELLING

Frame Element

Frame element has been used in model of building beams and columns. The frame element is a very powerful element that can be used to model beams, columns, braces, and trusses in planar and three-dimensional structures. A Frame element is modeled as a straight line connecting two points. Each element has its own local coordinate system for defining section properties and loads, and for interpreting output.

Each Frame element may be loaded by gravity (in any direction), multiple loads (concentrated, distributed, strain deformations etc.). Element internal forces are produced at the ends of each element and at a user specified number of equally spaced output stations along the length of the element **,CSI, 2009.**

Shell Elements:

SAP shell element that could accommodate arbitrary geometry, and which could interact with edge beams and supports, has been used in slab modelling for floors and roofs **,Wilson,2002.**

Mass Modelling

In SAP, mass and weight serve different functions. Mass is used for the inertia in dynamic analyses, and for calculating the built-in acceleration loads. Weight is a load that one defines and assign to one or more members, and could then be applied to one or more load cases.

SAP offers three different methods, shown in the interactive box below, to generate mass matrix see **Fig**.**2**

The two approaches in **Fig**.**2** could be combined together with From Element and Additional Masses and Loads option,

In this work, the applied load that consists of dead and live loads have been applied through From Loads option.

SAP Wind Idealization:

2.1.1 Spatial modeling of wind load

With SAP, the following steps could be followed to define spatial variation in drag wind pressure:

- Create an area with "None" properties (SAP offers such types of area object to be used in cladding modeling).
- Assign uniform pressure to the created area with a magnitude, which depends on story level (calculated from wind profile).

2.1.2 Temporal modelling of wind load:

With SAP, time function is used to define temporal variation in wind pressure.

2.1.3 Load case definition

Finally, temporal and spatial time variation are merged together through load case definition.

This procedure is called the mode superposition method, or more precisely the mode displacement superposition method**, ,Clough, and Penzien, 2003.**

3. CASE STUDY

Structural system for all case studies of this chapter has been assumed as Bundled Tube system, as this system is the most suitable one for considered height range.

Within case studies of these sections, dynamic load factor for mean wind pressure has been determined for different: (Heights, Modes, Roughness, Aspect Ratio, and Gust.

In all case studies, following data have been used, see **Table 2.**

- Building self-weight has been computed automatically by the SAP
- Mean wind speed has been assumed to be 45 m/sec with a sinusoidal time history.
- Slab thickness for floors, roofs, and shear walls has been assumed 0.2m.
- Damping ratio has been assumed 0.03 for all modes**, ,Arkawa, and Yamamoto, 2004.**

Height Versus Dynamic Load Factor:

Five buildings with different heights of 60, 120, 180, 240, and 300 m have been considered. For all buildings, plan dimensions have been assumed 63m by 63m.

Exposure B and wind gust time duration of 5 sec have been assumed with all heights with drag coefficient 1.18.

Results for above different heights have been presented, summarized, and discussed in sub-sections below:

For example, one hundred story (300m height) has been presented

3.1.1 One hundred story high building

SAP rendering view for the building has been shown in **Fig**.**3**:

Time history for tip displacement and building base shear are shown in **Fig**.**4** and **5**.

3.1.2 Summary of results for different heights

Variation of tip displacement and building base shear with building height have been summarized in **Table.3**, **Fig**.**6**, and **7**

From **Table 3.** and **Fig**.**6** and **Fig**.**7**, maximum DLF occurs in height range from (100-150)m. Comparing between wind response spectrum that discussed in section 1.5 (reproduce here for convince), one can conclude that within this height range, fundamental building frequency is so close as to dominate wind frequency.

Modes Versus Dynamic Load Factor:

This section aims to discuss the effect of higher modes on accuracy of estimating DLF under mean wind pressure.

- Dynamic responses for five buildings with different heights (60, 120, 180, 240, and 300 m) have been estimated based on and including (first mode only, first and second mode, and lower 12 modes.

For all buildings, plan dimensions have been assumed 63m by 63m with drag coefficient 1.18 and with gust time 5sec.

Results for tip displacement and building base shear with different modes are summarized in the **Fig**.**8** and **Fig**.**9** below. From these Figures, one can conclude that for buildings that have plan similar to considered in this study, effects of higher modes become insignificant for building height greater than 175m. While for lower heights, at least lowest two modes, they should be considered in building dynamic response.

Roughness Versus Dynamic Load Factor:

Effects of terrain exposure on DLF have been considered in this section. Wind pressures that are derived based on three different exposures (B, C, and D) have been subjected on buildings with different heights (60, 120, 180, 240 and 300 m). All buildings considered in this section have plan dimensions of 63m by 63m with drag coefficient 1.18 and with gust time 5sec.

Results for DLF for tips displacement and DLF for building base shear versus height for the three terrain exposures have been summarized in **Fig.10** and 11. From these Figures, one can conclude that for buildings that are considered in this section, terrain exposure has insignificant effect on response of tip displacement and building base shear.

Aspect Ratios Versus Dynamic Load Factor:

Effect of aspect ratio for building plan on DLF for tip displacement and building base shear are considered in this section. Aspect ratio in this section is defined as Eq. (6)

Four different "D" values (20, 40, 100, and 200) with constant "B" value of 20m have been considered. These lead to four different aspect ratios "λ" of 1, 2, 5, and 10. For each aspect ratio, corresponding drag coefficient "CD" has been determined based available wind tunnel data**, ,Simiu, and Robert, 1996.**

Exposure B, wind gust duration of 5 sec, and building height 150m have been assumed with all case studies of this section.

Results of DLF for tips displacement and DLF for building base shear versus aspect ratio are summarized in **Table 4. Fig.12, and 13**. Tables and Figures, show that maximum DLF tip displacement occurs when λ approaches 2. Comparing between wind response spectrums discussed in section 1.5, one can conclude that within this λ range, fundamental building frequency is so close to dominate wind frequency.

4. CONCLUSIONS

- Based on modeling of building beams and columns as frame elements, and modeling of floors, roofs and shear walls as shell elements, and modeling of wind gust as a sinusoidal function, following results and conclusions have been obtained:
- For different building heights considered in this study, it has been noted that the maximum dynamic load factor (DLF) occurs in height range from 100-150m. Within this height range, fundamental building frequency is so close as to dominate wind frequency.
- In an attempt to determine effects of higher modes on dynamic response of tall buildings, different numbers of mode shapes have been included in this study. From tip displacement and base shear results, it has been noted that for buildings, that have a plan similar to that considered in this study, effects of higher modes become insignificant for height greater than 175m. While for lower heights, at least lowest two modes they should be considered in building dynamic response.
- Effects of three different terrain exposures B, C, and D on DLF for tips displacement and DLF for building base shear have been considered. Based on obtained results, it has found that terrain exposure has insignificant effect on response of tip displacement and building base shear.
- Dynamic load factor (DLF) for tips displacement and for building base shear have been determined for different aspect ratios of building plan. Based on obtained results, it is noted that maximum DLF occurs when λ approaching 2, where within this λ range, fundamental building frequency is so closed to dominate wind frequency.

REFERENCES

- Arkawa, T., and Yamamoto, K.,2004, *Frequencies and Dampingr Ratios of a High Rise Building Based on Micromtremor Measurment [Report]. - Vancouver, B.C., Canada : Conference on Earthquake Engineering.*
- Balendra, T.,1993, *Vibration of Buildings to Wind and Earthquake Loads [Book]. Springer.*
- Clough, R., and Penzien J.,2003, *Dynamic of Structures [Book]. - [s.l.] : Computers& Structures.*
- CSI, Analysis Reference Manual. - Berkeley : Computers and Structures, Inc., 2009.
- Kwon, D., and Kareem A.,2013, *Generalized gust-front factor: A computational framework for wind load effects [Journal]. - [s.l.] : Engineering Structures, Vol. 48. - pp. 635-648.*
- Simiu, E., and Robert S.,1996, *Wind Effect on Structures (Fundimental and Applications on Design) [Book]. - Canada : John Wiley&Sons, Inc.*
- Taranath B.,2005, *Wind and Earthquake Resistant Buildings [Book]. - New York : Marcel Dekker..*
- Wilson E.,2002, *Three-Dimensional Static and Dynamic Analysis of Structures [Book]. - Berkeley : Computers and Structures,Inc.*

NOMENCLATURE

A= cross sectional area, m2
B= plan dimension across wind direction, m
C_D= drag Coefficient, unit less
D=plan dimension along wind direction, m
DLF =dynamic load factor $\frac{x_{max}(t_d)}{x_{Static}}$
$\boldsymbol{F_D}$ =drag Force
$\boldsymbol{p_d}$ =drag pressure in Pa
$\boldsymbol{t_d}$ =pulse duration
$\boldsymbol{T}$ period of motion
$\bar{\dot{x}}(z)$ =velocity in time domain, m/sec
$\bar{\dot{x}}(z)$ =mean wind speed, m/sec
$\bar{\dot{x}}(z_{ref})$ =mean wind speed depending on building site, m/sec
$\bar{\dot{x}}_{G-F}(t)$ =mean wind speed on gust front, m/sec
$\boldsymbol{z}$ =height above the ground, m
$\boldsymbol{z_o}$ =roughness length, m
$\boldsymbol{z_{max.}}$ =height where $\bar{V}_{max.}$occurs , m
$\boldsymbol{Z_{ref}}$ =gradient height (thickness of boundary layer) , m
$\boldsymbol{\alpha}$ =power law
$\boldsymbol{\rho}$ =air density
$\boldsymbol{\lambda}$ =aspect ratio D/B, unit less

$\emptyset_n$ =the nth mode shape
$\boldsymbol{\phi}$ =modal Matrix

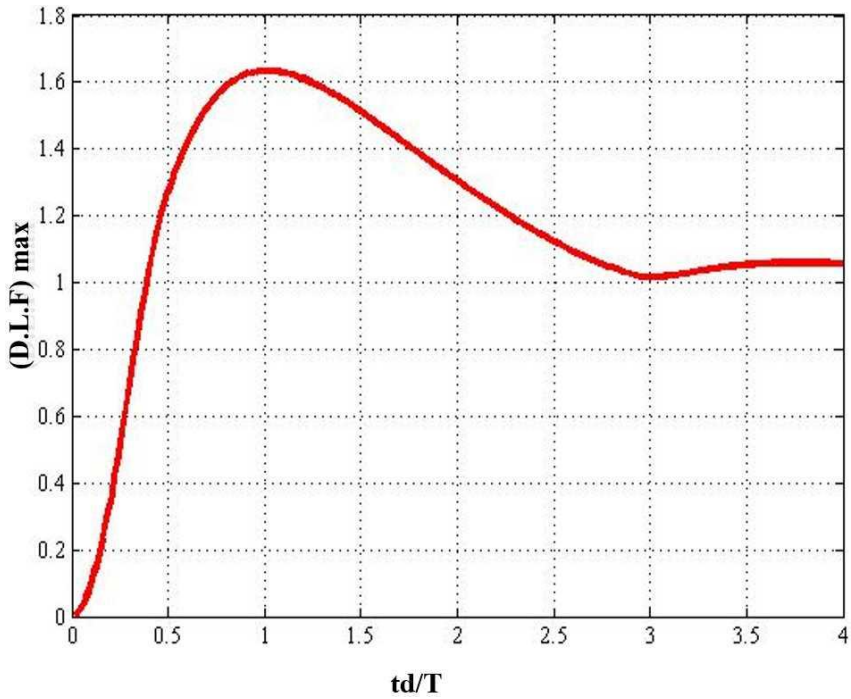

Figure 1. Response spectrum for square of-sinusoidal pressure of duration td

where $\mathbf{t_d}$, is pulse duration of the excitation, **T** is the period of motion, $\boldsymbol{T} = 2\pi\sqrt{\frac{m}{k}}$, $\mathbf{D.L.F} = \frac{x_{max}(t_d)}{x_{Static}}$.

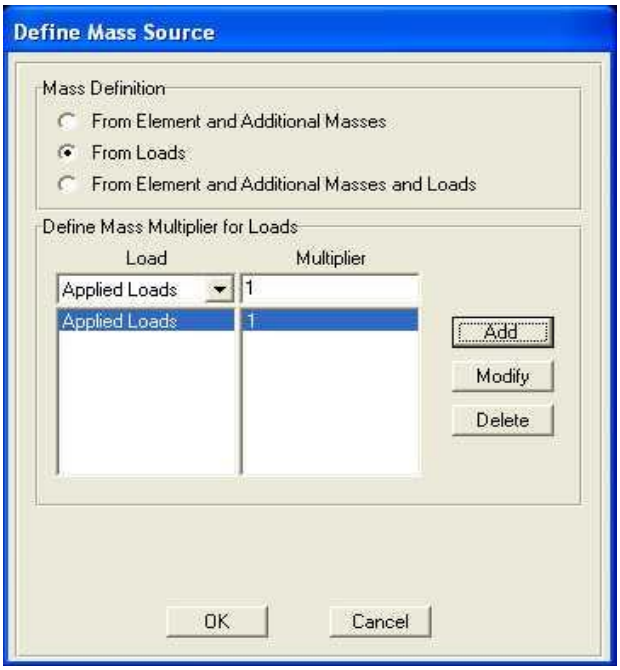

Figure 2. SAP Interactive box for mass definition.

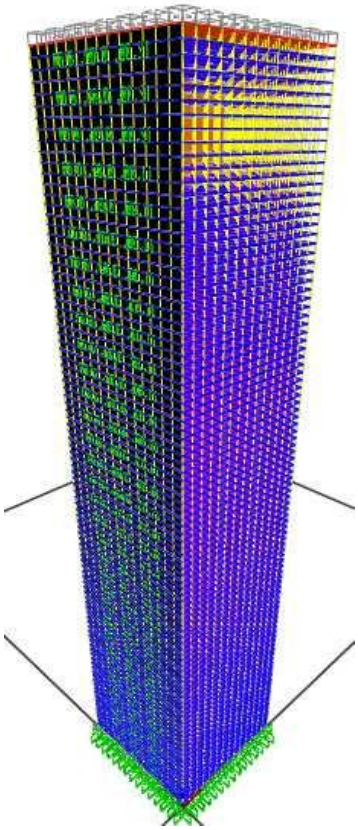

Figure 3. Isometric for 100 stories building.

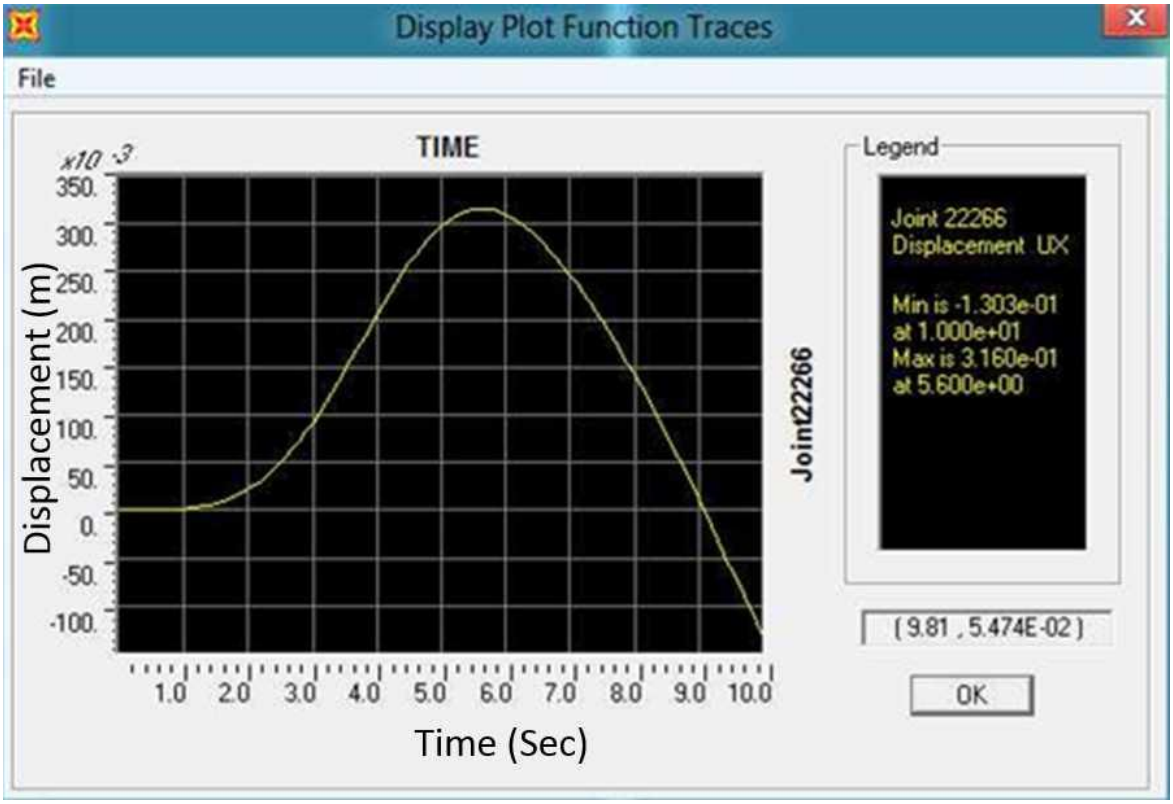

Figure 4. Tip displacement on **10**0 stories.

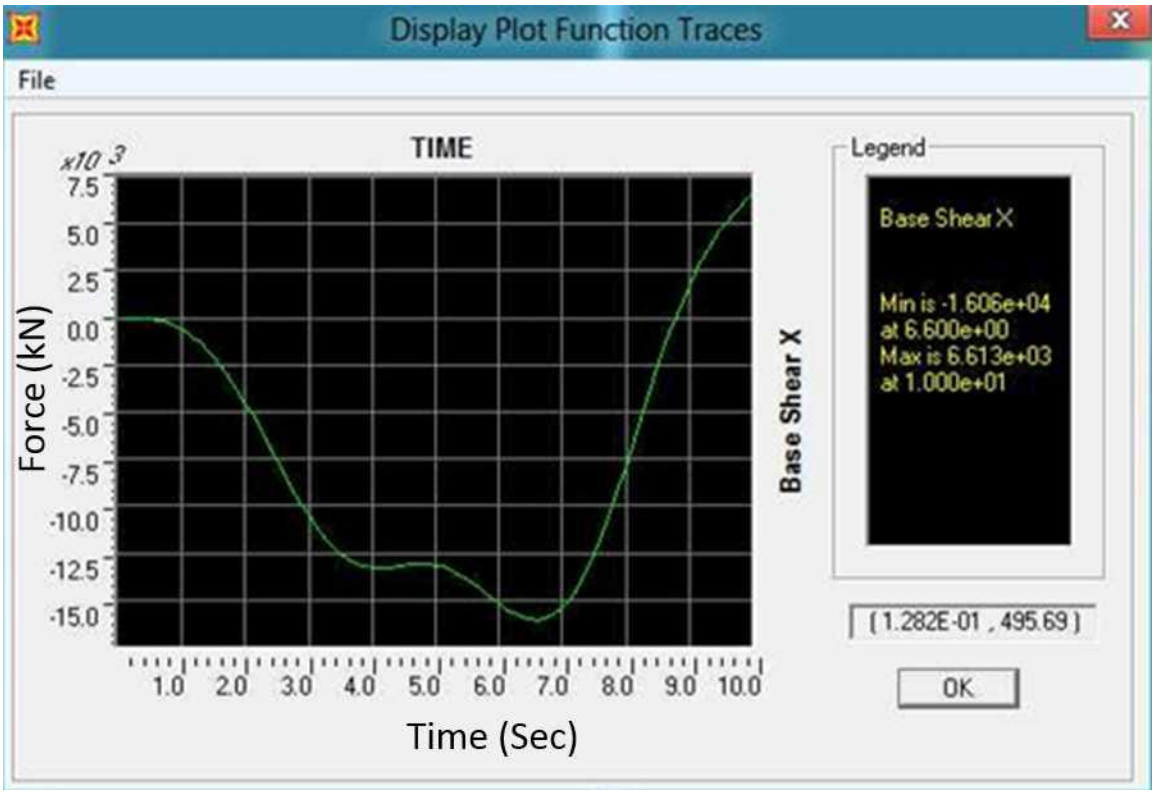

Figure 5. Building base shear at X-coordinate on **100** stories.

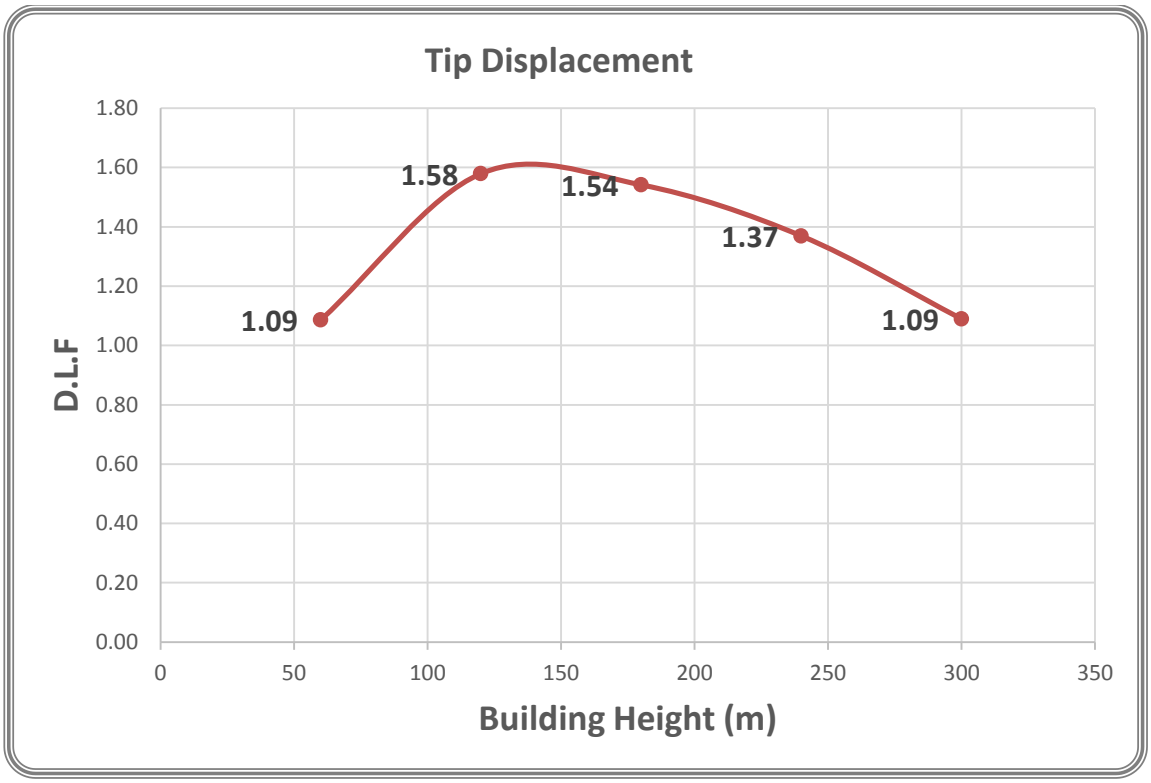

Figure 6. Height versus dynamic load factor for tip displacement.

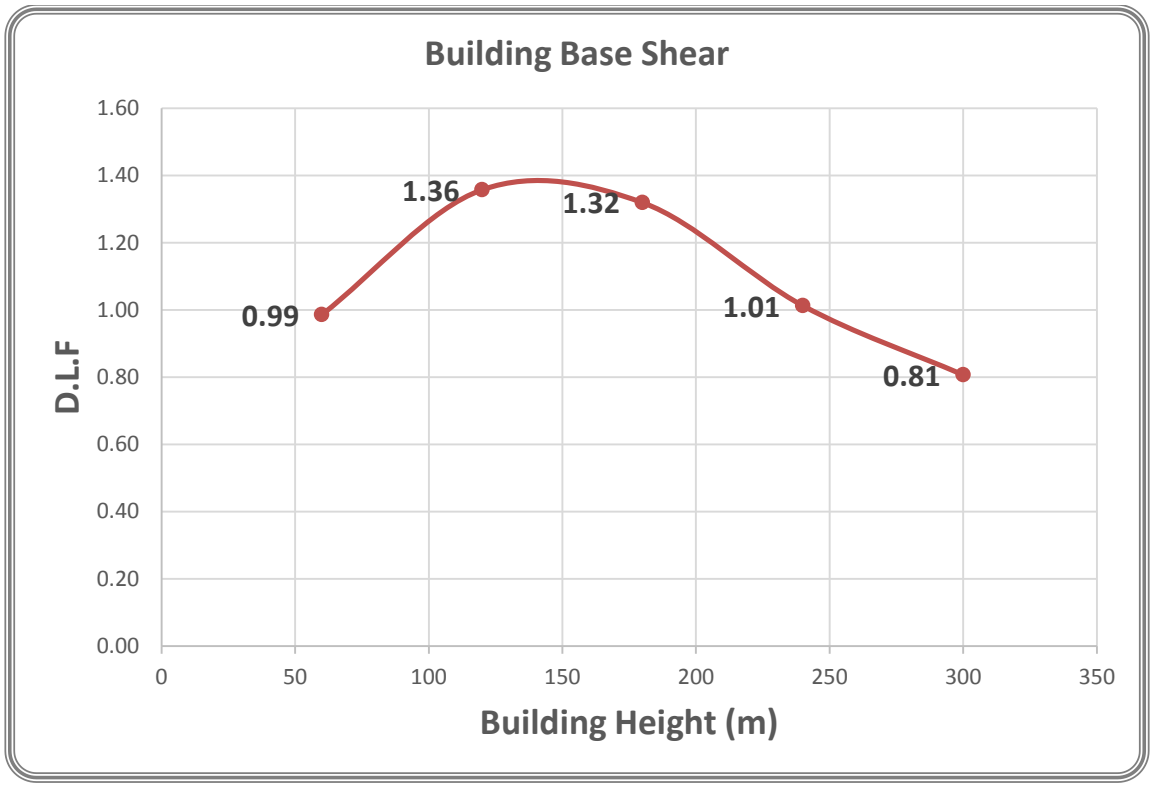

Figure 7. Height versus dynamic load factor for building base shear.

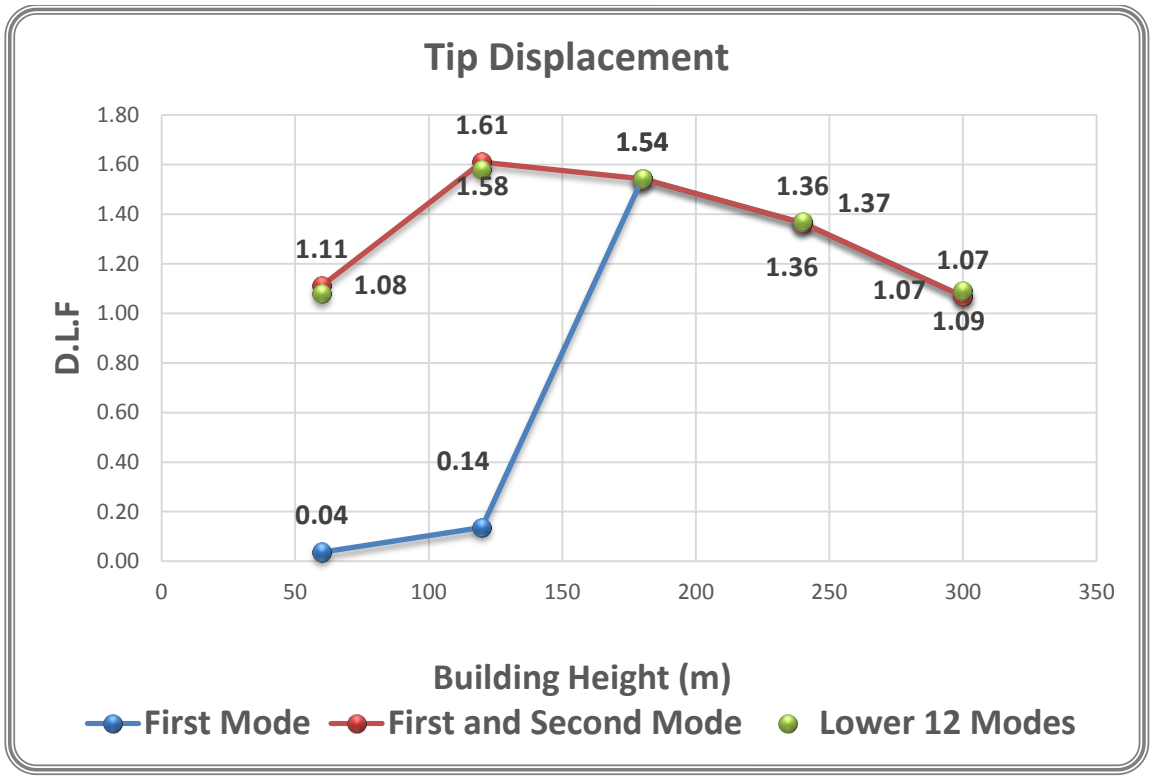

Figure 8. Modes versus dynamic load factor for tip displacement.

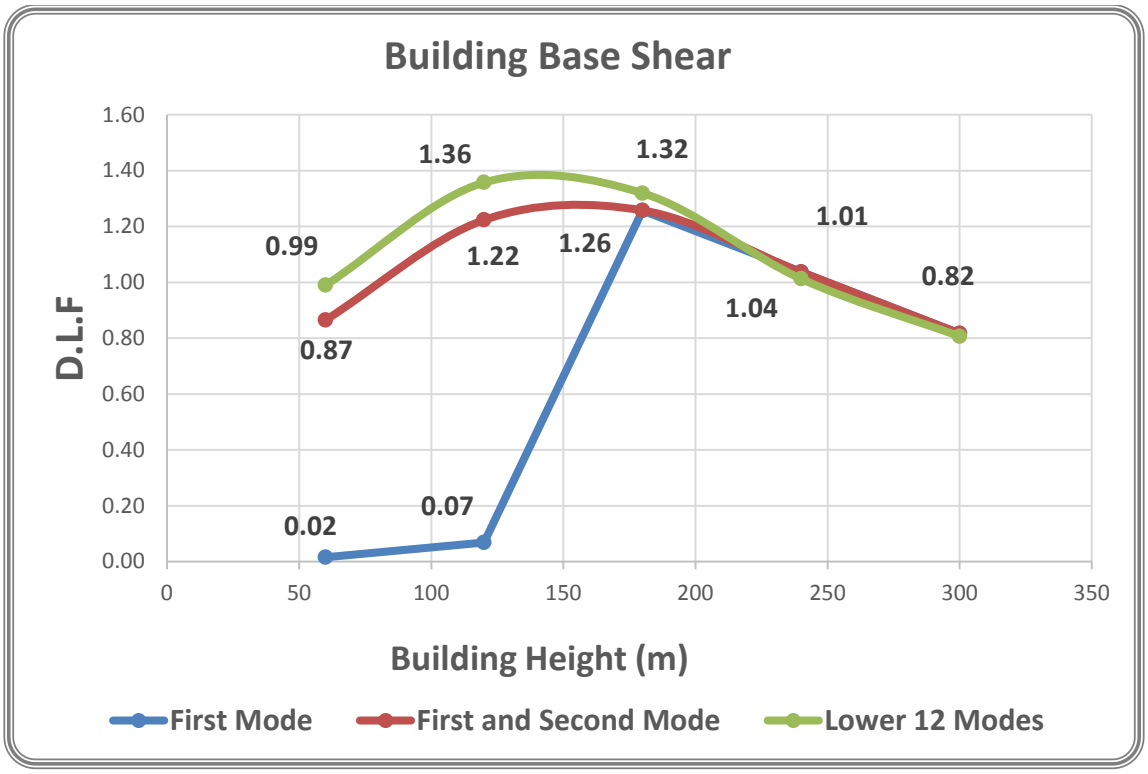

Figure 9. Modes versus dynamic load factor for building base shear.

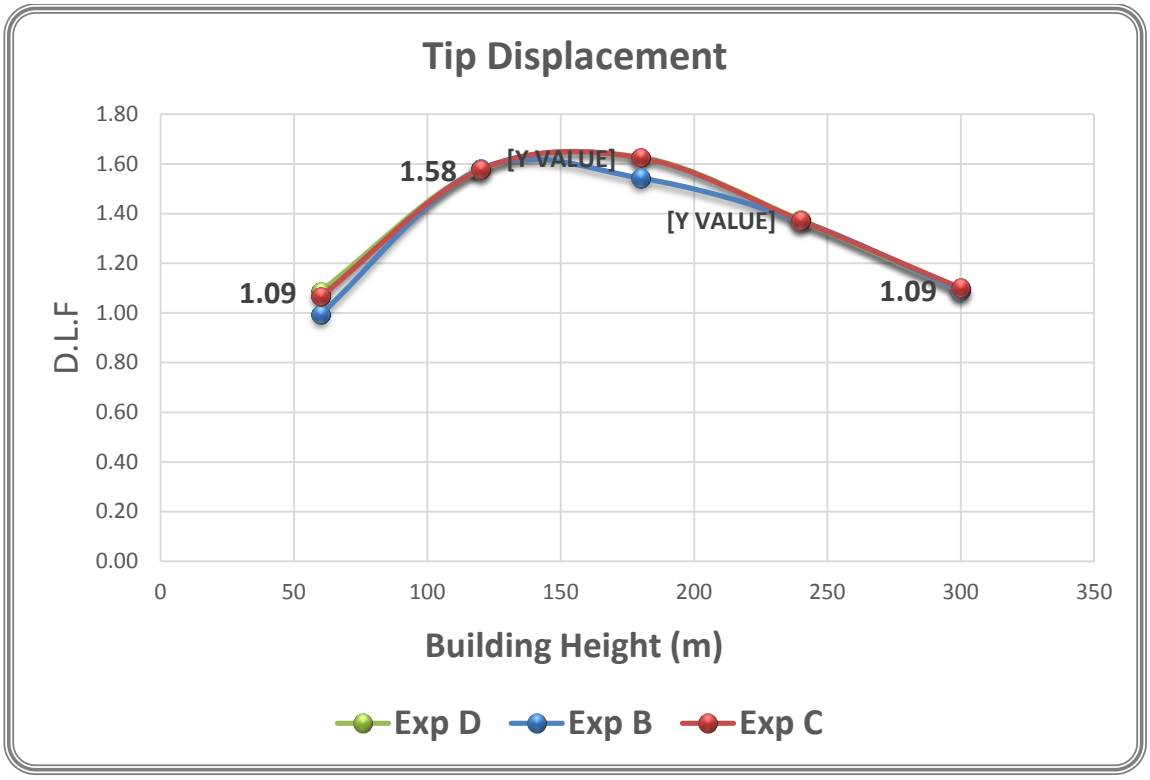

Figure 10. Roughness versus dynamic load factor for tip displacement.

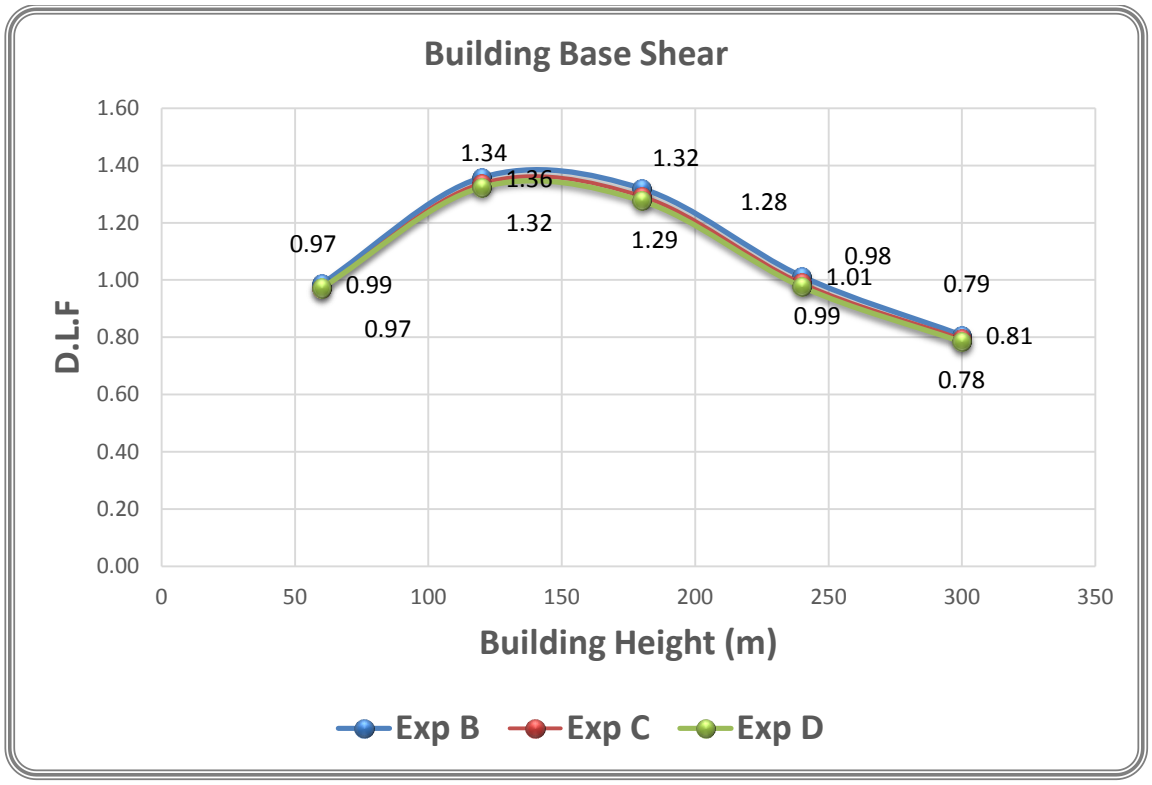

Figure 11. Roughness versus dynamic load factor for building base shear.

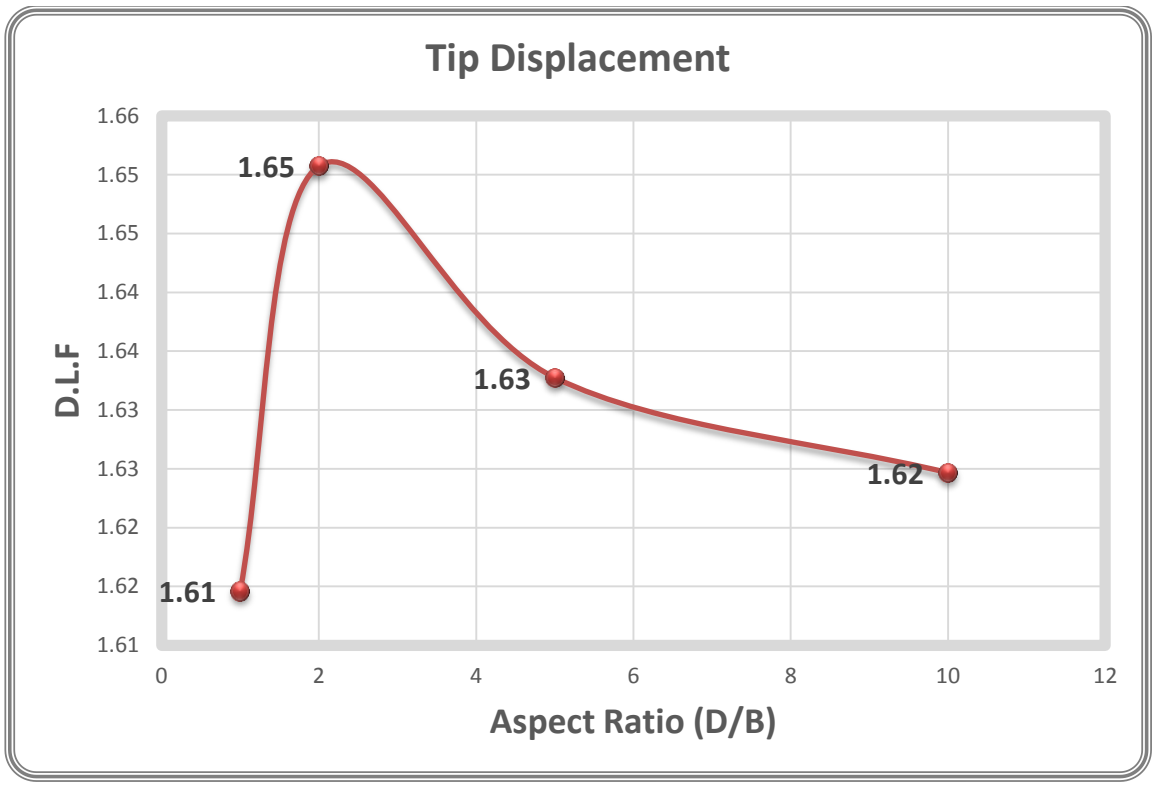

Figure12. Aspect ratios versus dynamic load factor for tip displacement.

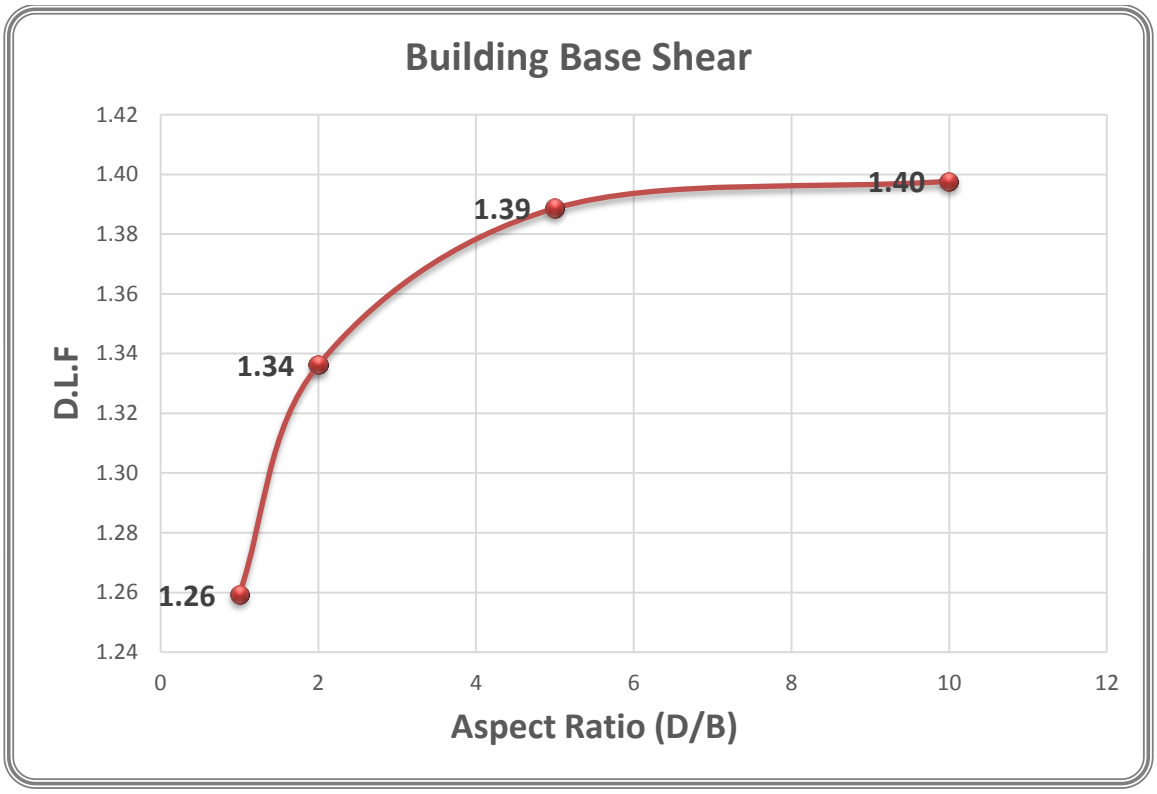

Figure 13. Aspect ratios versus Dynamic load factor for building base shear.

Table 1. Drag coefficients for a rectangular plate normal to smooth flow.

	Rectangular Plate in Normal Wind				Rectangular Plate on Ground Standing on Long Side					
Aspect Ratio	1.0	2.0	5.0	10.0	20.0	40.0	∞	1.0	10.0	∞
C_D	1.18	1.19	1.20	1.23	1.48	1.66	1.98	1.10	1.20	1.20

Table 2. Specifications of structural buildings with loads and cross sections.

Structure	Loads				
	Dead kN/m^2	Live kN/m^2	Line kN/m	Span	Cross Section
Beams	2.5	3.0	-	4.5	0.4 × 0.6
Columns	4.0	1.5	-	3.0	0.5 × 0.5
Portions	-	-	1.5	-	-

Table 3. Different heights with tip displacements and base shear.

Building Ht. (m)	Fund. Time Period (sec.)	Static Load		Dynamic Load		DLF	
		Tip Disp. (m)	Building Base Shear (kN)	Tip Disp. (m)	Building Base Shear (kN)	Tip Disp. (m)	Building Base Shear (kN)
60	0.46	0.0201	2419.2	0.022	2386.0	1.09	0.99
120	0.65	0.0165	6066.9	0.026	8237.0	1.58	1.36
180	0.83	0.060	10376.1	0.092	13690.0	1.54	1.32
240	0.98	0.140	15157.8	0.191	15350.0	1.37	1.01
300	1.19	0.290	19901.7	0.316	16060.0	1.09	0.81

Table 4 Aspect ratios versus dynamic load factor on displacement and building base shear.

Aspect Ratio λ	Drag Coefficient C_D	Static Load		Dynamic Load		DLF	
		Tip Disp. (m)	Building Base Shear (kN)	Tip Disp. (m)	Building Base Shear (kN)	Tip Disp. (m)	Building Base Shear (kN)
1	1.18	0.1754	2604	0.2832	3279	1.61	1.26
2	1.19	0.069	2538	0.1139	3391	1.65	1.34
5	1.20	0.0281	2640	0.0458	3666	1.63	1.39
10	1.23	0.0146	2718	0.0237	3799	1.62	1.40

Strain Analysis of Surface Cracked Thin Flat Plate under Cycling Impact Loading Effect

Asst. Prof. Dr. Fathi Abdulsahib Alshamma
Department of Mechanical Engineering
College of Engineering
University of Baghdad
Email: fathi_alshamma@yahoo.com

Asst. Lect. Bassam Ali Ahmed
Department of Electromechanical Engineering
College of Engineering
University of Technology
Email: bsmty77@yahoo.com

ABSTRACT

In this work, strains and dynamic crack growth were studied and analyzed in thin flat plate with a surface crack at the center, subjected to cycling low velocity impact loading for two types of aluminum plates (2024, 6061). Experimental and numerical methods were implemented to achieve this research. Numerical analysis using program (ANSYS11-APDL) based on finite element method used to analysis the strains with respect to time at crack tip and then find the velocity of the crack growth under cycling impact loading. In the experimental work, a rig was designed and manufactured to applying the cycling impact loading on the cracked specimens. The grid points was screened in front of the crack tip to measure the elastic-plastic displacements in the x and y direction by grid method, from which the strains are calculated. The results show that the strains increase with increasing in the crack length. It was found that the cumulative number of cycles leads to increase in the strain values with increasing in crack growth velocity.

Key words: strain, velocity, crack tip, analysis, plate.

تحليل الأنفعال لشق سطحي في صفيحة رقيقة تحت تأثير حمل صدمة متكرر

أ.م. د. فتحي عبد الصاحب الشماع
قسم الهندسة الميكانيكية
كلية الهندسة / جامعة بغداد

م.م. بسام علي احمد
الهندسة الكهروميكانيكية
كلية الهندسة / الجامعة التكنولوجية

الخلاصة

في هذا العمل تم دراسة وتحليل الأنفعالات وحركة نمو الشق لصفائح رقيقه ومستوية تحتوي على شق سطحي في وسطها ومعرضة لحمل صدمة دوري ذات سرعة منخفضة ولنوعين من سبائك ألالمنيوم (2024,6061) .تم استخدام طرق عملية وعددية لانجاز هذا

العمل. في التحليل العددي تم أستخدام برنامج (ANSYS11-APDL) بألاعتماد على طريقة العناصر المحددة وذلك لتحليل الأنفعالات بالنسبة للزمن عند قمة الشق ومن ثم حساب سرعة نمو الشق تحت تأثير حمل الصدمة المتكرر. في الجزء العملي تم تصميم وتصنيع جهاز لتسليط حمل الصدمه المتكرر على مركز العينه. حيث تم طباعة شبكه النقاط عند مقدمة قمة الشق وذلك لقياس الازاحات بطريقة الشبكة وبالتالي ايجاد الانفعالات المتوزعه حول قمة الشق الصدمه التكراري. وقد أظهرت النتائج بأن الأنفعالات المتولده تزداد بأزدياد طول الشق كذلك أظهرت بأن عدد الدورات التراكمي يؤدي الى زيادة قيم الأنفعالات وبالتالي زيادة سرعة نمو الشق .

الكلمات الرئيسية : أنفعال, سرعة, قمة الشق, تحليل, صفيحة.

1. INTRODUCTION

In real life cracks may occur in some parts of structure that may lead to failure like accidental cracking of welded connection, explosion of pressure vessel, buildings and sudden failure of jet aircraft. Therefore, strain analysis and study the cracks propagation within structures is very important to improve the design against fracture, **,Ayoub, 1984.** In this work, strain of surface cracked thin plate under cyclic loading was analyzed. Cycling load involved in many structures such as automobiles (piston inside cylinder), wing of aircraft, bridges, and machines structures. In general, three different fluctuating stress-time modes are possible. One is represented schematically by regular and sinusoidal time dependence. Where in the amplitude is symmetrical about mean zero stress level, alternating from a maximum tensile stress to a minimum compressive stress of equal magnitude, this is a reversed stress cycle. Another type, termed repeated stress cycle, is illustrated the maximum and minimum are asymmetrical relative to the zero stress level. Finally the stress may vary randomly in amplitude and frequency. Gears are subjected to reversed stress cycles, while the connected rod in a petrol engines and the wing of an aircraft are subjected to repeated stress cycles**, ,Stephens, et al., 2001.**

There are many researcher were studied the strain at crack tip with different fluctuating stress-time modes. **,Toribio, and Kharin, 2009.** studied the plane-strain crack subjected to mode I cyclic loading under small scale yielding. **,Sahoo, et al., 2007.** analyzed the effects of plasticity on the stress and deformation field near the crack tip, while **,Boljanovic, 2012.** proposed a computational model for estimating the crack growth behavior and fatigue life of a plate with a semi-elliptical surface crack.

The aim of this work is to build up a model described the strain behavior at crack tip to thin plate under cyclic loads. A rig system will be designed and manufacturing for this purpose. ANSYS11-APDL package will be employed to build up the model and analysis the strains.

2. NUMERICAL ANALYSIS

Numerical analysis of structures subjected to various kinds of actions is an important issue for structural safety. A numerical method can be used to obtain an approximate solution; approximate numerical procedures have become very accurate and reliable for the solution with the advent of high speed digital computers**, Kareem, 1998.** Solving fracture mechanics problems involves performing a linear elastic or elastic-plastic state analysis and then using specialized post processing commands or macros to calculate desired fracture parameters. The following topics describe the two main aspects of procedure:

1. Modeling the crack region.
2. Selecting of element and meshing.
3. Calculating fracture parameters.

In this research, the ANSYS software APDL is used for solving fracture problem. Selecting of element and meshing: The element Solid185 is used for 3D modeling of solid structures. It is defined by eight nodes having three degrees of freedom at each node, translations in the nodal x, y and z directions. The element has plasticity, hyper elasticity, stress stiffening, creep, large deflection, and large strain capabilities. It also has mixed formulation capability for simulating deformations of nearly incompressible elastoplastic materials, and fully incompressible hyper elastic materials. The boundary conditions are clamped-clamped with simply supported at the other edges plate and clamped-clamped with free at the other edges plate.

2.1 The Crack Region Modeling

Stress and deformation fields around the crack tip generally have high gradients. The precise nature of these fields depends on the material, geometry and other factors. To capture the rapidly varying stress and deformation fields, use a refined mesh in the region around the crack tip. For linear elastic problem the displacement near the crack tip (or crack front) vary as $\sqrt{r}$, where (r) is the distance from the crack tip. The stresses and strains are singular at the crack tip, varying as $1/\sqrt{r}$. To produce this singularity in stresses and strains, the crack tip mesh should have certain characteristics, the crack faces should be coincident and the elements around the crack tip (or crack front) should be quadratic, with the mid side nodes placed at the quarter points. Such elements are called singular elements. **Fig.1**

2.2 Loads and Boundary Conditions

The cycling impact loading is applied at the cracked thin flat plate; the boundary conditions are clamped-clamped with simply supported at

the other edges plate and clamped-clamped with free at the other edges plate. **Fig.2**

3. EXPERIMENTAL WORK

A rig system was designed and built up to achievement this work. The main purpose of rig system design to get a cycling impact loading to strike vertically at center of plate's surface and measurement the induced deformations and calculated the strains. It consists of electric motor, control number of cycle's equipment, gearbox, one step of pulleys and impactor arm. The specifications of electric motor were, power (100watt), voltage (220 volt), frequency (50Hz), and rotation velocity (780rpm) was reduced by gearbox that have a reduction ratio (1:40), the step of pulleys having (53mm) diameter of pinion pulley and (64mm) diameter of wheel pulley so as a reduction ratio (1:1.2), so that have a velocity for pinion pulley (19.5rpm) and suitable velocity for the wheel pulley (16.25rpm). A control number of cycle's equipment determinates the number of cycles needed to strike a plate's surface, for this work, the number of cycles was (1000 cycle/sec). The impactor mass (1.5kg), which have a hemispherical end (R=1.5mm), moves vertically to strike the plate's surface. The distance between end of impactor and the surface of plate was constant (80mm). The samples were hold from four sides (clamped-clamped with simply supported at the other edges) and once again through (clamped-clamped with free at the other edges). **Fig.3** is shown the experimental rig. Two types of metals were used in this work, aluminum (2024) and aluminum (6061). The specifications of metals have shown in **tables 1. and 2**. A grid has been printed in the front of the crack tip with square grid for measuring the displacements of each point after deformation by cycling impact load.

3.1 Procedure of Work

Grid method is one of the methods of strain analysis, which is whole field in nature. In order to determine displacements and strain components at given points of arbitrarily shaped surfaces a grid can be engraved on the surface to be studied. This grid acts as a reference element and the changes that the grid experiences from the unreformed to the deformed conditions can be utilized to determine either displacements or strains. Two difficulties are encountered which limit the use of grids for measuring deformations; firstly, the strains to be measured are usually very small, and in most cases the displacement readings are difficult to make with sufficient accuracy. This is particularly true in strain analysis. However, this method is very much suitable for the study of deformation in materials .Secondly, when the photographs of the grid network are magnified by microscope, the images of the grid lines are usually poorly

defined introducing appreciable errors into the displacement readings. This method has the advantages that a photographic record of deformations covers the entire field of the specimen. This record can be obtained for either static, dynamic elastic or plastic deformations. The strain was measured directly. The distance between the grid lines on the model was measured by a microscope by keeping the magnification of microscope same before and after loading. The specimen was impacted vertically through a number of cycles by the impactor on the center of the sample. The number of the cycles was controlled by controlling equipment. The grid method was used to calculate the displacement in X-axis (u) and in Y–axis (v). The dimensions of grid were (30 mm×30 mm) and the length of square is (1mm) .The grid was photographic before and after the cycle of the sample and the measurements of the displacements was taken by microscope as shown in **Fig.4** for all the samples. Then the strains at the surface crack tip were calculated in the plate.

3.2 Boundary Conditions Change under Cyclic Impact Load

Two types of boundary conditions were used in this work. The first, clamped-clamped with simply supported at the other edges plate (CSCS) as shown in **Fig.5**. The second of boundary condition, clamped-clamped with free at the other edges plate (CFCF) as shown in **Fig.6.**

4. RESULTS AND DISCUSSION

The results showed substantial convergence in the numerical analysis with experimental work and illustrated the effect of cyclic impact load on the strains and crack growth velocity at surface crack tip due to number of cycles.

4.1 Numerical Analysis (ANSYS Program)

4.1.1 The effect of the crack lengths on the strains

The extension in length (deflection) is direct proportional with applied stresses that means the increasing in crack length which leads to increase the values in strain as shown in **Fig.7 to 10**. The instantaneous length of crack for aluminum 6061 is greater than aluminum 2024.Because the aluminum 6061 is more ductile than the aluminum 2024 (young modulus for aluminum 2024 greater than aluminum 6061). Increasing in the cumulative number of cycles leads to increase in the strains with nonlinear behavior so that the increasing in crack length also will be nonlinear .The yield region will be not appoint, so that there is some limiting values that strain hardening will affect the results therefor the rate of increasing curve slope will be low till nearly 600 cycles then after that, the rate of curve slope will have a high increasing. Materials especially metals tend to exhibit a yield stress, above which they deform plastically. This means that there is always a region around the tip of a

crack in a metal, where plastic deformation occurs, and this plastic region is known as the crack tip plastic zone. The plastic zone size vary with the number of cycles and it increases with increase the number of cycles, because the increase in the number of cycles means increasing in the applied stresses that is leading to increase in the plastic zone size.

4.1.2 The effect of the boundary conditions on the strains

Fig. 11 to 14. show, the results of the strain values at clamped-clamped with free at the other edges boundary condition will be higher from the clamped –clamped with simply supported at the other edges boundary condition by maximum error percentage (17%) for Al-6061 and (18.9%) for Al-2024 between numerical analysis and experimental work, this is because the value of the deflection at clamped-clamped with free at the other edges will be higher from clamped-clamped with simply supported at the other edges, that is leading to the stress and strain values become higher.

4.1.3 The effect of the crack growth velocity on the strains

The crack growth velocity depends on the applied stress which increases with increase the cumulative number of cycles that means the crack growth velocity increases with increasing in the number of cycles. As shown in the **Fig. 15 and 16.** noticed after 500 cycles nearly for aluminum 2024, the crack propagation values were started more increasing and faster propagate before500 cycles, while for aluminum 6061 after 525 cycles nearly the crack propagation values were started more increasing before 525 cycles, So that the plastic zone consists at aluminum 6061 before aluminum 2024 and the crack propagation at aluminum 6061 faster from aluminum 2024. The main reason of this case, the effect of ductility of material on the stress and strain values under cycling impact loading will become more clearly appeared in aluminum 6061rather than in aluminum 2024 and noticed from ANSYS program results the crack growth velocity values were increased with increasing the crack length and aspect ratio of plate. The crack propagation don't occur under impact load only because the plastic zone due to low velocity impact with applied cyclic loading which cause crack propagation.

4.2 Experimental Work

4.2.1 The effect of the crack lengths on the strains

Fig. 17 to 20. illustrate the effect of the experimental combined load (cycling impact load) on the strains at surface crack tip due to number of cycles with crack lengths (7mm, 10mm) and constant depth (2mm) for aspect ratio (1) of aluminum plates. Maximum error percentage of strains

(12.5%) for aluminum 6061 and (13%) for aluminum 2024 between experimental work and numerical analysis.

4.2.2 The effect of the boundary conditions on the strains

Fig. 21 to 24. illustrate the effect of the experimental under cycling impact load on the strains at surface crack tip due to number of cycles with boundary conditions, clamped-clamped with free at the other edges and clamped-clamped with simply supported at the other edges, with crack length (6mm) for aspect ratio (1).

5. VERIFICATION

Fig. 25 to 28. show the behavior of metal in the distribution of strains with number of cycles at different crack lengths for methods, numerical analysis and experimental work. Noticed that the behavior of metal for the ANSYS program more regularly than experimentally, because ANSYS program be more accurate while it is natural there would be an error in the proportion of experimentally. When the results of experimental work were compared with the results of the numerical analysis found the maximum error in strain (18.9%). In experimental work was found that values of displacements were higher at crack-tip and reduced when leaving the crack tip. Thus, the strains have greatest value at crack tip. The determination time of entry of the specimen in the plastic zone in experimental work was very difficult. But in the ANSYS program it was identified as the time when the specimen in the region of the plastic zone. Also it was found that in numerical analysis (ANSYS program), the strains have greatest value at crack tip.

6. CONCLUSIONS

1. Plastic zone has a significant effect on crack growth velocity under cycling impact loading for two materials used in this work. There are some specific values of strains at which strain hardening effect on the results. Therefore the rate of curve slope will be lower until about 600 cycles. After that, the rate of curve slope will back to increase.

2. The number of cycles has a significant effect on crack growth velocity specially at 400 cycles were the rate of increasing of crack growth velocity will be very high which is reflect the effect of plastic zone.

3. The effect of ductility of material on the strains under cycling impact loading will become more pronounced in aluminum 6061rather than in aluminum 2024.

4. With cumulative number of cycles under the cycling impact loading on the plate, using clamped-clamped with simply supported at the other

edges boundary condition was better than clamped-clamped with free at the other edges.

REFRENCES

- Ayoub, M.T., 1984, A*n Introduction to Mechanics and Fracture of Solids*.
- ASM Hand Book, Volume 2, 1992, *Properties and Selection: Nonferrous Alloys and Special-Purpose Materials*, The Materials Information Company.
- Boljanovic, S., 2012, *Fatigue Strength Analysis of Semi-Elliptical Surface Crack*, Science Technical Review, Vol.62, No.1,p.p10-16.
- Kareem, A. A., 1998, *Evaluation of the Elastoplastic Fracture Parameters Using Finite Element Method*, M.SC. thesis submitted to the University of Baghdad in mechanical engineering.
- Sahoo, A. K., Dubey, R. N., and Pandey M. D., 2007, *Crack Induced Stress and Deformation Field*.
- Stephens, R.L., 2001, *Metal Fatigue in Engineering*, Second Edition, John Wiley and Sons, Inc., New York.
- Toribio, J., and Kharin, V., 2009, *Finite-Deformation Analysis of the Crack-Tip Fields under Cyclic Loading*, Department of Materials Engineering, University of Salamanca, E. P. S., Campus Viriato, Zamora, Spain.

NOMENCLUTURE

Ar = aspect ratio, dimensionless.
Lc = crack length, mm.
ϵ_x, ϵ_y = Strains at crack- tip region, dimensionless.

Table1. The specifications of aluminum 2024.

Young modulus (E)Gpa	Yield Tensile Strength (σ_y) Mpa	Ultimate tensile strength ($\sigma_{ult.}$) Mpa	Poissons ratio(ν)	Density (ρ)Kg/m^3
73	325	470	0.33	2780

Table2. The specifications of aluminum 6061.

Young modulus (E)Gpa	Yield Tensile Strength (σ_y) Mpa	Ultimate tensile strength ($\sigma_{ult.}$) Mpa	Poisson's ratio(ν)	Density (ρ)Kg/m^3
69	275	310	0.33	2700

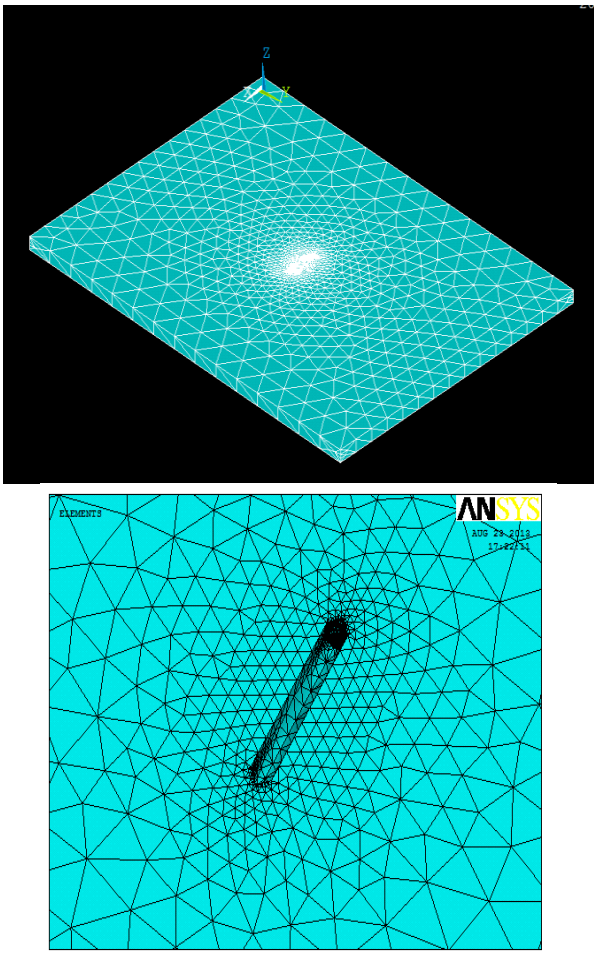

Figure1. 3D Model with solid185.

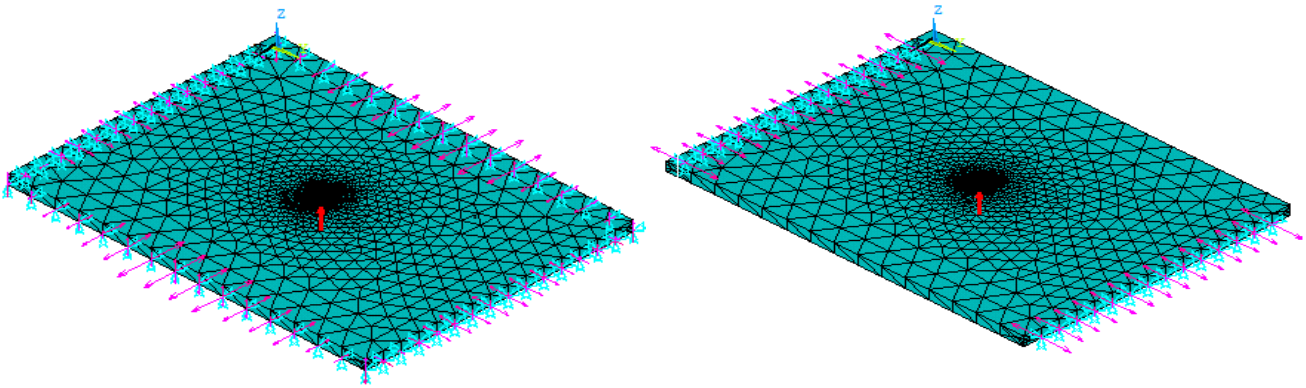

Figure2. Load and B.C.

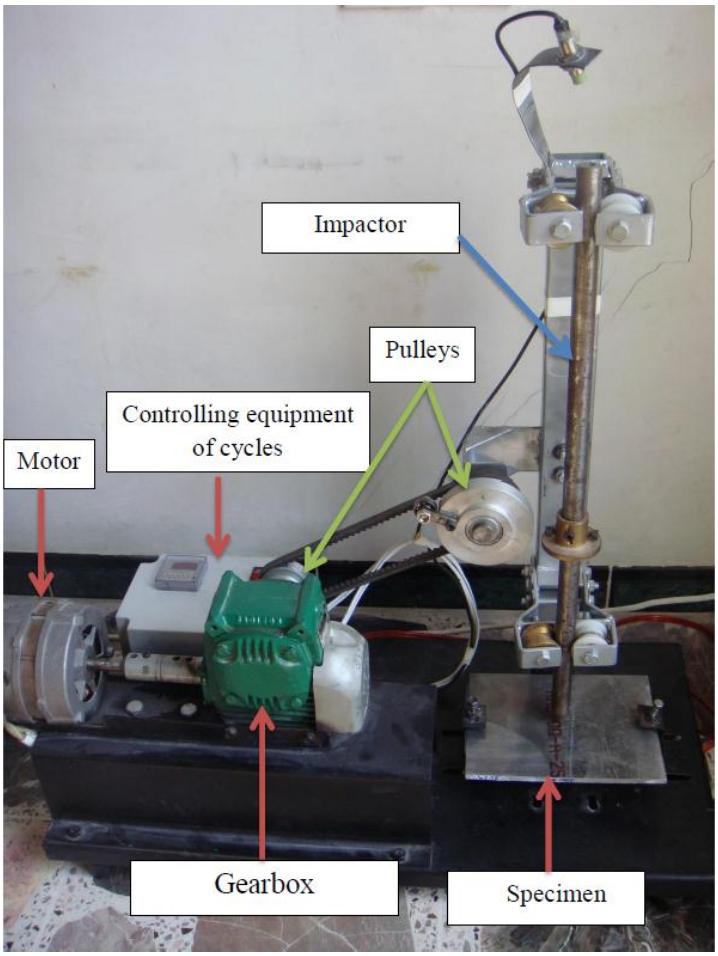

Figure3. Rig system.

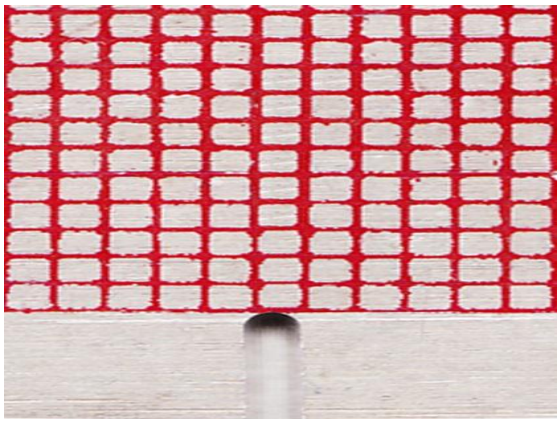

Figure4. Crack with grid.

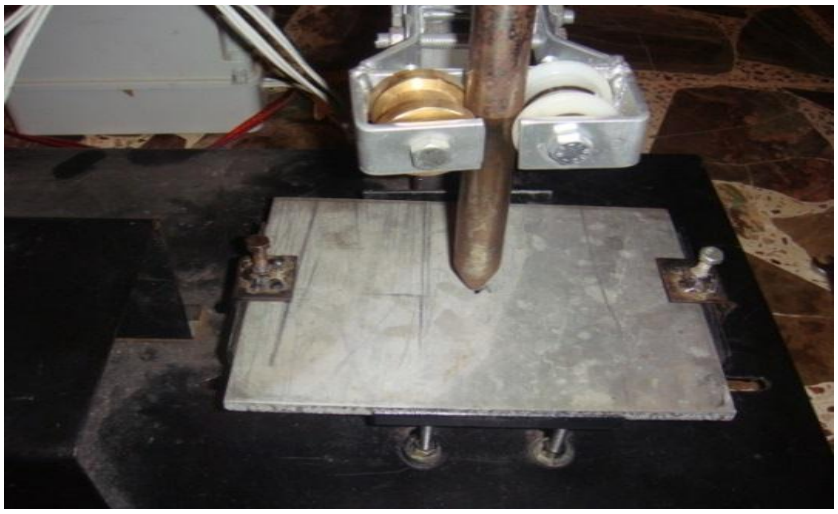

Figure5. CSCS-Boundary Condition.

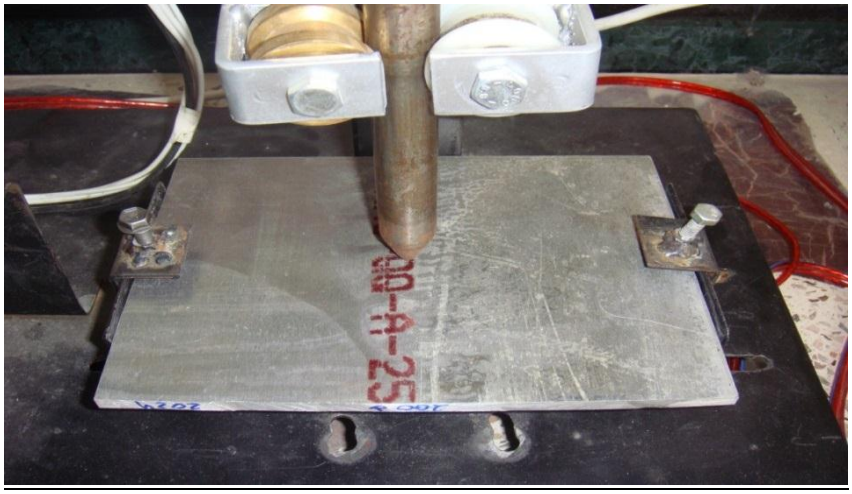

Figure6. CFCF-Boundary Condition.

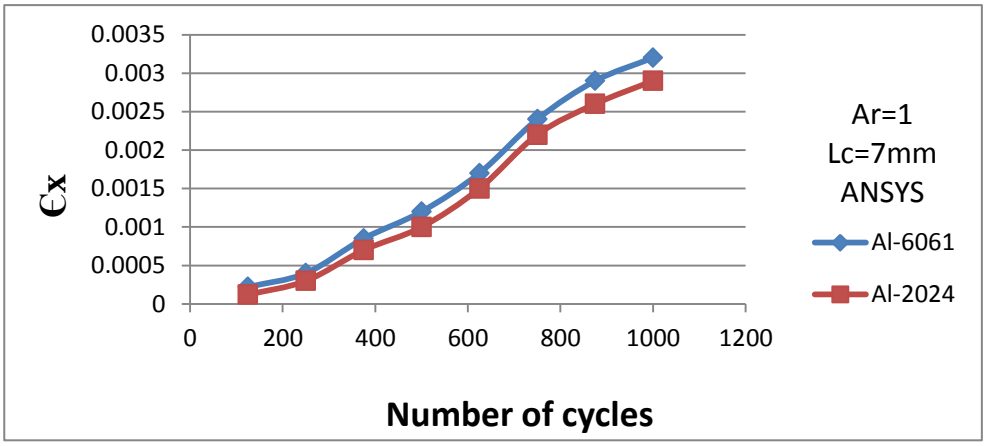

Figure7. $Є_x$ Numerical with number of cycles (Ar=1&Lc=7mm).

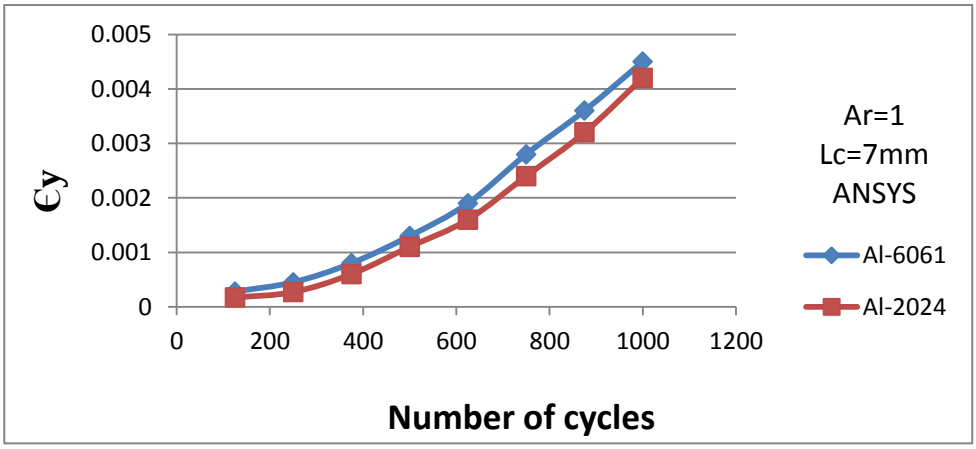

Figure8. $Є_y$ Numerical with number of cycles (Ar=1&Lc=7mm).

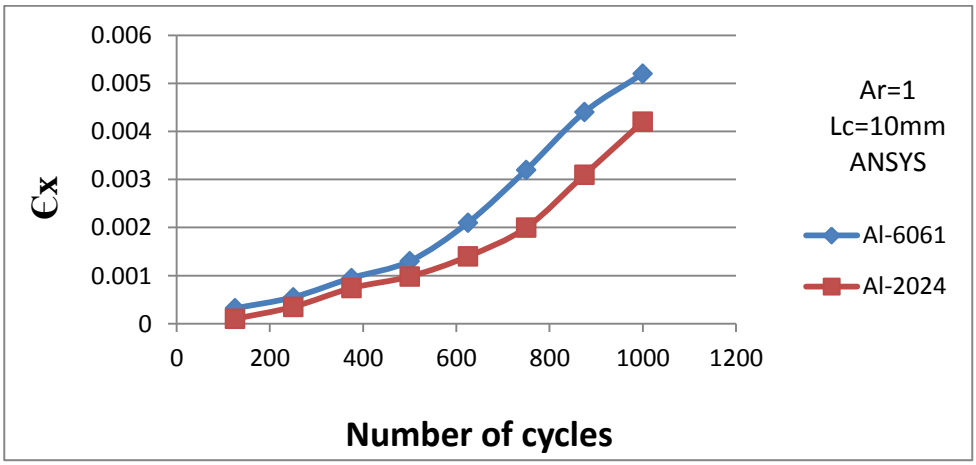

Figure9. $Є_x$ Numerical with number of cycles (Ar=1&Lc=10mm).

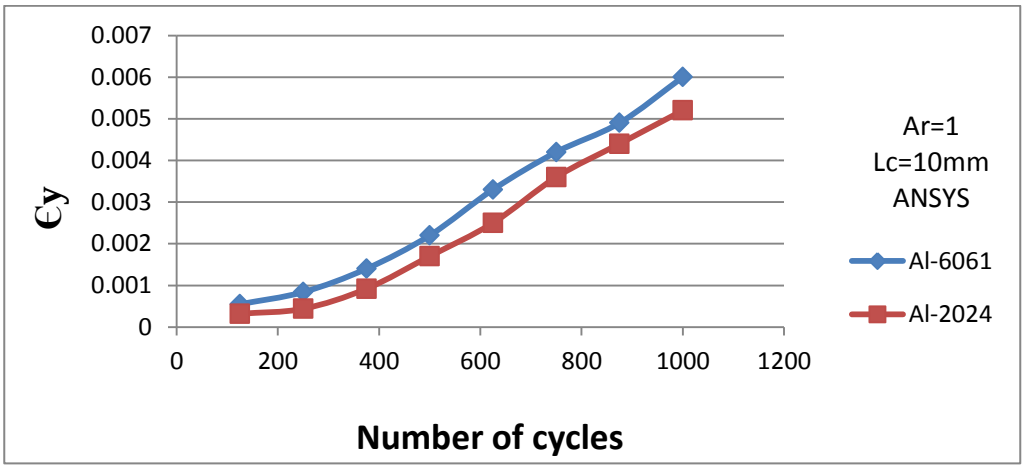

Figure10. $Є_y$ Numerical with number of cycles (Ar=1&Lc=10mm).

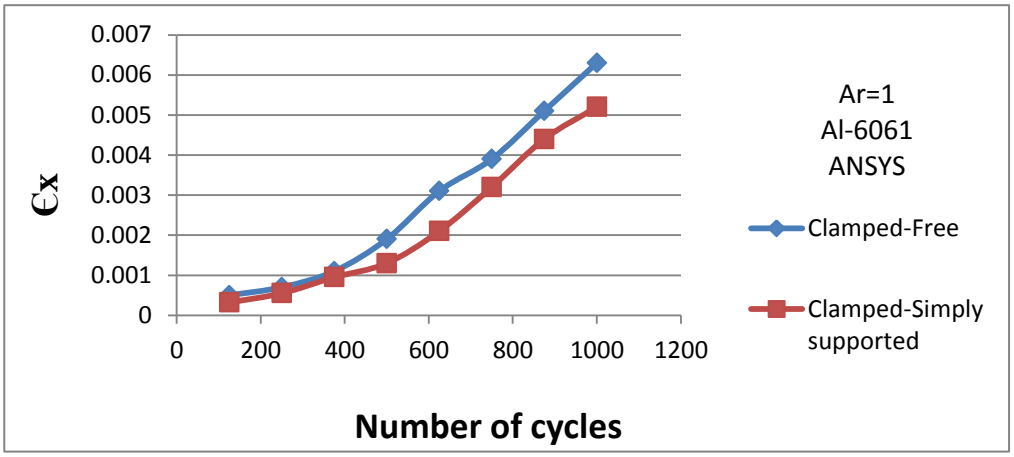

Figure11.$Є_{x.}$ Numerical with number of cycles (B.C for Al-6061).

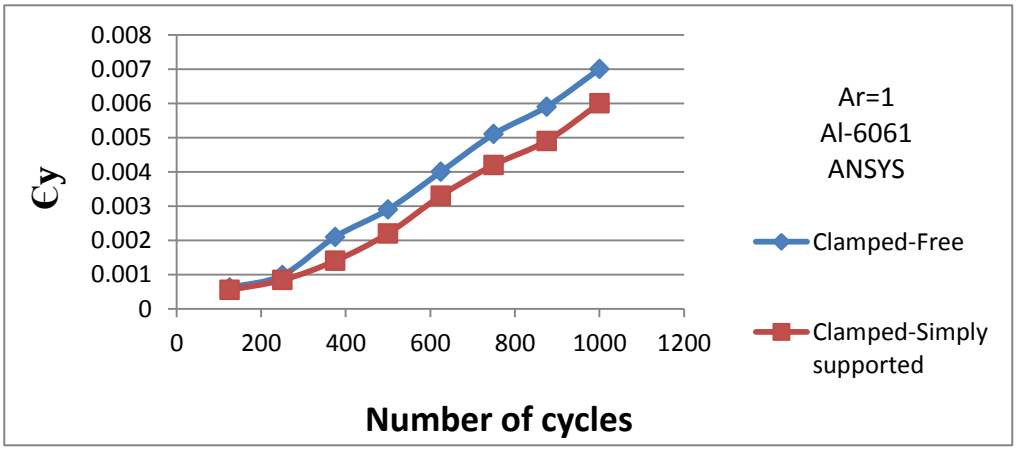

Figure12. $Є_y$ Numerical with number of cycles (B.C for Al-6061).

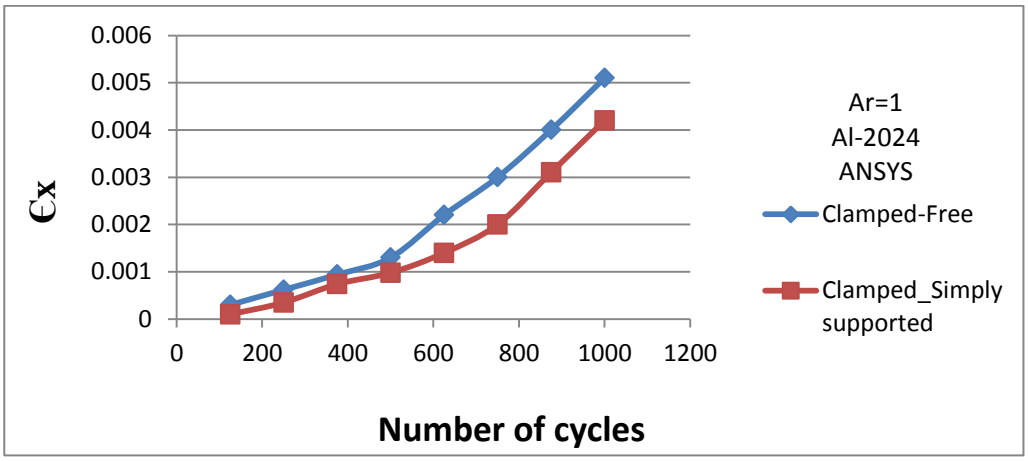

Figure13.$Є_x$ Numerical with number of cycles (B.C for 2024).

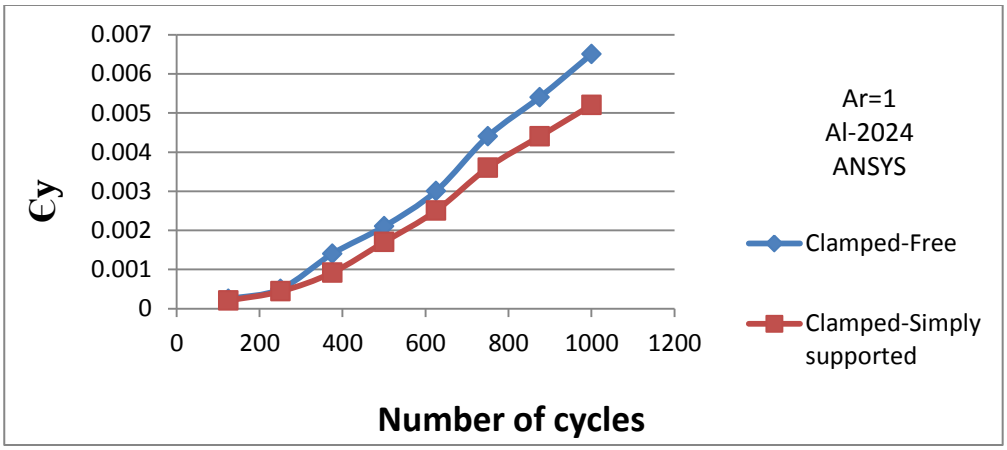

Figure14.$Є_y$ Numerical with number of cycles (B.C for 2024).

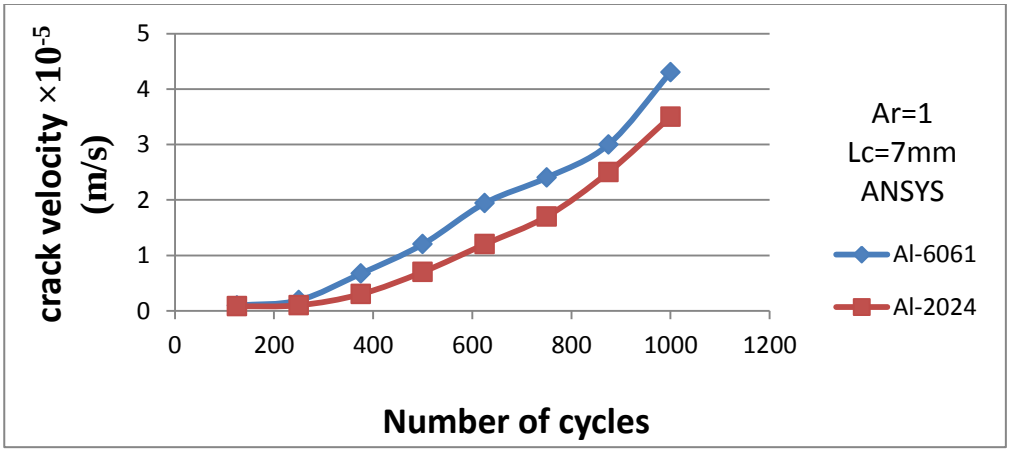

Figure15. Crack velocity numerical with number of cycles (Ar=1&Lc=7mm).

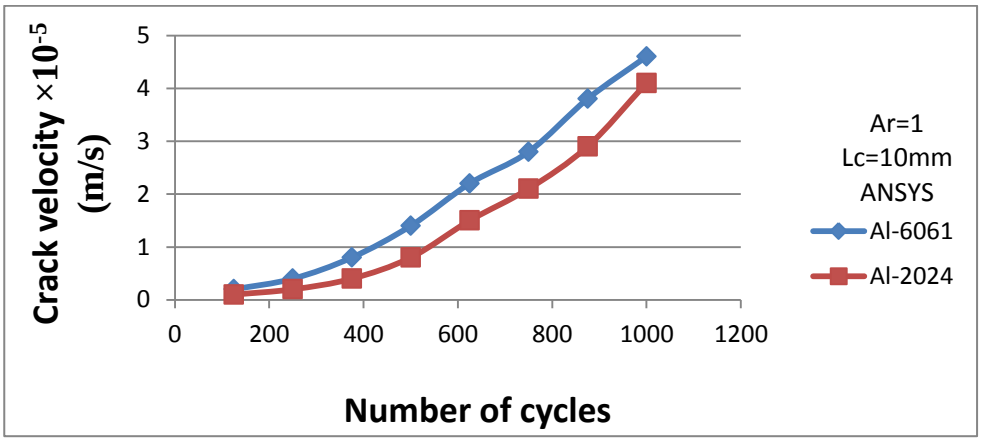

Figure16. Crack velocity numerical with number of cycles (Ar=1&Lc=10mm).

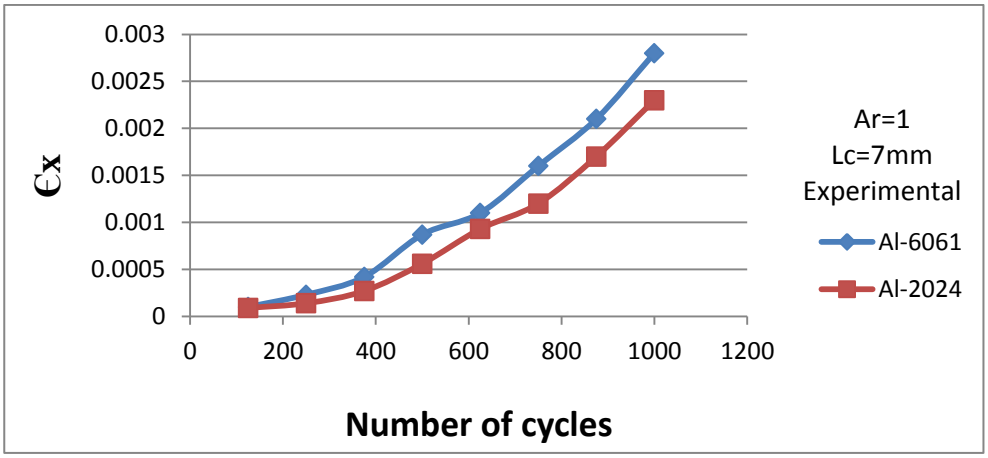

Figure17. $Є_x$ Experimental with number of cycles (Ar=1&Lc=7mm).

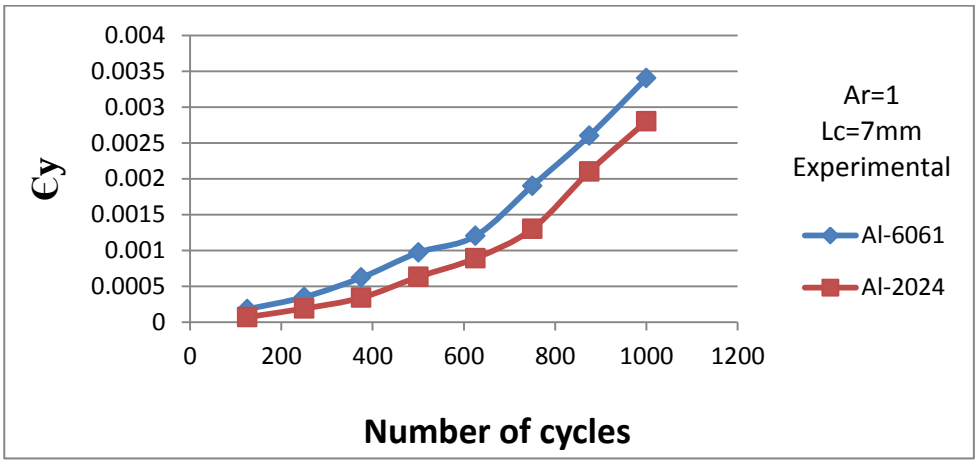

Figure18. $Є_y$ Experimental with number of cycles (Ar=1&Lc=7mm).

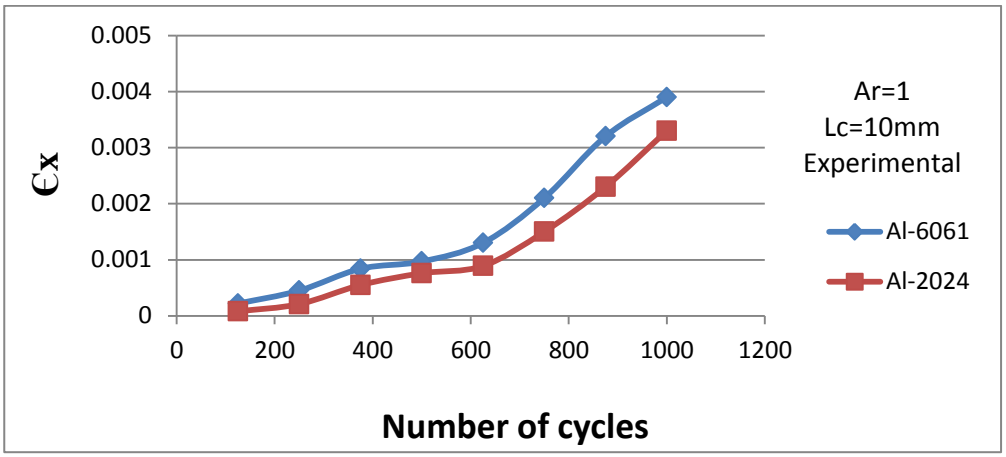

Figure19.$Є_x$ Experimental with number of cycles (Ar=1&Lc=10mm).

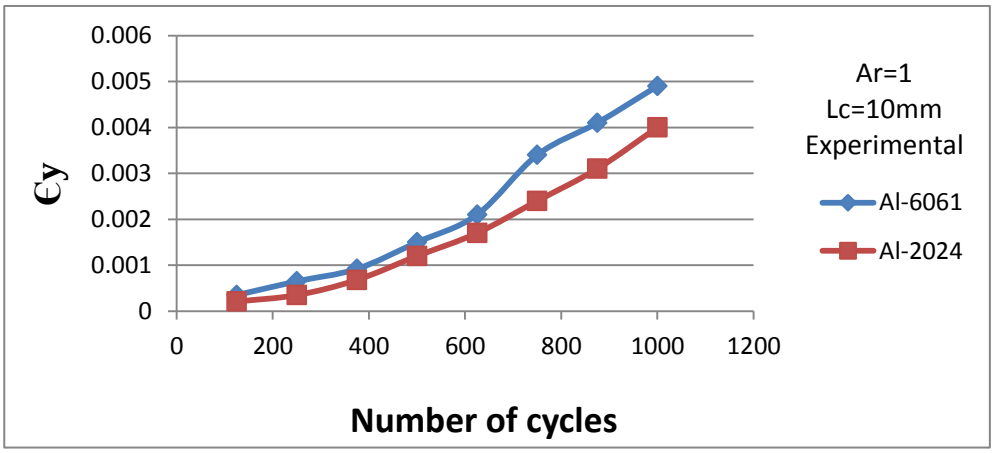

Figure20 .$Є_y$ Experimental with number of cycles (Ar=1&Lc=10mm).

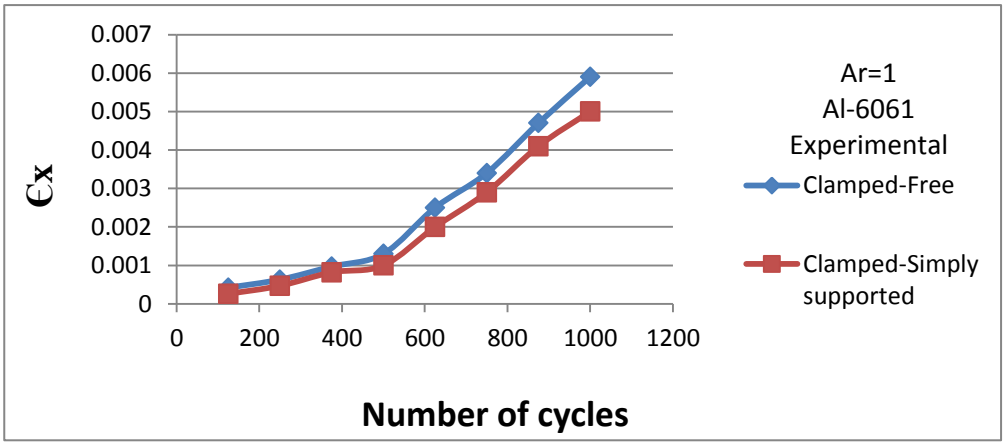

Figure21. $Є_x$ Experimental with number of cycles (B.C for Al-6061).

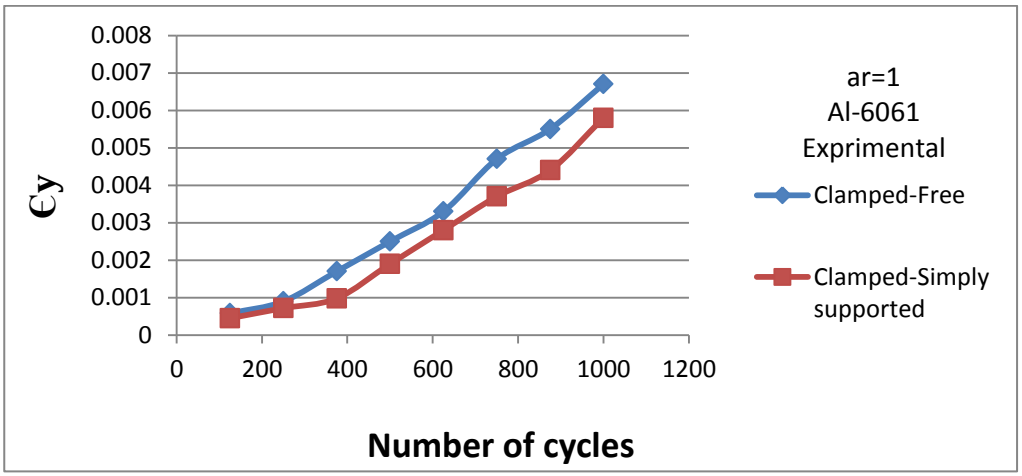

Figure22. $Є_y$ Experimental with number of cycles (B.C for Al-6061).

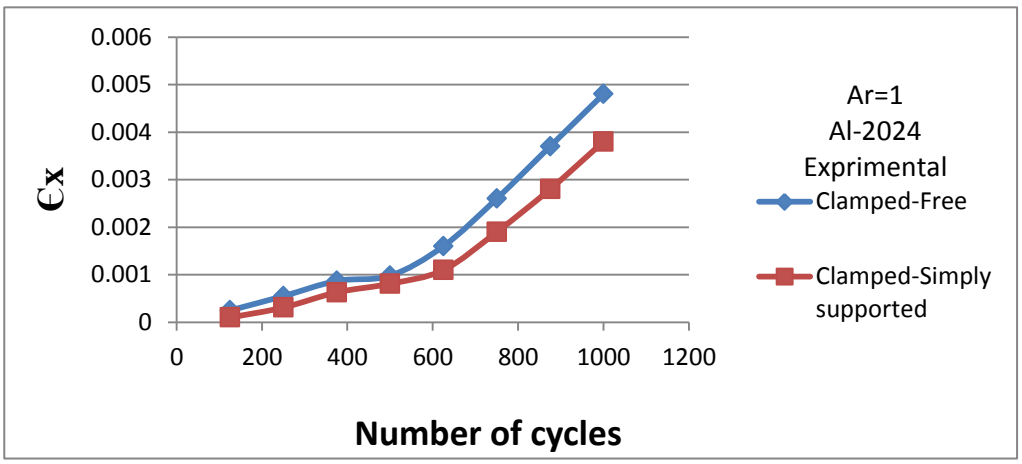

Figure23. $Є_x$ Experimental with number of cycles (B.C for 2024).

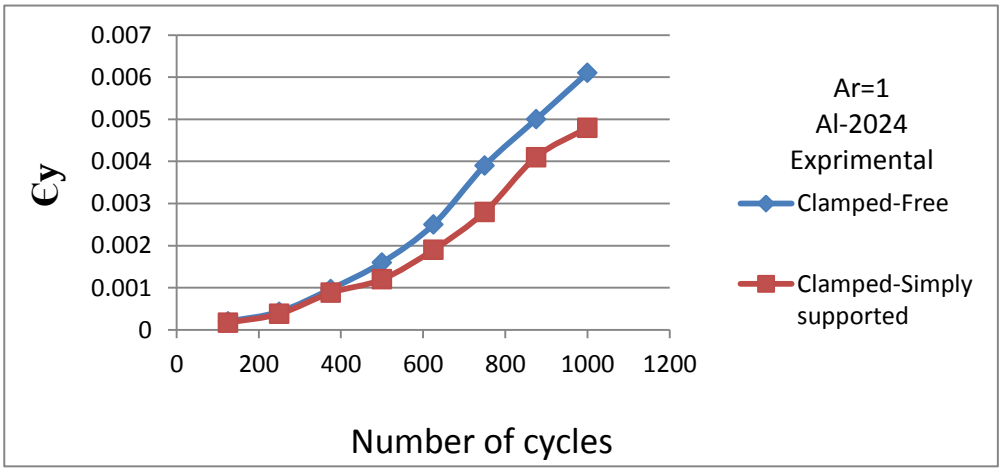

Figure24. $Є_y$ Experimental with number of cycles (B.C for 2024).

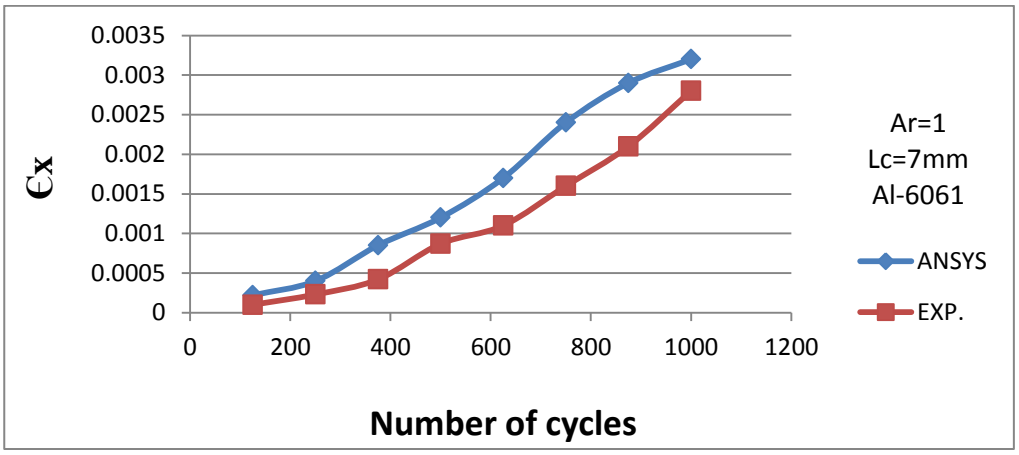

Figure25.$Є_x$ Numerical and experimental with number of cycles (Ar=1&Lc=7mmforAl-6061).

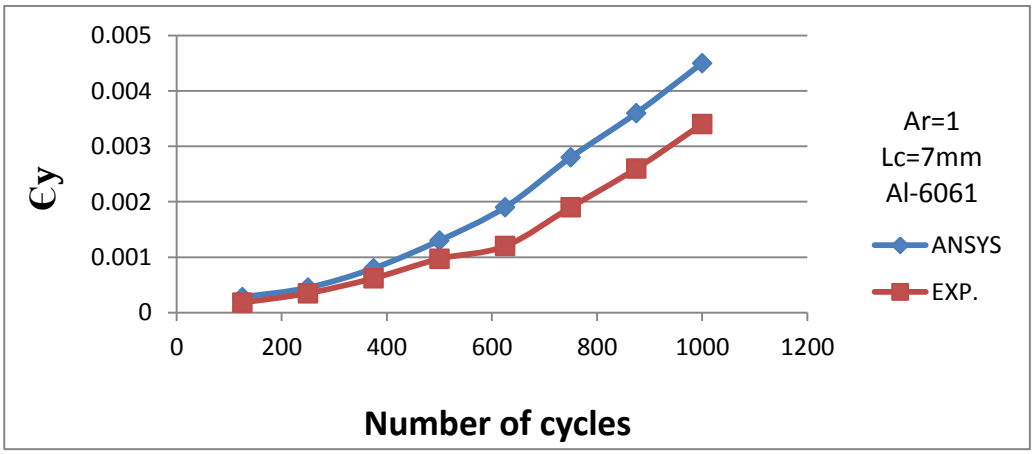

Figure26.$Є_y$ Numerical and experimental with number of cycles (Ar=1&Lc=7mm forAl-6061).

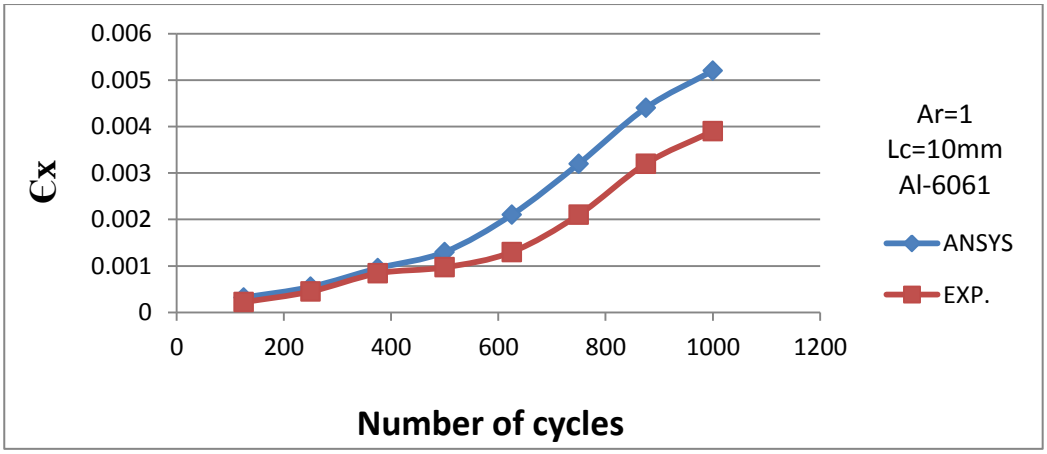

Figure27. $Є_x$ Numerical and experimental with number of cycles (Ar=1&Lc=10mm for Al-6061).

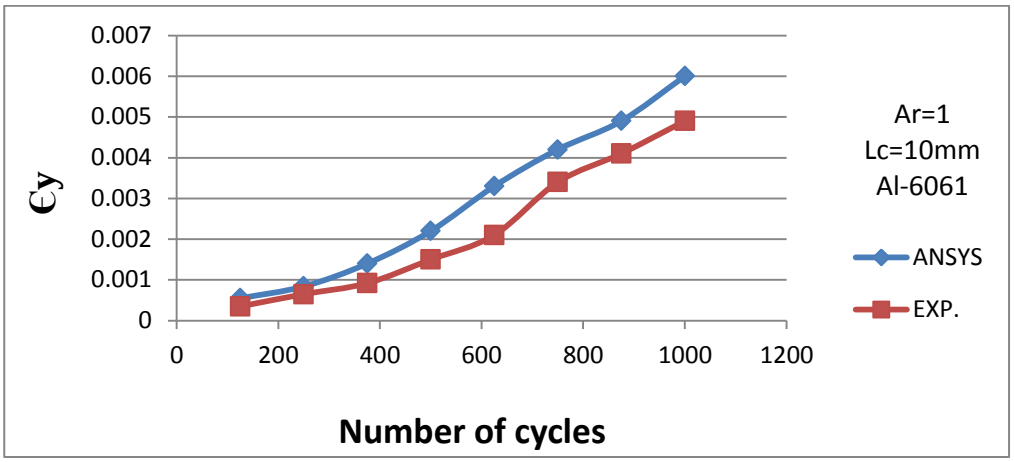

Figure28. $Є_y$ Numerical and experimental with number of cycles (Ar=1&Lc=10mm for Al-6061).

Ten Years of OpenStreetMap Project: Have We Addressed Data Quality Appropriately? – Review Paper

Dr. Maythm al-Bakri
Lecturer
Department of Surveying
College of Engineering
University of Baghdad
Email: m.m.m.s.albakri@gmail.com

ABSTRACT

It has increasingly been recognised that the future developments in geospatial data handling will centre on geospatial data on the web: Volunteered Geographic Information (VGI). The evaluation of VGI data quality, including positional and shape similarity, has become a recurrent subject in the scientific literature in the last ten years. The OpenStreetMap (OSM) project is the most popular one of the leading platforms of VGI datasets. It is an online geospatial database to produce and supply free editable geospatial datasets for a worldwide. The goal of this paper is to present a comprehensive overview of the quality assurance of OSM data. In addition, the credibility of open source geospatial data is discussed, highlighting the difficulties and challenges of VGI data quality assessment. The conclusion is that for OSM dataset, it is quite difficult to control its quality. It therefore makes sense to use OSM data for applications do not need high quality spatial datasets.

Key words: OpenStreetMap; VGI; spatial data quality; geometrical similarity; positional accuracy.

عشر سنوات منذ بداية مشروع OpenStreetMap : هل تمت السيطرة على جودة بياناته

م.د. ميثم مطشر شرقي
قسم هندسة المساحة
كلية الهندسة / جامعة بغداد

الخلاصة

أثبتت الدراسات الحديثة المتعلقة بتحليل البيانات المكانية ان الاتجاهات البحثية المستقبلية في معالجة هذه البيانات ستتركز على دراسة طبيعة وجودة البيانات المكانية المجانية المنشورة على شبكة الانترنيت Volunteered Geographic Information (VGI). يُنتج هذا النوع من الخرائط عن طريق جمع البيانات الجغرافية بالمسح الأرضي باستخدام مستقبلات نظام التموضع العالمي المحمولة Global Positioning System (GPS) المتوفرة حالياً في اغلب اجهزة الهاتف المحمول ، و كذلك بالاستعانة بمصادر حرة أخرى كالصور الفضائية المجانية المنشورة على شبكة الانترنيت. يمكن للمستخدمين تحرير المسارات والطرق وتحديثها من خلال وسائل التحرير المتاحة. شهدت العشر سنوات الاخيرة دراسة وتحليل دقة وتجانس مواقع واشكال العوارض على الخرائط المنتجة على شبكة الانترنيت وبالاخص مشروع خرائط الشارع المفتوح OpenStreetmap (OSM). خريطة الشارع المفتوح تقدم خريطة حرة للعالم بأكمله قابلة للتحرير من قبل أي شخص، شبيهة بطريقة عمل موسوعة ويكيبيديا. يهدف هذا البحث إلى تقديم نظرة شاملة عن ضمان جودة بيانات OSM ، بالإضافة الى مناقشة مصداقية

المصدر المفتوح للبيانات الجغرافية المكانية، وتسليط الضوء على الصعوبات والتحديات التي تواجه مستخدمي VGI في تقييم جودة بياناتها. إستنتج هذا البحث انه من الصعب جدا السيطرة على جودة بيانات OSM لذا فمن المنطقي استخدام هذه البيانات لتطبيقات لا تحتاج الى دقة عالية ، وللاغراض الاستطلاعية وعمل الدراسات الاحصائية.

1. INTRODUCTION

The past 30 years has seen the start and the development of the Internet technologies, which were initially used to obtain information only, **Harris, 2008**. However, in recent years, the advancement of web technologies has favoured the design of new patterns and practices models on the web extending beyond passive receiving of data. These cumulative developments are grouped under a common concept known as Web 2.0. The first official introduction of the term Web 2.0 was in the first conference of Web 2.0 (O'Reilly Media) by Tim O'Reilly in October 2004. Although the term Web 2.0 indicated a major change in the approaches of software developers on the web, it did not mean a new version of the World Wide Web. Web 2.0 has been described essentially as being a platform that can collect together different sites and software and make them easily available and useable to users, **,O'Reilly, 2005**.

The emerging of Web 2.0 technologies has led to significant changes in the methods of producing, processing, sharing and spreading information through the Internet, **,Rinner et al., 2008**. One consequence is enabling users to collaborate and interact among each other more easily and effectively. This is represented by the availability of a variety of social networking and communicating sites such as Facebook, Twitter, Flickr and You Tube. By using these facilities, it is possible to upload pictures or videos for public sharing; at the same time, it is also possible to make comments on the postings of others. Both of these practices facilitate the sharing of huge amounts of information on the web. Hence, nowadays not only professional users, but also non-experts, can generate and publish information on the Internet. This free sharing system was known as User Generated Content (UGC), **,Krumm et al., 2008**.

Since the term UGC refers to a variety of activities and applications, it is difficult to offer a standard definition for it. For instance, in their review of UGC, **,Vickery and Wunsch-Vincent, 2007.** identified the meaning of UGC as the ability of creating publicly, data on the Internet which can be achieved by amateurs or professionals with limited creative efforts. However, other authors did not accept this description as a common UGC definition; for example, ,**Ochoa and Duval, 2008.** reported that the UGC concept may be considered local rather than universal, as uploaded data may be available only for a specific group and not for common usage, or it may be simply rearranging such information and not making new contributions. Nonetheless, generally speaking, UGC can refer to information or media that may appear on the web which was contributed by volunteers without anticipation of any type of income, **,Krumm et al., 2008**.

A classical example of this kind of provision of information is Wikipedia (the free encyclopaedia). Wikipedia was originally established and founded by Larry Sanger and Jimmy Wales in 2001, **Miliard, 2008**. As Wikipedia adopts an open model for uploading and editing the contributions of others, which are in most cases articles, the numbers of the registered users and the articles in Wikipedia have increased significantly according to its statistics. However, the question of accuracy will arise when comparing this freely available data with professional productions. Inaccurate structure, bad quality and wrongly edited articles might be expected. Nevertheless, this is not the case in some situations when the free data is created by a group of people rather than single person, a factor that has been emphasised by, ,**Goodchild and Glennon, 2010**. They reported that the information obtained from a few contributors will be less

accurate than that obtained from many people. Furthermore, the Wikipedia community has developed its regulations and rules through a specific section of wiki space. This offers an opportunity to members to contact each other and decide upon standards for documented data in Wikipedia. This is why the concept of UGC expanded to several fields rapidly. For instance, the trend towards user-generated content which can be provided or shared online has had profound impacts on the geo-data scene.

By using Web 2.0 practices, an amateur can readily upload geo-data on the Internet. For example, nowadays any person can pick up the geographical information regarding their routes by using GPS in their driving or biking activities. Then, it is possible to contribute to updating and extending existing road databases on the web. It is also possible to add names or photographs to these datasets by means of the geotagging process. As these data are typically produced by volunteers, they have been labelled by **,Goodchild, 2007.** as volunteered geographic information (VGI). There are many alternative names and definitions for the phenomenon of geospatial information on the web. For instance, the term 'geospatial information bottom-up' was used by ,**Bishr and Kuhn, 2007.** to refer to geo-data on the Internet, whereas according to a definition provided by **,Turner, 2006**. this kind of information was coined as 'neogeography' and the same concept was also used by **,Haklay et al., 2008**. On the other hand, for **,Sui, 2008.** VGI means 'geography without geographers'. Whatever concepts that have been used to describe the open spatial data enabled on Web 2.0, the term VGI is the most widely adopted by many authors; see for example, **,Mooney et al., 2010**. ,**Coleman et al., 2009.** and ,**Elwood, 2008**. The term VGI was generally used to refer to creating, disseminating and updating geospatial data voluntarily on websites. This basically means combining the efforts of individuals or collaborative communities in such a way as to supply this new kind of geospatial data. Similar to UGC applications, VGI data can be effectively utilised by people other than the producers without any restrictions or rules.

VGI is similar to other open source productions in that producers and users of VGI data come from a variety of backgrounds because any person can become involved in this activity. In addition, there are no standard methods for uploading this kind of data. Since most VGI data are created by non-professionals, interest in integrating VGI with formal data, for instance, to develop and update formal datasets, may raise some concerns. From this point of view, ,**Elwood, 2008.** highlighted the need to investigate the different types of VGI with specific emphasis on examining the impacts of VGI services, such as tools and procedures that were used to collect, create and share this data, on the accuracy and the validation of using VGI for multiple purposes. Therefore, these databases are easily subject to heterogeneity and errors. However, VGI does suggest a new and powerful approach that could be efficiently used to create up to date datasets. Real time geospatial data that can be obtained from VGI are necessary for several purposes such as emergency actions; for example, ,**Zook et al., 2010.** reported that the flexibility of free web-based mapping services played a major role in aiding and rescuing people when an earthquake hit Haiti in January 2010. After the earthquake free information technologies such as aerial photographs were used in order to supply the necessary information about the most devastated areas and to produce route maps to deploy resources. Therefore, VGI can offer the most interesting and the cheapest geographic information to users and sometimes it will be the only source of information, especially for remote areas, **,Goodchild, 2007.**

In view of the fact that this article focuses on OpenStreetMap (OSM) data quality investigations in general, as OSM is the leading example of VGI projects that are concerned with geospatial

data development around the world, the OSM project will be discussed in greater detail than other VGI data types.

2. CHARACTERSTICS of OPENSTREETMAP

The OpenStreetMap (OSM) is an online geospatial database launched in England (London) by Steve Coast in 2004, **,Chilton, 2009**. In particular, it aims to produce and supply free editable geospatial datasets for a worldwide audience. The OSM fundamentally relies upon the collaborative volunteers' contributions for collecting and uploading geographic data to the common data base on the Internet, **,Ciepluch et al., 2009**. In general, contributors can collect the OSM data by controlling handheld portable GPS devices (navigation mode) such as the Garmin series. Nowadays, it is also possible to use built-in GPS applications which are available in most mobile phones models such as iPhone. In order to map a certain area using GPS technique, for instance, the OSM community gathers volunteers through an activity called 'mapping parties'. An example of this can be found in the study carried out by ,**Perkins and Dodge, 2008.** in which they illustrated a case study of a mapping party in Manchester, UK, in 2006. Although the GPS receivers may probably be considered as being the most important information source for the OSM project, there are also alternative data sources such as tracing data Yahoo imagery and /or Landsat images, **,Ramm et al., 2011**.

The OSM database allows for every user to reproduce or edit its datasets without the necessity for any authorization although attributing the data to OSM is required. Thus, the OSM project is technically similar to the Wikipedia (free encyclopaedia) concept. The users of these systems are able to modify and add or even delete the contributions made by others. The underlying OSM map data can be uploaded by creating a user account and edited online through a wiki-like interface. There are many other services that provide mapping on the Internet freely. For example, Microsoft offers Bing Maps, and Yahoo Maps and Google Maps are readily available. However, the users of these alternative map sources have only been provided with a very limited right to use their datasets. It is not permitted for users of these services to edit or update their datasets. Compared to the OSM data, there are several restrictions and conditions for using the Google Map service, as illustrated in ,**GoogleMaps, 2012.** For example, the raw data of Google Maps is not available to the users at all; however, it can be used by commercial companies such as TeleAtlas and Navteq, as they pay for downloading these, while OSM data can be downloaded by any user. Consequently, the OSM project can be considered as being one of the most useful online mapping services in that it is suitable for education in schools and undergraduate studies. The survey conducted by **,Bartoschek, and Keßler, 2013.** revealed that OSM is the most renowned online mapping service among students. The above mentioned positive aspects of OSM data, in addition to the possibility of using OSM as a base map for studies in cartography, make OSM a flexible tool in education.

The main other difference that may be noticed when comparing OSM data to other public mapping services is the level of detail as far as features are concerned. It is clear from **Fig. 1** that the site of Newcastle upon Tyne appears more complete in the OSM map than in the Google Maps version. However, the levels of detail of OSM maps vary around the world, ,**Ramm et al., 2011**. There are some places, such as the UK, that are mapped very well, whereas there are other parts of the world, such as Iraq for example, that have a little coverage for the centres of the big cities only. In fact, there is no detailed data for the countryside or the suburban areas, see **Fig. 2**. The detail of OSM maps is fundamentally based on the number of the volunteers that are available in each place around the globe.

The amounts of OSM data are increasing every day on the Internet. The number of registered users of this project is also growing at a remarkable rate. For example, ,**Haklay, and Weber, 2008.** reported that in 2008 the number of registered users of the OSM project was approximately 33,000, while at the time of writing this paper there are about 1,600,000 registered users, see **Fig. 3 and Table.1 ,OSM-stats, 2014.** It is clear that the number of registered people has increased by more than forty five times during the last six years. However, the number who edit is a minority of these. This view is supported by **,Neis, and Zipf, 2012.** who concluded that the rate of the registered users who achieved at least one edit of OSM data was only 38% of the total number of members. They also found that only 5% of the registered members have contributed more than 1000 nodes. Information can also be obtained from the **,OSM-stats, 2014.** with regard to the total number of uploaded GPS points, nodes, ways and relations for the real time OSM database. These statistics reflect the rapid growth of OSM data on the web, as shown in **Fig. 4 and Table. 2**.

There are various aspects to the most important motivations for these developments, for instance, gaining advantages from the free accessibility of OSM data (licence, cost, sharing) and opening up a new paradigm of 'geo-data-people's' Spatial Data Infrastructures (SDI). Access to current OSM data without any charge is available to anybody with web connections. In addition, the wide-ranging coverage of OSM data sources (around the world) allows visitors to search a world map and download different portions from a distance for any part of the world. Although these are positive aspects, the problem of heterogeneous data quality has emerged, **,Al-Bakri, and Fairbairn, 2011.** as will be discussed in more details in section 3.

3. THE ASSERTION of DATA QUALITY and CREDIBILITY of OPEN SOURCE DATA

Before discussing the problems of VGI data quality, it is necessary to understand the meaning of 'data quality'. Data quality as a concept may be defined differently, depending on the context in which it applies. There are many definitions of data quality in the literature. Each varies from organisation to organisation, application to application or person to person. For instance, the term 'quality' can be defined as an indication of high degree of craftsmanship or creativity, ,**Veregin, 1999.** In contrast, **,Jakobsson**, **2002**. regards data quality as a function of the difference between a dataset and the universe of discourse, when the universe of discourse is the actual objective world view and the dataset is the identifiable collection of any related dataset. In terms of spatial data, the notion of quality has been clarified by **,Korte, 2001.** as being the degree of how accurately the GIS data can be represented or meet a specific accuracy standard.

In most cases, the VGI data on the web may not contain any information about their quality. From this perspective, **,Flanagin, and Metzger, 2008.** supposed that the VGI data may improve spatial data content in general; however, the quality and accuracy of this data has still attracted the most attention to date. There are many reasons making VGI quality information extremely significant. For instance, the increasing of the decision making procedure based on the information of spatial data and the possibility of integrating different datasets which can be used for more GIS analysis and applications. The dependability of VGI data quality should be taken into consideration by people who have been collecting and disseminating this information. VGI data is usually collected by volunteers; thus its quality will vary and nobody can guess or know the value of it. This drawback has been agreed upon by authors such as, **,Haklay, 2010.** and **,Auer and Zipf, 2009.**

There are several legitimate criticisms that make the assessment of VGI quality difficult. For example, there is an enormous variety of people who contribute VGI data and there is no unified

authority whose role is to assess the quality of spatial data. Additionally, because of the different perspectives of data developers, it is highly likely that heterogeneities will be found in resulting datasets, **,Elwood, 2009.** This inspired **,Exel et al., 2010.** to include crowdsourced dynamics as an indicator of crowdsourced spatial data quality determination. They aimed to establish spatial data quality operational indicators for both user and feature quality. Their proposed approach fundamentally considered different crowdsourced activities such as the number of editors or edits per feature and the historical (or temporal) information of the features which includes the development of such features over time. This suggested framework may assist in measuring the density of edits to an area of crowdsourced data and ultimately assessing its data quality.

Elsewhere, **,Goodchild and Li., 2012.** have argued that although VGI may offer numerous advantages such as the free availability and accessibility of spatial datasets, the quality of VGI data should be considered as a vital issue as VGI data does not follow a standard structural design. Therefore, they investigated three different approaches to assess the quality of VGI data. Such quality assurance approaches are firstly, validation by crowdsourcing, secondly the social approach, relying on a hierarchy of 'trusted' individuals, and finally the geographic approach, which examines the probability of features being correctly located with reference to the surrounding context and geographical area. Subsequently, they compared these approaches with the quality assurance approach that is usually used by traditional mapping agencies. Some analysts e.g. ,**Hagenauer, and Helbich, 2012.** have pointed out that VGI data quality issues, especially completeness, can affect the fitness for use for such applications (e.g. urban planning). Therefore, they suggested a methodology to calculate through OSM data which urban areas in Europe are mapped or partially mapped. Their results found that the delineations of urban areas are based on the location.

The increase in the amount of data has also led to an increase in the heterogeneity between datasets. For instance, within different datasets, the features may be varying in accuracy due to the methods or skills that were employed for the purpose of collecting data. According to **,Haklay, 2010.** the distribution of errors in VGI data is usually based on the carefulness of each contributor. Therefore, the concern of trust of VGI data quality is the main issue facing the GI community. These heterogeneities may be especially problematic when the integration of multi-source spatial datasets is the target, for example.

4. HISTORY of OSM GEOMETRICAL SIMILARITY MEASUREMENT

4.1 Positional Discrepances

In order to understand the legitimate criticisms that the assessment of VGI quality is difficult, it is necessary to study previous researches and investigations which place emphasis on the assurance of VGI data quality. Furthermore, it is important to present research literatures related to quantitative measures for evaluating VGI quality. For instance, **,Ather, 2009.** carried out a research to look at the positional accuracy of OpenStreetMap data through comparison with the OS MasterMap dataset. Further map quality tests were also conducted in terms of a completeness study of road name attribution, and an analysis of number of users per area. The results of this analysis found that the positional accuracy of OpenStreetMap data to be very good in comparison to OS MasterMap, with over 80% overlap between most the road objects tested between the two datasets. The results also found there to be a positive correlation between road name attribute completeness and number of users per area.

,Haklay, 2010. examined the positional quality of OSM information by comparing it with OS-Meridian 2 datasets. The Meridian 2 dataset supplies detailed data of road networks in Great

Britain such as motorways, minor and major roads. In addition to use more data sources in order to complete this investigation. These involved the 1:10,000 raster files from OS, and some data about the neighbourhood size which is based on Census from OS and national statistics office. The main focus of Haklay's work was limited to the measuring of the quality of roads or motorways of OSM datasets. The findings of Haklay's study also showed that the quality of OSM data is variable when compared to OS datasets within the average of 6m of positional accuracy.

,Girres and Touya, 2010. assessed the quality of OSM datasets in France. In their investigation, many quality elements for OSM data were evaluated. The more interesting parameters that will be illustrated and described in this paper is geometric accuracy. Their analysis included the comparison of OSM data with the French National Mapping Agency geographic datasets. The results of their positional analysis of the road intersections indicated that the most frequent positional differences ranged between 2.5m to 10m, and the average value of the positional differences was nearly 6.65 m.

The differences between linear features were calculated by applying two techniques: the Hausdorf distance approach, which computes the maximum distance between the compared linear features, and the average distance approach, which takes the average distance between the compared polylines, a method suggested by McMaster (as cited in **,Girres and Touya, 2010.**). The principles of these methods can be seen in **Fig. 5**. The results of their study showed that the mean difference values between the compared roads were about 13.57m and about 2.19m for the Hausdorf distance and average distance methods respectively.

,Fairbairn, and Al-Bakri, 2013. also investigated the positional similarity of OSM dataset. They presented a methodology for assessing positional quality for Volunteered Geographic Information (VGI), such as OpenStreetMap (OSM) data, and authoritative large-scale data, such as Ordnance Survey (OS) UK data and General Directorate for Survey (GDS) Iraq data. The analyses are presented with a user-friendly interface which eases data input, computation and output of results, and assists in interpretation of the comparison. The results showed that a comparison of positional of OS data or GDS data, with those of OSM data, indicates that their integration for large scale mapping applications is not viable.

In another study **,Ming et al., 2013.** proposed a quality analysis model for OpenStreetMap crowd sourcing geographic data. Firstly, a quality analysis framework was designed based on data characteristic analysis of OSM data. Secondly, a quality assessment model for OSM data by three different quality elements: completeness, thematic accuracy and positional accuracy was presented. Finally, take the OSM data of Wuhan for instance, the research analysed and assessed the quality of OSM data with 2011 version of navigation map for reference. The result showed that the high-level roads and urban traffic network of OSM data has a high positional accuracy and completeness so that these OSM data can be used for updating of urban road network database.

In **,2014,Yang et al..** published a paper in which they developed an approach for integrating VGI POIs and professional road networks. The proposed method first generates a POI connectivity graph by mining the linear cluster patterns from POIs. Secondly, the matching nodes between the POI connectivity graph and the associated road network are fulfilled by probabilistic relaxation and refined by a vector median filtering VMF. Finally, POIs are aligned to the road network by an affine transformation according to the matching nodes. Experiments demonstrate that the

proposed method integrates both the POIs from VGI and the POIs from official mapping agencies with the associated road networks effectively and validly, providing a promising solution for enriching professional road networks by integrating VGI POIs.

4.2 Shape Similarity Measurement

In addition to the investigation of the positional similarity issue, there are several authors have examined various issues and problems that may relate to OSM data quality assessment such as measuring the quality of the shapes. For example, **,Haklay, 2010.** investigated the linear quality of OSM information by comparing it with OS-Meridian 2 datasets as mentioned above. The methodology which was applied to assess the quality of motorways of OSM data was based on approaches by **,Hunter, 1999.** and ,**Goodchild and Hunter, 1997**. The method of buffer was adopted to determine the accuracy of such lengthy objects by applying a certain distance of buffer size for this test. The results of the analysis showed that the average of overlap percentages when comparing OSM with OS datasets were approximately 80%, 88% and 77% for motorways, A-roads and B-roads respectively.

The quality of VGI data has received more attention from the GI community; for example, the investigation that was carried out by **,Zielstra and Zipf, 2010.** They studied the quality of the routes and roads of OSM data in Germany. The OSM information has been compared with a commercial dataset known as Tele Atlas. They based their approach on that suggested by **,Goodchild and Hunter, 1997.** to measure the quality of linear features. Their results found that the overlap percentages between the roads of OSM data and Tele Atlas datasets were ≥ 80% for most of the roads in major cities. In addition, they reported that the overlap percentage in towns of medium size was between 50% and 80%. They argued that the results of their comparisons revealed that the accuracy seems quite good and the OSM data can be used for many routing applications. However, they found that there are still shortcomings in the accuracy of the regional OSM datasets.

,Girres, and Touya, 2010. assessed the shape quality of OSM datasets in France. In their study, they considered the differences between polygonal objects of lakes. The surface distance method which was proposed by Vauglin (as cited in ,**Girres, and Touya, 2010.**) was adopted to quantify polygon differences. The method based on the common area of the two compared objects. The *ds* value will be zero if polygon *A* is equal to polygon *B*, while it will be one if *A* is not equal to *B*. The results of this method showed that there is a small difference between the polygons of the comparison datasets.

,Koukoletsos et al., 2012. suggested an automated feature-based matching method specifically designed for VGI, based on a multi-stage approach that combines geometric and attribute constraints. It was applied to the OSM dataset using the official data from Ordnance Survey as the reference dataset. The results were then used to evaluate data completeness of OSM in several case studies in the UK. The method combined geometric and attribute constraints (road name and type) in order to deal with heterogeneous datasets, taking into account that attributes may be missing. When tested on OSM (VGI) and ITN (Reference) datasets for the selected rural and urban areas, the process lasted eight and 15 hours, respectively. Data matching proved to be efficient, with matching errors between 2.08% (urban) and 3.38% (rural areas). Data completeness of the VGI dataset is then calculated for smaller areas (tiles), giving more representative results of its heterogeneity.

,Neis et al., 2012. outlined the development of Volunteered Geographic Information in Germany from 2007 to 2011, using the OpenStreetMap project as an example. Specifically, they considered the expansion of the total street network and the route network for car navigation. With a relative completeness comparison between the OSM database and TomTom‘s commercial dataset, they showed that the difference between the OSM street network for car navigation in Germany and a comparable proprietary dataset was only 9% in June 2011. The results of thier analysis regarding the entire street network revealed that OSM even exceeds the information provided by the proprietary dataset by 27%. Further analyses showed on what scale errors can be reckoned with in the topology of the street network, and the completeness of turn restrictions and street name information. In addition to the analyses conducted over the past few years, projections have additionally been made about the point in time by which the OSM dataset for Germany can be considered complete in relative comparison to a commercial dataset.

A recent study by ,**Fairbairn, and Al-Bakri, 2013.** involved creating a user-friendly interface incorporating quantitative and visual analysis of dataset comparison that could be used to assess geometrical similarity of OSM data. The interface was designed for assessing linear and shape matching, in this case comparing the formal data OS and GDS, with the rigorous field survey (FS), and the informal OSM data. The results of this analysis showed that the shape measurements of the informal OSM data do not match the formal data in any of the case study areas examined.

5. DISCUSSION and CONCLUSION

This paper has shown that there are significant incompatibilities preventing the matching of VGI with formal datasets. However, some of these can be addressed in a positive manner with regard to certain aspects such as the richness of datasets that have been offered by VGI data sources, **,Ballatore, and Bertolotto, 2011.** For example, the richness of feature type definition in OSM could enhance the value of integration. The growing availability of the subclasses of OSM features may enable a wealth of new opportunities to enhance and update the quality of feature classification of formal or governmental data. For instance, by comparing the children levels (i.e. fourth level) of XML schema trees of OSM datasets with those of formal datasets, as shown in **,Al-Bakri, and Fairbairn, 2012.** it can be seen that the schema of OSM feature classifications display more distribution and classes especially at the latest or end levels. The dynamic nature in terms of the frequency of updating and gathering detailed features of OSM data have established these aspects of feature types of OSM project as being particularly useful. This can be considered as one positive aspect of OSM or informal datasets which could enable these kinds of spatial datasets to be beneficial or advantageous.

Although the current study demonstrated that a divergence exists when evaluating the geometrical elements of VGI and formal spatial data sources, **,Zielstra, and Hochmair, 2011.** showed that the integration of pedestrian routes’ accessibility to transit stations (bus and metro stations) of VGI data, such as the OSM project, into the data produced from Tele Atlas and/or NAVTEQ can be useful in US and German cities. The reason for including OSM data in this integration process as a worthy source of pedestrian routes has been explained by the authors as being a potential rich and valuable source of pedestrians’ data that can be supplied from OSM project. This merit of OSM data has been proved by the findings of the numerical analysis of, ,**Zielstra, and Hochmair, 2011.** They showed that the information about pedestrian segments of OSM data can increase the usage of the transit facilities when the commercial data is not available, as in the case studies in Germany and some US cities such as Chicago and San Francisco. It seems possible that these results are due to the effective efforts of OSM

communities in Germany and some US cities to develop comprehensive OSM pedestrian path networks.

The positive aspects of VGI data that were mentioned in Section 2, such as the easy access, free use and the rapid growth of these kinds of datasets, makes it possible to envisage further practical applications of them. For example, the combining of the richness of the OSM database into the addresses of places around the world, by following mapping mashup technologies, may produce a compatible and helpful database. This could be used for tourist or navigation purposes rather than using traditional formal and expensive tourist maps. Another useful VGI application was suggested by ,**Neis et al., 2010.** They explained that the integration of up-to-date OSM data into the UN Spatial Data Infrastructure for Transportation would make it possible to manage disaster relief by creating crisis maps. The obvious example of this situation was when an earthquake hit Haiti in 2010 and how the use of OSM helped in the rescue of people, as described in introduction.

The availability of other VGI data sources beyond OSM can also be useful and valuable for such applications. The other VGI data sources, especially those which do not provide pure spatial datasets, such as Flickr, may be used for such applications that do not need to consider the spatial data quality elements in the processing flowline. For instance, ,**Schade et al., 2011.** proposed a workflow for using VGI data such as Flickr images for risk detection events. They initially described the positive characteristics of this kind of dataset and why it can be applied for this application. The massive growth of images through this website, the multiplicity of options for uploading images and the ability of users to geotag images can be considered the main positive aspects of this service. As an example of their application, Flickr images were used to detect the risk of flood in the UK for the period from 2007 to 2009. The analysis of the approach taken was basically based on the fundamental information that can be obtained from the Flickr website, such as the location of the picture, the time and date a picture was taken and the time and the data the pictures were uploaded onto the website.

Another example of a benefit gained from VGI data was illustrated by ,**Spinsanti, and Ostermann, 2010.** They developed a methodology to test the framework of assessing the contribution of VGI data to detecting the spread of fire events, and compared this with the official information sources that can be obtained from the European forest fire information system. For their project, the authors used picture data from Flickr and text data from Tweeter. They argued that using VGI data for communicating during disasters is an effective method of crisis management which may reduce the amount of risks and losses.

The above discussion has shown that although this paper concluded that it is difficult to integrate VGI data with formal spatial datasets, there is a wide range of applications that VGI data can serve and assist with; especially those which do not need high quality spatial datasets. Updating transit maps, enhancing pedestrian navigation systems and addressing disaster scenarios are all examples of small-scale topographic data which can be more easily integrated with formal datasets. Large-scale data show more limited promise due to geometric and semantic mismatching. Therefore, the conclusion that formal data providers would not be interested in integrating their datasets with, for example, OSM data is correct. VGI users, on the other hand, are certainly keen to incorporate official datasets into their own, and the results obtained in this research would give confidence to such procedures. The issue of data quality is taken seriously throughout the OSM community, for example. The section on Quality Assurance in the OSM blog shows that a number of tools are available and in development for detection, reporting and monitoring of data quality **,Wiki-OpenStreetMap, 2012.**

References

- Al-Bakri, M. and Fairbairn, D., 2011, *User generated content and formal data sources for integrating geospatial data,* 25th International Cartographic Conference Paris, France, pp. 1-8.
- Al-Bakri, M. and Fairbairn, D., 2012, *Assessing similarity matching for possible integration of feature classifications of geospatial data from official and informal sources*, International Journal of Geographical Information Science, 26, (8), pp. 1437-1456.
- Ather, A., 2009, *A quality analysis of OpenStreetMap data*. M.Sc. thesis, UCL.
- Auer, M. and Zipf, A., 2009, *How do free and open geodata and open sdtandards fit together? from sceptisim versus high potential to real applications,* The First Open Source GIS UK Conference. Nottingham, UK, pp. 1-6.
- Ballatore, A. and Bertolotto, M., 2011, *Semantically enriching VGI in support of implicit feedback analysis*, in Tanaka, K., Fr¨ohlich, P. and Kim, K.-S.(eds) Web and Wireless Geographical Information Systems, volume 6574 of Lecture Notes in Computer Science. Springer Berlin / Heidelberg, pp. 78-93.
- Bartoschek, T. and Keßler, C., 2013, *VGI in education–from K-12 to graduate studies*, in Sui, D., Elwood, S. and Goodchild, M.(eds) Crowdsourcing Geographic Knowledge. Volunteered Geographic Information (VGI) in Theory and Practice. Springer, pp. 341-360.
- Bishr, M. and Kuhn, W., 2007, *Geospatial information bottom-up: A matter of trust and semantics*, The European Information Society - Leading the Way with Geo-information. Springer-Verlag Berlin Heidelberg, pp. 365-387.
- Chilton, S., 2009, *Crowdsourcing is radically changing the geodata landscape: case study of OpenStreetMap,* 24th International Cartographic Conference Santiago, Chile, pp. 1-7.
- Ciepluch, B., Mooney, P., Jacob, R. and Winstanley, A. C., 2009, *Using OpenStreetMap to deliver location-based environmental information in Ireland*, SIGSPATIAL Special, 1, (3), pp. 17-22.
- Coleman, D., Georgiadou, Y. and Labonte, J., 2009, *Volunteered geographic information: the nature and motivation of producers*, International Journal of Spatial Data Infrastructures Research, 4, (1), pp. 332 - 358.
- Elwood, S., 2008, *Volunteered geographic information: future research directions motivated by critical, participatory, and feminist GIS*, Geojournal, 72, (3), pp. 173–183.
- Elwood, S., 2009, *Geographic information science: new geovisualization technologies – emerging questions and linkages with GIScience research*, Progress in Human Geography, 33, (2), pp. 256–263.
- Exel, M. v., Dias, E. and Fruijtier, S., 2010, *The impact of crowdsourcing on spatial data quality indicators,* GIScience 2010. Zurich, Switzerland pp. 1-4.

- Fairbairn, D.; Al-Bakri, M., 2013, *Using geometric properties to evaluate possible integration of authoritative and volunteered geographic information*, ISPRS Int. J. Geo-Inf., 2, pp. 349–370.
- Flanagin, A. J. and Metzger, M. J., 2008, *The credibility of volunteered geographic information*, Geojournal, 72, pp. 137–148.
- Girres, J.-F. and Touya, G., 2010, *Quality assessment of the French OpenStreetMap dataset*, Transactions in GIS, 14, (4), pp. 435-459.
- Goodchild, M. F. and Hunter, G. J., 1997, *A simple positional accuracy measure for linear features*, International Journal of Geographical Information Science, 11, (3), pp. 299 - 306.
- Goodchild, M. F., 2007, *Citizens as sensors: the world of volunteered geography*, Geojournal, 69, (4), pp. 211–221.
- Goodchild, M. and Glennon, A., 2010, *Crowdsourcing geographic information for disaster response: a research frontier*, International Journal of Digital Earth, 3, (3), pp. 231-241.
- Goodchild, M. F. and Li, L., 2012, *Assuring the quality of volunteered geographic information*, Spatial Statistics, 1, pp. 110-120.
- GoogleMaps, 2012, *Google maps/earth additional terms of service* Available at: http://maps.google.com/help/terms_maps.html (Accessed: 27-05-2014).
- Hagenauer, J. and Helbich, M., 2012*Mining urban land-use patterns from volunteered geographic information by means of genetic algorithms and artificial neural networks*, International Journal of Geographical Information Science, 26, (6), pp. 963-982.
- Haklay, M., 2010, *How good is volunteered geographical information? A comparative study of OpenStreetMap and Ordnance Survey datasets*, Environment and Planning B: Planning and Design, 37, (4), pp. 682 -703.
- Haklay, M., Singleton, A. and Parker, C., 2008, *Web mapping 2.0: The neogeography of the GeoWeb*, Geography Compass, 2, (6), pp. 2011-2039.
- Haklay, M. M. and Weber, P., 2008, *OpenStreetMap: user-generated street maps*, IEEE Pervasive computing, 7, (4), pp. 12-18.
- Harris, D., 2008, *Web 2.0 evolution into the intelligent Web 3.0.* London, UK: Emereo Pty Ltd.
- Hunter, G. J., 1999, *New tools for handling spatial data quality: moving from academic concepts to practical reality*, URISA Journal, Vol. 11, (No. 2), pp. 25-34.
- Jakobsson, A., 2002, *Data quality and quality management - examples of quality evaluation procedures and quality management in European national mapping agencies*, in Shi, W., Fisher, P. F. and Goodchild, M. F.(eds) Spatial Data Quality. London: Taylor & Francis, pp. 216–229.
- Korte, G. B., 2001, *The GIS Book, How to Implement, Manage, and Assess the Value of Geographic Information Systems.*5th ed Albany, New York: Onword Press.
- Koukoletsos, T., Haklay, M. & Ellul, C., 2012, *Assessing data completeness of VGI through an automated matching procedure for linear data*, Transaction in GIS, 16, pp. 477-498.

- Krumm, J., Davies, N. and Narayanaswami, C., 2008, *User-generated content*, Pervasive Computing, IEEE, 7, (4), pp. 10-11.
- Mooney, P., Corcoran, P. and Winstanley, A. C., 2010, *Towards quality metrics for OpenStreetMap*, GIS: Proceedings of the ACM International Symposium on Advances in Geographic Information Systems. San Jose, CA, pp. 514-517.
- Miliard, M., 2008, *Wikipediots: who are these devoted, even obsessive contributors to Wikipedia*, City Weekly. Available at: http://www.cityweekly.net/utah/article-5129-feature%20wikipediots-%09who%20are-these-devoted-even-obsessive-contributors-to-%09wikipedia.html.
- Ming, W., Qingquan, L., Qingwu, H. & Meng, Z., 2013, *Quality analysis of OpenStreetMap data*, International Archives of the Photogrammetry, Remote Sensing and Spatial Information Sciences, Volume XL-2/W1, 8th International Symposium on Spatial Data Quality , 30 May - 1 June 2013, Hong Kong, pp. 155-158.
- Neis, P., Singler, P. and Zipf, A., 2010, *Collaborative mapping and emergency routing for disaster logistics -Case studies from the Haiti earthquake and the UN portal for Afrika*, Geoinformatik 2010. Kiel, Germany, pp. 1-6.
- Neis, P. and Zipf, A., 2012, *Analyzing the contributor activity of a volunteered geographic information project -The case of OpenStreetMap*, ISPRS International Journal of Geo-Information, 1, (2), pp. 146-165.
- Neis, P., Zielstra, D. & Zipf, A., 2012, *The street network evolution of crowdsourced maps: OpenStreetMap in Germany 2007-2011*, Future Internet, 4, pp. 1-21.
- Ochoa, X. and Duval, E., 2008, *Quantitative analysis of user-generated content on the web*, Proceedings of the First International Workshop on Understanding Web Evolution Beijing, China, pp. 19-26.
- OSM-stats, 2014, *OpenStreetMap stats*. Available at: http://www.openstreetmap.org/stats/data_stats.html (Accessed: 21-05-2014).
- O'Reilly, T., 2005, *What is Web 2.0: design patterns and business models for the next generation of software*. Available at: http://oreilly.com/web2/archive/what-is-web-20.html?page=1 (Accessed: 11-03-2014).
- Perkins, C. and Dodge, M., 2008, *The potential of user-generated cartography:a case study of the OpenStreetMap project and Mapchester mapping party*, North West Geography, 8, pp. 19-32.
- Ramm, F., Topf, J. and Chilton, S., 2011, *OpenStreetMap - using and enhancing the free map of the world.* Cambridge, England: UIT Cambridge Ltd.
- Rinner, C., Kebler, C. and Andrulis, S., 2008, *The use of Web 2.0 concepts to support deliberation in spatial decision-making*, Computers, Environment and Urban Systems, 32, (5), pp. 386-395.
- Schade, S., Díaz, L., Ostermann, F., Spinsanti, L., Luraschi, G., Cox, S., Nuñez, M. and Longueville, B. D., 2011, *Citizen-based sensing of crisis events: sensor web enablement for volunteered geographic information*, Applied Geomatics, Online First™, 19 July 2011. DOI 10.1007/s12518-011-0056-y, pp. 1-16.

- Spinsanti, L. and Ostermann, F. O., 2010, *Validation and relevance assessment of volunteered geographic information in the case of forest fires*, 2nd International Workshop on Validation of Geo-Information Products for Crisis Management. Ispra, Italy, pp. 1-9.
- Sui, D., 2008, *The wikification of GIS and its consequences: Or Angelina Jolie's new tattoo and the future of GIS*, Computers, Environment and Urban Systems, 32, (1), pp. 1-5.
- Turner, A. J., 2006, *Introduction to Neogeography.* Short Cuts Series: O'Reilly Media, Inc.
- Veregin, H., 1999, *Data quality parameters*, in Longley, P., Goodchild, M., Maguire, D. and Rhind, D.(eds) *Geographical Information Systems Principles and Technical Issues.* USA: John Wiley & Sons, Inc, pp. 177-189.
- Vickery, G. and Wunsch-Vincent, S., 2007, *Participative Web and User-Created Content: Web 2.0, wikis and social networking.* USA: OECD.
- Wiki-OpenStreetMap, 2013, *State of the map 2012/call for venues/Tokyo*. Available at: http://wiki.openstreetmap.org/wiki/State_Of_The_Map_2012/Call_for_venues/Tokyo (Accessed: 03-06-2014).
- Yang, B., Zhang, Y. & Lu, F., 2014, *Geometric-based approach for integrating VGI POIs road networks*, International Journal of Geographical Information Science, 28, (1), pp. 126-147.
- Zielstra, D. and Zipf, A., 2010, *Quantitative studies on the data quality of OpenStreetMap in Germany*, Sixth International Conference on Geographic Information Science,GIScience 2010. Zurich, Switzerland, pp. 1-7.
- Zielstra, D. and Hochmair, H., 2011, *Comparative study of pedestrian accessibility to transit stations using free and proprietary network data*, Transportation Research Record: Journal of the Transportation Research Board, 2217, pp. 145-152.
- Zook, M., Graham, M., Shelton, T. and Gorman, S., 2010, *Volunteered geographic information and crowdsourcing disaster relief: a case study of the Haitian earthquake*, World Medical & Health Policy, 2, (2), pp. 7-33.

Table 1. The growth of OSM registered users **,OSM-stats, 2014.**

Date	Numbers of OSM Registered Users
Aug 2005	1,000
Jan 2006	1,500
Aug 2006	2,500
Jan 2007	3,000
Aug 2007	5,000
Jan 2008	10,000
Aug 2008	50,000
Jan 2009	100,000

Aug 2009	150,000
Jan 2010	200,000
Aug 2010	300,000
Jan 2011	350,000
Aug 2011	450,000
Jan 2012	530,000
Aug 2012	700,000
Jan 2013	1,000,000
Aug 2013	1,300,000
Jan 2014	1,500,000

Table 2. The growth of OSM data **,OSM-stats, 2014.**

Date	No. of Nodes	No. of Ways	No. of Relations
08/08/2005	8,000,000	8,000,000	8,000,000
23/01/2006	10,000,000	10,000,000	10,000,000
10/07/2006	20,000,000	15,000,000	15,000,000
25/12/2006	25,000,000	18,000,000	18,000,000
11/06/2007	30,000,000	20,000,000	20,000,000
26/11/2007	200,000,000	22,000,000	21,000,000
12/05/2008	230,000,000	24,000,000	22,000,000
27/10/2008	290,000,000	26,000,000	23,000,000
13/04/2009	320,000,000	27,000,000	24,000,000
28/09/2009	450,000,000	28,000,000	25,000,000
15/03/2010	580,000,000	31,000,000	26,000,000
30/08/2010	760,000,000	65,000,000	27,000,000
14/02/2011	1,000,000,000	80,000,000	28,000,000
01/08/2011	1,200,000,000	100,000,000	29,000,000
16/01/2012	1,300,000,000	110,000,000	30,000,000
02/07/2012	1,500,000,000	130,000,000	31,000,000
03/06/2013	1,100,000,000	200,000,000	32,000,000
05/05/2014	2,200,000,000	220,000,000	32,000,000

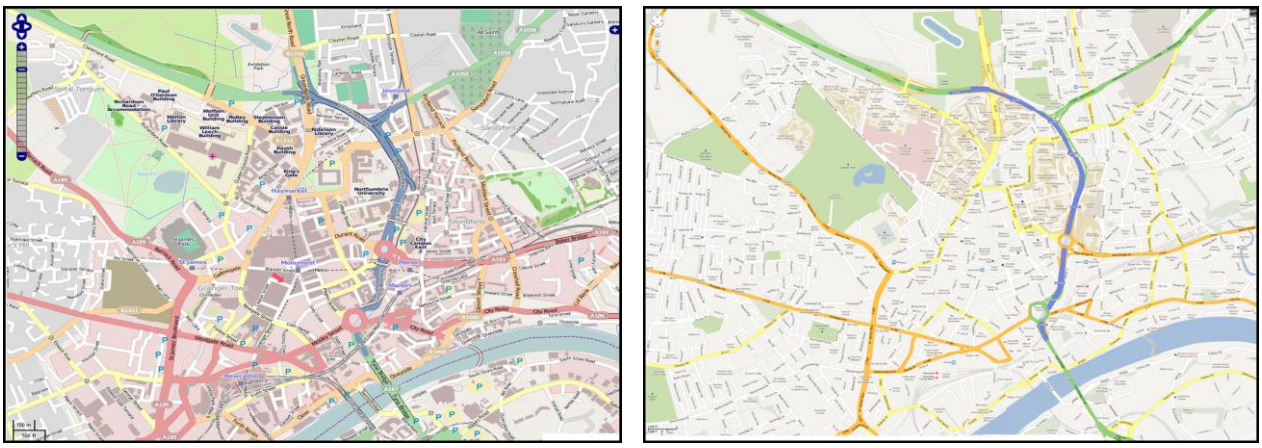

a-OpenStreetMap data (http://www.openstreetmap.org/). b- Google maps data (http://maps.google.co.uk/).

Figure 1. A comparison of the details of maps for the centre of Newcastle upon Tyne – UK (images sampled on 01/05/2014, both rendered at equivalent zoom levels – 16/19 for OSM, 15/18 for Google maps). This comparison facility is now available at http://tools.geofabrik.de/mc/.

a-London / UK b- Baghdad / Iraq

Figure 2. A comparison of the details of OSM data for the capital of UK (London) and the capital of Iraq (Baghdad). Images sampled on 1/05/2014, both rendered at equivalent zoom levels – 11/19 (http://www.openstreetmap.org/).

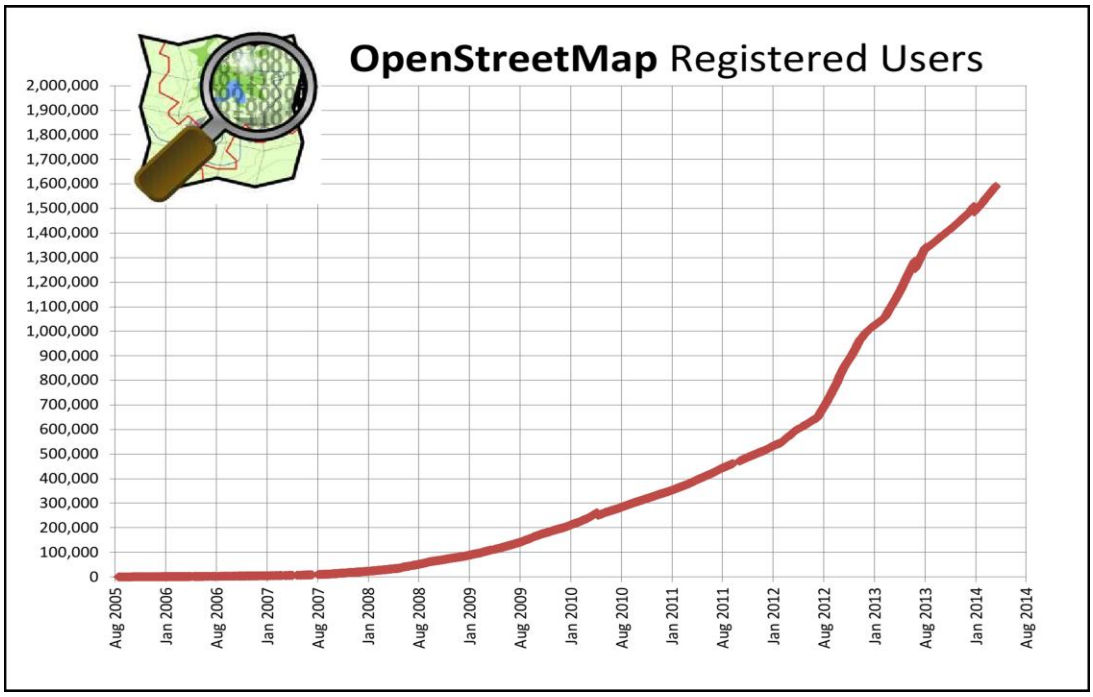

Figure 3. Statistics account graph reflecting the growth of OSM registered users **,OSM-stats, 2014.**

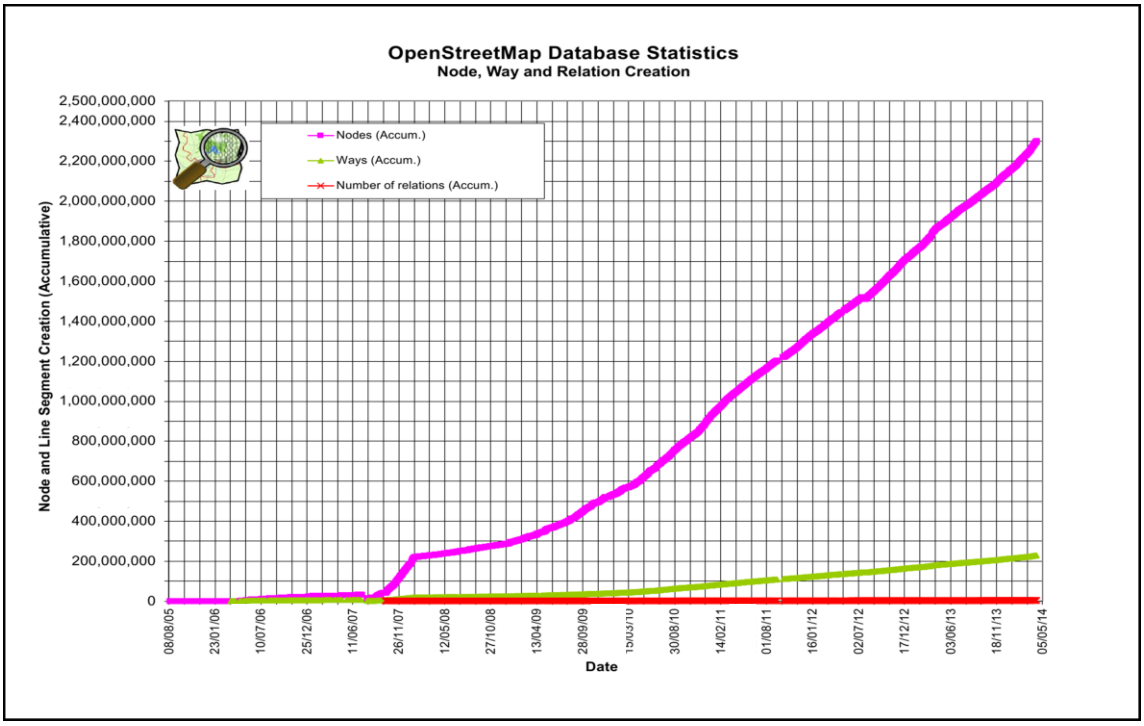

Figure 4. Statistics account graph reflecting the growth of OSM data (nodes, ways, and relations) on the web **,OSM-stats, 2014.**

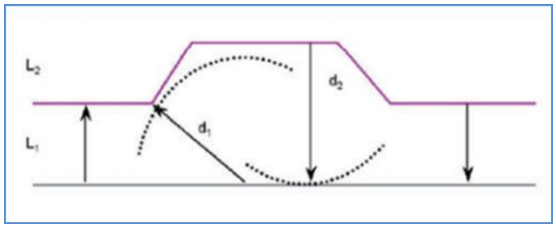

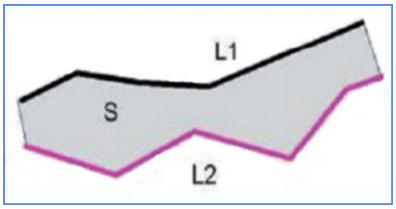

a-Hausdorff distance method b- average distance method

Figure 5. The methods that have been adopted by Girres and Touya (2010) to determine the linear differences between road features.

ISSN 1726 - 4073

Journal of Engineering

A Scientific Refereed Journal
Published by
College of Engineering
University of Baghdad

April
2015

Number 4
Volume 21

تقييم تأثير المخاطر على اهداف وسلامة المشاريع الانشائية في العراق

أ.م.د. انتصار كاظم رشيد
قسم الهندسة المدنية
كلية الهندسة / جامعة بغداد

الخلاصة

تعتبر مشاريع التشييد ذات طبيعة خاصة وتؤثر عليها عوامل كثيرة مما يجعلها تتعرض الى مخاطر متعددة وذلك نتيجة لطول فترة التنفيذ وتعدد المراحل ابتداءً من مرحلة القرار مروراً بالتنفيذ وحتى التسليم النهائي، الامر الذي يؤدي الى زيادة عدم التأكد وزيادة احتمالية وقوع المخاطر، تعد عملية تحليل وادارة المخاطر من الاساليب الفعالة والمثمرة التي تستخدم في ادارة مشاريع التشييد لغرض زيادة فرص انهاء المشروع بنجاح من ناحية الكلفة والوقت والجودة وبأقل ما يمكن من المشاكل.

يهدف البحث اولاً الى التخطيط الفعال لتحليل وادارة المخاطر ذات مستويات الاهمية المختلفة وفق استراتيجية محددة وفعالة معتمدة على خبراء متخصصين في مجال ادارة المخاطر، وثانياً التوصل الى اجراءات للاستجابة للمخاطر بما يكفل ادارة هذه المخاطر في مشاريع البناء.

حددت في هذا البحث عدد من المخاطر التي تم حدوثها فعلاً من دراسة عدد من مشاريع البناء المنجزة ومن الدراسات النظرية ومقابلة عدد من خبراء صناعة التشييد لتحديد مدى تأثير هذه المخاطر في كل من أهداف المشروع وسلامته.

ظهر ان من اهم المخاطر في المشاريع الانشائية في العراق هي (عدم توفر المخططات للشبكات الخدمية المارة خلال الموقع كالمخططات الكهربائية , الهاتف , الماء , وغيرها) و (فروقات بين التنفيذ والمواصفات المطلوبة نتيجة لسوء فهم المخططات والمواصفات)، كما ظهر ان اكبر تاثير للمخاطر هو على مدة تنفيذ المشروع وأقلها كان على السلامة المهنية، وان اجراء الاستجابة للمخاطر بوضع شروط عقدية هو الاجراء المفضل ثم يليه الاجراءات الاخرى.

الكلمات الرئيسية: المخاطر، عدم التأكد، ادلرة المخاطر، تحليل المخاطر، مشاريع التشييد

Valuation the impact of Risks on the Goals and the Safety of Construction Projects in Iraq

Asst. Prof.Dr. Entisar Kadhim Rasheed
Department of Civil Engineering
College of Engineering
Baghdad University
E-mail:int.pros_62@yahoo.com

ABSTRACT

Construction projects have a special nature and affect them many factors making them exposed to multiple risks as a result of the length of the implementation period and the multiplicity of stages, starting from the decision stage through implementation until the final delivery, which leads to increased uncertainty and the likelihood of risk.
The process of analysis and risk management is one of the effective and productive methods that are used in managing the construction projects for the purpose of increasing the chances of ending the project successfully in terms of cost, time and quality and at the lowest possible problems.
The research aims first to the effective planning for analysis and risk management with different levels of importance according to specific strategy and effective based on experts in the field of risk management and, secondly, reaching measures to respond to the risks in order to ensure the management of these risks in construction projects. In this research a number of risks are identified which that have been incurred actually after studying a number of completed construction projects and theoretical studies and interview a number of experts in the construction industry to determine the impact of these risks in each of the project's objectives and safety.
It appeared that the most important risks in construction projects in Iraq is (the lack of drawings for networks service through the site such as electrical drawings, phone, water, etc.) and (differences between the implementation and the required specifications because of a misunderstanding of the plans and specifications, It also appeared that the biggest effect of the risks is the on the duration of the project and the least was on occupational safety, and the best response to the risk is to fix certain conditions in the contract followed by other responses.

Key words: risk, uncertainty, risk management, risk analysis, construction projects

1. المقدمة:

يتكون قطاع البناء والتشييد من مجموعة نشاطات ترتبط باعمال المباني والانشاءات الهندسية بأنواعها بالاضافة الى اعمال الصيانة ، وتميز هذا القطاع بعلاقة وثيقة مع جميع القطاعات الاقتصادية الاخرى مما جعله مؤشراً مهماً وموثوقاً لحركة الاقتصاد الوطني واتجاهاته ، الا ان الكثير من المخاطر تواجهها مشاريع البناء والتشييد وهذه المخاطر قد تؤثر على تنفيذ المشروع وقد تؤدي الى تأخير التسليم وزيادة الكلفة وأحياناً تؤثر على جودة العمل. ان من اهم ما يجب أخذه في الاعتبار ان صناعة التشييد بطبيعتها محفوفة بالمخاطر والتي يصعب تجنبها او التنبؤ بها او بتأثيرها، وقد دعا ذلك الى الاهتمام بموضوع المخاطر في هذه الصناعة في العقدين الاخيرين على المستوى الدولي واتفق الخبراء على انه من مصلحة صاحب العمل الاقتصادية ان يتم تجنب او تقليل او قبول او تحويل المخاطر الى طرف اخر ذو قدرة وكفاءة على تحملها و ادارتها وانه يجب التخلي عن الفكرة العقيمة بأن يتحمل المقاول وحده كل هذه المخاطر وذلك خدمة لمصلحة المشروع. (Malcolm,1997). لقد أصبح الآن من الضروري فهم طبيعة المخاطر وتحليلها بهدف وضع استراتيجية معينة لإدارتها والتعامل معها. فادارة المخاطر في قطاع التشييد هي عملية تحقيق أهداف المشروع (زمن, كلفة، جودة، سلامة مهنية وبيئية)، وتساعد ادارة المخاطر

مديري المشاريع في جدولة أولوياتهم وتخصيص الموارد وتساعدهم ايضاً في عملية صنع القرار بشكل أكثر وثوقاً مما يسهم في إنجاح المشروع وتحقيق أهدافه.(منى واخرون،2012)

2. واقع ادارة المخاطر في العراق :

يمكن التعرف على واقع ادارة المخاطر في العراق من خلال توضيح مبررات انجاز هذا البحث وهي اولاً – محاولة لجلب انتباه أصحاب العلاقة لخطورة واهمية الموضوع، حيث ان الملاحظ عدم إلاكتراث وقلة الخبرة لدى المقاولين وأصحاب العمل بموضوع المخاطر وتأثيراتها. ثانياً – ان وجود المخاطر وعدم التنبؤ بها او التنبؤ بها ولكن عدم إتخاذ الإحتياطات اللازمة لمواجهة تأثيراتها يعتبر أمراً مكلفاً جداً للاقتصاد الوطني وللمقاول وصاحب العمل مع استنزاف للموارد وهدر للوقت. ثالثاً – لتزويد المقاولين بهيكلية لإدارة المخاطر وتبيان ماهية تأثير تلك المخاطر في أهداف المشروع، ولتحقيق هذه الاهداف لابد من دراسة مفهوم المخاطر وادارتها في صناعة التشييد، ثم تحديد المخاطر الاكثر احتمالاً والأكثر تأثيراً في مشاريع التشييد في العراق لكي نصل الى تحديد مستوى اهمية هذه المخاطر المحددة ومن ثم تحديد الاستجابة الممكنة والملائمة لها ولمخاطر اخرى المحتملة.

3. تعاريف اساسية :

3.1 المخاطر (Risks) وعدم التاكد (Uncertainty)

تعرف المخاطر بأنها إمكانية حدوث شئ خطيرنتيجة عدم توقع مخرجات العملية التي تقوم بتنفيذها بسبب عدم التأكدية (Uncertainty) المحيطة بالعملية قيد التنفيذ. وترجع عدم التأكدية الى تعدد المتغيرات المدخلة للعملية الواحدة وتغيرها، وقد صنف الباحثون والعلماء عملية صناعة التشييد بأنها متعددة المتغيرات وذات طابع حاد التغير والتذبذب خلال مراحل تنفيذه. ومن هنا تظهر أهمية دراسة المخاطر من خلال ما يسمى بإدارة المخاطر (Risks Management) (د.عاطف واخرون،2008) ، كما تم تعريف المخاطر بانها احتمالية حدوث أية حادثة مستقبلية والتي يمكن أن تؤثر على الخطط الموضوعة للمشروع ومنها المالية والزمنية وبالتالي الانحراف عما مخطط له (علاء،2013). هناك وجهة نظر تشير الى ان المخاطرة هي حدث محتمل له تأثير سلبي فقط في اهداف مشروع معين. وقد نشأت هذه الفكرة من مفهوم عدم التأكد (Uncertainty) الذي ينتج عنه نتيجتين مختلفتين، اما الفرصة التي ينجم عنها الربح أو المخاطرة التي ينجم عنها الخسارة، كما هو موضح في الشكل رقم (1) (Malcolm,1997).

ويمكن تعريف المصطلحات الاتية: (منى واخرون،2012)

- المخاطرة : عامل أو حدث مجهول له احتمال حدوث، وفي حال حدوثه له تأثير سلبي في هدف واحد على الاقل من جدولة وكلفة وجودة وسلامة المشروع.
- عدم التأكد : حدث او عامل لايمكن تحديده بدقة ولكن له احتمال حدوث، ولا يمكن توقع نتيجته بدقة بسبب ندرة المعلومات حول ما سيحدث في المستقبل ومتى التأثير ومداه.
- الفرصة : حدث حدوثه غير مؤكد إلا انه داعم لإنجاز الأهداف في حال حدوثه.

فالمخاطرة والفرصة لهما العناصر نفسها من احتمال الحدوث ومستوى التأثير ولكن تختلف عن الفرصة بنوع التأثير اذا حدثت (منى واخرون،2012)، كما وتعرف المخاطرة (عدي،2008) بأنها كل مكروه لا يمكن توقعه بشكل دقيق لاعتماده على

ظروف مستقبلية غير معروفة مسبقاً، ويتم الاعتماد على الطرق الاحصائية والاستفادة من المشاريع السابقة المماثلة لتحديد المخاطر التي يمكن حدوثها واحتمالية حدوث كل منها وكيفية تفاديها او تقليل آثارها خدمة لأهداف المشروع.

ويقترب البحث من هذه التعريفات.

2.3. ادارة وتحليل المخاطر :

تعرف ادارة وتحليل المخاطر بأنها العملية التي تمكن من معرفة المخاطر وتحليل تلك المخاطر باستخدام الطريقة المناسبة ومن ثم وضع الحل المناسب الذي يزيل ذلك الخطر او يقلل من تأثيره وبذلك تزيد من نجاح والمشروع وتحقيق اهدافه (Taylor et al,1997). ان تحليل وادارة المخاطر في المشروع تعتبر عملية مستمرة ويمكن ان تبدأ في اي مرحلة من دورة المشروع ويمكن ان تدوم وتستمر الى ان تصبح تكاليف استخدامها اكثر من فائدتها المحتملة والتي يمكن كسبها، وكلما تقدم المشروع تقل المخاطر وبهذا فان فعالية استخدام تحليل وادارة المخاطر تميل الى التقلص لذلك فانه من المستحسن استخدامها في الاطوار المبكرة من دورة حياة المشروع(Malcolm,1997)، كما ويرى الباحث (عدي،2008) بأن دراسة مركبات الخطر والتحقق منها والالتباس الحاصل في اتخاذ القرارات هو لتوفير وإعطاء الاجابات لأي شخص في موقع اداري أو تنفيذي يعلم مدى صلاحياته وماعليه من واجبات تجاه اي مشكلة او حالة او عند ادارة الفعاليات للمشروع وهذا يحصل من خلال استيعاب افضل الفرص الممكنة للنجاح وتقليل فرص الفشل.

4. تقنيات ادارة المخاطر ومراحلها :

هناك العديد من التقنيات لكل مرحلة من مراحل ادارة المخاطر، اذ يحتاج اي اجراء في ادارة المخاطر الى ادوات لتطبيقه(منى واخرون،2012) ، وهذه المراحل هي:

- مرحلة تحديد المخاطر : تستخدم فيها تقنية العصف الدماغي (Brainstorming) وقائمة التحقق (Check List) بشكل كبير أكثر من اي تقنيات اخرى، ويعد الاستبيان ايضاً من التقنيات المستخدمة في هذا المجال.
- مرحلة تحليل المخاطر وتقييمها : تصنف التقنيات المستخدمة في هذه المرحلة الى نوعين : نوعية (Qualitative) وكمية (Quantitative) اذ تستخدم التقنيات النوعية اكثر من الكمية. ومنها ايضاً مصفوفة الاحتمال والتأثير (Probability _ Impact Matrix) وطريقة التدرج التحليلي AHP (Analytical Hierarchical Process) .
- مرحلة الاستجابة للمخاطر ذكر العديد من الباحثين انه يوجد اربع وسائل للاستجابة للمخاطر في مشاريع التشييد وهي : الاحتفاظ بالمخاطر (Risks Retention) وتخفيض (احتمال او تأثير) المخاطر (Risk Reduction) وتحويل المخاطر (Risk Transfer) وتجنب المخاطر (Risk avoidance).
- التحكم في رد المخاطر : الاستجابة للتغييرات في المخاطر على مدى فترة المشروع.

5. فوائد تطبيق تحليل وادارة المخاطر:

ان من اهم الفوائد التي يمكن تحقيقها من عملية تحليل وادارة المخاطر في مشاريع التشييد هي:(Taylor et al،1997)

- فهم جيد للمشروع ويقودنا هذا الفهم الى تكوين خطط واقعية ومنطقية في تقدير تكلفة المشروع وتحديد مدة المشروع، كما وان هذا الفهم يمكن جميع الاطراف المتعلقة بالمشروع من معرفة التعامل مع تلك المخاطر.
- الفهم الجيد للمخاطر يساعد على الاختيار الانسب لنوع العقد.

- معرفة المخاطر في المشروع تسمح بتقدير منطقي مدروس بعيداً عن العشوائية لاحتياطي الطوارئ الذي يعكس فعلاً المخاطر وكذلك يوجه بعدم تشجيع قبول مشاريع غير فعالة من الناحية المالية.
- المساهمة في بناء معلومات احصائية للمخاطر تساعد في التصميم الجيد للمشاريع.
- تسهيل الأخذ بالمخاطر الكبيرة بمعقولية اكثر مما يزيد الفائدة المكتسبة من الأخذ بالمخاطر.
- المساعدة في التمييز بين الحظ والادارة الجيدة وبين سوء الحظ والادارة السيئة.

6.جمع البيانات وتحليلها :

1.6. تحديد المخاطر:

تم تحديد اهم المخاطر التي حدثت فعلاً في المشاريع الانشائية قيد الدراسة والتي شملت (مشاريع الطرق والجسور، المباني، المستشفيات، المشاريع النفطية، شبكات الماء والمجاري، الابنية المدرسية) في عموم المحافظات في العراق اضافة الى المراجعة النظرية للبحوث والادبيات وعدد من المقابلات مع خبراء في مجال صناعة التشييد ونتائج الاستبيان، وبذلك تم تصنيف هذه المخاطر والبالغ عددها (42) والتي ادت الى تغييرات في الكلفة والوقت وجودة المشروع وكما يلي:

مخاطر تنظيمية، مخاطر مكانية، مخاطر فنية، مخاطر مالية، مخاطر قانونية ومخاطر سياسية وكما موضحة في جداول التحليل المرفقة، يتضح من الدراسة الاولية للبيانات الحقلية التي تم جمعها من هذه المشاريع مايلي:

1- ان المخاطر التنظيمية تركزت بشكل كبير في مشاريع الطرق والجسور بينما المخاطر الفنية والسياسية فكانت في مشاريع المعالجة وشبكات المياه اما المخاطرالمكانية والقانونية والمالية فقد تركزت في الابنية المدرسية والمستشفيات وغيرها.

2- ان اكثر عدد مرات حدوث للمخاطر في هذه المشاريع هي المخاطر الفنية تليها المخاطر المكانية ثم التنظيمية ثم السياسية واخيراً المخاطر القانونية ثم المالية، ويفهم من عدد المرات مستوى الاهمية لكل من هذه المخاطر.

3- ان العدد الكلي كحد اعلى للمخاطر مجتمعة كانت في مشاريع المعالجة وشبكات المياه أما المشاريع الاخرى فكان العدد اقل.

2.6. تأثير المخاطرفي أهداف المشروع وسلامته:

اعتمد في هذا البحث معياران في تحليل المخاطر:

- احتمال حدوث المخاطر
- درجة تأثير المخاطر في اهداف المشروع اذا حدثت تلك المخاطر

دمج هذان المعياران في المعادلة الاتية لتقدير اهمية المخطرأو درجة المخطر(Godfrey,1996):

$$R = P * I \quad (1)$$

حيث ان :

R = مؤشر المخاطر او درجة المخطر، وقيمه تتراوح بين (0 ، 1)

P = احتمال حدوث المخطر وقيمه تتراوح بين (0 ، 1)

I = تأثير المخطر وقيمه تتراوح بين (0 ، 1)

ولتقدير احتمال حدوث المخاطر وتأثيرها صممت استمارة استبيان تضمنت اربعة محاور:

المحور الاول: يهدف الى الحصول على معلومات عامة لافراد العينة المختارة من المستبينين كالاختصاص، التحصيل الدراسي، قطاع العمل، المركز الوظيفي وعدد سنوات الخبرة كما في الجدولين رقم (1) و (2).

المحور الثاني: يصف المقياس المستخدم لاحتمال الحدوث والتاثير للمخاطر وكما يلي:

الاحتمالية	قليل جداً	قليل	متوسط	عالي	عالي جداً
	0.1	0.3	0.5	0.7	0.9
التأثير	0.05	0.1	0.2	0.4	0.8

ووضع هذا المقياس بالاعتماد على مقياس وضعه (المعهد الأمريكي للمقاييس القومية، 2004).

المحور الثالث: صمم لتحديد احتمال حدوث المخاطر ونسبة تاثير المخاطر على اهداف المشروع.

المحور الرابع: صمم لتحديد نوع اجراء الاستجابة المتبع لمواجهة تلك المخاطر.

وزعت عدد من استمارات الاستبيان الى مدراء المشاريع الانشائية ومهندسين في المكاتب الاستشارية وفي شركات المقاولات القطاع العام والخاص واساتذة الجامعات ودعم الاستبيان بالمقابلات الشخصية استرد منها (44) استمارة اعتمدت لاغراض التحليل.

1.2.6. تحليل و معالجة البيانات:

استخدم البرنامج الحاسوبي (Excel) لمعالجة البيانات، لقد تبين ان مايقارب نصف حجم العينة من المستبينين لديهم خبرة اكثر من (15) سنة مما يزيد من وثوقية المعلومات التي وفرها المستبينون لتصوير الواقع من خلال خبرتهم في مجال صناعة التشييد، ولغرض الاستفادة من هذه النتائج وتوحيدها لتكون ذات معيار موحد تم اعطاء اوزان معادلة لنوع الشهادة وعدد سنوات الخبرة كما موضح في الجدول رقم (3)(عدي،2008) وهذه التقنية قلما استخدمت في مجال ادارة المخاطر، وبتطبيق المعادلتين التاليتين يمكن استخدام اجوبة المستبينين في احتساب معدل الاحتمالية والتأثير لكل نوع من انواع تلك المخاطر (حسين،2001):

$$\text{معدل احتمالية حدوث الخطر} = \frac{\text{مجموع (احتمالية حدوث الخطر * تكرارها)}}{\text{مجموع التكرارات}} \qquad (2)$$

$$\text{معدل تأثير حدوث الخطر} = \frac{\text{مجموع (تأثير حدوث الخطر * تكرارها)}}{\text{مجموع التكرارات}} \qquad (3)$$

حيث ان :

احتمالية وتأثير حدوث الخطر= القيم القياسية لكل منها

التكرار = عدد مرات تكرار اجابة معينة مضروبة بالاوزان المعادلة لكل اجابة

مجموع التكرارات = المجموع التراكمي للتكرارات لجميع العوامل مع الاوزان

وقد تم ترتيب قيم مؤشر المخاطر تنازلياً كما في الجدول رقم (4) حيث يتضح ان احتمالية حدوث كثير من المخاطر التنظيمية والفنية والمكانية تكون عالية وهذا مالوحظ ايضاً من دراسة البيانات الحقلية الفعلية كما ورد في الفقرة (1.6) اعلاه. هناك عدة مقاييس للاحتمال والتأثير عند استبدال المقياس الكيفي بأرقام عند التحليل الاحصائي وقد اعتمد المقياس الآتي: (منى واخرون،2012)

المقياس	منخفض جداً	منخفض	متوسط	عالي
المجال %	10 – 0	30 – 11	60 – 31	60 <

تم تحديد مستوى ألأهمية بالاعتماد على هذا المقياس للاحتمال والتأثير للمخاطر ووفق مبدأ حساب الفرق بين اكبر قيمة لمؤشر المخاطر واصغر قيمة له من الجدول رقم (4) والرمز له بالحرف (D) وهذا المبدأ يمكن الاعتماد عليه لتحديد حدود مؤشر المخاطر لغرض معالجتها وفقاً للموارد المخصصة لذلك وكما يلي:

$$D = 0.112555 - 0.002564 = 0.109991$$

وبذلك يمكن حساب الحد الادنى والحد الاعلى لمؤشر المخاطر (المجال) في كل مستوى ، كما في الجدول رقم (5) علماً بأنه تم تقريب الارقام الى اربعة مراتب للسهولة، فيكون الحد الاعلى لكل مجموعة هو الحد الأدنى لمجموعة المخاطر التي تليهافي الأهمية، فيقع مؤشر المخاطر المنخفضة الأهمية جداً بين (0.0026 و 0.0134) بينما يقع مؤشر المخاطر منخفضة الأهمية بين (0.135 و 0 0.465) وهكذا، وقد تم ترتيب المخاطر حسب مستوى اهميتها في الجدول رقم (4) حيث تقع الأعلى أهمية أولاً، كالمخطر (عدم توفر المخططات للشبكات الخدمية المارة خلال الموقع كالمخططات الكهربائية , الهاتف , الماء , وغيرها) يعد عالي الأهمية بمؤشر (0.1126)، وهذا يعكس أهمية معالجة هذه المخاطر. أما المخطر (تأخر اجراءات تحويل العمل الى الورثة) فان مؤشرها (0.0026) اي ان مستوى اهميته منخفض جداً في اهداف المشروع.

2.2.6 اختبارالفرضية:

1.2.2.6اختبار الاستقلالية (اختبار – كاي تربيع X^2) بين احتمال وتأثير المخاطر:

يتم فرض الاستقلال لأي علاقة بين متغيرين يراد التأكد من انهما مستقلان عن بعضهما، وتقوم طريقة مربع كاي (X^2) على ايجاد مقياس الأخطاء الناجمة عن تقريب القيم المشاهدة بفرض الاستقلال وهذا المقياس هو(محمد،1983):

$$X2 = \sum_{IJ}^{n} \frac{(Oij - Eij)2}{Eij} \quad (4)$$

حيث ان : Oij : عدد المشاهدات في السطر الذي ترتيبه (i) والعمود الذي ترتيبه (j)

Eij : عدد القيم المتوقع وجودها في السطر الذي ترتيبه (i) والعمود الذي ترتيبه (j) بفرض الاستقلال ويتم ايجاده كما يلي:

$$Eij = \frac{(ni+)(n+j)}{n} \quad (5)$$

حيث ان: n_{i+} : مجموع قيم المشاهدات في السطر الذي ترتيبه (i)

n_{+j} : مجموع قيم المشاهدات في العمود الذي ترتيبه (j)

يقبل فرض الاستقلال اذا كانت قيمة (X^2) المحسوبة من المعادلة (4) اعلاه اقل من قيمة (X^2) الجدولية. وقد كانت نسبة الخطأ المسموح به مساوية الى (5%) ودرجة الحرية تساوي (C−1) (R−1) حيث ان:

R = عدد الاسطر في جدول التوافق

C= عدد الاعمدة في جدول التوافق

لقد كانت قيمة (X^2) المحسوبة تساوي (1) اصغر من قيمتها الجدولية والمساوية الى (27. 1345) وهذا يثبت عدم وجود العلاقة بين المتغيرات فلاعلاقة بين احتمالية حدوث المخطر وتأثيره فقد تكون الاحتمالية عالية لكن التاثير منخفض.

وفي حالة الاستقلال بين المتغيرين يتم استخدام العلاقة الآتية لمعرفة درجة الاحتمالية ((Contingency Coefficient (G)) :

$$G = \sqrt{X2 / (X2 + 1)} \quad (6)$$

حيث ان : $G < 1$

فكلما اقتربت (G) من العدد (1) تعد ذات درجة عالية من الاحتمالية. وقد كانت قيمة (G) مساوية الى (0.71) وهذا يؤكد علاقة الاستقلال اي وجود عدم اعتماد بين المتغيرين الاحتمالية والتأثير.

2.2.2.6اختبار معامل الارتباط (R – Correlation Coefficient) بين احتمال وتأثير المخاطر:

لقد تمت كذلك دراسة مدى الارتباط بين النتائج عن طريق احتساب معامل الارتباط وكانت قيمته مساوية الى (R= 0.854) لمستوى دلالة (أهمية) مساوية الى (α=0.05) مما يدل على وجود ارتباط قوي بين النتائج.

3.2.6 مناقشة نتائج تاثير المخاطر على اهداف المشروع وسلامته:

يمكن دراسة النتائج في الجدول رقم (4) حيث يتضح مايلي:

1− ان المخاطر ذات المستوى العالي من الاهمية كانت من صنف المخاطر التنظيمية والفنية حيث ظهر ان كل من المخاطر الثلاث (عدم توفر المخططات للشبكات الخدمية المارة خلال الموقع كالمخططات الكهربائية , الهاتف , الماء , وغيرها) بدرجة تاثير= 0.3159 يليه المخطر (المناسبات الدينية والعطل المفاجئة) بدرجة تأثير = 0.2682 ثم المخطر (فروقات بين التنفيذ والمواصفات المطلوبة نتيجة لسوء فهم المخططات والمواصفات) بدرجة تأثير = 0.277، اضافة الى الاحتمالية العالية لحدوثها لذا كان مستوى اهميتها عالي في الجدول رقم (4) وهذا ما يعكس اولوية اتخاذ اجراءات الاستجابة لها عند ادارة المخاطر .

2− ان المخاطر متوسطة الاهمية كانت ايضاً من صنف المخاطر التنظيمية والفنية حيث نرى ان المخطر (ضعف التنسيق والاتصالات بين صاحب العمل والمقاول) بدرجة تاثير = 0.205 والمخطر (تلزيم العمل لمقاول غير كفوء) حيث لم تكن درجة تاثيره عالية = 0.1955 لكن احتمالية حدوثه عالية = 0.3125 وبالتالي كان مؤشره عالٍ فاصبحت له اهمية متوسطة

ثم يليه المخطر (تصنيع القطع الكونكريتية الجاهزة في اماكن بعيدة عن العمل) ذو درجة تأثير = 0.2045 ثم المخطر (عدم توفر المعلومات الضرورية (تأخر وصول المخاطبات الرسمية الى موقع العمل)) درجة تاثير= 0.2114 ، وبالتالي فان هذه المخاطر تاتي اولوية الاستجابة لها بالدرجة الثانية عند ادارة المخاطر.

3- اما بقية المخاطر فقد توزعت بين منخفضة الاهمية ومنخفضة الاهمية جدا .

ولكن من الجدير بالملاحظة ان المخطر الفني (عدم دقة المسوحات المتعلقة بموقع المشروع من قبل الطرف الاول) كان مستوى اهميته منخفضاً برغم تساوي درجة تاثيره مع المخطرالتنظيمي متوسط الاهمية (عدم توفر المعلومات الضرورية (تأخر وصول المخاطبات الرسمية الى موقع العمل)) وذلك لان احتمال حدوثه كان منخفضاً = 0.1057 ، نستخلص من ذلك انه لادارة المخاطر فان اجراءات الاستجابة تعتمد على مستوى اهمية المخطر والذي بدوره يعتمد على العوامل الثلاثة وهي احتمالية ودرجة حدوث المخطرو مؤشره.

ولتحديد الأهداف التي تتأثر بكل مخطر حسبت النسب المئوية للتكرار لكل هدف من أهداف المشروع في الاستبيانات المستردة، ويبين الجدول (6) هذه النسب المئوية، ويظهر ان تأثير المخاطر في السلامة المهنية منخفض جداً مقارنةً بالتأثير في المدة والكلفة والجودة. فهناك فقط ثلاثة من المخاطر (تصنيع القطع الكونكريتية الجاهزة في اماكن بعيدة عن العمل) و (عدم تخصيص مكان لرمي الانقاض) و (صعوبة الوصول الى الموقع (الموقع في منطقة نائية)) أثرت وبشكل واضح في السلامة المهنية بتكراراكثر من (30%). سنعتبر ان المخطر يؤثر في الهدف اذا كانت النسبة اكبر من (30%) اي من متوسط فأكثر حسب مقياس الاحتمال والتأثير المعتمد سابقاً وقد تم تظليلها في الجدول. يبين الجدول رقم (7) نسب تكرار كل هدف بالنسبة الى تكرار أهداف المشروع جميعها ضمن الاجابات المستردة. يلاحظ ان المدة تكررت بنسبة (47.69 %) كاعلى نسبة تكرار، اما السلامة المهنية فكان تكرارها (6.7%) اقل نسبة تكرار وهذا يعكس قلة الاهتمام بالسلامة المهنية في مشاريع التشييد وضعف ثقافة السلامة في ادارة المخاطر.

3.6 اجراءات الاستجابة للمخاطر:

لدراسة الاجراءات الممكنة والمطبقة في مشاريع التشييد في العراق للاستجابة للمخاطر مع التركيز فقط على المخاطر(عالية ومتوسطة الاهمية)، صمم استبيان مغلق بعدد من الخيارات للاجابة عليه اضافة الى خيار(غير ذلك) لتحديد اجراءات الاستجابة للمخاطر التي لم تذكر في استمارة الاستبيان، لقد عرضت في هذا الاستبيان الاجراءات الشائعة الاستخدام للاستجابة للمخاطر وهي :(منى واخرون،2012) ، (علاء،2013):

- اضافة شروط عقدية.
- تجنب حدوث المخاطر: وهو مجموعة التغييرات في خطة المشروع للتخلص من المخاطر او للمحافظة على اهداف المشروع من التاثيرات لهذه المخاطر.
- قبول المخاطر: وهو مفهوم معاكس لمفهوم تجنب المخاطر ويعني قبول الخسائر عند حدوثها ويقسم الى:

- القبول المخطط للمخاطر باتخاذ اجراء داخلي: كترتيب نظام إنذار ضد الحريق عند التعامل مع مادة سريعة الاحتراق.
- القبول غير مخطط: باهمال المخطر او الجهل بوجودها.

- تخفيض الخسائر بادخال تأثير المخطر بالحسابات عند تحديد سعر العرض.

● تحويل المخطر الى طرف آخر: اي ترحيل المخطر ونقل التاثيرات المالية له الى طرف اخر كالتعاقد مع مقاول ثانوي لتنفيذ بعض الاعمال التي تتسبب في حدوث مخطر ما.

1.3.6 جمع البيانات:

لقد تم توزيع (50) استمارة استبيان الى عددمن الخبراء اعتمدت منها (37) استمارة فقط لعدم دقة الاستمارات الاخرى ، وقد اختلفت عدد سنوات الخبرة للمستبينين وقد لوحظ ان اكثر من نصف العينة كانت خبرتهم اكثر من (15) سنة وهذا مؤشر الى موثوقية اجاباتهم.

2.3.6 تحليل البيانات ومناقشة اجراءات الاستجابة:

استخدم ايضاً برناج (Excel) لتحليل البيانات التي تم جمعها من استمارات استبيان اجراءات الاستجابة، ويوضح الجدول رقم (8) النسب المئوية لتكرار اجراءات الاستجابة في اجابات المستبينين لكل مخطر على حدة. فقد ظهرمثلاً ان (57.5%) من المستبينين يعالجون المخطر (عدم توفر المخططات للشبكات الخدمية المارة خلال الموقع كالمخططات الكهربائية , الهاتف , الماء , وغيرها) باضافة شروط تعاقدية كاجراء للاستجابة لذلك المخطر وهذا يوضح اهمية هذا المخطر حيث انه يجب ان وتوفر المخططات ضمن دراسة الجدوى في المرحلة الاولى للمشروع وهي مرحلة اتخاذ القرار. ظلل الاجراء ذو نسبة التكرار الأكبرمن (30% وفق مقياس الاحتمال السابق) باللون الرمادي الغامق في الجدول (8) كي يعتمد كاجراء اساسي لمعالجة المخطر المعني، اما الاجراء ذو النسبة الأقل من (30%) فقد ظلل باللون الرمادي الفاتح كي يعتمد كاجراء ثانٍ للاستجابة كما في المخطر(المناسبات الدينية والعطل المفاجئة).لوحظ ايضاً ان المخاطرعدا (عدم توفر المخططات للشبكات الخدمية المارة خلال الموقع كالمخططات الكهربائية , الهاتف , الماء , وغيرها) لها نسبة تكرار اقل من (50%) مما يدل على عدم اتفاق أغلب المستبينين في معالجة هذه المخاطر. ولمعرفة اجراءات الاستجابة الاكثر استخداماً للمخاطر حسبت النسب المئوية لتكرار كل اجراء في الاجابات المستردة كما مبين في الجدول رقم (9)، حيث ظهر ان الاجراء (شروط عقدية) هو اجراء الاستجابة الأكثر استخداماً بشكل عام (اي المجموع الكلي لجميع الاجابات) بنسبة تكرار مساوية الى (21.05%) يليها اجراء (قبول المخاطر) بنسبة تكرار (20.22%) واجراء (تجنب المخاطر) بنسبة تكرار (17.59%) ثم الاجراءات الاخرى.

3.3.6 شجرة القرار:

وهي طريقة بيانية تستخدم كثيرا لدراسة القرارات في حالة عدم التأكد مع وجود احتمالات، واسم الطريقة هو دلالة على شكلها، فهذه الطريقة تعتمد على رسم القرارات والحالات المتوقعة على شكل شجرة. وتتفرع الشجرة إلى أفرع بناء إما على اختيار نختاره أوبناء على أحداث مستقبلية لا ندري أيها يقع، فهناك نقاط للقرار يتفرع منها القرارات المختلفة ويرمز لها بالمستطيل وهناك نقاط للأحوال يتفرع منها الأحوال المستقبلية المختلفة ويرمز لها بالدائرة. لقد تم رسم الاستنتاجات التي تم التوصل اليها في الجدولين رقم (6) و(8) حول تأثير المخاطر على أهداف المشروع واجراءات الاستجابة للمخاطر ذات نسبة تأثير اكبر من (30%) في شجرة القرار الموضحة في الشكلين رقم (2) و(3) وذلك لتسهيل العمل على متخذي القرار بشأن اختيار الاجراء المناسب للاستجابة للمخاطروعلى اي هدف لتخصيص الميزانية المطلوبة وتدريب العاملين لمواجهة ذلك الخطر على ذلك الهدف.

7. الاستنتاجات والتوصيات:

لقد توصل البحث الى بعض النتائج في موضوع تقييم تأثير وادارة المخاطر في المشاريع الانشائية في العراق ومنها :

● ان اهم المخاطر في مشاريع التشييد هي عدم توفر المخططات للشبكات الخدمية المارة خلال الموقع كالمخططات الكهربائية , الهاتف , الماء , وغيرها) و(فروقات بين التنفيذ والمواصفات المطلوبة نتيجة لسوء فهم المخططات والمواصفات).

● توجد علاقة عدم استقلال اي علاقة ارتباط بين احتمال وتاثير المخاطر مما يدل على وجود علاقة بين المخاطر وان حدوث بعض المخاطر يكون سبباً في حدوث مخاطر اخرى مما يوضح اهمية متابعة ومراقبة المخاطرحيث ان تخفيف بعض المخاطر يؤدي الى تخفيف مخاطر اخرى في نفس الاجراء.

● ظهر ان اكبر تاثير للمخاطر هو على مدة تنفيذ المشروع ثم على كلفة المشروع واقلها كان على السلامة المهنية.

● اتضح ان الاستجابة للمخاطر بشكل عام ولجميع الاجابات بوضع شروط عقدية هو الاجراء المفضل للاستجابة للمخاطر يليه قبول المخاطر ثم اجراء تحويل المخاطر ثم تليها الاجراءات الاخرى.

ومن التوصيات التي يمكن اعتمادها في هذا البحث ما يلي :

● ضرورة تطوير الثقافة الادارية لمدراء المشاريع من خلال الاستفادة من التكنلوجيا الحديثة في جميع مرافق المشاريع الانشائية

● تأهيل وتطوير الكوادر الهندسية في مجال تحليل وادارة المخاطر من خلال الدورات التعليمية والتأهيلية للمهندسين لغرض تطبيقها والاستفادة منها في مشاريع التشييد.

● العمل على تطوير الصيغ التعاقدية بين صاحب العمل والمقاول فيما يتعلق بتحليل وادارة المخاطر بما يضمن حقوق جميع الاطراف مع عمل برامج لادارة هذه المخاطر.

المصـادر العربية:

- منى حمادة و د.محمد نايفة و د.عمر عاموري،" إدارة مخاطر التشييد لمشاريع التشييد في سورية"، مجلة جامعة دمشق للعلوم الهندسية، المجلد الثامن والعشرون، العدد الأول ،2012.
- د.عاطف عبد المنعم و محمد محمود الكاشف، " تقييم إدارة المخاطر"، جامعة القاهرة 2008.
- علاء محسن مهدي،" إدارة المخاطر المسببة للمطالبات في المشاريع الانشائية الحكومية"، رسالة ماجستير، كلية الهندسة، جامعة بغداد 2013.
- عدي لطيف قاسم،" التقنيات الحديثة في دراسة العمل في المشاريع"، رسالة ماجستير، كلية الهندسة، جامعة بغداد 2008.
- المعهد الأمريكي للمقاييس القومية، معهد ادارة المشروعات،" الدليل المعرفي لادارة المشروعات"، مكتبة الكونجرس، الاصدار الثالث 2004.
- حسين هشام مصطفى،" تقييم التقنيات: دراسة العمل في قطاع التشييد في العراق "، رسالة ماجستير، كلية الهندسة، جامعة بغداد 2001.
- محمد صبحي ابو صالح وعدنان محمد عوض،" مقدمة في الاحصاء"، جامعة اليرموك، إربد، الاردن، الناشر: جون وايلي وابناءه، نيويورك، 1983.

المصادر الاجنبية:

- Godfrey. P," Control of Risk: A Guide to the Systematic Management of Risk from Construction Published by CIRIA, London, UK,1996.

- Malcolm, N.E. and McKennon, J. ,"A Process Driven Approach to Integrated Environments", Proceedings INCOSE International Symposium 1997.
- Taylor,I and Bassler, J.," Application of ANSI Standard to Space Station Resources", Proceedings INOSE International, 1997.

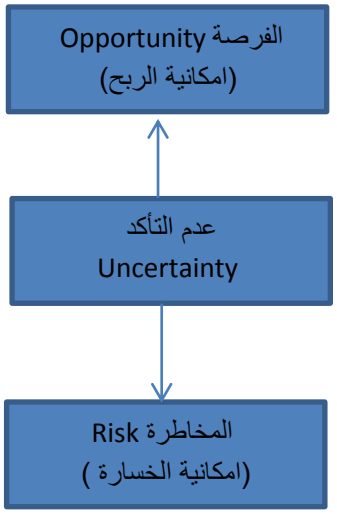

الشكل (1) نتائج عدم التأكد (منى واخرون،2012)

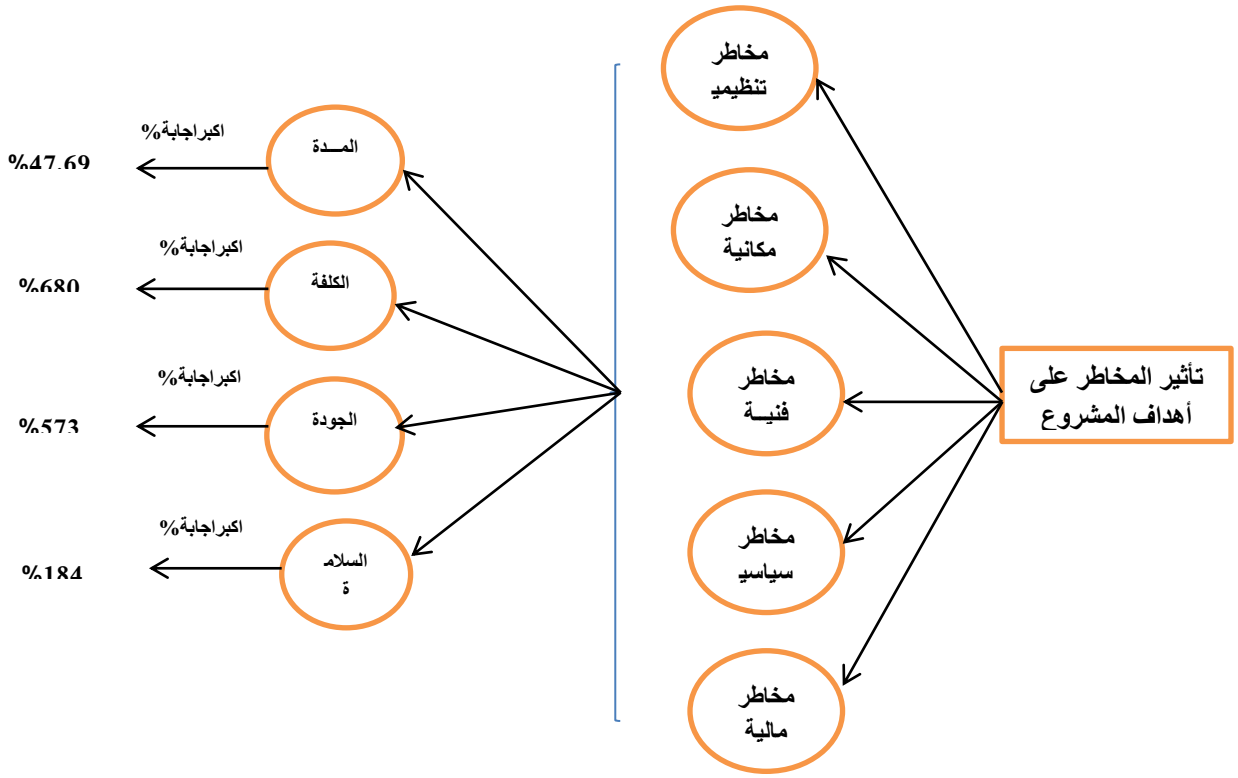

شكل رقم (2): شجرة القرار لتأثير المخاطر على أهداف المشروع الانشائي

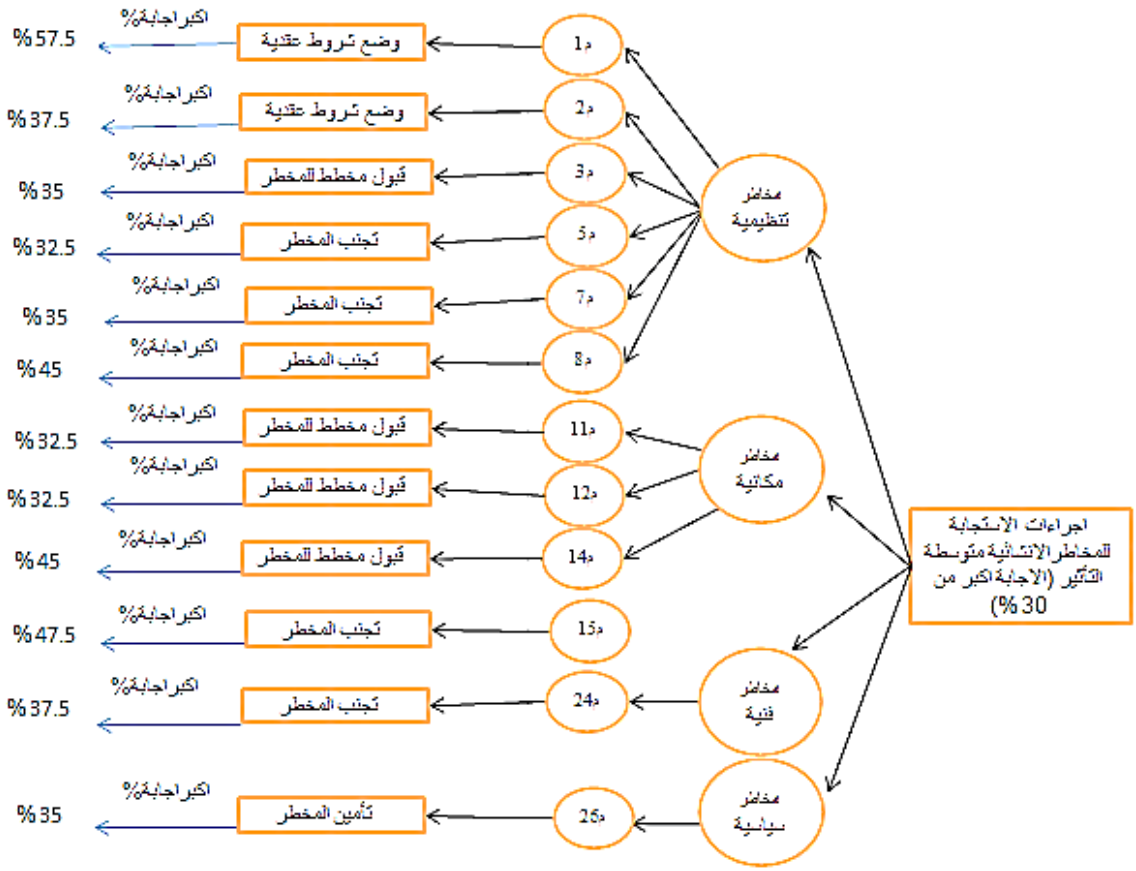

الشكل رقم(3): شجرة القرار لاجراءات الاستجابة للمخاطر

جدول رقم (1) : التحصيل الدراسي لافراد العينة

التحصيل الدراسي	التكرار	النسبة المئوية
بكالوريوس هندسة	22	50
ماجستير هندسة	15	34
دكتوراه هندسة	7	16
المجموع	44	%100

جدول رقم (2) : سنوات الخبرة لافراد العينة

سنوات الخبرة	التكرار	النسبة المئوية	
1 – 5	7	16	%52 اقل من 15 سنة
6 – 15	16	36	
اكثر من 15	21	48	%48 اكثر من 15 سنة
المجموع	44	%100	

جدول رقم (3) : الاوزان المعادلة لافراد العينة(حسين،2001)

المعلومات الشخصية العامة	وصف البيانات	الوزن المعادل
التحصيل الدراسي	بكالوريوس	1
	ماجستير	1.25
	دكتوراه	1.5
الخبرة	اقل من 15 سنة	1
	اكثر من 15 سنة	2

جدول رقم (4): ترتيب المخاطر تنازلياً حسب مؤشرها ومستوى أهميتها

التسلسل	المخاطر	الاحتمالية	التأثير	مؤشر المخاطر	مستوى الاهمية
-1	عدم توفر المخططات للشبكات الخدمية المارة خلال الموقع كالمخططات الكهربائية , الهاتف , الماء , وغيرها)	0.3563	0.3159	0.112555	عالية الأهمية
-2	المناسبات الدينية والعطل المفاجئة	0.3449	0.2682	0.092502	
-3	فروقات بين التنفيذ والمواصفات المطلوبة نتيجة لسوء فهم المخططات والمواصفات	0.3216	0.2773	0.08918	
-4	ضعف التنسيق والاتصالات بين صاحب العمل والمقاول.	0.321	0.2205	0.070781	متوسطة الأهمية
-5	تلزيم العمل لمقاول غير كفوء.	0.3125	0.1955	0.061094	
-6	تصنيع القطع الكونكريتية الجاهزة في اماكن بعيدة عن العمل 0.2960.2045	0.296	0.2045	0.060532	
-7	عدم توفر المعلومات الضرورية (تأخر وصول المخاطبات الرسمية الى موقع العمل).	0.2494	0.2114	0.052723	
-8	عدم وضوح الالتزامات التعاقدية.	0.2869	0.1568	0.044986	منخفضة الأهمية
-9	تأخر وصول بعض المواد والتجهيزات من بلد المنشأ	0.2057	0.1602	0.032953	
-10	تأخر المصادقة على المخططات التنفيذية من قبل الجهة الاستشارية	0.225	0.1239	0.027878	
-11	عدم دقة المسوحات المتعلقة بموقع المشروع من قبل الطرف الاول	0.1057	0.2114	0.022345	
-12	تأخر اكمال التصاميم او تغيير في التصميم	0.1784	0.125	0.0223	
-13	تأخر المباشرة بالعمل في المشروع	0.2068	0.1063	0.021983	
-14	تأخر في تسليم الموقع الى المقاول بسبب عدم تهيئة الموقع	0.1381	0.1114	0.015384	
-15	حدوث مشاكل داخلية بين اعضاء فريق المقاول	0.1653	0.0898	0.014844	
-16	عدم كفاية التخصيصات المالية لاكمال الاعمال	0.138	0.1057	0.014587	
-17	تاخيرانجاز الفقرات بسبب عدم توفرالسيولة المالية لدى المقاول (عدم التحكم بالتدفق النقدي)	0.1256	0.1114	0.013992	منخفضة الأهمية جداً
-18	وجود عوائق في الموقع كالمياه الجوفية, انابيب المياه, تاسيات كهربائية --- الخ	0.1438	0.0886	0.012741	
-19	تأخر استلام السلف التشغيلية وفق العقد لحين اكمال الاجراءات القانونية	0.1398	0.0841	0.011757	
-20	عدم تطابق المخططات (انشائي , معماري) او وثائق العقد	0.1034	0.1125	0.011633	
-21	تدهور الاوضاع الامنية في المشروع بالاضافة الى تكرار تفجير المعدات	0.1193	0.0858	0.010236	
-22	نزاعات خلال مرحلة التشييد بين اطراف العمل	0.1034	0.0875	0.009048	

	0.00891	0.075	0.1188	التضخم وتقلبات الاسعارخلال فترة تنفيذ المشروع	-23
	0.008629	0.0591	0.146	عدم تخصيص مكان لرمي الانقاض	-24
	0.008341	0.0716	0.1165	سوء الظروف الجوية	-25
	0.007092	0.0671	0.1057	ارض المشروع مستملكة من قبل الدولة ولكن لم يتم تسديد استحقاقات المالكين	-26
	0.007061	0.0807	0.0875	جدولة غير دقيقة للمشروع	-27
	0.006715	0.0969	0.0693	وفاة المقاول	-28
	0.00659	0.0648	0.1017	ارتفاع كبير في اسعار حديد التسليح	-29
	0.006577	0.0804	0.0818	تأخر وصول المواد بسبب الاجراءات الامنية	-30
	0.006487	0.0466	0.1392	اختلاف طبيعة الارض	-31
	0.006182	0.0693	0.0892	تبديل موقع العمل	-32
	0.006022	0.0896	0.0693	عدم استطاعة المقاول استلام الموقع بسبب احداث امنية	-33
	0.005899	0.058	0.1017	عدم امكانية الاستفادة من المشروع بسبب وجود نواقص كالمصاعد	-34
	0.005219	0.0835	0.0625	ظروف الحرب (استقرار وحدة عسكرية في المشروع لمدة طويلة)	-35
	0.004886	0.0432	0.1131	مطالبة المقاول بفرق سعر لارتفاع اسعار المواد بسبب التاخير	-36
	0.004819	0.0364	0.1324	ضيق المساحة داخل الموقع وصعوبة حركة المعدات وعدم توفر مكان لتجهيز المواد، اضافة الى الزخم المروري في المنطقة	-37
	0.004818	0.0597	0.0807	حدوث اضرار في بعض اجزاء المشروع بسبب الاحداث الامنية	-38
	0.00427	0.0648	0.0659	تعرض المشروع الى اطلاقات نارية نتيجة احداث امنية	-39
	0.004229	0.0517	0.0818	تأخر تنفيذ بعض الفقرات بسبب عدم استملاك المناطق المحرمة للمشروع	-40
	0.003298	0.0324	0.1018	صعوبة الوصول الى الموقع (الموقع في منطقة نائية)	-41
	0.002564	0.0389	0.0659	تأخر اجراءات تحويل العمل الى الورثة	-42

جدول رقم (5) : حدود مؤشرالمخاطر لكل مستوى أهمية

أهمية المخاطر(مستوى الاهمية)	الحد الادنى	الحد الاعلى
منخفضة الأهمية جداً	0.0026	0.0134 = D 10% + 0.0026
منخفضة الأهمية	0.0135	0.0465 = D 30% + 0.0135
متوسطة الأهمية	0.0466	0.0796 = D 30% + 0.0466
عالية الأهمية	0.0797	0.1127 = D 30% + 0.0797

تصنيف المخاطر	ت	المخاطر	كلفة	مدة	جودة	سلامة

جدول رقم (6): النسب المئوية لتكرارتأثير كل مخطر في أهداف المشروع

تنظيمية	1-	عدم توفر المخططات للشبكات الخدمية المارة خلال الموقع كالمخططات الكهربائية , الهاتف , الماء , وغيرها)	30	87.5	7.5	0
	2-	المناسبات الدينية والعطل المفاجئة	37.5	87.5	5	0
	3-	ضعف التنسيق والاتصالات بين صاحب العمل والمقاول	17.5	92.5	7.5	0
	4-	تصنيع القطع الكونكريتية الجاهزة في اماكن بعيدة عن العمل	40	60	52.5	32.5
	5-	عدم توفر المعلومات الضرورية (تأخر وصول المخاطبات الرسمية الى موقع العمل)	25	52.5	47.5	2.5
	6-	عدم وضوح الالتزامات التعاقدية	67.5	37.5	35	17.5
	7-	تأخر المصادقة على المخططات التنفيذية من قبل الجهة الاستشارية	7.5	62.5	52.5	0
	8-	تأخر المباشرة بالعمل في المشروع	5	65	40	17.5
	9-	حدوث مشاكل داخلية بين اعضاء فريق المقاول	10	85	12.5	2.5
مكانية	10-	تأخر في تسليم الموقع الى المقاول بسبب عدم تهيئة الموقع	15	90	2.5	0
	11-	وجود عوائق في الموقع كالمياه الجوفية, انابيب المياه, تاسيات كهربائية --- الخ	52.5	67.5	20	17.5
	12-	عدم تخصيص مكان لرمي الانقاض	20	27.5	37.5	50
	13-	سوء الظروف الجوية	35	52.5	12.5	20
	14-	اختلاف طبيعة الارض	17.5	77.5	35	20
	15-	تبديل موقع العمل	42.5	77.5	10	0
	16-	ضيق المساحة داخل الموقع وصعوبة حركة المعدات وعدم توفر مكان لتجهيز المواد، اضافة الى الزخم المروري في المنطقة	35	32.5	42.5	5
	17-	صعوبة الوصول الى الموقع (الموقع في منطقة نائية)	47.5	20	30	50
فنية	18-	فروقات بين التنفيذ والمواصفات المطلوبة نتيجة لسوء فهم المخططات والمواصفات	15	87.5	5	0
	19-	تلزيم العمل لمقاول غير كفوء	32.5	12.5	77.5	0
	20-	تأخر وصول بعض المواد والتجهيزات من بلد المنشأ	27.5	82.5	7.5	0
	21-	عدم دقة المسوحات المتعلقة بموقع المشروع من قبل الطرف الاول	20	47.5	72.5	0
	22-	تأخر اكمال التصاميم او تغيير في التصميم	20	45	52.5	5
	23-	عدم تطابق المخططات (انشائي , معماري) او وثائق العقد	27.5	52.5	47.5	5
	24-	نزاعات خلال مرحلة التشييد بين اطراف العمل	5	65	27.5	10

	-25	جدولة غير دقيقة للمشروع	20	82.5	17.5	0
سياسية	-26	تدهور الاوضاع الامنية في المشروع بالاضافة الى تكرار تفجير المعدات	20	75	12.5	12.5
	-27	تأخر وصول المواد بسبب الاجراءات الامنية	17.5	85	5	2.5
	-28	بسبب احداث امنية لم يستطع المقاول استلام الموقع	57.5	47.5	20	20
	-29	ظروف الحرب (استقرار وحدة عسكرية في المشروع لمدة طويلة)	42.5	32.5	25	10
	-30	حدوث اضرار في بعض اجزاء المشروع بسبب الاحداث الامنية	22.5	85	10	30
	-31	تعرض المشروع الى اطلاقات نارية نتيجة احداث امنية	22.5	85	15	7.5
مالية	-32	عدم كفاية التخصيصات المالية لاكمال الاعمال	17.5	80	17.5	0
	-33	تاخيرانجاز الفقرات بسبب عدم توفرالسيولة المالية لدى المقاول (عدم التحكم بالتدفق النقدي)	5	55	47.5	10
	-34	التضخم وتقلبات الاسعارخلال فترة تنفيذ المشروع	37.5	70	12.5	0
	-35	ارتفاع كبير في اسعار حديد التسليح	67.5	42.5	22.5	0
	-36	عدم امكانية الاستفادة من المشروع بسبب وجود نواقص كالمصاعد	90	17.5	5	0
	-37	مطالبة المقاول بفرق سعر لارتفاع اسعار المواد بسبب التاخير	85	17.5	5	0
قانونية	-38	تأخر استلام السلف التشغيلية وفق العقد لحين اكمال الاجراءات القانونية	42.5	57.5	5	0
	-39	ارض المشروع مستملكة من قبل الدولة ولكن لم يتم تسديد استحقاقات المالكين	25	75	2.5	0
	-40	وفاة المقاول	15	80	2.5	0
	-41	تأخر تنفيذ بعض الفقرات بسبب عدم استملاك المناطق المحرمة للمشروع	12.5	85	7.5	0
	-42	تأخر اجراءات تحويل العمل الى الورثة	10	87.5	12.5	0

جدول رقم (7): تكرار أهداف المشروع بشكل عام

أهداف المشروع	التكرار	النسب المئوية
الكلفة	680	24.75
المدة	1310	47.69
الجودة	573	20.86
السلامة المهنية	184	6.70
المجموع	**2747**	**%100**

جدول رقم (8): نسبة تكرار اجراءات الاستجابة للمخاطر في الاجابات المستردة

تصنيف المخاطر	تسلسل المخاطر	المخاطر	شروط عقدية	تجنب	قبول مخطط	إهمال أو جهل	بسعر العرض	التأمين	تحويل لطرف آخر	غير ذلك
تنظيمية	م1	عدم توفر المخططات للشبكات الخدمية المارة خلال الموقع كالمخططات الكهربائية , الهاتف , الماء , وغيرها)	57.5	12.5	12.5	5	0	2.5	2.5	7.5
	م2	المناسبات الدينية والعطل المفاجئة	37.5	35	17.5	2.5	0	2.5	2.5	2.5
	م3	ضعف التنسيق والاتصالات بين صاحب العمل والمقاول	5	5	35	10	2.5	5	2.5	15
	م4	تصنيع القطع الكونكريتية الجاهزة في اماكن بعيدة عن العمل	10	20	25	0	5	12.5	15	7.5
	م5	عدم توفر المعلومات الضرورية (تأخر وصول المخاطبات الرسمية الى موقع العمل)	22.5	32.5	20	5	2.5	7.5	5	5
	م6	عدم وضوح الالتزامات التعاقدية	15	30	17.5	5	10	5	2.5	12.5
	م7	تأخر المصادقة على المخططات التنفيذية من قبل الجهة الاستشارية	25	35	7.5	10	0	7.5	7.5	7.5
	م8	تأخر المباشرة بالعمل في المشروع	5	45	17.5	5	2.5	5	5	7.5
	م9	حدوث مشاكل داخلية بين اعضاء فريق المقاول	12.5	30	20	7.5	0	7.5	5	10
مكانية	م10	تأخر في تسليم الموقع الى المقاول بسبب عدم تهيئة الموقع	30	15	25	7.5	0	10	5	7.5
	م11	وجود عوائق في الموقع كالمياه الجوفية, انابيب المياه, تاسيات كهربائية --- الخ	12.5	5	32.5	2.5	5	15	5	20
	م12	عدم تخصيص مكان لرمي الانقاض	12.5	15	32.5	7.5	2.5	10	10	12.5
	م13	سوء الظروف الجوية	12.5	7.5	27.5	5	0	17.5	0	25

	م14	اختلاف طبيعة الارض	5	2.5	45	10	5	10	15	7.5
	م15	تبديل موقع العمل	10	47.5	10	5	0	0	2.5	12.5
	م16	ضيق المساحة داخل الموقع وصعوبة حركة المعدات وعدم توفر مكان لتجهيز المواد، اضافة الى الزخم المروري في المنطقة	22.5	15	22.5	2.5	2.5	0	10	12.5
	م17	صعوبة الوصول الى الموقع (الموقع في منطقة نائية)	25	15	10	5	2.5	5	7.5	15
فنية	م18	فروقات بين التنفيذ والمواصفات المطلوبة نتيجة لسوء فهم المخططات والمواصفات	17.5	7.5	30	5	2.5	20	2.5	7.5
	م19	تلزيم العمل لمقاول غير كفوء	15	15	25	2.5	2.5	15	17.5	2.5
	م20	تأخر وصول بعض المواد والتجهيزات من بلد المنشأ	22.5	25	7.5	0	2.5	10	25	2.5
	م21	عدم دقة المسوحات المتعلقة بموقع المشروع من قبل الطرف الاول	7.5	25	20	0	2.5	10	17.5	7.5
	م22	تأخر اكمال التصاميم او تغيير في التصميم	32.5	27.5	5	0	0	5	12.5	2.5
	م23	عدم تطابق المخططات (انشائي , معماري) او وثائق العقد	15	12.5	10	0	0	20	20	15
	م24	نزاعات خلال مرحلة التشييد بين اطراف العمل	7.5	37.5	15	7.5	0	7.5	2.5	15
	م25	جدولة غير دقيقة للمشروع	17.5	25	25	5	0	2.5	12.5	0
سياسية	م26	تدهور الاوضاع الامنية في المشروع بالاضافة الى تكرار تفجير المعدات	7.5	2.5	12.5	5	0	35	15	17.5
	م27	تأخر وصول المواد بسبب الاجراءات الامنية	5	2.5	17.5	5	0	25	20	20
	م28	بسبب احداث امنية لم يستطع المقاول استلام الموقع	2.5	15	20	2.5	0	27.5	15	15
	م29	ظروف الحرب (استقرار وحدة عسكرية في المشروع لمدة طويلة)	2.5	7.5	20	7.5	5	27.5	15	12.5
	م30	حدوث اضرار في بعض اجزاء المشروع بسبب الاحداث الامنية	10	7.5	22.5	2.5	0	25	15	10
	م31	تعرض المشروع الى اطلاقات نارية نتيجة احداث امنية	12.5	10	20	5	5	15	20	10
مالية	م32	عدم كفاية التخصيصات المالية لاكمال الاعمال	37.5	12.5	15	5	5	10	2.5	7.5
	م33	تاخيرانجاز الفقرات بسبب عدم توفرالسيولة المالية لدى المقاول (عدم التحكم بالتدفق النقدي)	35	17.5	2.5	10	2.5	5	5	15

	م34	التضخم وتقلبات الاسعارخلال فترة تنفيذ المشروع	22.5	15	12.5	7.5	7.5	12.5	10	10
	م35	ارتفاع كبير في اسعار حديد التسليح	32.5	2.5	12.5	5	10	20	0	12.5
	م36	عدم امكانية الاستفادة من المشروع بسبب وجود نواقص كالمصاعد	12.5	0	27.5	7.5	5	22.5	0	10
	م37	مطالبة المقاول بفرق سعر لارتفاع اسعار المواد بسبب التاخير	42.5	5	20	2.5	5	7.5	7.5	7.5
	م38	تأخر استلام السلف التشغيلية وفق العقد لحين اكمال الاجراءات القانونية	25	10	10	2.5	2.5	10	10	20
	م39	ارض المشروع مستملكة من قبل الدولة ولكن لم يتم تسديد استحقاقات المالكين	47.5	17.5	2.5	2.5	0	10	7.5	10
	م40	وفاة المقاول	37.5	10	22.5	0	0	10	2.5	22.5
	م41	تأخر تنفيذ بعض الفقرات بسبب عدم استملاك المناطق المحرمة للمشروع	20	5	20	0	0	15	17.5	20
	م42	تأخر اجراءات تحويل العمل الى الورثة	15	5	17.5	2.5	0	12.5	22.5	30
عدد المخاطر التي تعالج بالاجراء المعين بنسبة اكبر من 30%			2	6	4	0	0	1	0	0

جدول رقم (9): تكرار اجراءات الاستجابة في الاجابات المستردة

اجراء الاستجابة	التكرار	النسب المئوية
شروط عقدية	329	21.05
تجنب المخاطر	275	17.59
قبول مخطط	316	20.22
إهمال او جهل	74	4.73
بسعر العرض	40	2.56
التأمين	201	12.86
التحويل لطرف آخر	132	8.45
غير ذلك	196	12.54
المجموع	**1563**	**%100**

أهمية الإستخدام الحديث لمادة الخرسانة في العراق
دراسة تحليلية لتطور إنتاج وإستخدام مادة الخرسانة في العمارة

محمد رضا شاكر مجيد
مدرس
كلية الهندسة – جامعة بغداد
إيميل:mridhachalabi@gmail.com

الخلاصة

ليست مادة الخرسانه بإمكاناتها ومواصفاتها المميزة كأي مادة أخرى حيث ساعدت منذ إكتشافها لأول مرة على إحداث طفرة في عالم التصميم وتنويع إنتاج الأعمال المعمارية العظيمة بعيداً عن الشكل الهندسي المعتاد وذلك مما ساعد على الخروج عن المألوف وتحقيق مالم يكن ممكناً.

و تعتبر مادة الخرسانة الى وقتنا الحاضر الحل الأفضل والأسهل والأوفر لأغلب مشاكل الإنشاء بما فيها المشكلة الاقتصادية.

لذا بدأ أغلب المعماريين المبدعين في الحداثة (بالذات) مسيرتهم المهنية وذاع صيتهم من خلال تصاميم تميزت بإستخدام مادة الخرسانة كمادة إنشائية أساسية في فتره مابين الحربين[1] حيث كانت الحل الإقتصادي لأزمة الإسكان في العراق، ومن ثم تطورت مع الحداثه لتنتقل من الجانب الوظيفي البحت الى الجوانب التعبيرية والنحتية أيضاً.

وتبرز هنا أهمية الخرسانة كمادة إنشائية وإستغلال مواصفاتها وتحسينها كمادة أساسية في العمل المعماري حيث لايزال هنالك قُصور واضح في إستخدام مادة الخرسانة في العمل المعماري في العراق ولاتزال تستخدم هذه المادة بصيغتها الإنشائية أكثر من كونها مادة يمكن إستثمار خصائصها وتطويرها للعمل المعماري.

لقد عمل الكثير من المعماريين المحليين والعالميين لإستغلال خصائص هذه المادة خلال أربعينيات وخمسينات القرن الماضي لإنتاج أعمال ومباني معمارية متميزة وظهرت من خلالها حركات وتوجهات معمارية مرموقة أثرت بشكل كبير على العمارة.

من هنا تبرز مشكلة البحث حيث لانرى تطوراً واضحاً في إستخدام هذه المادة في العراق وإنما هنالك مايوصف بالتردي في الشكل وحتى في مواصفات المادة المنتجة من الناحية الإنشائية والتنفيذ.

ويهدف البحث الى التعريف بإمكانات مادة الخرسانة التقليدية ومواصفاتها وكيف أستخدمت هذه الخصائص بشكل إيجابي من قبل رواد العمارة، وبيان العلاقة بين الشكل المعماري والشكل المنشاي للأبنية والدور الذي تلعبه هذه المادة في هذا المجال، لتشكل

[1] الحرب العالمية الأولى والحرب العالمية الثانية

إطاراً نظرياً للبحث ومن ثم إستخلاص أهم التجارب التي توصل إليها المعماريون في إنتاج وإستخدام هذه المادة للخروج بإستنتاجات وتوصيات تعين المعمار للدخول وفهم هذه المادة وإستخدامها وتطويرها لإنجاز مباني ذات طابع معماري متميز.

الكلمات الرئيسة: الخرسانة، قحطان المدفعي، مواصفات، الوحشيه، ميتابولزم، العضويه، دوكتل، لافارج، الإجيليا، الخرسانة الشفافه.

Importance of New Use of Concrete in Iraq
Analysis of Development And Use of Concrete in Architecture

Mohammed Ridha Shakir Majeed
Lecturer
Engineering College – Baghdad University
E-mail:mridhachalabi@gmail.com

ABSTRACT

Since its invention by the Ancient Romans and later developed during the mid-18th century, the concrete structure and finish, has been considered as the most powerful, practical, economic and constructional material that meets the building's architectural and aesthetical requirements. By creating unique architectural forms, the pioneer architects used concrete widely to shape up their innovative designs and buildings.

The pre-mixed ultra-high performance concrete which manufactured by Lafarge.

The transparent concrete and cement that allow the light beams to pass through them, introduces remarkable well-lit architectural spaces within the same structural criteria. This product is a recyclable, sustainable, friendly environmental and cost efficient back up .

Due to its characteristics, strength, flexibility, affordability and long term performance, the concert integrated and contributed in modern architecture, urbanism and civil developments. Apparently, most of the 20th Century architects employed high-tech concrete method to deliver Iconic and bespoke architectural monuments world-wide. The interaction between the architectural form and the concrete as a buildable, executable, structural and constructional material has been always the main concern for architects over generations .

The formalism in architecture was first identified by the Art-Nouveau movement during the early 20 century in Europe as well as in Northern America. It formed, utilized and sculptured the concert to meet the use, function, aesthetical and spatial needs of spaces. This wave generated series of most significant, outstanding and impressive buildings in the architectural symbolized record .

This was followed by the Brutalism architecture presented by Alison and Peter Smithson in England and also by Le Corbusier works in Marseille and India. However, Alvar Alto and Louis Khan have participated and established a tremendous use of concrete to erect public interest developments on the same era

The concert as a structural element dominated the Metabolism architecture that represented by the Japanese architects like Kiyonori Kikutake, Kisho Kurokawa, Noboru Kawazoe, Masato Otakaand and Fumihiko Maki. They visualized the city of the future to be viable, evaluable, expandable, flexible structures that evoked the processes of organic growth as it is in nature. Their developments are often called technocratic and described as avant-garde with a rhetorical character. The Metabolist mega structures heavily relied on advanced technology and adaptable plug-in building techniques in using this material .

The research concluded the influences of the concrete as a building material upon the modern and building forms from the outsets. By exploring the history of the material, expanding its characteristics and specifications and later demonstrating the modern architecture movements and architects, this research has achieved its targets to acknowledge the importance of concrete in the current construction market and architectural developments.

Key Word: Concrete, Kahtan Al Madfai, Specification, Brutalism, Metabolism, Organism, Ductal, Lafarge, Agilia, Translucent concrete.

1- المقدمة

إن مادة الخَرَسَانَة المشهورة إنشائياًوالمتكونة من الإسمنت والرمل والماء مع إضافة الركام، التي تعد من أهم مواد البناء في العصر الحديث خصوصاً مع تدعيمها بالحديد لتصبح خرسانة مسلحة كانت قد أستخدمت من قبل الرومان حيث إستخدموا الخرسانة العادية Plain Concrete قبل حوالي ألفي عام وقد أستعملت في معظم مبانيهم لسهولة تشكيلها وإمكان تنفيذها بعمالة مدربة تدريباً بسيطاً.

إن الصفات التقليدية للخرسانة هي التصلب عند إضافة الماء ولكنها لها خصائص أخرى هي:

- تأخذ شكل صلد ومتين مع الزمن تدريجيا وتبدأ بالتصلب الابتدائى Initial setting وتنتهى بالتصلب النهائى Final setting.
- شديدة المقاومة لقوى الإنضغط Compressive Forces ولكنها في نفس الوقت ضعيفة جداً في مقاومتها لقوى الشد Tensile Forces لذلك فالخرسانة العادية (غير المسلحة) لا تستخدم أبداً في الأماكن التي تحدث فيه إإجهادات الشد (مثل العتبات Beams). وللتغلب على هذه المشكلة، يوضع قضبان حديد التسليح وهو مقاوم ممتاز لقوى الشد وقوى الضغط في آن واحد، في حين أن قضبان حديد التسليح الطويلة يمكن أن تتحمل قوى الشد كلها فإن الخرسانة لا تتحمل قوى الضغط كلها إذا كانت قطاعاتها نحيفة Slender فيحدث نتيجة لهذا إنبعاج الخرسانة Buckling.

وكما هو معروف إن مركبا خليطاً من الخرسانة والحديد يعطى مادة مثالية لمقاومة الإجهادات المختلفة المؤثرة عليها، وهذا المركب هو ما يعرف باسم الخرسانة المسلحة Reinforced Concrete (مصدر 21).

ولقد أدرك الرومان إمكانية بناء الجسور من خرسانتهم الجديدة وأصبح بناء القباب أقل كلفة عندهم وأكثر سهولة، ومهد الطريق لفن عمارة جديد، ولبناء القناطر من هياكل خشبية وتُصب الخرسانة فوقها، لتتمكن من حمل وزن السقف ككل حين جفاف الخرسانة، وأحيانًا إذا لم تكن الألواح الخشبية ناعمة فستخلف خطوطًا في السقف، وبالتالي تعكس مكان وجودها وتعطي ملمساً وشكلاً معمارياً.

ولم تكن الخرسانة عاملاً مساعداً على حل المشكلة الجمالية فقط بل وأصبحت عاملاً مساعداً وبشكل فعّال من ناحية الوظيفة أيضاً، حيث منحت المصمم فرصة عدم التقيد بأحجام الفضاءات أو فتحات الشبابيك أو إرتفاعات الأبواب كما في إستخدام الطابوق أو الحجر كونهما يتألفان من وحدات بقياسات محددة وصغيرة.

هذا وقد خدمت الخرسانة المنشأ من ناحية سهولة إدخال الخدمات والحفاظ عليها بخلق أنفاق لها داخلها من دون التأثير على هيكل المنشأ وجماليته بالإضافة الى كونها مادة عازلة للحرارة مما سيحافظ على البيئة الداخلية المريحة للمنشأ وسلامته من التأثيرات الخارجية.

أما في العصر الحديث فبعد معماريي الفن الجديد (الآرت نوفو كما سبق) وإن من الأوائل الذين إستخدموا الخرسانة في الواجهات هو المعماري الشهير فرانك لويد رايت Frank Lloyd Wright وذلك في بيوت البراري وبيت الشلال (شكل-1)، حيث لم يكن من المتعارف سابقاً له (في الولايات المتحدة) إستخدام الخرسانة كمادة إنهاء، ولكن أبداع رائد الحداثة (رايت) في تصاميمه وجه الأنظار لإمكانيات الخرسانة التعبيرية.

وإستمرت مادة الخرسانة بإستقطاب إهتمام المعماريين الكبار ومقلديهم في بداية القرن العشرين ولغاية الآن، وبرزت أسماء مثل لو كوربوزيه Le Corbusier ، ووالتر غروبيوس Walter Gropius، ولويس كان Louis Kahn ،

وإيرو سارينين Eero Saarinen، وكيشو كاراكاوا Kisho Kurokawa، وبيير لويجي نيرفي Pier Luigi Nervi كأهم من إستخدموا المادة بصفاتها التعبيرية وقد أبدع الأخير في إستخدامه للخرسانة حيث لقب بشاعر الخرسانة، فضلاً عن كنزو تانغه Kenzo Tange، والمعمارية العراقية زها حديد Zaha Hadid وغيرهم، وتتواصل التصاميم لإكتشاف إمكانيات جديدة ومواصفات محسنة تساعد في سهوله التشكيل وجمالية التصميم.

ولقد شهدت فترة الخمسينات في العراق عودة عدد من الفنانين التشكيليين والمعماريين الى العراق يحملون معهم ذات الأفكار والمفاهيم الفلسفية إزاء العمارة التي أشاعتها الأنماط والمدارس التي إنتشرت في أمريكا وأوروبا من معطيات التكنلوجيا الغربيه وما ظهر في ميدان التداول الفعلي من مواد وأساليب تنفيذية...فكان من جراء ذلك أن قفزت سمات جديدة الى واقع المدينة العراقية وخاصة بغداد ومجتمعها ومنها إستخدام متجدد للمواد الإنشائية مع ما أفرزته مادتي الفولاذ والخرسانة من طواعية ومتانة لم تكن مألوفة في واقع التنفيذ فأعطت هذه الإستخدامات متسعاً من المرونة نحو التلاعب بالأشكال بإتجاه خالٍ نسبياً من تعقيدات المادة وكان في مقدمتها إمكانية الحصول على بحور مترامية...من خلال إستخدام النظم المنشاية الهيكلية.

إن الإنفتاح على التقنية الغربية وكذا الأمر بالنسبة لتقنيات المعسكر الإشتراكي بعد أن كانت العلاقات والخطوط العريضة لسياسات الدولة ترسمها الدوائر البريطانية..

لقد ساهم المعمار قحطان المدفعي برفد النتاج المعماري العراقي (مع غيره من رواد العمارة العراقية المعاصرة) بحيوية إضافية من خلال تحركه وتطلعاته وتقصيه لكل مايظهر على الساحة من شواخص الأعمال...وكما يشير د.خالد السلطاني إنه قد إستهوتنا وراقت لنا تلك التكوينات الديناميكية والتكوينات المتناغمة التي طالعناها في متنزه الأوبرا ومدينة الألعاب في بغداد والتي أقترنت بإسم المعمار قحطان المدفعي..وحيوية الشباب التي تتوافق مع كل مايوحي بالحركة والتغيير (شكل–2). (مصدر 22)

2– المواصفات التقليدية لمادة الخرسانة وميزاتها :

a. المواصفات الفيزيائيه والكيمياوية:

- بطيئة الإشتعال.
- درجة نفاذيتها للماء 0.1% مقاومة للأملاح والأحماض.
- مقاومة للاحتكاك والكسر.
- رديئة التوصيل للكهرباء.
- ضعيفة التوصيل الحراري.
- تتحمل إجهاد ضغط يصل إلى 50 نيوتن / مم2.
- مقاوم للأشعة فوق البنفسجية.

b. ميزات مادة الخرسانة:

- إحدى مواد البناء الأكثر طواعية المتوفرة للمهندسين والمعماريين.
- عملية لإعادة الإنتاج والترميم وذات جمالية عالية وصديقة للبيئة.
- تخفف الحمولات على الأبنية بعوامل أمان كبيرة للهياكل الضخمة والأساسات.
- يمكن تلوينها بالصباغات والدهانات.
- الإكساء بواسطتها يمكن أن يحل محل الخرسانة مسبقة الصنع عندما تكون هناك مشكلة في الوزن والشكل.
- سهلة التصنيع والقولبة لإنتاج الاشكال والتفاصيل الدقيقة كما تعطي الملمس المطلوب للسطوح النهائية بأفضل نوعية.
- شديدة الصلابة ومقاومة للاحتكاك.

- مقاومة للتآكل والظروف الجوية الخارجية من حرارة ورطوبة وخاصة الاجواء البحرية.
- عازلة للحرارة والصوت وتتسم بمقاومة عالية للحريق وتسرب الماء.
- غير قابلة لتكاثر الحشرات ونمو الفطريات والمكروبات.

3-1 طرق العمل بمادة الخرسانة :

- الصب بالموقع مباشرة (Cast in situ)
- الخرسانه المسبقه الصب (Pre-cast)
- الخرسانه المسبقه الاجهاد (Pre-stressed)
- القوالب المنزلقه (Slip form)

3- الإستخدامات التقليدية لمادة الخرسانة:

تستخدم الخرسانة في الكثير من الأعمال المعمارية والبنائية وأهمها:

- تكسيات واجهات المباني
- الأعمدة والجسور
- الشبابيك أو المشربيات الإسلامية
- تغطية الأسقف بديلاً للأسبستوس والقرميد
- الأسقف المعلقة
- جدران المباني
- وحدات معمارية وزخرفية مختلفة
- الشرفات
- القباب
- التماثيل
- أقنية للري والصرف
- النافورات
- أحواض زهور
- جدران عزل الضوضاء

4- أهم التوجهات المعمارية التي إستخدمت مادة الخرسانة:

a. التعبيرية العضوية Organic expressionism:

كانت بدايتها بحركه الآرت نوفو Art Nouveau[2]التي إبتدأت بتصميم الفضاء الداخلي وإتسعت لتشمل العمارة، وإمتدت في أنحاء أوربا لتمثل بداية تجسيد الفكر المبدع في العمارة والتعبير عن شخصيه المصمم خلال البناية.

ومن ثم نمت هذه الحركه لتصل الى مستوى النحت والتعبير الجمالي المتفرد في كل بناية الذي هو توجه النحتية، ولكي نعرف النحتية في العماره نستطيع القول إنها المباني التي أنشأت بالإعتماد على أسلوب النحت لإنشاء مباني تتوافر فيها شروط الإنتفاع

[2] أرت نوفو (الكلمة الفرنسية ل' الفَنّ الجديد 'Art Nouveau,) أسلوبُ دوليُ مِنْ الفَنِّ والهندسة المعماريةِ والتصميمِ الذي بَلغ الذروة في الشعبيةِ في بِداية القرنِ العشرونِ (1880-1914) ويتمَيَّزُ بتصميماته المتُجَدِّدِة جداً، المتَدَفُّقة، وتصميمات ذات خطوط منحنية وأشكال الأزهار والأشكال المستوحاة من النباتات.

والمتانة والجمال والإقتصاد وتفي بحاجات الإنسان المادية والنفسية و الروحية والإجتماعية في حدود الإمكانات المتوافرة وبأحسن الوسائل في ظل محددات المكان والبيئة المحيطة.

برج انيشتاين (شكل – 3) من أشهر أعمال المعماري الألماني إريك مندلسون Erich Mendelsohn، والذي هو عبارة عن مرصد فلكي أقيم ما بين سنتي 1917 – 1921 ، تكريماً للفيزيائي ألبرت أنيشتاين في بوتسدام في ألمانيا. (مصدر 15)

يوضح المبنى أفكار مندلسون في التصميم البلاستيكي بدون زوايا أي بخطوط منحنية، وكانت الخرسانة هي المادة المطواعة لتنفيذ هذا المبنى، ولكن بسبب الحرب تم تنفيذ بعض الأجزاء بواسطة الطابوق وطليت بطلاء نهائي للبرج.

و يعد هذا المبنى من المباني المتألقة المعبرة عن عمارة القرن العشرين.

تغطي البرج قبة صغيرة تسمح للراصد الفلكي بالنظر من خلالها بواسطة مرقابه إلى قبة السماء، وتسمح بإنتقال الضوء إلى مستوى تحت الأرض داخل المبنى، يمكن فيه رصد حركة الأفلاك، ويتميز المبنى من الخارج بخطوطه الانسيابية، والديناميكية الفائقة للشكل الخارجي للبرج وقاعدته التي تحتوي المدخل الذي يرتفع بضع درجات عن الأرض.

إن إستخدام الخطوط والمستويات المنحنية وعدم إستخدام الزوايا القائمة، والرمزية في التشكيل، والتكوينات المعمارية الحرة (غير المنتهية) النحتية المعبرة والمؤثرة في النفس، ومادة الخرسانة هي المادة الطيعة لتنفيذ فكر التعبيريين. .(مصدر 3)

وهنالك كما سنرى لاحقاً نماذج رائعة من العمارة النحتية، حيث تشكل الأنظمة المنشأية القشرية الخرسانية (الأنظمة المنشأية السطحية) الأنظمة الأكثر نقاءاً في تراكب الأشكال المعمارية مع الأشكال المنشأية.

b. العماره الوحشيه [3] Brutalism Architecture

ظهر هذا الاتجاه المعماري في النصف الثاني من خمسينات القرن الماضي حيث إنطلقت من إنكلترا من خلال أعمال الزوجين سميتسون أليسون وبيتر Alison & Peter Smithson.

وهناك من ينسب بداية العمارة الوحشية إلى المعمار لو كوربوزيه Le Corbusier من خلال طابع المبنى السكني الشهير في مرسيليا (شكل – 4) ومن خلال إستخدام الخرسانة العارية والتأكيد على مبدأ صرامة المادة، وتكرار العناصر الشاقولية، وتغيير مقياس الفتحات في واجهات المبنى ، كما إن كنيسة رونشام في فرنسا تعكس بعض صفات الوحشية هذه إلا أن البعض يقول أنها ذات إتجاه فريد وخاص.

ومن الأعمال الأخرى للمعمار لو كوربوزيه التي تعكس صفات الوحشية مبنى قصر العدل في مدينة شنديغار (شكل – 5) وهو مشيد من الخرسانة المسلحه ويوضح أسلوب المصمم في استخدام هذه المادة وتطويعها لتخدم أفكاره.(مصدر 3)

- **اهم ميزات هذا الاتجاه المعماري :**
  - صياغة التكوين الأساسي للمبنى من عدد من الحجوم المعمارية المترابطة والمتداخلة.
  - إظهار مادة البناء الاساسية بشكل صريح في المظهر الخارجي والفراغات الداخلية للمبنى وإظهار الهيكل الخرساني المسلح.
  - إستخدام الجدران الخرسانية والاجرية العارية وذلك للحصول على خشونة متعمدة في الطابع المعماري للمبنى للرغبة المقصودة في التوصل الى حجوم معمارية ضاغطة توحي بثقل المبنى.

[3] **العمارة الوحشية** Brutalist architecture هو نمط معماري ازدهر في فترة الخمسينيات حتى منتصف السبعينيات من القرن العشرين، وقد إنبثق من الحركة المعمارية الحداثية في البداية، وتمثّل هذا النمط بالمباني الحكومية والمساكن منخفضة الإيجار ومراكز التسوق لخلق هياكل وظيفية بتكلفة منخفضة، حتى أتى بعض المصممين في نهاية المطاف وغير الاستخدامات بطريق أخرى مثل مباني الكليات.

- كثيرا ما تشكل الجدران الخارجية والداخلية القاطعة زوايا مختلفة (منفرجة، حادة، قائمة) وذلك من أجل الإبتعاد عن الأشكال التقليدية.
- يلاحظ في الواجهات عدم الإنتظام والعشوائية المقصودة في توزيع الفتحات.
- في الكثير من شواهد العمارة الوحشية إتبعت حلول وأساليب معمارية قريبة من أصول العمارة التعبيرية.
- إستخدام التأثيرات الجمالية والحسية الناجمة عن تكرار المرازيب الخرسانية الضخمة ذات المقطع المربع أو الدائري كما لا تخلو عمارتهم من لمسات تميزها كالأعمدة المفردة او المزدوجة التي تتقدم سطوح الواجهات والتضاد ما بين المقياس الصغير الناعم والمقياس الكبير الضخم لعناصر واجهات المباني الرئيسية والثانوية.
- لم يلتزموا بان تعكس واجهات المبنى طبيعة الفراغات المعمارية الداخلية.

- **أهم معماريو هذا الإتجاه وأهم أعمالهم:**

- **سميتسون أليسون وبيتر Alison & Peter Smithson**

ومن أعمالهما مدرسة نورفلك في إنكلترا عام 1954 والمبنى السكني في واتفوورد 1956 , حدائق روبن هود في لندن (شكل – 6). (مصدر 23)

- **ألفار آلتو Alvar Aalto**

المعمار الفنلندي الذي تأثر نوعما بالوحشية لكنه بقي مؤكداً للأفكار التي صاغها لنفسه ويظهر هذا التأثر في إحدى الكنائس في فنلندا(شكل – 7).

- **لويس كان Louis Isadore Kahn**

الأمريكي الذي ركز على الكتل الشاقولية والسطوح الصماء وإستخدام الجدران الخرسانية العارية ومن أهم أعماله مبنى الأقسام الداخلية في ولاية بنسلفانيا (شكل – 8).

c. حركة الميتابولزم Metabolism:

نظر معماريو الميتابولزم الى المجتمع الإنساني على إنه عملية حيوية وتتطور بإستمرار وإن التعامل مع المجتمع الإنساني لابد أن يؤخذ كوحدة واحدة أو جزء من إستمرارية الوجود الطبيعي الذي يشمل جميع الحيوانات والنباتات وعليه تعتبر التكنولوجيا إمتداداً للإنسانية. (مصدر 2)

إن معماريوا الميتابولزم هم مجموعة من المعماريين اليابانيين من المشاركين في الإعداد والمشاركة في مؤتمر التصميم العالمي الذي إنعقد في طوكيو 1960، وظهرت هذه المجموعة عقب الحرب العالمية الثانية إذ كان الدمار سائدا و الناس في حالة تشرد تام دون مأوى، وقد حاول هؤلاء وضع الحلول لهذه الكارثة.

المعماريون هم :

- كيونوري كيكوتيKIYONORI KIKUTAKE
- كيشو كوروكاو KISHO KUROKAWA
- نوبور كاوازوي NOPORU KAWAZOE
- ماساتو اوتاما MASATO OTAK
- فومهيكو ماكي FUMIHIKO MAKI
- كيوشي اوازو KIYOSHI AWAZU

وإنضم إليهم كنزو تانغي KENZO TANGE بصورة غير رسمية تأييداً للأفكار.

وتضمن البيان الاول للمجموعة:

إختيار مصطلح Metabolism للتعبير عن المجموعة يعود الى الايمان بان التقنية والتصميم يجب أن يرمزا الى حيوية الكائنات الحية.

ولايعبر الميتابوليزم Metabolism فقط عن التلاؤم والتوافق مع التقدم الطبيعي والتاريخي بل يشجع التطور والنشاط الميتابوليزمي وذلك لسببين:

- يجب أن يمثل المجتمع الإنساني جزءاً من الإستمرارية الطبيعية للكون.
- التقنية هي إمتداد إنساني.

- **الأفكار الأساسية للميتابوليزم Metabolism:**
  - الهدف من استعمال هذا الرمز هو أن العمارة يجب أن تتمتع بالحيوية الإنشائية التي تتمتع بها الكائنات الحية.
  - النتاج المعماري الجديد يجب أن يتصف بإمكانية التطور والنمو وإستبدال بعض أجزاء المبنى المستهلكة.
  - أنظمة تخطيطية تسمح بالتطور والنمو.
  - تطويع التقنيات وإستخدامها الى أقصى الحدود في مجال العمارة.
  - إعتماد الأفكار الخاصة بالبنى العملاقة.
  - تمييز الفراغات المعمارية وتصنيفها وفقاً لتغير الإحتياجات الإنسانية ووفقاً للمدة التي تصلح فيها للإستخدام.
  - إعتماد الأفكار الخاصة بالمباني ذات الإستمرارية الزمنية القليلة والعمل على تطوير أنظمة معمارية وإنشائية تحقق ذلك. (مصدر 1)
- **أهم الأعمال للميتابولزم:**
  - مشاريع الحضارة البحرية Marine City للمعمار كيونوري كيكوتيك في عام 1960(شكل – 9)

حيث نرى إن المجموعة المحيطية العائمة عبارة عن مباني برجية أسطوانية ترتكز على جزر إصطناعية في المحيط ترتبط مع بعضها بجسور عائمة وكل برج يتسع ل5000 نسمة و1250 شقة سكنية وبارتفاع 300 م.

  - المدينة اللولبية HELIX CITY لكيشو كوروكاوا (شكل – 10)

البنية الحجمية تقوم على بنى حلزونية مروحية الشكل (كلاستر مروحي).

d. عمارة ما بعد الحداثة (Postmodern architecture)

بعد أن أصبحت ما ذكر سابقاً من تيارات وحركات معمارية تخلق الملل الرتيب صار الميل إلى إستحداث أشكال ضد مايعتبره الأسلوب العالمي (International). فظهر إتجاه بتمجيد الفوضى بدلاً من النظام وكذلك تحميل الشكل المعماري أساليب معمارية تعود الى عصور مختلفة ومتباينة بدلاً من الشكل الموحد.

وكان من أهم رواد هذه العمارة روبرت فنتوري (شكل – 11) ، كما وظهر إتجاه آخر وهو الحنين الى الماضي وتكييف الأطر التقليدية القديمة لتلائم الحاجات والمضامين الحالية.(مصدر رقم 3).

وقد لعب إستخدام مادة الخرسانة المسلحة دوراً متميزاً في بروز هذه المفاهيم

5- العلاقة بين الشكل المعماري والشكل المنشأي ودور مادة الخرسانة في إغنائها:

كما يظهر وإن النظام المنشأي هو العنصر الأكثر تأثيراً وقوة للشكل عندما لايكون آخر سلسلة القرارات المتخذة لتحديد شكل المبنى وإنه يعدل ويغير كافة القرارات الأخرى المتخذة بشأن المبنى.

إن الأبنية التي يتخذ فيها القرار المتعلق بالأفكار المبدأية للنظام المنشأي بفترة متأخرة خلال العملية التصميمية ينتج عنها نظام منشأي لايتكامل مع وظيفة المبنى ونواحيه الجمالية.

هنالك الكثير من الأمثلة للهياكل المنشأية تتكلم وتصرخ وتعبر بشدة عن ملامحها المعمارية وفي هذه الحالة فأن مصمميها المعماريين والإنشائيين قد إتخذوا قرارهم لكي تكون قراراتهم المنشأية بحيث لاتقلل من بل تعزز الأفكار المعمارية ومتطلباتها، حيث لايمكن أن يستمر الهيكل المنشأي صامتاً بل يتوجب أن يكون صوتاً مسموعاً، وعندما يعطى الهيكل المنشأي صوتاً فأنه يسهم بإعطاء العمارة معناها ويغنيها وأحياناً يكون العنصر المعماري الأكثر تميزاً في المبنى.

وهنالك الكثير من الفرص المنشأية لإغناء وتقوية خبراتنا المعمارية، فبإمكاننا السماح للهيكل المنشأي أن يتكلم ويُسمع وبإمكاننا تصميم الهيكل المنشأي بحيث لايكتفى بالنظر إليه وتحليله ولكن يغري المتلقي لقراءة خصائصه المعمارية المتفردة.

وهنا تدخل الخرسانة كمادة عاملاً مهماً في هذا المجال.

وتنقل الأنظمة المنشأية المنحنية والمتدلية كالأنظمة النسيجية الأحمال الى نقاط الأسناد من خلال إجهادات الشد، ويمكن أن يكون الحبل المتدلي الذي يغطي بحر معين بين نقطتي إسناد عاليتين أبسط مثال عن هذه الأنظمة، وتصمم هذه الأنواع من الأنظمة عادة للسقوف بحيث يتغلب وزنها على قوى الرياح الشافطة أو قوى الضغط الرافعة والتي قد تؤدي الى حركة عمودية مفرطة للسقف، وتستخدم الخرسانة المسلحة أحياناً لهذا النوع من الأنظمة لتلافي ماورد أعلاه، وتدعم الخرسانة بحديد التسليح وللسطوح الخارجية والداخلية ليوفر الحماية الكافية ضد قوى الشد، ويتم تثقيل الأنظمة التي تشيد من مواد أخف وزناً أو تربط بنظام ربط منفصل ومحكم بالأرض لتلافي قوة رفع الرياح.

ويبين الآتي من الأمثلة التنوع بالعلاقة مابين الشكليين المعماري والمنشأي وهي أعمال معمارية تم فيها بشكل أساس تراكب الأشكال المعمارية والمنشأية معاً.

ولعل سقف قاعة الجناح البرتغالي في لشبونة (شكل – 12) للمعمار ألفارو سيزا Álvaro Siza [4] عام 1998 خير مثال لهذه الأنظمة، حيث سقف ألفارو سيزا ساحة إحتفالات بعرض 58متر وطول 65متر في الجناح البرتغالي لمعرض 98 بسقف خرساني منحني متدلي وبسمك لايتجاوز 200ملم، وهذا إنجاز كبير وتحدي في آن واحد.

ويمكن وصف صبة السقف كحجاب أو برقع أو خيمة لنحافة سمكها وشكلها المتدلي بشكل واضح، وقد تم تشييد رواقيين معمدين تعمل عمل الكتل الضخمة النهائية التي تقاوم سحب السقف المتدلي، وقد تم تعزيز هذه الأروقة بتسعة جدران متوازية تعمل كأكتاف تقاوم السحب الكبير الداخلي للسقف المعلق.

إن بساطة تصميم تفاصيل التعليق من خلال الأروقة لاتعكس ضخامة وأهمية الحمل واللعبة الإنشائية للمبنى، ويتألف المبنى المصمم للجناح البرتغالي من شكلين، السقف المتدلي والأروقة المتعامدة.

وتشكل الدعائم الخرسانية المستخدمة في قاعة مطار دالاس للمعمار إيرو سارينين (شكل – 13) التقرب التقليدي لمعالجة مثل هذا النوع من الأنظمة المنشأية كونها مسلوبه ومائلة تعكس ضخامة الكتلة الخرسانية المسلحة الثقيلة للسقف. ويتجه التصميم البارع للمبنى بشكل مبدأي لتشتيت قسوة السطوح الخارجية المائلة مع إستخدام التطليعات المقوسة العليا والتأكيد على المداخل والفضاءات المحصورة بين الدعامات المستخدمة من قبل المستعملين للإنتظار والإستقبال.

ومن وجهة نظر بيير لويجي نيرفي Pier Luigi Nervi فإن قناعته فيما يتعلق بالمنشآت العالية الإرتفاع والكبيرة البحور كأبنية القاعات الرياضية والملاعب فإن الهيكل المنشأي لها سيكون خادعاً في حالة عدم الإلتزام الصارم بتكامل الهيكل المنشأي مع الأفكار التصميمية. وذلك واضح في مبنى قصر الرياضة في روما (شكل – 14) كونها:

[4] ألفارو سيزا فييرا (Álvaro Siza Vieira) من أشهر المعماريين من مواليد 25 حزيران 1933 البرتغال.

- تقاوم الأحمال من خلال أسماكها الخرسانية الرقيقة (قليلة السمك).
- تعتمد هذه الأنظمة المنشأية بأداءها المنشأي على ثلاثية أبعادها وأشكالها المنحنية وإتجاهاتها الدقيقة ومواقع نقاط الإسناد.
- القشرة التي تشكل سقف القاعة الرياضية لاتتصل بالأسس بشكل مباشر ولكنه ينتهي بحافات عليا وتلتقي بدعامات خرسانية مائلة تقاوم الدفع بإتجاه الخارج.

وتشكل القشرة الخارجية في آن واحد شكل السقف وتعمل إنشائياً وكغالق للمبنى وتم تضليع سقفها من الداخل، حيث تظهر الأضلاع المتشابكة من الداخل طبيعة القوالب المسبقة الصب والتي تزيد من إستقرار المنشأ القشري وتعطي إنطباع متميز للملمس الداخلي للسقف (شكل – 15).

في هذه الأمثلة تعرف الأنظمة المنشأية الأشكال المعمارية وغالباً الوظائف ولو بشكل جزئي للقشرة الغالقة للمبنى، وتشكل الأنظمة المنشأية القشرية الأنظمة الأكثر نقاءاً في تراكب الأشكال المعمارية مع الأشكال المنشأية، وتقاوم الأنظمة المنشأية القشرية وتسمى أيضا بالأنظمة المنشأية السطحية الأحمال من خلال أسماكها الرقيقة' بإعتمد هذه الأنظمة المنشأية أداءها المنشأي على ثلاثية أبعادها وأشكالها المنحنية وإتجاهاتها الدقيقة ومواقع نقاط الإسناد.

هانز آشلر Heinz Isler أحد المصممين الأوروبيين الرواد لأنظمة الهياكل القشرية أنشأ العديد من المنشأت القشرية بإستخدام الخرسانة المسلحة وبسطوح ملساء من الداخل والخارج وتشبه الى مدى كبير بيضة الدجاجة. (مصدر 23) وحدت المنشآت القشرية التي صممها هانز آشلر الأشكال المعمارية والمنشأية وجعلها تنبع من الأسس وتنحني بشكل مستمر لتغلق الفضاء الداخلي (شكل – 16).

ويمثل مبنى السفارة المكسيكية في برلين للمعمار فرانسيسكو سيرانو Francisco Serrano (شكل – 17) مثالاً آخراً لإنجازات الخرسانة والذي يوضح عمل الواجهة كشاشة أو حاجب للمبنى، وتشكل العناصر العمودية الخرسانية المتقاربة ضرورة لنقل أحمال الجاذبية وأحمال الرياح وتهيأ الأمان والنواحي الجمالية للمبنى، وهدف المعماري خلق تكوين متكامل لايعطي صورة خاطئة عن المبنى.

إن تشكيل هذه العناصر العمودية بهذه الطريقة لإعطاء الناحية الجمالية والناحية الإنشائية في نفس الوقت، وكلما تحركت العين بشكل تدريجي بإتجاه العناصر العمودية فتبدو وكأنها تتحرك، ويكمل المظهر الإيجابي للنظام المنشأي إستخدام مادة الإنهاء الخشنة الملمس وبلون أبيض من الخرسانة ولتعكس التصنيف العالي لتصميم وإنشاء السفارة.

6- الأستخدام المعاصر لمادة الخرسانة:

تكمن أهمية الخرسانة في الوقت الحالي بإعتبارها عصب البناء، وذلك لشيوع إستخدامها كمادة إنشائية رئيسة، وإن حركة الإعمار التي تمضي قدماً في العراق تحتاج إلى التعرف بآخر المستجدات والتطوير الحاصل في إستخدامات الخرسانة بأنواعها عالمياً، وبما يتلائم مع طبيعة العمل الهندسي والظروف المحلية، وعلى سبيل المثال لا الحصر نذكر هنا تطوير بعض المواد الجديدة من قبل شركات ضخمة لصناعة الإسمنت، لتشييد إنشاءات أرخص و قابلة للدوام بشكل أكبر و هذا يشمل الجسور و الطرق السريعة و المباني.

حيث أنتجت مواد حديثة وتم تطوير إنتاج مادة الخرسانة وتحديث إستخداماتها لتتلائم مع العصر الحالي والمتطلبات الإقتصادية والبيئية:

a. مادة الدوكتل (Ductal):

وهو المنتج الأحدث من مادة الخرسانة الخاص بشركة لافارج (Lafarge)[5] الفرنسية، (مصدر – 7) حيث إنها وعلى الضد من الخرسانة التقليدية الهشة و القابلة للتحطم تحت تأثير الضغط الكبير فإن مادة الدوكتل تعطي إشارات للتشقق قبل أن تصل الى حد الإنهيار وهي من ميزاتها الجديدة والجيدة.

إن مادة الدوكتل هو نوع من مادة الخرسانة المسلحة بالألياف وتحتوي على 2–4% من الألياف المعدنية أو العضوية، وتتمتع بأداء فائق يتميز بما يلي (شكل – 18):

- مقاومة الضغط بما يتراوح من 6 إلى 8 أضعاف الخرسانة العادية. ليونة عالية. السيولة وسهولة الصب.
- عمرها الافتراضي أطول من مادة الخرسانة التقليدية بما يتراوح من ضعفين إلى 3 أضعاف.
- مقاومة عالية للصدأ، والكشط، والصدمات.
- منتج متعدد الاستعمالات إلى حد بعيد.
- صديقة للبيئة ومعترف بها من قبل المهندسين والعاملين في حقل الهندسة المعمارية لما تتمتع به من صفات جمالية وبنائية بارزة.
- أكثر صلابة بخمس مرات من الخرسانة التقليدية بسبب إضافة ألياف صغيرة مضافة الى تركيبتها وهذه الألياف المكونة من الفولاذ أو مادة البوليمر تعزز صلابة الخرسانة و تنهي الحاجة الى قضبان حديد التسليح وإن الجسر المشيد من مادة الدوكتل أكثر إشراقاً وأخف وزناً من الجسر المشيد من مادة الخرسانة التقليدية.

إن إنهاء إستخدام قضبان حديد التسليح يتضمن فوائد أخرى منها إطالة عمر الأعمال الإنشائية فعلى سبيل المثال، فإن الملح المستخدم في عملية إزالة الثلوج يتسرب الى الخرسانة المكون لجسر ما، الأمر الذي يؤدي الى صدأ قضبان حديد التسليح وإن هذا التآكل يؤدي الى فصل أجزاء الخرسانة عن بعضها البعض و عن قضبان الحديد الداعم و في نهاية الامر سينهار الجسر.

إن الطبقة السطحية لجسر من الخرسانة التقليدية تحتاج الى تصليحات كبيرة أو إعادة بناء بعد 25 سنة من التشييد، بينما الطبقة السطحية للجسر المنشأ من الدوكتل يدوم على الاقل الى ضعف هذه المدة، لقد أخذت هذه المادة طريقها في العديد من جسور المشاة حول العالم.

b. خرسانة الإجيليا (Agilia)

حيث أنتجت الشركة نفسها مادة أخرى هي مادة خرسانة الإجيليا (Agilia)، وهو نوع من الخرسانة ينضج ذاتياً ولا يتطلب هزه، مما يؤدي إلى تقليل التكلفة والجهد والضوضاء في مواقع البناء، فهي خرسانة سهلة الإستخدام وتتدفق داخل أصغر الزوايا لتتناسب تماما مع كافة الأشكال، كما وإن تركيبتها السائلة تزيل الحاجة إلى عملية الهز المرهقة والمفعمة بالضجيج حتى تنتشر بشكل سلس، مما يوفر الوقت والجهد ويقلل من الضجيج (شكل – 19).

ووفقاً لإختبارات الشركة إذا قمنا بمزج الإجيليا مع الخرسانة فان ذلك يؤدي الى تخفيض عملية صب كتلة حجمها 60 متر مكعب من مادة الخرسانة من 8 ساعات الى ساعتين كما يؤدي الى خفض عدد العاملين من 8 أشخاص إثنين فقط (مصدر – 7).

ويتطلب عادةً بعد صب الخرسانة أن يقوم عاملاً بالمرور على السطح بآلة تستخدم لإزالة الفقاعات الهوائية وهذه العملية طويلة وتصدر أصواتاً عالية، ولكن باستخدام مادة الإجيليا فإن ذلك يساعد الخرسانة على التصلب دون الحاجة لعملية الذبذبة لإن هذه المادة تحتوي على مزيج من الاضافات الكيمياوية مثل المواد السوبر بلاستيكية التي تجعل الخرسانة سائلاً، فضلاً عن إستخدام مواد كيمياوية أخرى للتقليل من الحاجة الى الماء الأمر الذي يساعد الخرسانة على التصلببشكل أسرع.

[5] لافارج شركة تصنيع فرنسية متخصصة بإنتاج ثلاثة منتجات أساسية هي الإسمنت والركام المستخدم في التشييد والخرسانة. وأصبحت هذه الشركة الرائدة في مجال مواد البناء.

وبسبب هذا السيلان فإنه باستطاعة الخرسانة ان تملأ القوالب المعقدة وأن تغطي الإنشاءات المعقدة كلها تاركةً نهاية ملساء وإن الرطوبة المتزايدة تجعل هذه المادة مثالية للإستخدام في المناطق الزلزالية حيث يتم إستخدام العوارض الحديدية بكثافة.

c. الخرسانة الشفافة Translucent Concrete

وهي نوع جديد من مادة الخرسانة يختلف عما ورد سابقاً عن مادة الدوكتل حيث قامت شركة ليتراكون LiTraCon (Light-Transmitting Concrete) بالكثير من التجارب والجهود لتغير المفهوم السائد عن مادة الخرسانة التقليدية بأنها شيئاً جامداً قاسياً غير قابل للتفنن فى إستخدامه، الى أن وصلت الى ما نحن بصدده اليوم وهو الخرسانة الشفافة Translucent Concrete (التى تسمح بمرور الضوء خلالها)، حيث يتم مزج الخرسانة بنوع معين من الألياف البصرية Optical Fibers، مما تسمح لمرور الضوء من خلالها (مصدر 8).

وقد أضيفت الألياف البصرية Optical Fibers بسماكة الشعرة لتسمح للضوء بالدخول من الطرف الاول للخرسانة الى الطرف الآخر، وقد اخترع المهندس المعماري الهنغاري آرون لوسونكزي (شكل – 20) Áron Losonczi الخرسانة نصف الشفافة بالقيام بتجارب على المواد الإنشائية، ولكنه قام بانشاء قطع من البلوك بمراحل متعددة لضمان إتصال الألياف الزجاجية مع الأسطح الجانبية للخرسانة.(مصدر 23)

وهنالك طريقة أخرى لإنتاج هذا النوع من الخرسانة وذلك بصب طبقة رقيقة وطويلة من الخرسانة و من ثم صبّ طبقة من الألياف الزجاجية فوقها، وبعد عدة تجارب لهذه العملية نتج عنها لوح طويل يمكن أن يتم تقطيعه الى قطع من البلوك القصيرة الممزوجة بالألياف الزجاجية الضوئية المتنوعة التي تتراوح أقطارها بين 2 ميكرون الى 2 ميلي ميكرون (شكل – 21).

وبإستخدام هذه الألياف المتعددة الأقطار يمكننا الحصول على تأثيرات ضوئية متعددة، وإن تنويع حجم قطع البلوك لا يؤدي الى أي تأثير على الأثر الضوئي بإستخدام هذه القطع المضيئة من البلوك فضلاً عن إن المهندسين المعماريين بإستطاعتهم بناء عدد متنوع من الإنشاءات التي تتراوح بين جدار خرساني نصف مضيء الى الأرضيات المضاءة من الأسفل.(مصدر 10)

و قد إزدادت رغبة المهندسين المعماريين لإستخدام هذه المادة الخرسانية الجديدة في العديد من دول العالم، وعلى سبيل المثال طلبت إحدى الشركات إستخدام هذه المادة الخرسانية في إنشاء كلية الشرطة في مدينة الكويت، لأن مادة البيتون ممتازة أيضاً في عزل حرارة الصحراء وإنها تسمح بإدخال أشعة الشمس الى البناء بدون الشعور بالحرارة اللاهبة، ونرى إستخدام ذلك أيضاً في مبنى الجناح الإيطالي في المعرض العالمي بمدينة شنغهاي في الصين وهو مشيد بالخرسانة الشفافه (شكل – 22).

وتستخدم تقنية أخرى في الخرسانة وهي بوضع ثقوب صغيرة في الخرسانة لا تؤثر على فعاليتها ولكنها تزيد من الشفافية لتصبح شفافية الخرسانة20%. (شكل – 23)

وأرى من مجهة نظري كباحث ضرورة إستخدام مثل هذه الخرسانة في العراق وعلى نطاق واسع وضرورة التوعية بإستخدامها لنبدا عصراً جديداً من العمارة والحد من الجوانب السلبية للعمارة في الوقت الحاضر والتي يتم تداولها دون دراية ولا تخطيط مسبق ومن قبل حرفين ليس لهم إلمام كامل بالمظهر المعماري اللائق (شكل – 24).

لقد حاولت المعمارية العراقية زها حديد إضفاء لمسة معمارية جميلة ومعاصرة في تصميمها لمنى البنك المركزي العراقي في بغداد ووضفت فيه إستخدام معاصر وجميل وبمن للخرسانة المسلحة نتمنى أن نراه في تصاميم أخرى مستقبلية (شكل – 25).

7- الإستنتاجات

- تعتبر مادة الخرسانة لوقتنا الحاضر الحل الأمثل والأسهل والأوفر لأغلب مشاكل الإنشاء والتشييد بما فيها المشكلة الإقتصادية.
- لازال هنالك قصوراً في إستخدام مادة الخرسانة في العمل المعماري في العراق.

- لمادة الخرسانة مواصفات مهمة ومتعددة تخدم النواحي الوظيفية والمعمارية والبيئية في آن واحد، وقد أستخدمها جيل واسع من المعماريين الرواد العراقيين والعالميين ونشأت توجهات معمارية متعددة كانت لمادة الخرسانة الأساس في نشأتها.
- لقد أستخدمت مادة الخرسانة كمادة إنشائية أساسية لتقوية العلاقة بين الشكل الإنشائي والشكل المعماري ومن خلال مواصفات هذه المادة مكنت المهندسين المعماريين والإنشائيين من عمل التداخل والتراكب بين الشكلين معاً، وقد أنتج المعماريون أمثلة عديدة ورائعة في هذا الإتجاه في مختلف بلدان العالم.
- تقوم شركات عديدة ضخمة بإنتاج أنواع جديدة من مادة الخرسانة وبمواصفات حديثة تختلف عن مادة الخرسانة التقليدية وتعطي إنطباعاً معمارياً جديداً وتوسع من مجال إستخداماتها

8- التوصيات

- ضرورة معرفة المعمار بخصائص مادة الخرسانة التقليدية وطبيعتها وصفاتها وميزاتها المختلفة لكي يتم إستخدامها بشكل كفوء.
- توسيع القاعدة المعرفية للمهندسين والتواصل والتفاعل مابين الإختصاصات المختلفة لإستخدام مادة الخرسانة بشكلها الأمثل من النواحي الإنشائية والمعمارية والخدمية.
- الإطلاع على المباني التي أنشأت بشكل أساسي من مادة الخرسانة والتي أخذت شهرتها من هذه المادة وتحليلها ودراستها وتحديد كيفية معالجة النواحي المعمارية بإستخدام هذه المادة والتي أوصلتها الى هذه الشهرة.
- التعرف على مستجدات الإنتاج الجديد لمادة الخرسانة الحديثة وإستخداماتها في دول العالم المختلفة ومحاولة إدخالها في المشاريع والتصاميم الجديدة في العراق.
- البدء مما إنتهت إليه دول العالم في مجال تطوير إستخدامات مادة الخرسانة ومحاولة الإبتكار وإيجاد مواد خرسانية حديثة وجديدة تتلائم وبيئتنا المحلية والنواحي الإقتصادية والحاجة الملحة للمشاريع والأبنية المختلفة.
- إعداد البحوث والدراسات المتخصصة في هذا المجال والتعمق في كيفية تطوير إستخدام مادة الخرسانة وإدخالها ضمن مجال البحوث والدراسات العليا المشتركة بين الإختصاصين المعماري والإنشائي.
- إدخال مادة الخرسانة الحديثة في مناهج تدريس طلبة الدراسات الأولية وبالأخص مناهج تركيب المباني وتقنيات البناء المتقدمة والإنشاء التقني في القسام المعمارية لكليات الهندسة في الجامعات العراقية.

9- المصادر والمراجع

- شيرزاد، شيرين إحسان، الأسلوب العالمي في العمارة بين المحافظة والتجديد، الطبعة الثانية، 2002، المؤسسة العربية للدراسات والنشر، بيروت.
- شيرزاد، شيرين إحسان، الحركات المعمارية الحديثة، الأسلوب العالمي في العمارة، الطبعة الأولى، 1999، المؤسسة العربية للدراسات والنشر، بيروت.
- شيرزاد، شيرين إحسان، لمحات من تاريخ العمارة والحركات المعمارية وروادها، الطبعة الثانية، 2002، المؤسسة العربية للدراسات والنشر، بيروت.
- Asensio, Francisco, New Architecture An International Atlas, Printed in China, 2007.
- Charleson, Sebestyen, Gyula, Associated Editor: Chris Pollingten, New Architecture and Technology, architectural Press, first published 2003.

- Ching, Francis D.K. and Cassandra Adams, Building Construction Illustrated الواضح في إنشاء , المباني، ترجمة الدكتور سليم صبحي الفقيه، الجامعة الأردنية منشورات عمادة البحث العلمي 2004/4
- http://www.lafarge.com.eg/wps/portal/eg/ar/5_1-Innovation.
- http://www.litracon.hu/downloads.php
- http://www.engpal.net/vb3/t11806.html
- Hunt, Sara, The Wright Experience Amaster Architect's Vision, Glasgow GII SLX, Scotland 2008.
- Hunts, Tony, Tony Hunt's Structures Notebook, Architectural Press, Second Edition 2003.
- Kuhl, Isabel, and others, 50 Architects you should know, Germany, 2008.
- LLC, Build, Build Bios, Significant Work by Important People, Heinz Isler: a few important things.
- Schenk, Mack, On The Shape of Cables, arches, Vaults, and Thin shells, November 10, 2009.
- Sharp, Dennis, Twentieth century architecture, A visual study, Australia, 2002.
- W., Andrew, Structure as Architecture A source Book for Architects and Structural Engineers, Architectural Press, First Published 2005.
- With apreface by Ralph Rapson and an article by Hannslart Bandel, Struture Systems, 1967 by Deutsche Verlags – Anstalt Gmbttgart.
- www.arab-eng.org
- www.mahjoob.com
- www.majddoc.com
- www.wikipedia.org
- الراوي، خالد ثابت، عمارة قحطان عوني دراسه تحليليه وتوثيقيه، أطروحه مقدامه الى مجلس كلية الهندسة – جامعة بغداد، 1990

شكل -1 بيت الشلال للمعمار فرانك لويد رايت 1935

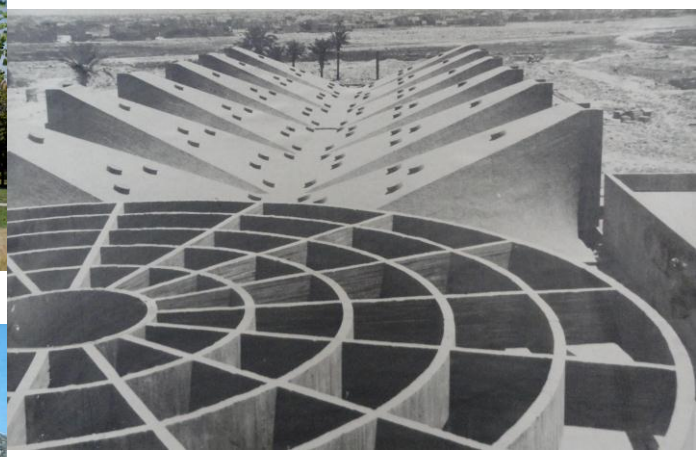

شكل -2 متحف التاريخ الطبيعي، قحطان المدفعي، بغداد، 1965

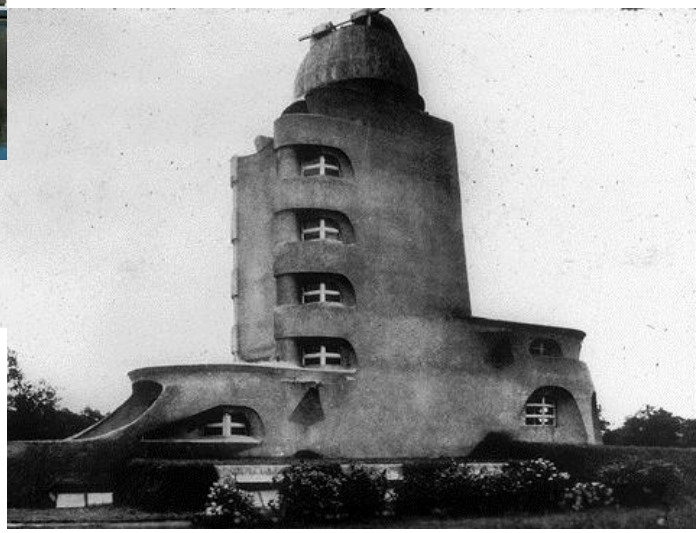

شكل - 3 برج انيشتاين للمعمار إريك ميندلسون 1921-1917

شكل -4 مبنى مرسيليا السكني- 1952- 1947

شكل - 5 مبنى قصر العدل في مدينة شنديغار 1953- 1963

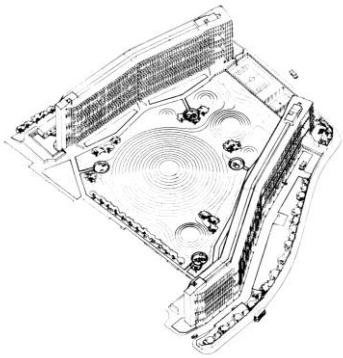

شكل -6 حدائق روبن هود لأليسون وبيتر سميتثون (1966-1972) في لندن

شكل -7 كنيسة لاكويدن ريستسي في فنلندا للمعمار ألفر آلتو 1957-1959

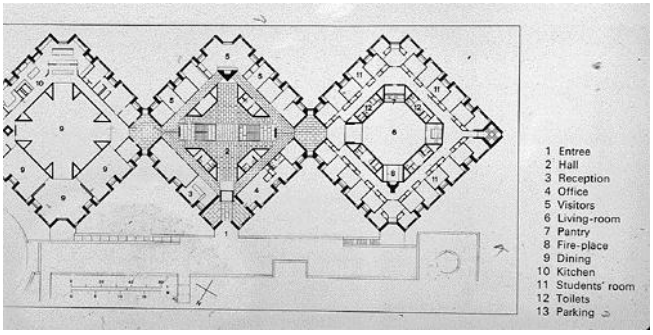

شكل -8 مبنى الأقسام الداخلية في ولاية بنسلفانيا للمعمار لويس كان 1960

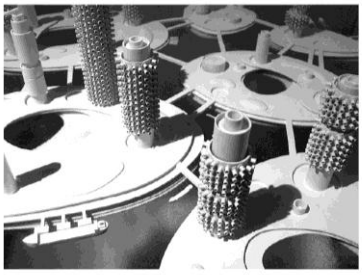

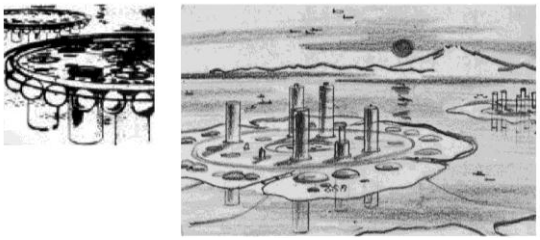

شكل -9 مشاريع الحضارة البحرية للمعمار كيونوري كيكوتي 1960

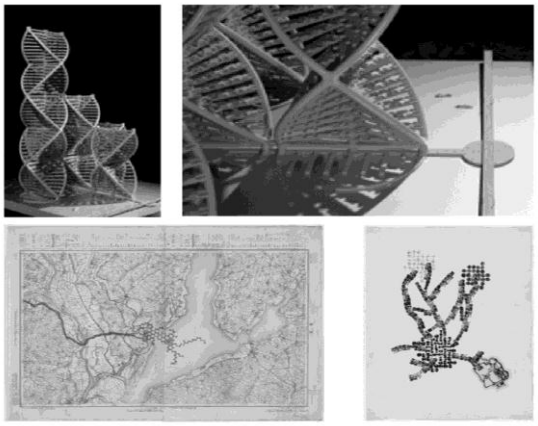

شكل -10 المدينة اللولبية للمعمار كيشو كوروكاوا 1961

شكل -11 دار جست نت في فيلادلفيا للمعمار روبرت فنتوري 1975

شكل -12 سقف قاعة الجناح البرتغالي في لشبونة للمعمار ألفارو سييزا 1998

شكل - 13 مطار دالاس للمعمار إيروو سارينين 1958-1962

شكل -14 مبنى قصر الرياضة في روما للمعمار بيير لويجي نيرفي 1956-1958

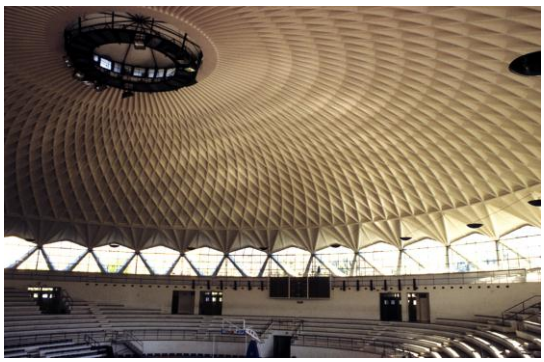

شكل -15 مبنى قصر الرياضة في روما للمعمار بيير لويجي نيرفي 1956-1958

شكل -16 مسبح مغلق للمعمار هانز آشلر في سويسرا 1981

شكل -17 مبنى السفارة المكسيكية للمعمار فرانسيسكو سيرانو برلين 2000

شكل -18 إستخدام مادة الدوكتل في الواجهات

شكل –19 بالإمكان إستخدام مادة الإجيليا لأغراض تزيين الواجهات

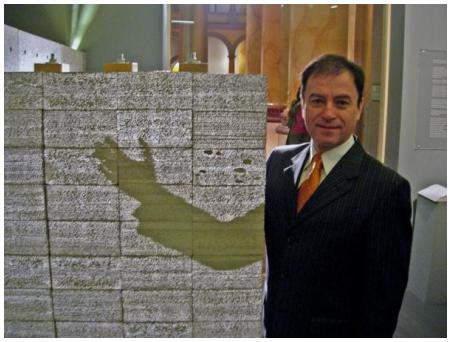

شكل –20 المهندس المعماري الهنغاري آرون لوسونكزي

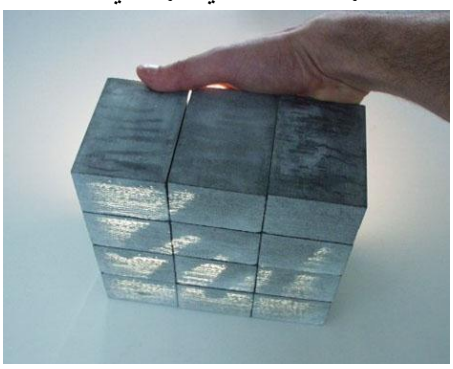

شكل –21 الخرسانة الشفافة

شكل –22 مبنى الجناح الإيطالي في معرض شنغهاي

شكل –23 منتجات من الخرسانة الشفاف

شكل –24 بعض الجوانب السلبية في لعمارة العراق اليوم

شكل –25 مبنى البنك المركزي العراقي للمعمارية زها حديد، بغداد، 2015